Conservative numerical schemes for high-frequency wave propagation in heterogeneous media

Joan Staudacher

CENTRALE PARIS

Laboratoire de Mécanique des Sols, Structures et Matériaux – UMR 8579

École Doctorale "Sciences pour l'Ingénieur" (ED 287)

Conservative numerical schemes for high-frequency wave propagation in heterogeneous media

THÈSE

présentée et soutenue publiquement le `\ThesisDate`

pour l'obtention du grade de

Docteur de l'École Centrale de Paris

par

Joan Staudacher

Composition du jury

ONERA/DADS – 29, avenue de la Division Leclerc, F-92322 Châtillon cedex

ONERA
THE FRENCH AEROSPACE LAB

Mis en page avec la classe thloria.

Contents

1

General introduction

Outline of this research

This thesis is concerned with the modelisation of the propagation of high-frequency (HF) waves in an heterogeneous medium constituted by piecewise homogeneous acoustic or elastic subdomains. Thus the overall domain contains several interfaces, and the aforementioned problem is then split into:

i. the issue of HF wave propagation in an homogeneous acoustic or elastic medium on the one hand,

ii. and the issue of reflection and transmission of these waves at the interfaces of the medium, on the other hand.

We note at the outset that tangential diffraction and critical diffraction phenomena (yielding surface waves) may also occur, but are not considered here. Some bibliographical comments are introduced, though, in the next chapter. A typical application is the propagation of HF waves induced by pyrotechnical shocks, within a satellite structure for the unfolding of solar panels, or for the separation between the launcher and the payload, for example. For these cases, the propagation medium (the structure) can be modeled at a first glance as a piecewise homogeneous linear elastic medium carrying HF waves. One important issue is then to quantify the energy released by the shocks in order to be able to predict (and subsequently alleviate) the potential damages they may induce to the devices attached to the structure, or to the structure itself. It is thus desirable to describe as precisely as possible the distribution of energy density and energy fluxes caused by those loads. In our modeling, the latter shall typically be considered as highly oscillating initial conditions having the form of localized HF waves; see the Section 2.1.4 in the subsequent chapter.

In this setting, classical engineering approaches such as the Statistical Energy Analysis (SEA) may be invoked [49, 50]. SEA describes the energy distribution in built-up structures by the computation of average mechanical energies in the different subsystems constituting the main system. Despite its numerous developments and improvements since the earlier works of Lyon & Maidanik [48], SEA remains an approximate, heuristic method. It does not give any indication on the local distribution and direction of propagation of the energy in the considered structure. In addition, SEA is restricted to the steady-state, frequency domain. A more precise approximation of the problem is thus necessary. In this respect, engineers have considered approaches based on an analogy of high-frequency vibration phenomena with heat conduction phenomena (Vibrational Conductivity Analogy, VCA) [10, 37, 39, 54]. In VCA, a vibrational temperature is introduced and identified to the classical physical notion quantifying the motions and interactions of particles. Note that in SEA, VCA or in the approach developed in this thesis, the energy (or the energy density) and more generally quadratic quantities will arise as the most relevant observables for the characterization of HF wave propagation, since the highly oscillatory features of quantities such as the pressure field (for acoustic waves) or the displacement field (for elastic waves) are more difficult to understand in a high-frequency regime. We shall thus consider in this work the problem of the evolution of the energy density associated to HF initial conditions in a piecewise homogeneous medium characterized by its physical parameters (the density, the compressibility and/or the Lamé moduli in isotropic materials) for acoustic waves (see the Eq. (2.9)) or for elastic waves (see the Eq. (2.13)). We seek in this

way a characterization of the highly oscillating solutions of the wave or the Navier equation considered in homogeneous subdomains, supplemented with reflection and transmission boundary conditions at the interfaces between these subdomains.

The direct approach to solve this boundary value problem by classical numerical methods such as finite differences or finite elements are limited by the number of points necessary to discretize the spatial domain. Other approximation methods are then envisaged, which are based on the use of asymptotic expansions (in powers of the relative wavelength which is a small parameter $\varepsilon \ll 1$) as approached solutions. We may consider different classes of methods, that both have pros and cons. We basically refer to the WKB method [13, 59, 65, 67], which relies on an asymptotic expansion and leads to the resolution of a couple of equations, the (non-linear) eikonal equation and the transport equation. The latter may be solved by the method of characteristics or ray tracing; see [18] and references therein. This approach allows to estimate the solutions of evolution equations as the relative wavelength ε goes to 0. Nevertheless, it is limited by the facts that it does not take into account the diffraction effects at boundaries straightforwardly, and it fails at the caustics, which are envelope curves where the waves intersect. Thus it needs to be completed by refined theories to deal with such phenomena.

An alternative approach has been investigated after the earlier works of Tartar [71], Paul and Lions [45], Papanicolaou *et al.* [61], Gérard *et al.* [22], or Markowich *et al.* [65] among others. It consists in introducing a Wigner transform of the solution of a wave equation, from which the energy density and the energy flux density are derived in the limit of a small relative wavelength $\varepsilon \to 0$. These limits are related to the limit Wigner transform, the so-called Wigner or semi-classical measure. The characterization of HF wave propagation phenomena reduces then to the resolution of a system of Liouville transport equations that allows to determine the Wigner measures of acoustic or elastic wave motions. More precisely, their solutions correspond to angularly resolved energy densities lying in the phase space position $\times$ wave vector, the so-called specific intensities, each of them corresponding to a different mode of propagation, or polarization. In acoustics, the modes are purely compressional, while in isotropic elasticity the modes are both compressional (axial strains) and transversal (shear strains). The specific intensities satisfy boundary conditions (typically reflections and transmissions whenever diffraction phenomena are ignored) at the interfaces within a piecewise homogeneous medium, that can be determined in terms of the wave celerities and physical parameters on each side of the interfaces. A rigorous mathematical treatment of the reflection/transmission conditions for the energy flux densities of the HF solutions of a scalar wave equation is proposed in [4, 52]. It has been extended recently to the vector, elastic wave equation in [5]. The analysis developed in these works shows that the same kind of boundary conditions as for plane waves applies at the limit of high frequencies. They embed the well-established Snell-Descartes laws of refraction, stating that the tangent components of the wave vectors at the interfaces remain constant. Such considerations apply to the propagation of HF waves within built-up structures [64], for example. To sum up, the approach elaborated in this thesis consists in adopting a kinetic point of view of wave propagation phenomena, where energy "particles" associated to such highly oscillating waves are tracked in the phase space. This setting also allows to obtain a relevant description of the energy flux density, which implies that the leading directions of propagation of the energy are properly resolved.

The kinetic approach basically reduces to the resolution of Liouville equations supplemented with HF initial conditions, and boundary conditions at the interfaces and the outer boundary of the physical domain. For arbitrary geometries, one has to resort to numerical methods. Typically Monte-Carlo (MC) methods, finite element (FE) methods or finite difference (FD) methods may be adopted. From a computational point of view, the kinetic approach presents some drawbacks in that the numerical resolution of the Liouville transport equation requires a large number of discretization points in order to encompass the whole phase space (position and wave vector domains) with FE or FD methods. MC methods allow to compute local solutions, a decisive advantage over such energetic methods for large-scale computations. They converge slowly, but it is always possible to control their accuracy. The MC method for solving a transport partial differential equation is based on its interpretation as a Fokker-Planck equation for the marginal probability density of an underlying homogeneous Markov process having its values in phase-space [7, 38]. The latter corresponds to the position and velocity of particles with possible different polarizations. The algorithm thus consists in simulating trajectories of these particles and subsequently averaging over these paths. It extends to a bounded domain by constructing those trajectories from the broken bicharacteristic flow within the phase-space. This is practically done by

reflecting and transmitting those rays according to Snell-Descartes laws, with possible mode conversions in elastodynamics.

The main drawback of MC methods is their lack of versatility for complex geometries as typically encountered in structural acoustics. FE methods are better adapted to complicated geometries, but require more memory spaces for the numerical simulations than FD methods. In our work, we shall rather consider the classical approach by a FD scheme that is adapted to first order linear partial differential equations, as proposed by Jin and his co-workers in *e.g.* [27–32]. The major difficulty arising from that scheme is that for low discretization numbers, the energy may be not conserved as it is numerically reflected and transmitted at the interfaces within the computational domain. In particular, if one takes relatively low discretization numbers it is observed that some energy may be lost at an interface between two different subdomains, due to a poor interpolation of the specific intensities in phase space. More precisely, the difference of wave celerities on each side of that interface induces a difference of variation scales in the distribution of the transmitted wave vectors obtained by Snell-Descartes laws. This difference increases with the ratio $\frac{c^+}{c^-}$, where c^+ and c^- denote the wave celerities on both sides of an interface with $c^+ > c^-$. This implies that a classical interpolation of the specific intensities as proposed in [27, 31] is not always adapted in order to obtain a conservative numerical solution of the Liouville equation, since it induces a loss of the overall energy brought by the initial conditions. This defect may be corrected by a direct method consisting in correcting the difference of scale on each side of an interface. To this purpose, one can define two different grids of wave vectors on each side of the interface of the medium, with different discretization steps adapted to each variation scale. However this strategy clearly lacks versatility. Alternatively, the energy loss may be corrected by computing *ad hoc* interpolation coefficients, when possible, defined so as to cancel the numerical loss of energy at an interface. This may lead to interpolations extending over more than two points, contrary to what is done in [27, 31]. Both methods can also be combined in order to construct the desired conservative numerical schemes. This construction is the main concern presented in this thesis. It is illustrated by different examples showing how the proposed modified FD schemes correct the loss of energy obtained with the classical unmodified schemes, considering also a relatively low number of discretization points.

This thesis is organized as follows. The following chapter 2 introduces the setting of high-frequency wave propagation both for acoustic and elastic media, and different approaches that can be used in order to address it: especially the WKB method and the kinetic approach. The consideration of boundary conditions is also outlined in this chapter, which is concluded with a summary of the kinetic model that shall be adopted in the remaining of the thesis. The numerical treatment of this problem by FD schemes, and the issue of discretizing the computational phase-space domain as well as the interfaces between the different homogeneous subdomains, are exposed in the subsequent chapter 3. The general form of the investigated numerical schemes and the issue of numerical energy loss at the interfaces of the propagation medium are also presented in this part. The correction of these losses by different approaches is the subject of the chapter 4. Validations and illustrations of the proposed developments by numerical examples are presented in the last chapter 5. It also brings out an analysis of the convergence of the solutions obtained for different discretization refinements to a theoretical analytical solution, which is computed in the particular case of a straight interface. This chapter concludes with the conservation of the energy obtained with these numerical schemes, for any number of discretization points. Finally, chapter 6 offers a few conclusions and prospects on this work.

Résumé de cette recherche

L'objet de cette thèse est la modélisation de la propagation d'ondes hautes fréquences (HF) dans un milieu hétérogène consituté de sous-domaines acoustiques ou élastiques, homogènes par morceaux. Par conséquent, l'ensemble du domaine comprend plusieurs interfaces, et le problème prédéfini se décompose en :

i. un problème de propagation d'ondes dans un milieu homogène acoustique ou élastique, d'une part,
ii. et un problème de réflexion et transmission de ces ondes aux interfaces du domaine, d'autre part.

Nous pouvons remarquer d'entrée que des diffractions critique et tangentielle peuvent aussi se produire (et engendrer des ondes surfaciques), mais ne sont pas prises en compte dans la modélisation considérée ici.

Certains détails bibliographiques concernant ces points sont toutefois évoqués dans le prochain chapitre. Une application classique consiste en la propagation d'ondes HF produite par des chocs pyrotechniques au sein de la structure d'un satellite, pour le déploiement d'un panneau solaire, ou lors de la séparation entre les étages d'une fusée (séparation entre le lanceur et la charge utile) par exemple. Dans ces cas précis, le domaine de propagation (la structure) peut être modélisée au premier abord, par un milieu homogène par morceaux, linéaire, élastique, dans lequel se propagent des ondes HF. Un des problèmes majeur qui se posent alors, est de quantifier l'énergie libérée par les chocs, de manière à être capable de prédire (et donc d'éviter) les dégâts éventuels qu'ils peuvent causer aux instruments solidaires de la structure, ou à la structure elle-même. Il est donc intéressant de pouvoir décrire aussi précisément que possible, la répartition de la densité d'énergie et de la densité de flux d'énergie provoquée par ces chargements. Dans la modélisation adoptée, ces dernières peuvent être considérées comme des conditions initiales oscillantes, qui prennent la forme d'ondes HF localisées (voir la section 2.1.4 du chapitre correspondant).

Des approches d'ingénierie classiques telles que la SEA (Statistical Energy Analysis) peuvent être mentionnées [49, 50]. La SEA décrit la répartition d'énergie vibratoire dans des assemblages mécaniques par le calcul d'énergies mécaniques moyennes dans les différents sous-systèmes qui constituent le système tout entier. Malgré de nombreux développements et améliorations depuis les premiers travaux de Lyon & Maidanik [48], la SEA reste une méthode heuristique approximative. Elle ne donne aucune indication sur la répartition locale et la direction de propagation de l'énergie dans le système considéré. Il faut ajouter à cela que la SEA se réduit au domaine fréquentiel en régime permanent. Une meilleure approximation du problème est donc nécessaire. Dans cette optique, des ingénieurs ont considéré des approches, basées sur l'analogie entre les phénomènes de vibrations hautes-fréquences, et les phénomènes de conduction thermique (Vibrational Conductivity Analogy, VCA) [10, 37, 39, 54]. En VCA, une température de vibration est introduite et identifiée à la notion physique classique qui quantifie le mouvement et les interactions des particules. Il faut remarquer qu'en SEA, VCA, ou dans l'approche développée dans cette thèse, l'énergie (ou densité d'énergie) et plus généralement des quantités quadratiques apparaissent comme étant les observables les plus pertinentes, pour la caractérisation d'ondes HF, puisque les caractéristiques de quantités telles que le champ de pression (pour les ondes acoustiques) ou le champ de déplacement (pour les ondes élastiques) sont plus difficiles à apprécier dans le régime hautes fréquences. Nous considérons donc dans le présent ouvrage, le problème de l'évolution de la densité d'énergie associé à des conditions initiales HF, dans un milieu homogène par morceaux et caractérisé par ces paramètres physiques (densité, compressibilité et paramètres de Lamé dans les milieux isotropes) pour les ondes acoustiques (*cf.* Eq. (2.9)) ou pour les ondes élastiques (*cf.* Eq. (2.13)). On essaye de déterminer de cette manière une caractérisation des solutions oscillantes de l'équation des ondes ou des équations de Navier, considérées dans des sous-domaines homogènes, auxquelles s'ajoutent des conditions de réflexion transmission aux interfaces entre ces sous-domaines.

L'approche classique directe pour résoudre ces problèmes aux limites par des méthodes numériques classiques telles que des méthodes de différences finies ou d'éléments finis, sont limitées par le nombre de points nécessaires pour discrétiser le domaine spatial. D'autres méthodes d'approximation peuvent alors être envisagéees, basées sur l'utilisation de développements asymptotiques (en la longueur d'onde relative qui est un petit paramètre $\varepsilon \ll 1$), comme solution d'approximation. On considère différentes classes de méthodes qui présentent des avantages et des inconvénients. On renvoie classiquement à la méthode WKB [13,59,65,67], fondée sur un développement asymptotique et qui conduit à la résolution d'un couple d'équations, l'équation Eikonale (non-linéaire), et l'équation de transport. Celles-ci sont résolues par des méthodes de tracé de rayon ou par la méthode des caractéristiques, voir [18]. Cette approche permet d'approximer les solutions d'équations d'évolution pour lesquelles la longueur d'onde relative ε tend vers 0. Toutefois, elle est limitée par le fait qu'elle ne permet pas de prendre en compte les phénomènes de diffraction aux interfaces, ni de modéliser les caustiques, qui sont des enveloppes (courbes) où les rayons se croisent. Elle doit donc être complétée par des théories plus fines, qui prennent en compte ces phénomènes.

Une approche alternative a été développée après les premiers travaux de Tartar [71], Lions & Paul [45], Papanicolaou *et al.* [61], Gérard *et al.* [22], ou Markowich *et al.* [65] parmi d'autres. Elle consiste à introduire la transformée de Wigner de la solution d'une équation d'ondes, de laquelle sont déduites les densités d'énergie et densités de flux d'énergie, dans la limite des petites longueurs d'ondes relatives $\varepsilon \to 0$. Ces limites sont reliées à la limite de la transformée de Wigner appelée aussi mesure de Wigner.

La caractérisation des phénomènes de propagation d'ondes HF se réduit alors à la résolution d'un système d'équations de Liouville, qui permet de déterminer les mesures de Wigner associées aux déplacements d'ondes acoustiques ou élastiques. Plus précisément, les solutions correspondent à des densités d'énergie résolues selon la direction de propagation, qui évoluent dans l'espace des phases position × vecteur d'ondes, et appelées intensités spécifiques, chacune d'entre elles correspondant à différents modes de propagation. En acoustique les modes sont purement des modes de compression, tandis qu'en élasticité isotrope, les modes sont à la fois des modes de compression et des modes transverses (cisaillement). Les intensités spécifiques satisfont des conditions aux limites (réflection et transmission, si l'on ne tient pas compte des phénomènes de diffraction) aux interfaces d'un sous-domaine homogène, qui peuvent s'exprimer en fonction de la célérité des ondes et des paramètres physiques de part et d'autres de ces interfaces. Un traitement mathématique rigoureux des conditions de réflexion/transmission pour les densités de flux d'énergie des solutions HF de l'équation des ondes scalaire est proposée dans [4, 52]. Il a été étendu récemment au cas de l'équation des ondes élastiques vectorielle dans [5]. L'analyse développée dans ces travaux montre que l'on obtient le même type de conditions aux limites à la limite des hautes fréquences que pour des ondes planes. Elles intègrent les lois classiques de la réfraction de Snell-Descartes, qui expriment que les composantes tangentielles des vecteurs d'ondes aux interfaces restent constantes. Ces considérations s'appliquent par exemple au cas de la propagation d'ondes HF dans des assemblages de structures élancées [64]. Pour résumer, l'approche élaborée dans cette thèse consiste à adopter un point de vue cinétique du phénomène de propagation d'ondes où l'on considère des particules d'énergie associées aux ondes à oscillations rapides et l'on examine leur évolution dans l'espace des phases. Ce point de vue permet d'obtenir par ailleurs une description pertinente des flux d'énergie, ce qui implique que les directions principales de propagation de l'énergie sont bien déterminées.

L'approche cinétique se réduit fondamentalement à la résolution d'équations de Liouville complétées par des conditions initiales HF, et des conditions aux limites aux interfaces et aux frontières extérieures du domaine physique. Pour des géométries arbitraires, il faut avoir recours à d'autres types de méthodes numériques. D'un point de vue calcul, l'approche cinétique présente des inconvénients, dans la mesure où le résolution numérique des équations de Liouville nécessite un nombre important de points de discrétisation, pour le discrétisation de l'espace des phases tout entier (position et vecteurs d'ondes). Typiquement des méthodes de Monte-Carlo (MC), d'éléments finis (FE) et de différences finies (FD) peuvent être utilisées. Du point de vue des résolutions numériques, l'approche cinétique présente un certain nombre d'incovénients, essentiellement parce qu'elle exige de recourir à un grand nombre de points de discrétisation afin d'englober tout l'espace des phases (position et vecteur d'onde) avec des méthodes FD ou FE. Les méthodes MC permettent quant à elles de ne calculer que des solutions locales si besoin est, un avantage qui peut s'avérer décisif par rapport aux méthodes énergétiques précédentes pour des simulations à grande échelle. En revanche elles convergent lentement, mais il est toujours possible de contrôler leur précision. L'approche MC pour la résolution d'une équation aux dérivées partielles du type transport est fondée sur son interprétation comme une équation de Fokker-Planck pour la densité de probabilité marginale d'un processus de Markov sous-jacent, à valeurs dans l'espace des phases [7, 38]. Ce dernier correspond à la position et la vitesse de "particules" d'énergie ayant éventuellement des polarisations différentes. L'algorithme consiste ainsi à simuler des trajectoires de ces particules, et ensuite en prendre leur moyenne. Il s'étend à des domaines bornés en construisant ces trajectoires à partir du flot bicaractéristique brisé dans l'espace des phases. Pratiquement cela revient à réfléchir et transmettre les rayons d'énergie suivant les lois de Descartes, avec des conversions de modes possibles en élastodynamique.

Les méthodes d'éléments finis sont mieux adaptées aux géométries complexes, mais requièrent plus d'espace mémoire en moyenne au cours des simulations numériques que les méthodes de différences finies. Dans le cas présent, on fait le choix d'utiliser des méthodes différences finies mieux adaptées à la résolution d'équations aux dérivées partielles du premier ordre, comme proposés par Jin et ses coauteurs dans [27–32]. Une des difficultés principales de ces schémas est que pour de faibles nombres de discrétisation, on peut observer des pertes d'énergie dues à la présence d'interfaces (réflection et transmission numériques) à l'intérieur du domaine de calcul. En particulier, si l'on considère de faibles nombres de discrétisation, on observe que de l'énergie est perdue à une interface entre deux sous-domaines en raison d'une interpolation trop simple des intensités spécifiques dans l'espace des phases. En effet, la différence de célérité des ondes de part et d'autres d'une interface induit une différence d'échelle de variation des vecteurs d'ondes incidents et transmis obtenus par les lois de Snell-Descartes de part

et d'autre de cette interface. Cette différence augmente avec le ratio $\nu = \frac{c^+}{c^-}$, où $c^+ > c^-$ désignent les célérités de part et d'autre de l'interface. Ceci implique qu'une interpolation linéaire classique à deux points des intensités spécifiques n'est pas toujours adaptée pour obtenir une solution numérique conservative de l'équation de Liouville, puisqu'elle induit une perte de l'énergie totale. On propose de remédier à ce défaut par une méthode directe qui consiste à corriger la différence d'échelle de part et d'autres d'une interface. Dans cette optique, on pourrait définir deux grilles différentes de vecteurs d'ondes, de part et d'autre de l'interface, avec des pas de discrétisation différents adaptée à chaque échelle de variation. Cette méthode présente toutefois l'inconvénient de manquer de versatilité. Une autre approche consiste à calculer des coefficients d'interpolation, quand ceci est possible, de manière à annuler la perte d'énergie numérique à une interface. Ceci peut conduire à des méthodes d'interpolation à plus de deux points, contrairement à ce qui est fait dans [27, 31]. Les deux approches évoquées ici peuvent aussi être combinées pour construire les schémas numériques voulus. Cette construction est la préoccupation principale de la thèse présentée ici. Elle est illustrée par différents exemples numériques qui montrent comment les schémas numériques modifiés suivant le principe énoncé plus haut corrigent la perte d'énergie obtenue avec les schémas classiques non modifiés de [27, 31], considérant également des nombres de discrétisation faibles.

Ce mémoire est organisé comme suit. Le chapitre 2 suivant introduit le cadre théorique de la propagation d'ondes pour l'acoustique et l'élastodynamique, et les différentes approches utilisées pour modéliser ces problèmes – en particulier la méthode WKB et l'approche cinétique. La prise en compte des conditions aux limites fait également l'objet de ce chapitre, qui est conclut par un résumé du modèle cinétique adopté dans le suite de cette thèse. Le traitement numérique de ce problème par des schémas DF, et le probléme de la discrétisation de l'espace des phases et des interfaces entre les différents sous-domaines fait l'objet du chapitre 3 qui suit. La forme générale des schémas numériques considérés et le problème de la perte d'énergie aux interfaces du milieu sont aussi présentés dans ce chapitre. La correction de ces pertes par différentes approches fait l'objet du chapitre 4. Les validations et les illustrations des développements proposés par des exemples numériques sont présentées dans le dernier chapitre 5. Celui-ci présente également une analyse de la convergence des solutions obtenues, pour différents niveaux de raffinement de la discrétisation, vers une solution théorique calculée dans le cas particulier d'une interface droite. Ce chapitre conclut quant à la conservation de l'énergie obtenue avec les schémas numériques développés, pour un nombre quelconque de discrétisation. Finalement le chapitre 6 propose quelques conclusions et perspectives à ce travail.

2

Addressing high-frequency wave propagation in heterogeneous media

High-frequency (HF) wave propagation may be treated in a specific manner compared to low-frequency (LF) wave propagation, because of the difference of scale between the size L of the computational domain, and the characteristic size of the spatial variations of the waves that propagate in it. Typically if λ denotes a wavelength, the parameter $\varepsilon = \lambda/L$ is small compared to 1. In the present case the wavelength is also small compared to the the microscopic structure of the medium, which can be considered as a low-frequency medium. Taking into account fine scales in the resolution of wave equations in acoustics or in elastodynamics requires an important computational cost, if one wants to obtain accurate solutions as for low or even mid-frequency waves. The use of alternative approaches, such as asymptotic methods relying on an expansion of the solution of the wave equation in powers of ε, is necessary to describe high-frequency wave phenomena. The Wentzel-Kramers-Brillouin (WKB) method for instance (see [67] for applications in solid mechanics) is based on an approximation of the solution of a wave equation in the form of an expansion in powers of ε multiplied by a phase exponential proportional to $1/\varepsilon$. It provides a system of first-order partial differential equations which describe the evolution of the phase (eikonal equation) and of the amplitude (transport equation) of the approximate solution. These equations can be solved by ray tracing among other methods. It consists in introducing a system of equations describing the co-evolution of the phase and of the amplitude of the wave on curves orthogonal to the iso-curves of the phase, called rays. An Hamiltonian is associated to each wave equation for the physics to be considered, typically acoustics or elastodynamics in the present case. It must be kept constant along the rays, while it also describes the evolution of the phase. Even though this method has been widely used in dealing with high-frequency waves, it has the drawback to yield a non linear (eikonal) equation, which precludes the analysis of multi-valued solutions. Therefore the approximate solutions obtained by this method are incomplete or inaccurate in the regions where the rays intersect, as for instance in the case of caustics. The WKB expansion is indeed insufficient to deal with diffraction problems. It must be replaced in this case by other types of expansion, or requires higher order terms developments. Finally even if it may be applicable for treating some boundary condition problems, it is however restricted by the regularity of the initial conditions. The latter is also a necessary condition to perform the WKB expansion (see [65], proposition 2.1).

Other types of approaches developed by Tartar [71], Lions & Paul [45], Gérard *et al.* [22], Markowich *et al.* [65], Papanicolaou *et al.* [61] are based on a kinetic point of view in dealing with HF waves. They rest upon the derivation of a Liouville-type transport equation for the energy density associated to the HF solutions of wave equations. The Liouville equation describes the evolution of the latter in the phase space $(\mathbf{x}, \mathbf{k}) \in \mathbb{R}^d \times \mathbb{R}^d$, where d is the physical space dimension. For this reason these densities are also called specific intensities in the dedicated literature (see [61] for instance). This formulation has several advantages. The Liouville equation is linear hence it satisfies a superposition principle. This is a desirable property in order to model crossing rays, providing therefore with more accurate solutions than the WKB approach for instance. As a consequence, it lends itself to the description of caustics and to

refraction phenomena at an interface (see for example the related works of Buchal & Keller [11] or Lewis *et al.* [41] on creeping waves). The simple form of the Liouville equation, a first-order partial differential equation (PDE), is appropriate for a computation of its approximate solution by finite difference (FD) methods. Finite differences are easy to implement, leading to a discretization of the specific intensities on a regular grid. This approach is based intrinsically on an energetic point of view (an energy density in phase space is computed) and is a way to express the energy and flux densities in terms of the computed solution. Nevertheless it is restricted by its theoretical framework, raising a relevant problem related to the choice of boundary conditions for the specific intensities. This problem, of which solution is unknown in the general case, has been dealt with in particular cases solely. In [4, 52] for example the relations between incident, reflected and transmitted specific intensities already known for harmonic plane waves, are properly derived in case of HF wave transmission between two heterogeneous media or wave reflection at a convex boundary. These relations turn out to be the same in both cases. The kinetic approach also has serious drawbacks in its numerical application, since it is necessary to discretize the whole phase space. This may significantly increase the cost of numerical computations. Different ways to correct this problem have been outlined by Engquist & Runborg in [18], mainly wave front methods and moment methods. The basic objective of the latter is to reduce the dependence of the energy density toward the wave vectors domain. These last developments will not be presented in this work though.

2.1 Acoustic and elastic wave propagation

We begin this chapter by introducing the evolution equations ruling the propagation of acoustic and elastic waves in an open domain $\mathcal{O} \subset \mathbb{R}^d$, where $d = 2$ or $d = 3$ is the physical space dimension. It is occupied by an heterogeneous medium, considered as a piecewise homogeneous one described by the geometry of the various homogeneous subdomains. That geometrical description includes boundaries and interfaces. An interface corresponds to a discontinuity of the physical parameters between two homogeneous media occupying two subdomains of $\mathcal{O}$. The piecewise homogeneous media considered here are either gas, liquids or solids. We first consider the case of an acoustic medium, where a solution of the wave equation propagates at the wave velocity $c(\mathbf{x})$ at the location $\mathbf{x} \in \mathcal{O}$ defined in terms of the density $\rho(\mathbf{x})$, and the compressibility $\kappa(\mathbf{x})$ of the medium by:

$$c(\mathbf{x}) = \frac{1}{\sqrt{\rho(\mathbf{x})\kappa(\mathbf{x})}}\,. \tag{2.1}$$

Then we consider solutions of the elastodynamic wave equation in isotropic media. They can be split into two types of waves: longitudinal waves or pressure waves (also called P waves), and shear waves (also called S waves). Each type of wave is characterized by a different velocity expressed in terms of the density $\rho(\mathbf{x})$ and the Lamé parameters $\lambda(\mathbf{x})$ and $\mu(\mathbf{x})$ in the medium by:

$$c_{\mathrm{P}}(\mathbf{x}) = \sqrt{\frac{\lambda(\mathbf{x}) + 2\mu(\mathbf{x})}{\rho(\mathbf{x})}}\,, \quad c_{\mathrm{S}}(\mathbf{x}) = \sqrt{\frac{\mu(\mathbf{x})}{\rho(\mathbf{x})}}\,. \tag{2.2}$$

The following notations are adopted throughout this chapter. The boundaries $\partial\mathcal{O}$ are defined by an equation of the form $\Sigma_b(\mathbf{x}) = 0$, where $\mathbf{x} \in \mathbb{R}^d$. The interfaces splitting $\mathcal{O}$ into several subdomains are denoted by $\cup_{1\leq i\leq p}\mathcal{I}_i$, while the set of subdomains of $\mathcal{O}$ deprived of its interfaces is denoted by $\tilde{\mathcal{O}}$. Each interface $\mathcal{I}_i$ is oriented by its unit normal $\mathbf{n}_i$, and defined by an equation of the form $\Sigma_i(\mathbf{x}) = 0$.

2.1.1 Acoustic waves

We consider small perturbations $(\boldsymbol{\sigma}, \rho, \mathbf{u})$ of the stress tensor $\boldsymbol{\sigma}_{\mathrm{t}}$, density ρ_{t}, and velocity field $\mathbf{u}_{\mathrm{t}}$ of a fluid medium, respectively, with respect to a reference state of that fluid at rest characterized by $(\boldsymbol{\sigma}_0, \rho_0, \mathbf{u}_0 = \mathbf{0})$:

$$\begin{aligned}
\boldsymbol{\sigma}_{\mathrm{t}}(t,\mathbf{x}) &= \boldsymbol{\sigma}_0(\mathbf{x}) + \boldsymbol{\sigma}(t,\mathbf{x})\,,\\
\rho_{\mathrm{t}}(t,\mathbf{x}) &= \rho_0(\mathbf{x}) + \rho(t,\mathbf{x})\,,\\
\mathbf{u}_{\mathrm{t}}(t,\mathbf{x}) &= \mathbf{0} + \mathbf{u}(t,\mathbf{x})\,.
\end{aligned}$$

The linearized balance of momentum reads:

$$\rho_0(\mathbf{x})\partial_t \mathbf{u}(t,\mathbf{x}) = \mathbf{Div}_{\mathbf{x}}\boldsymbol{\sigma}(t,\mathbf{x})\,, \tag{2.3}$$

and the linearized equation of mass conservation (or continuity equation) reads:

$$\partial_t \rho(t,\mathbf{x}) + \mathrm{div}_{\mathbf{x}}(\rho_0(\mathbf{x})\mathbf{u}(t,\mathbf{x})) = 0 \tag{2.4}$$

for $(t,\mathbf{x}) \in \mathbb{R}\times\tilde{\mathcal{O}}$. Here the divergence of the stress tensor is defined by $(\mathbf{Div}_{\mathbf{x}}\boldsymbol{\sigma},\mathbf{c}) = \mathrm{div}_{\mathbf{x}}(\boldsymbol{\sigma}^{\mathsf{T}}\mathbf{c})$ for any constant vector $\mathbf{c}$, where $\mathbf{A}^{\mathsf{T}}$ stands for the transpose of matrix $\mathbf{A}$. In addition, it is assumed that:

– The fluid is inviscid, such that the shear component of the stress fluctuations is negligible. This yields a spherical stress fluctuation:

$$\boldsymbol{\sigma}(t,\mathbf{x}) = -p(t,\mathbf{x})\mathbf{I}_d\,, \tag{2.5}$$

where p is the fluid pressure fluctuation, and $\mathbf{I}_d$ is the identity matrix of $\mathbb{R}^d$.

– The total entropy $s_{\mathrm{t}} = s_0 + s$ remains constant considering the motion of any fluid particle, leading to the linearized energy conservation:

$$\partial_t s(t,\mathbf{x}) + \mathbf{u}(t,\mathbf{x})\cdot\boldsymbol{\nabla}_{\mathbf{x}} s_0(\mathbf{x}) = 0\,. \tag{2.6}$$

From the equation of state $p_{\mathrm{t}} = p(\rho_{\mathrm{t}}, s_{\mathrm{t}})$ and the balance of momentum applied to the reference pressure field $\boldsymbol{\nabla}_{\mathbf{x}} p_0 = \mathbf{0}$ with $p_0 = p(\rho_0, s_0)$, one has:

$$\mathbf{0} = \left(\frac{\partial p}{\partial \rho}\right)_s \boldsymbol{\nabla}_{\mathbf{x}}\rho_0 + \left(\frac{\partial p}{\partial s}\right)_\rho \boldsymbol{\nabla}_{\mathbf{x}} s_0\,,$$

from which the sound speed (2.1) in an heterogeneous medium arises as:

$$c^2(\mathbf{x}) = \left(\frac{\partial p}{\partial \rho}\right)_s\,. \tag{2.7}$$

The linearized equation of state thus reads:

$$p(t,\mathbf{x}) = c^2(\mathbf{x})\rho(t,\mathbf{x}) + \left(\frac{\partial p}{\partial s}\right)_\rho s(t,\mathbf{x})\,,$$

which together with Eq. (2.4) and Eq. (2.6) finally yields:

$$\frac{1}{c^2(\mathbf{x})}\partial_t p(t,\mathbf{x}) + \rho_0(\mathbf{x})\,\mathrm{div}_{\mathbf{x}}\,\mathbf{u}(t,\mathbf{x}) = 0\,. \tag{2.8}$$

Now taking the divergence of the linearized balance of momentum (2.3) and deriving with respect to the time t the continuity equation (2.8) above, yields the following scalar wave equation for the pressure field p:

$$\partial_t^2 p(t,\mathbf{x}) - \frac{1}{\kappa(\mathbf{x})}\boldsymbol{\nabla}_{\mathbf{x}}\cdot\left(\frac{1}{\rho_0(\mathbf{x})}\boldsymbol{\nabla}_{\mathbf{x}} p(t,\mathbf{x})\right) = 0\,; \tag{2.9}$$

or, deriving with respect to the time t the linearized balance of momentum (2.3) and taking the gradient of the continuity equation (2.8), yields the following vector wave equation for the velocity field $\mathbf{u}$:

$$\partial_t^2 \mathbf{u}(t,\mathbf{x}) - \frac{1}{\rho_0(\mathbf{x})}\boldsymbol{\nabla}_{\mathbf{x}}\left(\frac{1}{\kappa(\mathbf{x})}\boldsymbol{\nabla}_{\mathbf{x}}\cdot\mathbf{u}(t,\mathbf{x})\right) = \mathbf{0}\,. \tag{2.10}$$

Both hold for $(t,\mathbf{x}) \in \mathbb{R}\times\tilde{\mathcal{O}}$, while the compressibility of the fluid is introduced as $\kappa(\mathbf{x}) = (\rho_0(\mathbf{x})c^2(\mathbf{x}))^{-1}$. The fluid pressure field p shall satisfy in addition initial conditions of the form:

$$p(0,\mathbf{x}) = p_0(\mathbf{x})\,,\quad \partial_t p(0,\mathbf{x}) = q_0(\mathbf{x})\,,$$

where p_0 and q_0 are regular functions at least in $\mathcal{C}^2(\mathbb{R}^d)$ (the set of functions defined on $\mathbb{R}^d$ and twice differentiable) with compact supports in a sub-domain of $\mathcal{O}$. This regularity is required here by the structure of (2.9). It is however not necessarily required for other approaches presented further on, where the assumptions made on the initial conditions may be less restrictive (for instance p_0 and q_0 in $\mathrm{H}^2(\mathbb{R}^d)$).

For the scalar wave equation (2.9) in an homogeneous medium without any boundary conditions, solutions in the form of plane wave can be sought for in the following form $(t,\,\mathbf{x}) \to f(\mathbf{k}\cdot\mathbf{x} - \omega t)$, where f is any function which is at least twice differentiable. Plugging this ansatz into Eq. (2.9), leads to the dispersion equation below:

$$|\mathbf{k}| = \frac{\omega}{c} \tag{2.11}$$

which defines the type of waves, that can propagate at the frequency ω in the medium characterized by its (constant) sound speed c. The norm $|\mathbf{k}|$ of $\mathbf{k}$ is the so-called wave number.

If however (2.9) is considered with some boundary conditions defined at the edges of $\mathcal{O}$, for example:

$$\mathbf{u}(t,\mathbf{x})\cdot\mathbf{n} = 0\,, \quad (t,\mathbf{x}) \in \mathbb{R}\times\partial\mathcal{O}\,, \tag{2.12}$$

where $\mathbf{n}$ is the outward unit normal to $\partial\mathcal{O}$, its solutions can no longer be sought for in the form of plane waves, and other types of solutions must be considered (see the section 2.2). Note that these boundary conditions correspond to total reflection on the edges of $\mathcal{O}$. As for the boundary conditions used to model the behavior of waves at an interface, we refer to the next section 2.1.3 for a description of the interface conditions in the case of harmonic plane waves, and to the section 2.2.3 for further examples.

2.1.2 Elastic waves

The problem of wave propagation also finds applications in elastodynamics, where the evolution of the displacement field $\mathbf{u}$ is described by the following balance of momentum, assuming small perturbations of the elastic medium with respect to its reference configuration:

$$\rho(\mathbf{x})\partial_t^2\mathbf{u}(t,\mathbf{x}) = \mathbf{Div}_{\mathbf{x}}\boldsymbol{\sigma}(t,\mathbf{x})\,, \quad (t,\mathbf{x}) \in \mathbb{R}\times\tilde{\mathcal{O}}\,. \tag{2.13}$$

The right-hand-side of (2.13) is again the divergence of the stress tensor $\boldsymbol{\sigma}$ as already defined above. For a linear, isotropic homogeneous medium characterized by its Lamé parameters λ and μ, the stress tensor is given in terms of the linearized strain tensor $\boldsymbol{\epsilon}$ by:

$$\boldsymbol{\sigma}(t,\mathbf{x}) = \lambda(\mathbf{x})\,\mathrm{Tr}(\boldsymbol{\epsilon})\mathbf{I} + 2\mu(\mathbf{x})\boldsymbol{\epsilon}\,, \quad \boldsymbol{\epsilon}(t,\mathbf{x}) = \frac{1}{2}\left(\boldsymbol{\nabla}_{\mathbf{x}}\otimes\mathbf{u} + \boldsymbol{\nabla}_{\mathbf{x}}\otimes\mathbf{u}^{\mathsf{T}}\right)\,. \tag{2.14}$$

Here $\mathbf{a}\otimes\mathbf{b}$ stands for the tensor product of two vectors $\mathbf{a}$ and $\mathbf{b}$, defined for any vector $\mathbf{c}$ by $(\mathbf{a}\otimes\mathbf{b}) = (\mathbf{b}\cdot\mathbf{c})\mathbf{a}$. In an homogeneous medium $\mathbf{Div}_{\mathbf{x}}\boldsymbol{\sigma} = (\lambda+\mu)\boldsymbol{\nabla}_{\mathbf{x}}(\boldsymbol{\nabla}_{\mathbf{x}}\cdot\mathbf{u}) + \mu\boldsymbol{\Delta}\mathbf{u}$ and Eq. (2.13) reads as the Navier equation:

$$\rho\partial_t^2\mathbf{u}(t,\mathbf{x}) = (\lambda+\mu)\boldsymbol{\nabla}_{\mathbf{x}}(\boldsymbol{\nabla}_{\mathbf{x}}\cdot\mathbf{u}) + \mu\boldsymbol{\Delta}_{\mathbf{x}}\mathbf{u}\,, \quad (t,\mathbf{x}) \in \mathbb{R}\times\tilde{\mathcal{O}}\,. \tag{2.15}$$

Here $\boldsymbol{\Delta}_{\mathbf{x}}\mathbf{u} = \mathbf{Div}_{\mathbf{x}}(\boldsymbol{\nabla}_{\mathbf{x}}\mathbf{u})$ and $\boldsymbol{\nabla}_{\mathbf{x}}\cdot\mathbf{u} = \mathrm{div}_{\mathbf{x}}\,\mathbf{u}$ stand for the Laplacian and the divergence operator of the displacement field $\mathbf{u}$, respectively. As in the case of acoustic waves, $\mathbf{u}$ satisfies initial conditions of the form:

$$\mathbf{u}(0,\mathbf{x}) = \mathbf{u}_0(\mathbf{x})\,, \quad \partial_t\mathbf{u}(0,\mathbf{x}) = \mathbf{v}_0(\mathbf{x}),$$

where $\mathbf{u}_0$ and $\mathbf{v}_0$ are regular functions at least in $\mathcal{C}^2(\mathbb{R}^d)$ with compact supports in $\mathcal{O}$.

If no boundary conditions are imposed, Eq. (2.15) admits solutions in the form of plane waves:

$$\mathbf{u}(t,\,\mathbf{x}) = \mathbf{d}f(\mathbf{k}\cdot\mathbf{x} - \omega t)\,, \tag{2.16}$$

where f is any function which is twice differentiable, $\mathbf{k}$ denotes the wave vector and $\mathbf{d}$ the direction of vibration, or the wave polarization. Seeking solutions of the Navier equation in this form shows that two types of waves arise in $\mathcal{O}$. Indeed, plugging the above ansatz into Eq. (2.15) yields $\boldsymbol{\Gamma}(\mathbf{k})\mathbf{d} = \omega^2\mathbf{d}$, such that $\mathbf{d}$ and ω^2 arise as the eigenvectors and eigenvalues, respectively, of the so-called Christoffel tensor $\boldsymbol{\Gamma}$ of the medium defined by:

$$\boldsymbol{\Gamma}(\mathbf{k}) = (c_{\mathrm{P}}^2 - c_{\mathrm{S}}^2)\mathbf{k}\otimes\mathbf{k} + c_{\mathrm{S}}^2|\mathbf{k}|^2\mathbf{I}_d\,. \tag{2.17}$$

The solvability condition $\det \mathbf{\Gamma}(\mathbf{k}) = 0$ for this eigen system provides with the dispersion relations:

$$|\mathbf{k}| = \frac{\omega}{c_{\mathrm{P}}} \quad \text{or} \quad |\mathbf{k}| = \frac{\omega}{c_{\mathrm{S}}}\,, \tag{2.18}$$

from which one may recover an expression of the celerities of plane waves in the medium. For P or S waves it is recalled that the latter (denoted by c_{P} and c_{S} respectively) are given by Eq. (2.2). The eigenvectors of the Christoffel tensor form an orthonormal basis of which directions are the polarization directions, with $\mathbf{d}_{\mathrm{P}} \parallel \mathbf{k}$ for the longitudinal wave and $\mathbf{d}_{\mathrm{S}} \perp \mathbf{k}$ for the two shear waves.

If some boundary conditions are imposed, for example the traction-free (Neumann) boundary condition:

$$\boldsymbol{\sigma}(t, \mathbf{x})\mathbf{n} = \mathbf{0}\,, \quad (t, \mathbf{x}) \in \mathbb{R} \times \partial\mathcal{O}\,, \tag{2.19}$$

other types of solutions than plane waves must be sought for, as presented for instance in the section 2.2. As for the interface conditions used between two homogeneous elastic media, we refer to the section 2.2.3 below and to [13] for further developments.

2.1.3 Interface conditions

Wave solutions of Eq. (2.9) or Eq. (2.13) propagate in the domain $\mathcal{O}$ from one sub-domain to the other by being reflected and/or transmitted by the interfaces within $\mathcal{O}$. We introduce in this section the laws, that rule the behavior of waves at that interfaces in terms of reflection/transmission coefficients for the amplitudes of plane waves impinging them. They play a role as important as the propagation equations, which in return describe the behavior of such waves in each sub-domain. The interface conditions may however be difficult to determine depending on the form of the solutions of (2.9) or (2.13), or on the approach chosen to approximate them. In particular, the type of initial conditions that have been imposed play an important role in the derivation of the reflection/transmission coefficients, as this is explained further on (see the section 2.2.3). In some particular cases an expression of these coefficients is easily obtained, as for example for harmonic plane waves impinging on a straight interface between two homogeneous media. We therefore present that case at first. Since it corresponds to a simplified configuration, we consider the elementary case of a single interface within $\mathcal{O}$, denoted by $\mathcal{I}$ and assumed to be plane. We denote by $\mathbf{n}$ the unit normal vector to $\mathcal{I}$, and by $x_{\mathbf{n}} = \mathbf{x} \cdot \mathbf{n}$ the so-called normal component of $\mathbf{x} \in \mathcal{O}$. More generally, for any vector $\mathbf{a} \in \mathbb{R}^d$ one shall introduce its normal component as $a_{\mathbf{n}} = \mathbf{a} \cdot \mathbf{n}$ and its tangent component as $\mathbf{a}' = (\mathbf{I}_d - \mathbf{n} \otimes \mathbf{n})\mathbf{a}$. Also $\hat{\mathbf{a}} = \mathbf{a}/|\mathbf{a}|$ is the associated unit vector provided that $\mathbf{a} \neq \mathbf{0}$. With these notations $\mathcal{I}$ is assumed to be defined as the set of points:

$$\mathcal{I} = \{\mathbf{x} \in \mathcal{O}\,;\, \Sigma(\mathbf{x}) = x_{\mathbf{n}} = 0\}\,.$$

The homogeneous sub-domain of $\mathcal{O}$ defined as the set of points $\{\mathbf{x} \in \mathcal{O}\,;\, x_{\mathbf{n}} > 0\}$ is then denoted by $\mathcal{O}^+$, while the set $\{\mathbf{x} \in \mathcal{O}\,;\, x_{\mathbf{n}} < 0\}$ is denoted by $\mathcal{O}^-$. In the next paragraph, we first consider the case of acoustic plane waves.

Reflection/transmission of acoustic plane waves at a straight interface

We adopt the following notations. The constant values of the celerity and of the density are denoted respectively by c^- and ρ^- in $\mathcal{O}^-$, and by c^+ and ρ^+ in $\mathcal{O}^+$. We also make the assumption that $c^- < c^+$ and that the unit normal $\mathbf{n}$ to the interface points toward $\mathcal{O}^-$. Let $\kappa^\pm = 1/\rho^\pm(c^\pm)^2$. We consider an harmonic plane wave impinging on $\mathcal{I}$ from the slow side $\mathcal{O}^-$ with the following form of the fluid velocity field:

$$\mathbf{u}_{\mathrm{i}}(t,\, \mathbf{x}) = c^- \hat{\mathbf{k}}\, \mathrm{e}^{\mathrm{i}(\omega t - \mathbf{k}\cdot\mathbf{x})}\,, \tag{2.20}$$

where ω denotes the frequency and $\mathbf{k}$ denotes the wave vector. The incidence of $\mathbf{u}(t, \mathbf{x})$ on $\mathcal{I}$ produces a reflected wave $\mathbf{u}_{\mathrm{R}}(t, \mathbf{x})$ of the form (2.20) with an amplitude A_{R} and wave vector $\mathbf{k}_{\mathrm{R}}$, and a transmitted wave $\mathbf{u}_{\mathrm{T}}(t, \mathbf{x})$ of the same form with an amplitude A_{T} and transmitted vector $\mathbf{k}_{\mathrm{T}}$:

$$\mathbf{u}_{\mathrm{R}}(t,\, \mathbf{x}) = A_{\mathrm{R}} \times c^- \hat{\mathbf{k}}_{\mathrm{R}}\, \mathrm{e}^{\mathrm{i}(\omega t - \mathbf{k}_{\mathrm{R}}\cdot\mathbf{x})}\,,$$
$$\mathbf{u}_{\mathrm{T}}(t,\, \mathbf{x}) = A_{\mathrm{T}} \times c^+ \hat{\mathbf{k}}_{\mathrm{T}}\, \mathrm{e}^{\mathrm{i}(\omega t - \mathbf{k}_{\mathrm{T}}\cdot\mathbf{x})}\,.$$

We refer to the Figure 2.1 for an illustration. The incident, reflected and transmitted pressure fields are related to the above velocity fields by the continuity equation (2.8):

$$
\begin{aligned}
p_{\mathrm{i}}(t,\,\mathbf{x}) &= \frac{1}{\kappa^-}\,\mathrm{e}^{\mathrm{i}(\omega t-\mathbf{k}\cdot\mathbf{x})}\,,\\
p_{\mathrm{R}}(t,\,\mathbf{x}) &= \frac{A_{\mathrm{R}}}{\kappa^-}\,\mathrm{e}^{\mathrm{i}(\omega t-\mathbf{k}_{\mathrm{R}}\cdot\mathbf{x})}\,,\\
p_{\mathrm{T}}(t,\,\mathbf{x}) &= \frac{A_{\mathrm{T}}}{\kappa^+}\,\mathrm{e}^{\mathrm{i}(\omega t-\mathbf{k}_{\mathrm{T}}\cdot\mathbf{x})}\,,
\end{aligned}
$$

owing to the dispersion relation (2.11) which yields $\omega = c^-|\mathbf{k}| = c^-|\mathbf{k}_{\mathrm{R}}| = c^+|\mathbf{k}_{\mathrm{T}}|$. The reflected and transmitted amplitudes are derived from the continuity of the pressure and normal velocity fields at the plane interface $\mathcal{I}$, namely $p_{\mathrm{i}}+p_{\mathrm{R}} = p_{\mathrm{T}}$ and $(\mathbf{u}_{\mathrm{i}}+\mathbf{u}_{\mathrm{R}})\cdot\mathbf{n} = \mathbf{u}_{\mathrm{T}}\cdot\mathbf{n}$ whenever $\mathbf{x}\in\mathcal{I}$. These conditions read:

$$
\begin{aligned}
\frac{1}{\rho^-\kappa^-}\left(k_{\mathbf{n}}\,\mathrm{e}^{-\,\mathrm{i}\,\mathbf{k}'\cdot\mathbf{x}'}+A_{\mathrm{R}}k_{\mathrm{R}\mathbf{n}}\,\mathrm{e}^{-\,\mathrm{i}\,\mathbf{k}'_{\mathrm{R}}\cdot\mathbf{x}'}\right) &= \frac{1}{\rho^+\kappa^+}A_{\mathrm{T}}k_{\mathrm{T}\mathbf{n}}\,\mathrm{e}^{-\,\mathrm{i}\,\mathbf{k}'_{\mathrm{T}}\cdot\mathbf{x}'}\,,\\
\frac{1}{\kappa^-}\left(\mathrm{e}^{-\,\mathrm{i}\,\mathbf{k}'\cdot\mathbf{x}'}+A_{\mathrm{R}}\,\mathrm{e}^{-\,\mathrm{i}\,\mathbf{k}'_{\mathrm{R}}\cdot\mathbf{x}'}\right) &= \frac{1}{\kappa^+}A_{\mathrm{T}}\,\mathrm{e}^{-\,\mathrm{i}\,\mathbf{k}'_{\mathrm{T}}\cdot\mathbf{x}'}\,,
\end{aligned}
\tag{2.21}
$$

for all $\mathbf{x}'$ on $\mathcal{I}$. We deduce from the previous relations that $\mathbf{k}_{\mathrm{R}}$ and $\mathbf{k}_{\mathrm{T}}$ are located in the same plane as $\mathbf{k}$ and $\mathbf{n}$, the so-called plane of incidence, and that their tangential components are conserved:

$$
\mathbf{k}' = \mathbf{k}'_{\mathrm{R}} = \mathbf{k}'_{\mathrm{T}}\,. \tag{2.22}
$$

These relations, that describe the reflected and transmitted components at $\mathcal{I}$, correspond to the well-known Snell-Descartes law. It gives the reflected and transmitted wave vector components in terms of the incident one. Indeed the normal components can be deduced using the dispersion equation for $\mathbf{k}_{\mathrm{R}}$ and $\mathbf{k}_{\mathrm{T}}$, and the fact that the incident, reflected and transmitted waves have the same circular frequency ω. They satisfy:

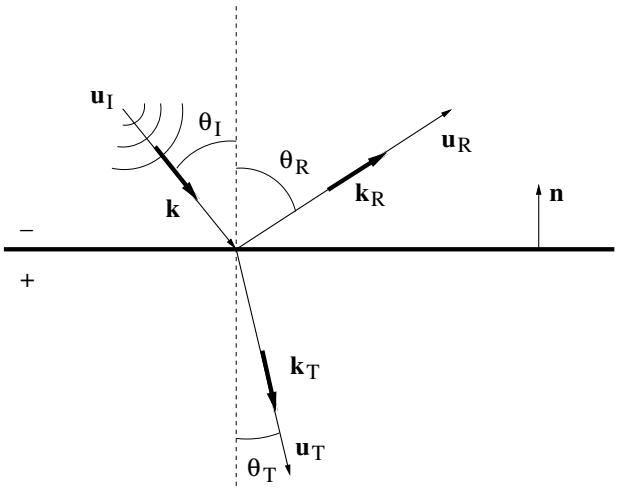

Figure 2.1: Reflected and transmitted vectors $\mathbf{k}_{\mathrm{R}}$ and $\mathbf{k}_{\mathrm{T}}$ at a straight interface with unit normal $\mathbf{n}$, and incident, reflected and transmitted angles θ_{i}, θ_{R} and θ_{T}.

$$
\begin{aligned}
-k_{\mathbf{n}} = k_{\mathbf{n}\mathrm{R}}(\mathbf{k}') &= \sqrt{\left(\frac{\omega}{c^-}\right)^2-|\mathbf{k}'|^2}\,,\\
-k_{\mathbf{n}\mathrm{T}}(\mathbf{k}') &= \sqrt{\left(\frac{\omega}{c^+}\right)^2-|\mathbf{k}'|^2}\,.
\end{aligned}
\tag{2.23}
$$

The last line above for transmission from $\mathcal{O}^-$ to $\mathcal{O}^+$ holds as long as $|\mathbf{k}'| < \omega/c^+$, otherwise the normal component of the transmitted wave vector is either null or purely imaginary. That condition is the expression of the fact that incident waves are transmitted only under critical incidence, $k_{\mathbf{n}} \leq \xi_c(\mathbf{k}')$, where $\xi_c(\mathbf{k}')$ is the so-called critical normal incidence. It is defined for a given tangential component $\mathbf{k}'$ by the following formula:

$$\xi_c(\mathbf{k}') = -|\mathbf{k}'|\sqrt{\left(\frac{c^+}{c^-}\right)^2 - 1}\,. \tag{2.24}$$

If $k_{\mathbf{n}} > \xi_c(\mathbf{k}')$, the wave is totally reflected and there is no transmission. Now the amplitude reflection and transmission coefficients R^- and T^-, respectively, can be derived from (2.21) in terms of the incident and transmitted wave vector components and have the following expressions:

$$\begin{aligned} \mathrm{R}^-(\mathbf{k}) &= A_{\mathrm{R}} = \frac{\rho^+ k_{\mathbf{n}\mathrm{R}}(\mathbf{k}') + \rho^- k_{\mathbf{n}\mathrm{T}}(\mathbf{k}')}{\rho^+ k_{\mathbf{n}\mathrm{R}}(\mathbf{k}') - \rho^- k_{\mathbf{n}\mathrm{T}}(\mathbf{k}')}\,, \\ \mathrm{T}^-(\mathbf{k}) &= A_{\mathrm{T}} = 2\left(\frac{\kappa^+}{\kappa^-}\right)\frac{\rho^+ k_{\mathbf{n}\mathrm{R}}(\mathbf{k}')}{\rho^+ k_{\mathbf{n}\mathrm{R}}(\mathbf{k}') - \rho^- k_{\mathbf{n}\mathrm{T}}(\mathbf{k}')}\,. \end{aligned} \tag{2.25}$$

Note that the corresponding reflection and transmission coefficients from $\mathcal{O}^+$ to $\mathcal{O}^-$, denoted R^+ and T^+ are deduced by interchanging κ^- and κ^+ and ρ^- and ρ^+ in the above formulas. Also one may observe that they depend on $\mathbf{k}$ rather than $\mathbf{k}'$ solely, since $k_{\mathbf{n}\mathrm{R}}$ and $k_{\mathbf{n}\mathrm{T}}$ are implicitly functions of ω, or $|\mathbf{k}|$.

Finally, the power flow reflection/transmission coefficients $\mathcal{R}^-$ and $\mathcal{T}^-$ are defined as the ratio of the normal flux components for the reflected and transmitted acoustic intensities $\boldsymbol{\pi}_{\mathrm{R}} = p_{\mathrm{R}}\overline{\mathbf{u}}_{\mathrm{R}}$ and $\boldsymbol{\pi}_{\mathrm{T}} = p_{\mathrm{T}}\overline{\mathbf{u}}_{\mathrm{T}}$, respectively, where $\overline{\mathbf{a}}$ stands for the complex conjugate of $\mathbf{a}$. They are deduced from $\mathrm{R}^-(\mathbf{k})$ and $\mathrm{T}^-(\mathbf{k})$ by:

$$\begin{aligned} \mathcal{R}^-(\mathbf{k}) &= -\frac{\boldsymbol{\pi}_{\mathrm{R}}\cdot\mathbf{n}}{\boldsymbol{\pi}_{\mathrm{i}}\cdot\mathbf{n}} = (\mathrm{R}^-(\mathbf{k}))^2\,, \\ \mathcal{T}^-(\mathbf{k}) &= \frac{\boldsymbol{\pi}_{\mathrm{T}}\cdot\mathbf{n}}{\boldsymbol{\pi}_{\mathrm{i}}\cdot\mathbf{n}} = 1 - \mathcal{R}^-(\mathbf{k})\,, \end{aligned} \tag{2.26}$$

where the superscript $-$ is used for reflection from the slow medium $\mathcal{O}^-$ to itself and transmission from $\mathcal{O}^-$ to the fast medium $\mathcal{O}^+$. A superscript $+$ shall be used for reflection from $\mathcal{O}^+$ to itself and transmission from $\mathcal{O}^+$ to $\mathcal{O}^-$. These expressions will be used several times from now onwards. In the next section, we present the same laws for elastic waves. In this case an additional phenomenon must be taken into account, which is the conversion of modes or polarizations.

Reflection/transmission of elastic plane waves at a straight interface

In elastodynamics, the description of reflection and transmission phenomena is slightly different from acoustics, since the conversion of modes at $\mathcal{I}$ must be taken into account. This means that an incident wave of any type (P or S) produces reflected and transmitted waves of both types. More precisely, if we use the same conventions as for acoustic waves ($\mathcal{I}$ is a plane interface between $\mathcal{O}^-$ and $\mathcal{O}^+$ oriented by the unit normal vector $\mathbf{n}$), one may observe that the interface phenomena can be decoupled for the P waves and S waves (the SV waves) defining the plane of incidence on the one hand, and for the S waves orthogonal to the plane of incidence (the SH-waves) on the other hand. This allows to treat the case of SH waves separately, and the case of P and SV waves as a two-dimensional problem, which takes place in the plane of incidence. Thus in the following, we restrict ourselves to the case of a P wave impinging from $\mathcal{O}^-$ on $\mathcal{I}$ (see Figure 2.2). However we do not make any assumption concerning the comparison between the relative values of the wave speeds on both sides of the interface, which means that we may have $c_{\mathrm{P}}^- > c_{\mathrm{P}}^+$ or $c_{\mathrm{P}}^+ > c_{\mathrm{P}}^-$ and $c_{\mathrm{S}}^- > c_{\mathrm{S}}^+$ or $c_{\mathrm{S}}^+ > c_{\mathrm{S}}^-$, where c_{S}^-, c_{P}^-, c_{S}^+ and c_{P}^+ stand respectively for the speeds of P waves and SV waves in $\mathcal{O}^-$ and of P waves and SV waves in $\mathcal{O}^+$. For the density, we keep the same notations as for the acoustic case.

We consider an harmonic plane wave impinging on $\mathcal{I}$ from $\mathcal{O}^-$ with the following form:

$$\mathbf{u}_{\mathrm{i}}(t,\mathbf{x}) = \hat{\mathbf{k}}\,\mathrm{e}^{\mathrm{i}(\omega t - \mathbf{k}\cdot\mathbf{x})}\,, \tag{2.27}$$

where ω denotes the frequency and $\mathbf{k}$ denotes the wave vector. Therefore $\mathbf{u}_{\rm i}$ corresponds to an incident P wave. It gives rise to reflected and transmitted waves denoted by:

$$\mathbf{u}_m(t,\mathbf{x}) = A_m \mathbf{d}_m \, \mathrm{e}^{\mathrm{i}(\omega t - \mathbf{k}_m\cdot\mathbf{x})} \,,$$

where the index $m \in \{\mathrm{PR},\mathrm{PT},\mathrm{SR},\mathrm{ST}\}$ denotes respectively, the reflected P wave, the transmitted P wave, the reflected SV wave and the transmitted SV wave. $\mathbf{d}_m$ and A_m denote respectively the direction of polarization and the amplitude of the wave indexed by m. If $\mathbf{k}_m$ denotes the wave vector and $|\mathbf{k}_m|$ denotes the wave number, we first recall that the dispersion equations read $\omega = c_m|\mathbf{k}_m|$. The polarization directions for P waves is the same as the direction of propagation $\hat{\mathbf{k}}_m$, $m = \mathrm{PR},\mathrm{PT}$, while for S waves both directions are orthogonal:

$$\begin{aligned} \mathbf{d}_m &= \hat{\mathbf{k}}_m \,, && m = \mathrm{PR},\mathrm{PT} \,, \\ \mathbf{d}_m &= \frac{(\hat{\mathbf{k}}_m \times \mathbf{n}) \times \hat{\mathbf{k}}_m}{|(\hat{\mathbf{k}}_m \times \mathbf{n}) \times \hat{\mathbf{k}}_m|} \,, && m = \mathrm{SR},\mathrm{ST} \,. \end{aligned}$$

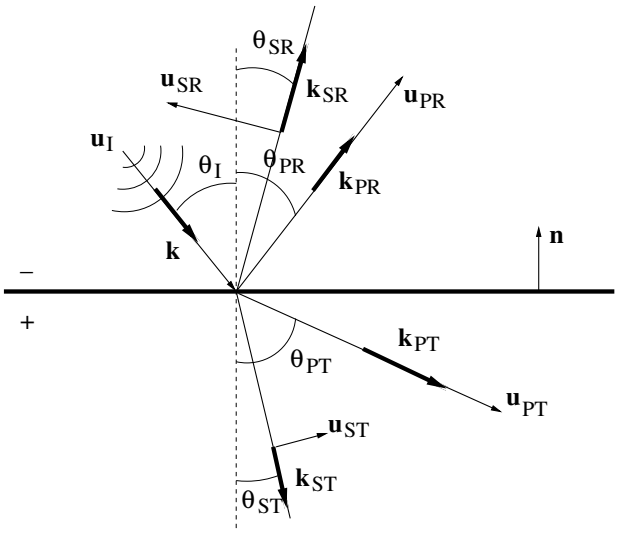

Figure 2.2: Reflection and transmission of a P wave impinging at a straight interface.

We then express the stress vectors $\mathbf{t}_m$ on the interface in terms of the components $\mathbf{u}_m$ for each $m \in \{\mathrm{i},\mathrm{PR},\mathrm{PT},\mathrm{SR},\mathrm{ST}\}$. The strain tensor $\boldsymbol{\epsilon}_m = \boldsymbol{\nabla}_{\mathbf{x}} \otimes_s \mathbf{u}_m$, where $\mathbf{a} \otimes_s \mathbf{b} = \mathrm{sym}(\mathbf{a} \otimes \mathbf{b})$, is given with these notations by:

$$\boldsymbol{\epsilon}_m(t,\mathbf{x}) = -\,\mathrm{i}\, A_m (\mathbf{d}_m \otimes_s \mathbf{k}_m) \, \mathrm{e}^{\mathrm{i}(\omega t - \mathbf{k}_m\cdot\mathbf{x})} \,,$$

so that:

$$\mathrm{div}_{\mathbf{x}}\, \mathbf{u}_m = \mathrm{Tr}\, \boldsymbol{\epsilon}_m = -\,\mathrm{i}\, A_m (\mathbf{d}_m \cdot \mathbf{k}_m) \, \mathrm{e}^{\mathrm{i}(\omega t - \mathbf{k}_m\cdot\mathbf{x})} \,.$$

If $\mu^{\pm}$ and $\lambda^{\pm}$ stand for the Lamé parameters on both sides of the interface, the stress vectors $\mathbf{t}_m$ are deduced by applying Hooke's law (2.14):

$$\begin{aligned} \mathbf{t}_m^{\pm}(t,\mathbf{x}) &= \boldsymbol{\sigma}_m^{\pm}(t,\mathbf{x})\mathbf{n} \\ &= \lambda^{\pm}(\mathrm{div}_{\mathbf{x}}\, \mathbf{u}_m)\mathbf{n} + 2\mu^{\pm}\boldsymbol{\epsilon}_m\mathbf{n} \\ &= -\,\mathrm{i}\, A_m \left[\lambda^{\pm}(\mathbf{d}_m\cdot\mathbf{k}_m)\mathbf{n} + \mu^{\pm}\left((\mathbf{d}_m\cdot\mathbf{n})\mathbf{k}_m + (\mathbf{k}_m\cdot\mathbf{n})\mathbf{d}_m\right)\right] \mathrm{e}^{\mathrm{i}(\omega t - \mathbf{k}_m\cdot\mathbf{x})} \,. \end{aligned} \tag{2.28}$$

We observe here that a convenient choice of $\mathbf{d}_m$ enables to decouple the problem of reflection and transmission for P, SV and SH waves in the incidence plane $(\mathbf{k},\mathbf{n})$ and in its orthogonal direction $\mathbf{k}\times\mathbf{n}$, since $\mathbf{d}_{\rm P} = \hat{\mathbf{k}}_{\rm P}$, $\mathbf{d}_{\rm S}\cdot\hat{\mathbf{k}}_{\rm S} = 0$, and $\mathbf{d}_{\rm SH}\cdot\mathbf{n} = 0$. The reflection and transmission coefficients are then obtained from

the continuity conditions at $\mathcal{I}$ for the displacement and stress vectors. The continuity of displacements reads:

$$\mathbf{u}_{\rm i}(t,\mathbf{x}) + \mathbf{u}_{\rm PR}(t,\mathbf{x}) + \mathbf{u}_{\rm SR}(t,\mathbf{x}) = \mathbf{u}_{\rm PT}(t,\mathbf{x}) + \mathbf{u}_{\rm ST}(t,\mathbf{x})\,, \quad (t,\mathbf{x}) \in \mathbb{R}\times\mathcal{I}\,, \tag{2.29}$$

and the continuity of stress vectors reads:

$$\mathbf{t}^-_{\rm i}(t,\mathbf{x}) + \mathbf{t}^-_{\rm PR}(t,\mathbf{x}) + \mathbf{t}^-_{\rm SR}(t,\mathbf{x}) = \mathbf{t}^+_{\rm PT}(t,\mathbf{x}) + \mathbf{t}^+_{\rm ST}(t,\mathbf{x})\,, \quad (t,\mathbf{x}) \in \mathbb{R}\times\mathcal{I}\,. \tag{2.30}$$

Both conditions imply the equality of each phase term, that is, for all $m \in \{\mathrm{PR},\mathrm{SR},\mathrm{PT},\mathrm{ST}\}$, relations that correspond to Snell-Descartes laws are deduced in the form $\mathbf{k}' = \mathbf{k}'_m$, where it is recalled that $\mathbf{k}'_m = (\mathbf{I}_d - \mathbf{n}\otimes\mathbf{n})\mathbf{k}_m$ denotes the tangential component of $\mathbf{k}_m$. Solving for the above set of equations one obtains expressions for the plane wave reflection/transmission coefficients corresponding to an incident P wave from $\mathcal{O}^-$, defined for $\alpha = \mathrm{P}$ or S by:

$$\mathrm{R}^-_{\mathrm{P}\alpha}(\mathbf{k}) = A_{\alpha\mathrm{R}}\,, \quad \mathrm{T}^-_{\mathrm{P}\alpha}(\mathbf{k}) = A_{\alpha\mathrm{T}}\,. \tag{2.31}$$

The detailed computations that give these coefficients are outlined in the Appendix A to which we refer. Obviously the same kind of computations allows to express the corresponding coefficients for an impinging SV wave. It can also be carried on symmetrically for a P wave and an SV wave crossing $\mathcal{I}$ from $\mathcal{O}^+$ to $\mathcal{O}^-$. Performing these computations leads to sixteen amplitude coefficients the describe the reflection and transmission phenomena at $\mathcal{I}$. We refer to [20] for example for an explicit expression of all these coefficients. We note that, as for the acoustic case, these coefficients depend on $\mathbf{k}'$ solely rather than $\mathbf{k}$.

Finally, the power flow reflection/transmission coefficients $\mathcal{R}^-_{\mathrm{P}\alpha}$ and $\mathcal{T}^-_{\mathrm{P}\alpha}$ are defined as for acoustic waves as the ratio of the normal flux components for the reflected and transmitted elastic intensities, or flux vectors $\boldsymbol{\pi}_m = -\boldsymbol{\sigma}_m\overline{\partial_t \mathbf{u}}_m$ (with the same convention for their orientation as for acoustic intensities):

$$\mathcal{R}^-_{\mathrm{P}\alpha}(\mathbf{k}) = -\frac{\boldsymbol{\pi}_{\alpha\mathrm{R}}\cdot\mathbf{n}}{\boldsymbol{\pi}_{\rm i}\cdot\mathbf{n}}\,, \quad \mathcal{T}^-_{\mathrm{P}\alpha}(\mathbf{k}) = \frac{\boldsymbol{\pi}_{\alpha\mathrm{T}}\cdot\mathbf{n}}{\boldsymbol{\pi}_{\rm i}\cdot\mathbf{n}}\,.$$

The normal fluxes are expressed with the use of the dispersion equations $\omega = c_m|\mathbf{k}_m|$, and derived as:

$$\begin{aligned}
\boldsymbol{\pi}_{\rm i}\cdot\mathbf{n} &= \omega\rho^-\boldsymbol{\Gamma}^-(\hat{\mathbf{k}})\mathbf{k}\cdot\mathbf{n}\,,\\
\boldsymbol{\pi}_{\alpha\mathrm{R}}\cdot\mathbf{n} &= \omega|A_{\alpha\mathrm{R}}|^2\rho^-\boldsymbol{\Gamma}^-(\mathbf{d}_{\alpha\mathrm{R}})\mathbf{k}_{\alpha\mathrm{R}}\cdot\mathbf{n}\,,\\
\boldsymbol{\pi}_{\alpha\mathrm{T}}\cdot\mathbf{n} &= \omega|A_{\alpha\mathrm{T}}|^2\rho^+\boldsymbol{\Gamma}^+(\mathbf{d}_{\alpha\mathrm{T}})\mathbf{k}_{\alpha\mathrm{T}}\cdot\mathbf{n}\,,
\end{aligned}$$

where $\boldsymbol{\Gamma}^\pm(\mathbf{k}) = \big(c_{\rm P}^\pm)^2 - (c_{\rm S}^\pm)^2\big)\,\mathbf{k}\otimes\mathbf{k} + (c_{\rm S}^\pm)^2|\mathbf{k}|^2\mathbf{I}_d$ stands for the Christoffel tensor (2.17) on both sides of the interface. The latter equalities lead to expressions of the power flow reflection/transmission coefficients in terms of the reflection/transmission coefficients for the amplitudes, that are detailed in the Appendix A. These coefficients satisfy in addition the following energy conservation law, obtained by writing the continuity of the overall normal energy flux at $\mathcal{I}$:

$$\mathcal{R}^-_{\mathrm{PP}}(\mathbf{k}) + \mathcal{T}^-_{\mathrm{PP}}(\mathbf{k}) + \mathcal{R}^-_{\mathrm{PS}}(\mathbf{k}) + \mathcal{T}^-_{\mathrm{PS}}(\mathbf{k}) = 1\,, \quad \forall\mathbf{k}\in\mathbb{R}^3\,.$$

As before, equivalent expressions for an SV wave impinging from $\mathcal{O}^-$ or for a P and a SV wave impinging from $\mathcal{O}^+$ can be computed exactly along the same lines as above.

We conclude that interface conditions are well described in the case of harmonic plane waves, that impinge on a straight interface between two homogeneous media. In some other cases it is possible to apply these conditions straightforwardly, as for high-frequency waves in slowly varying media as introduced in the next paragraph. In that case the difference of scales between the wave length and the characteristic dimension of $\mathcal{O}$ allows to approximate the interface conditions by the laws derived above, as seen in the section 2.2.3.

2.1.4 High-frequency setting

The consideration of high-frequency (HF) waves in the bounded domain $\mathcal{O}$ requires a modeling strategy which is *a priori* different from the approaches developed for the analysis of low to mid-frequency wave

propagation phenomena. For the latter, the transient dynamics of a bounded medium can be described by the superposition of its lowest eigenmodes. In the case of high-frequency excitations, the propagation of waves cannot be modeled by taking into account the higher-order eigenmodes as illustrated by the experiments outlined in [26, 62]. One possible way to perform this modeling is to introduce two scales of variations, which are the dimension of the propagation domain L on the one hand, and the characteristic wavelength λ of the waves on the other hand. The term "high-frequency waves" naturally understands that the second scale is small compared to the first one. In this work we also consider that λ is small compared to the typical size of the heterogeneities of the materials, that is the range of variation of the wave celerity $c(\mathbf{x})$. This separation of scales can thus be summarized by introducing the parameter $\varepsilon = \frac{\lambda}{L} \ll 1$ in the wave equations (2.10) or (2.13), through highly oscillatory initial conditions. For example, the latter may take the form:

$$\mathbf{u}(0,\mathbf{x}) = \varepsilon \mathbf{A}(\mathbf{x})\, \mathrm{e}^{\,\mathrm{i}\, S(\mathbf{x})/\varepsilon}\,, \quad \partial_t \mathbf{u}(0,\mathbf{x}) = \mathbf{B}(\mathbf{x})\, \mathrm{e}^{\,\mathrm{i}\, S(\mathbf{x})/\varepsilon}\,. \tag{2.32}$$

where $\mathbf{A}\,(\mathbf{x})$ and $\mathbf{B}(\mathbf{x})$ are smooth compactly supported functions defining the polarization directions and amplitudes, and $S(\mathbf{x})$ denotes a (real-valued) initial phase function. These functions vary on the slow scale. On the contrary, the whole phase terms $S(\mathbf{x})/\varepsilon$ vary on the fast scale. As an example we may consider a highly oscillatory harmonic plane wave with the following expression: $\mathbf{u}(0,\mathbf{x}) = \varepsilon \mathbf{A}(\mathbf{x})\, \mathrm{e}^{\,\mathrm{i}\, \mathbf{x}\cdot\mathbf{k}_0/\varepsilon}$, where $|\mathbf{k}_0|$ is of the same order as L^{-1}. For this kind of problem a direct numerical resolution of (2.10) or (2.13) is no longer an option, since it would require an increasingly finer spatial discretization. It must consequently be replaced by other analytical or numerical techniques, for example by seeking an approximate solution as an expansion in powers of ε. We may mention the Wentzel-Kramer-Brillouin (WKB) method (see for example [13, 18, 59, 65, 67]), or the consideration of the Wigner transform of the solution derivatives and its high-frequency weak limit (see for example [5, 8, 9, 22, 61]). The latter allows to derive the so-called kinetic models of high-frequency wave propagation in heterogeneous media, which are based on a description a the wave energy in the phase space position $\times$ wave vector. In order to take into account the fast scale variations in this approach, a rescaling of the variables $\mathbf{x}' = \frac{\mathbf{x}}{\varepsilon}$ and $t' = \frac{t}{\varepsilon}$ is performed. The wave field $\mathbf{u}(t,\mathbf{x})$ (or its derivatives) is rescaled by the function $\mathbf{u}_\varepsilon(t,\mathbf{x})$ defined by $\mathbf{u}_\varepsilon(t,\mathbf{x}) = \mathbf{u}(\frac{t}{\varepsilon},\frac{\mathbf{x}}{\varepsilon})$, satisfying (2.10) or (2.13) multiplied by $(\mathrm{i}\,\varepsilon)^2$. The problem obtained at the limit when ε goes to 0 has then to be carefully addressed in terms of semi-classical measures, independently from high-frequency numerical techniques. The WKB method and kinetic models are presented in the next two sections.

We must finally mention that the separation of scales introduced above naturally suggests to take into account the diffraction phenomena of the waves at interfaces. They occur in our setting through refraction at tangential and critical incidence (see the earlier works of Buchal & Keller [11] or Lewis *et al.* [41]). Though they will be not considered in this thesis due to the lack of existing results for their analysis in a semi-classical limit, they are briefly introduced in the next section.

2.2 WKB method

The WKB expansion method [13, 18, 59, 65, 67] is a classical way to construct high-frequency approximations of wave systems. It is based on the assumption that the solution of the acoustic wave equation (2.9), or the vector Navier equation (2.15), can be sought for as an expansion in powers of the frequency. This expansion arises here as a power series depending on the small parameter ε, which represents the relative wavelength of the initial conditions. Introducing it in a scalar or vector wave equation leads to a system of coupled equations governing the behavior of the phase (eikonal equation) and of the amplitudes of the different expansion coefficients (transport equations). This system can be solved by different methods, such as ray tracing or wave front methods (see [18]). Ray tracing consists in solving the eikonal and transport equations on curves called rays, where:

(i). the phase is constant and determined by the initial conditions,

(ii). the zeroth-order amplitude is determined as the solution of an ordinary differential equation, in terms of the initial conditions, the phase and the wave speed in the medium.

The behavior of the solution of a wave equation on the rays can be described by several approaches, see [13,18,59]. It can be shown in addition that the boundary conditions are the same as the ones obtained for harmonic plane waves in case of a straight interface between two homogeneous media [13, 59]. We present hereafter the derivation of this method for the wave equation of linearized acoustics, defining the boundary conditions for HF waves, and we mention the applications in the case of elastodynamics. In acoustic or elastic media when the wavelength is small compared to their heterogeneities or propagation distances, the plane-wave form (2.16) is locally valid in the HF range. This observation allows to intuit the form of approximate solutions of wave equations, and the conditions they must satisfy. It constitutes the starting point of the WKB method.

2.2.1 Eikonal and transport equations

We consider here the vector acoustic wave equation (2.10) or elastic wave equation (2.13) in heterogeneous media, supplemented with initial conditions of the WKB type (2.32). We assume that an approximate solution $\mathbf{u}_\varepsilon(t,\mathbf{x}) \simeq \mathbf{u}(t,\mathbf{x})$ can be sought for as an expansion in powers of $\varepsilon \ll 1$, the small length scale characterizing the spatial variations of the initial conditions. That expansion has the following form:

$$\mathbf{u}_\varepsilon(t,\mathbf{x}) = \mathbf{A}_\varepsilon(t,\mathbf{x})\,\mathrm{e}^{\mathrm{i}\,S(t,\mathbf{x})/\varepsilon}\,, \quad \mathbf{A}_\varepsilon(t,\mathbf{x}) = \sum_{p=0}^{\infty} \varepsilon^p \mathbf{A}_p(t,\mathbf{x})\,. \tag{2.33}$$

Here $\mathbf{A}_p$, $p>0$, denote the expansion coefficients of the amplitude and polarization $\mathbf{A}_\varepsilon$ of $\mathbf{u}_\varepsilon$ at order p with respect to ε. They are supposed to be regular functions in $\mathcal{C}^\infty(\mathbb{R}\times\mathbb{R}^d)$. The phase function S is also a regular function in $\mathcal{C}^\infty(\mathbb{R}\times\mathbb{R}^d)$, of which derivatives are all bounded to a certain order $p'>0$. Plugging Eq. (2.33) above into the wave equation (2.10) or the Navier equation (2.13) yields the different equations, that rule the behavior of the zeroth-order term $\mathbf{A}_0$ and the phase S. Let $\mathbf{s}=(t,\mathbf{x})\in\mathbb{R}\times\mathcal{O}$ be the time-space position and $\boldsymbol{\xi}=(\omega,\mathbf{k})\in\mathbb{R}\times\mathbb{R}^d$ be its dual counterpart. The equalities obtained in the expansion in powers of $1/\varepsilon$ for the term in front of $1/\varepsilon^2$ (resp. $1/\varepsilon$) read:

$$\begin{aligned} \mathbf{H}(\mathbf{s},\boldsymbol{\nabla}_\mathbf{s} S)\mathbf{A}_0 &= \mathbf{0}\,,\\ \boldsymbol{\nabla}_\mathbf{s}\cdot\left(\mathbf{A}_0^\mathsf{T}\boldsymbol{\nabla}_{\boldsymbol{\xi}}\mathbf{H}(\mathbf{s},\boldsymbol{\nabla}_\mathbf{s} S)\mathbf{A}_0\right) &= 0\,, \end{aligned} \tag{2.34}$$

where $\mathbf{H}(\mathbf{s},\boldsymbol{\xi})$ is the so-called $d\times d$ dispersion matrix (or the principal symbol) of the acoustic or elastic wave equation, defined by:

$$\mathbf{H}(\mathbf{s},\boldsymbol{\xi}) = \rho(\mathbf{x})\left(\boldsymbol{\Gamma}(\mathbf{x},\mathbf{k}) - \omega^2\mathbf{I}_d\right)\,. \tag{2.35}$$

The Christoffel tensor $\boldsymbol{\Gamma}(\mathbf{x},\mathbf{k})$ for acoustic waves reads $\boldsymbol{\Gamma}(\mathbf{x},\mathbf{k}) = c^2(\mathbf{x})\mathbf{k}\otimes\mathbf{k}$, whereas it is given by Eq. (2.17) for elastic waves in an isotropic medium: $\boldsymbol{\Gamma}(\mathbf{x},\mathbf{k}) = (c_\mathrm{P}^2(\mathbf{x}) - c_\mathrm{S}^2(\mathbf{x}))\mathbf{k}\otimes\mathbf{k} + c_\mathrm{S}^2(\mathbf{x})|\mathbf{k}|^2\mathbf{I}_d$. It is important to observe here that it is no longer assumed that the propagation media are homogeneous. However, the dispersion matrix is independent of the fast scale ε, that is we consider high-frequency wave propagation with $\varepsilon\ll 1$ in a slowly varying "low-frequency" medium. The solvability condition $\det\mathbf{H}(\mathbf{s},\boldsymbol{\nabla}_\mathbf{s} S)=0$ for the first equation obtained above is the eikonal equation for S, and the second one is the transport equation for $\mathbf{A}_0$. We detail them in the next paragraphs for each of the cases considered here.

Eikonal and transport equations for the acoustic wave equation

Let us first consider the case of the acoustic wave equation (2.10). The Christoffel tensor being $\boldsymbol{\Gamma}(\mathbf{x},\mathbf{k}) = c^2(\mathbf{x})\mathbf{k}\otimes\mathbf{k}$, the system (2.34) reads:

$$\begin{aligned} \left[c^2(\mathbf{x})(\boldsymbol{\nabla}_\mathbf{x} S\otimes\boldsymbol{\nabla}_\mathbf{x} S) - (\partial_t S)^2\right]\mathbf{A}_0 &= \mathbf{0}\,,\\ c^2(\mathbf{x})\left(\boldsymbol{\nabla}_\mathbf{x}(\mathbf{A}_0\cdot\boldsymbol{\nabla}_\mathbf{x} S) + (\boldsymbol{\nabla}_\mathbf{x}\cdot\mathbf{A}_0)\boldsymbol{\nabla}_\mathbf{x} S\right) - \left(2(\partial_t\mathbf{A}_0)(\partial_t S) + (\partial_t^2 S)\mathbf{A}_0\right) &= \mathbf{0}\,. \end{aligned}$$

The first line shows that $\boldsymbol{\nabla}_\mathbf{x} S$ and $\mathbf{A}_0$ are colinear. Its projection on $\boldsymbol{\nabla}_\mathbf{x} S$ leads to the following eikonal equations for S:

$$\partial_t S \pm c(\mathbf{x})|\boldsymbol{\nabla}_\mathbf{x} S| = 0\,, \tag{2.36}$$

which describe the general behavior of the phase of the wave in terms of the speed $c(\mathbf{x})$ in the medium. These equations can also be obtained by considering the roots of the determinant of $\mathbf{H}(\mathbf{s}, \boldsymbol{\xi})$, given here by 0 and $\pm c(\mathbf{x})|\mathbf{k}|$. Their resolution is presented in the next subsection. The eikonal equation can be used in one of the two forms (2.36), to rewrite the second line above as a transport equation for $|\mathbf{A}_0|^2$. Indeed, projecting the second line above along $\mathbf{A}_0$ yields:

$$\partial_t |\mathbf{A}_0|^2 \pm \boldsymbol{\nabla}_{\mathbf{x}} \cdot \left(|\mathbf{A}_0|^2 c(\mathbf{x}) \frac{\boldsymbol{\nabla}_{\mathbf{x}} S}{|\boldsymbol{\nabla}_{\mathbf{x}} S|} \right) = 0 \,. \tag{2.37}$$

The signs are in agreement with the conventions used for the eikonal equations. Thus the choice of one of the two eikonal equations above (2.36) leads to a system of two equations, one for the phase S and the other one for the energy $|\mathbf{A}_0|^2$. In the case of the Navier equation, the problem can be put in the same form, as outlined below.

Eikonal and transport equations for the Navier equation

We now turn to the case of the Navier equation (2.13) for a linear, isotropic medium. The Christoffel tensor being $\boldsymbol{\Gamma}(\mathbf{x}, \mathbf{k}) = (c_{\mathrm{P}}^2(\mathbf{x}) - c_{\mathrm{S}}^2(\mathbf{x}))\mathbf{k} \otimes \mathbf{k} + c_{\mathrm{S}}^2(\mathbf{x})|\mathbf{k}|^2 \mathbf{I}_d$, the system (2.34) reads:

$$\begin{aligned} \left[(c_{\mathrm{P}}^2(\mathbf{x}) - c_{\mathrm{S}}^2(\mathbf{x}))(\boldsymbol{\nabla}_{\mathbf{x}} S \otimes \boldsymbol{\nabla}_{\mathbf{x}} S) + c_{\mathrm{S}}^2(\mathbf{x}) |\boldsymbol{\nabla}_{\mathbf{x}} S|^2 - (\partial_t S)^2 \right] \mathbf{A}_0 = \mathbf{0} \,, \\ (c_{\mathrm{P}}^2(\mathbf{x}) - c_{\mathrm{S}}^2(\mathbf{x})) \left(\boldsymbol{\nabla}_{\mathbf{x}} (\mathbf{A}_0 \cdot \boldsymbol{\nabla}_{\mathbf{x}} S) + (\boldsymbol{\nabla}_{\mathbf{x}} \cdot \mathbf{A}_0) \boldsymbol{\nabla}_{\mathbf{x}} S \right) + c_{\mathrm{S}}^2(\mathbf{x}) \left(\boldsymbol{\nabla}_{\mathbf{x}} \mathbf{A}_0 (\boldsymbol{\nabla}_{\mathbf{x}} S) + (\Delta_{\mathbf{x}} S) \mathbf{A}_0 \right) \\ - \left(2(\partial_t \mathbf{A}_0)(\partial_t S) + (\partial_t^2 S) \mathbf{A}_0 \right) = \mathbf{0} \,. \end{aligned}$$

The analysis of these equations leads to eikonal equations for the P and S waves. More precisely, it can be shown that S must satisfy equations of the form (2.36), where $c(\mathbf{x})$ is either replaced by $c_{\mathrm{P}}(\mathbf{x})$ for P waves, or $c_{\mathrm{S}}(\mathbf{x})$ for S waves, c_{P} and c_{S} being given by (2.2). For P waves $\mathbf{A}_0$ has the direction of $\boldsymbol{\nabla}_{\mathbf{x}} S$, while for S waves $\mathbf{A}_0$ is orthogonal to $\boldsymbol{\nabla}_{\mathbf{x}} S$, say $\mathbf{A}_0 = B\mathbf{e}_1 + C\mathbf{e}_2$ such that $\mathbf{e}_1$, $\mathbf{e}_2$ are vectors forming an orthogonal basis with $\boldsymbol{\nabla}_{\mathbf{x}} S$. As previously, the eikonal equations can also be obtained by considering the roots of the determinant of $\mathbf{H}(\mathbf{s}, \boldsymbol{\xi})$, equal here to 0, $\pm c_{\mathrm{S}}(\mathbf{x})|\mathbf{k}|$, and $\pm c_{\mathrm{P}}(\mathbf{x})|\mathbf{k}|$. One may show in addition (see [13]) that $|\mathbf{A}_0|^2$, B^2 and C^2 satisfy transport equations of the form (2.37). In the case of P waves, $\mathbf{A}_0(\mathbf{s})$ satisfies the same transport equation (2.37) as the one obtained for acoustic waves, replacing c by c_{P}. In the case of S waves, it can be shown that for a judicious choice of the vectors $\mathbf{e}_1$ and $\mathbf{e}_2$ along the rays, the amplitudes $\mathcal{E}(\mathbf{s}) = B(\mathbf{s})^2$ and $\mathcal{E}(\mathbf{s}) = C(\mathbf{s})^2$ satisfy the following transport equations:

$$\partial_t \mathcal{E} \pm \boldsymbol{\nabla}_{\mathbf{x}} \cdot \left(\mathcal{E}\, c_{\mathrm{S}}(\mathbf{x}) \frac{\boldsymbol{\nabla}_{\mathbf{x}} S}{|\boldsymbol{\nabla}_{\mathbf{x}} S|} \right) = 0 \,,$$

where the convention for the signs is the same as for the eikonal equations. This shows that the system of equations obtained fro elastic waves can be put in a convenient form which is formally the same as the one obtained for acoustic waves. We thus focus in the next subsection on solving the equations (2.36) and (2.37) by the method of ray tracing. The phase $S(t, \mathbf{x})$ and the amplitude $|\mathbf{A}_0(t, \mathbf{x})|$ are determined for all $t > 0$ on curves called rays, in terms of the initial conditions for $t = 0$.

2.2.2 Ray equations

Ray equations are deduced from the method of characteristics. This method can be applied to different types of partial differential equations (PDE) of first order, which includes the eikonal and transport equations obtained by the WKB approach. It consists in solving these equations on curves of $\mathbb{R}^d$, along which the solution of the concerned PDE is conserved. The problem is then to determine these curves in the whole space, in terms of the initial conditions of the original problem. We present hereafter the resolution method for both the eikonal and transport equations, which can be solved on the same curves.

Eikonal equation

We recall that the eikonal equations (2.36) read in terms of the roots $\mathcal{H}^{\pm}(\mathbf{x}, \mathbf{k}) = \pm c(\mathbf{x})|\mathbf{k}|$ of the dispersion matrix of an acoustic medium as:

$$\partial_t S(t, \mathbf{x}) + \mathcal{H}(\mathbf{x}, \boldsymbol{\nabla}_{\mathbf{x}} S) = 0 \,, \tag{2.38}$$

where $\mathcal{H}(\mathbf{x},\mathbf{k}) \in \{\mathcal{H}^{\pm}(\mathbf{x},\,\mathbf{k})\}$ is called a Hamiltonian. We consider the possible solution S of (2.38) defined on $\mathbb{R}^+ \times \mathcal{O}$, and the corresponding system of bi-characteristics equations $t \to (\mathbf{x}(t),\,\mathbf{k}(t))$ with the initial conditions below:

$$\left\{\begin{array}{ll} \dfrac{\mathrm{d}\mathbf{x}}{\mathrm{d}t} = \boldsymbol{\nabla}_{\mathbf{k}}\mathcal{H}(\mathbf{x}(t),\mathbf{k}(t))\,, & \mathbf{x}(0) = \mathbf{x}_0\,, \\ \dfrac{\mathrm{d}\mathbf{k}}{\mathrm{d}t} = -\boldsymbol{\nabla}_{\mathbf{x}}\mathcal{H}(\mathbf{x}(t),\mathbf{k}(t))\,, & \mathbf{k}(0) = \boldsymbol{\nabla}_{\mathbf{x}}S(0,\,\mathbf{x}_0)\,, \end{array}\right. \tag{2.39}$$

where $\mathbf{x}_0 \in \mathcal{O}$. The problem (2.38) with the same initial conditions as above can then be solved by determining the solutions of the system (2.39). Indeed from the differentiation of the eikonal equation with respect to the space variable one obtains the variations of $\boldsymbol{\nabla}_{\mathbf{x}}S(t,\mathbf{x}(t))$ as follows:

$$\frac{\mathrm{d}}{\mathrm{d}t}\boldsymbol{\nabla}_{\mathbf{x}}S\left(t,\mathbf{x}(t)\right) = D^2_{\mathbf{x}}S\left[\frac{\mathrm{d}\mathbf{x}}{\mathrm{d}t} - \boldsymbol{\nabla}_{\mathbf{k}}\mathcal{H}\left(\mathbf{x}(t),\boldsymbol{\nabla}_{\mathbf{x}}S(t,\mathbf{x}(t))\right)\right] - \boldsymbol{\nabla}_{\mathbf{x}}\mathcal{H}\left(\mathbf{x}(t),\boldsymbol{\nabla}_{\mathbf{x}}S(t,\mathbf{x}(t))\right)\,, \tag{2.40}$$

where $D^2_{\mathbf{x}}S = \boldsymbol{\nabla}_{\mathbf{x}} \otimes \boldsymbol{\nabla}_{\mathbf{x}}S$ denotes the Hessian of S. This shows that, if $t \mapsto \mathbf{x}(t)$ is chosen so as to cancel the expression in the brackets of (2.40), the couple $(\mathbf{x}(t), \boldsymbol{\nabla}_{\mathbf{x}}S(t,\mathbf{x}(t)))$ is a system of bi-characteristics of the form (2.39). Moreover, the uniqueness of the solution of (2.39) for given initial conditions insures that for all $t \geq 0$, $\mathbf{k}(t) = \boldsymbol{\nabla}_{\mathbf{x}}S(t,\mathbf{x}(t))$. The study of the system (2.40) is thus interesting for the description of the solution of the eikonal equation.

Along the curve $t \mapsto \mathbf{x}(t)$ the phase is constant, as it can easily be verified by differentiating $t \to S(t,\mathbf{x}(t))$, so that $S(t,\mathbf{x})$ is entirely defined by the initial conditions $S(0,\mathbf{x})$. The determination of $S(t,\mathbf{x})$ reduces then to the computation of the curves $t \mapsto \mathbf{x}(t)$, called rays. These rays, of which derivatives have a norm equal to the speed $c(\mathbf{x})$ in $\mathcal{O}$, define the wave front at a given time t. The vector $\mathbf{k}$, which gives the direction of the rays is also called the slowness vector. The rays are determined by noticing that an equation for the evolution of $\mathbf{x}(t)$ deduced from (2.39) reads:

$$\frac{\mathrm{d}^2\mathbf{x}}{\mathrm{d}t^2} = -c(\mathbf{x})\boldsymbol{\nabla}_{\mathbf{x}}c(\mathbf{x})\,.$$

It enables to obtain the rays in most cases, formally or numerically. Once the latter are known, the phase S is determined along them with the help of the initial conditions, which reads:

$$S(t,\mathbf{x}(t)) = S(0,\mathbf{x}_0)\,, \quad \forall t \geq 0\,, \quad \mathbf{x}_0 \in \mathcal{O}\,. \tag{2.41}$$

We give an illustration of the integration of the system (2.39) in case of a constant speed $c(\mathbf{x}) = c_0$, and initial conditions $\mathbf{k} = \mathbf{k}(0) = \boldsymbol{\nabla}_{\mathbf{x}}S(0,\,\mathbf{x}_0)$. The second line of (2.39) shows that the curves are straight lines, given by the following relation:

$$\mathbf{x}(t) = \mathbf{x}_0 + c_0\hat{\mathbf{k}}_0 t\,.$$

$\mathbf{x}_0$ denotes the initial position, $\hat{\mathbf{k}}_0 = \mathbf{k}_0/|\mathbf{k}_0|$, and S is deduced for all $\mathbf{x} \in \{\mathbf{x}_0 + c_0\hat{\mathbf{k}}_0 t\}$ by the initial condition for S on the characteristics:

$$S(t,\mathbf{x}) = S(0,\mathbf{x} - c_0\hat{\mathbf{k}}_0 t)\,.$$

This example is essential and will be used several times in our numerical applications.

Transport equation

Let us now consider the case of the transport equation (2.37), that we recall here using the notation $\mathcal{E} = |\mathbf{A}_0|^2$ (or $\mathcal{E} = B^2$ or $\mathcal{E} = C^2$):

$$\partial_t\mathcal{E} + \boldsymbol{\nabla}_{\mathbf{x}} \cdot \left(\mathcal{E}\, c(\mathbf{x})\frac{\boldsymbol{\nabla}_{\mathbf{x}}S}{|\boldsymbol{\nabla}_{\mathbf{x}}S|}\right) = 0\,. \tag{2.42}$$

We suppose that $S(t,\,\mathbf{x})$ is known for $\mathbf{s}=(t,\mathbf{x})\in\mathbb{R}^+\times\mathcal{O}$. Adopting the same approach as for the eikonal equation, we consider the system of ray equations corresponding to (2.42):

$$\left\{\begin{array}{ll} \dfrac{\mathrm{d}\mathbf{x}}{\mathrm{d}t} & = \boldsymbol{\nabla}_{\mathbf{k}}\mathcal{H} \qquad\qquad\qquad\qquad\qquad\qquad\qquad\qquad\qquad\qquad\quad \mathbf{x}(0)=\mathbf{x}_0\,,\\ \dfrac{\mathrm{d}\mathbf{k}}{\mathrm{d}t} & = -\begin{pmatrix}\mathrm{div}_{\mathbf{x}}(\nabla_{\mathbf{k}}\mathcal{H}) & \partial_t\,\mathrm{div}_{\mathbf{x}}(\nabla_{\mathbf{k}}\mathcal{H})\\ \mathbf{0} & D^{\mathrm{T}}(\nabla_{\mathbf{k}}\mathcal{H})+\mathrm{div}_{\mathbf{x}}(\nabla_{\mathbf{k}}\mathcal{H})\mathbf{I}\end{pmatrix}\mathbf{k}(t)-z(t)\boldsymbol{\nabla}_{\mathbf{s}}\,\mathrm{div}_{\mathbf{x}}(\nabla_{\mathbf{k}}\mathcal{H})\,, \quad \mathbf{k}(0)=\boldsymbol{\nabla}_{\mathbf{s}}\mathcal{E}(\mathbf{s}_0)\,,\\ \dfrac{\mathrm{d}z}{\mathrm{d}t} & = \begin{pmatrix}1\\ \nabla_{\mathbf{k}}\mathcal{H}\end{pmatrix}\cdot\mathbf{k}(t)\,, \qquad\qquad\qquad\qquad\qquad\qquad\qquad\qquad\qquad\quad z(0)=\mathcal{E}(\mathbf{s}_0)\,.\end{array}\right. \tag{2.43}$$

As for the eikonal equation, the integration of the transport equation can be done by solving the system (2.43), and integral curves can be determined on which $(\mathbf{x}(t),\boldsymbol{\nabla}_{\mathbf{s}}\mathcal{E}(\mathbf{s}(t)),\mathcal{E}(\mathbf{s}(t)))$ is a solution. One may verify that if $(\mathbf{x}(t),\mathbf{k}(t),z(t))$ is a solution, the quantity $(\mathbf{k}\cdot(1,\boldsymbol{\nabla}_{\mathbf{x}}\mathcal{H})^{\mathsf{T}}+z\Delta_{\mathbf{x}}\mathcal{H})$ remains constant on these rays. But the definition of the first line of (2.43) shows that the rays defined for the latter system are the rays of the eikonal equation (the Cauchy theorem for ordinary differential equations applies), which are already known once the phase has been determined. The last line of the above system thus describes the evolution of z along these rays. In the particular case of the solution associated to the transport equation (2.42), this equation reads:

$$\frac{\mathrm{d}z}{\mathrm{d}t}=-z(t)\Delta_{\mathbf{x}}\mathcal{H}\,,$$

where $z(t)=\mathcal{E}(\mathbf{s}(t))$, which is an ordinary transport equation along the curve $t\mapsto\mathbf{s}(t)$. It may be solved explicitly in terms of $\Delta_{\mathbf{x}}\mathcal{H}$. We refer to [18], where an expression of $\mathcal{E}$ is given in the particular case of the Helmholtz equation (harmonic plane wave). The corresponding computation under the assumption that $\Delta_{\mathbf{x}}\mathcal{H}\neq 0$, leads to:

$$\mathcal{E}(\mathbf{s}(t))=\frac{h_0}{\mathrm{q}(t)}\,,\quad \frac{1}{\mathrm{q}}\frac{\mathrm{dq}}{\mathrm{d}t}=\Delta_{\mathbf{x}}\mathcal{H}\,, \tag{2.44}$$

where h_0 is defined by the initial conditions, and $\mathrm{q}(t)$ expresses the amplification of an infinitesimal area transported by the rays called the geometrical spreading. It depends on the speed $c(\mathbf{x})$ in the medium, and on the variations of S. Therefore the variations of $\mathcal{E}$ on a ray are obtained by the above formula, using the initial conditions $h_0=-\mathcal{E}(\mathbf{s}_0)\Delta_{\mathbf{x}}\mathcal{H}$ to determine that constant.

We illustrate these results once again in the case of a constant speed $c(\mathbf{x})=c_0$ in $\mathcal{O}$. In that case, the geometrical spreading is equal to 1, so that $\mathcal{E}$ is constant along the rays. As the latter are straight lines, as already seen for the phase function S, $\mathcal{E}$ is defined on the rays by the initial conditions:

$$\mathcal{E}(\mathbf{s})=\mathcal{E}(0,\mathbf{x}-c_0\hat{\mathbf{k}}_0t)\,,\quad \hat{\mathbf{k}}_0=\frac{\boldsymbol{\nabla}_{\mathbf{x}}S(\mathbf{s}_0)}{|\boldsymbol{\nabla}_{\mathbf{x}}S(\mathbf{s}_0)|}\,.$$

Approximate solution of the wave equation

Gathering the results of the previous paragraphs gives an expression of the zeroth-order term of the WKB expansion of the high-frequency solution of the wave equation on the rays. It reads:

$$\mathbf{u}_\varepsilon(t,\mathbf{x}(t))\simeq\mathbf{A}_0(t,\,\mathbf{x}(t))\,\mathrm{e}^{\,\mathrm{i}\,S(t,\mathbf{x}(t))/\varepsilon}\,,$$

where $|\mathbf{A}_0(t,\,\mathbf{x}(t))|=\sqrt{\mathcal{E}(\mathbf{s}(t))}$, and S and $\mathcal{E}$ are determined respectively by (2.41) and (2.44) along the rays.

2.2.3 Boundary conditions and diffraction phenomena

We consider a wave that hits a plane interface, adopting the notations of the section 2.1.3. We recall that the unit normal vector to $\mathcal{I}$ is denoted by $\mathbf{n}$, moreover we suppose that an equation for $\mathcal{I}$ is $x_{\mathbf{n}}\mathbf{x}\cdot\mathbf{n}=0$. We consider a wave of the form (2.33), where S denotes the phase, and $\mathbf{A}$ its amplitude. We denote by ω the quantity $\omega=2\pi c/(L\varepsilon)$, where L stands for a characteristic dimension of $\mathcal{O}$, and suppose that the incident wave impinges on $\mathcal{I}$ from $\mathcal{O}^-$.

A first example is given by the configuration analyzed in the section 2.1.3 of a piecewise homogeneous medium characterized by the constant speeds c^- and c^+ such that $c^- < c^+$, for example. We consider the approximation $\mathbf{u}_\varepsilon$ of the form (2.33), with an amplitude independent of ε:

$$\mathbf{u}_\varepsilon(t,\mathbf{x}) = \mathbf{A}_0(t,\mathbf{x})\,\mathrm{e}^{\,\mathrm{i}\,S(t,\mathbf{x})/\varepsilon}\,. \tag{2.45}$$

It corresponds to the zeroth-order WKB approximation of the exact solution of our wave propagation problem. In that case, we have seen that the phase can be expressed in terms of the initial condition S_0 as $S(t,\mathbf{x}) = S_0(\mathbf{x} - c\hat{\mathbf{k}}t)$, where $\mathbf{k} = \boldsymbol{\nabla}_\mathbf{x} S$ depends only on $\mathbf{x}$. In addition, the rays are straight lines defined by the initial conditions. We thus observe that the behavior of the solution at $\mathcal{I}$ depends directly on S_0. The constant values of the speed on each side of $\mathcal{I}$ imply that the ray equation for $\mathbf{k}(t) = \boldsymbol{\nabla}_\mathbf{x} S(t,\mathbf{x})$ has along $\mathcal{I}$ the form:

$$\frac{\mathrm{d}\mathbf{k}'}{\mathrm{d}t} = \mathbf{0}\,.$$

Here we have projected the first line of (2.40) on the tangential direction to the interface. This implies that if $\mathbf{k}$ denotes the incident wave vector, and $\mathbf{k}_\mathrm{R}$ and $\mathbf{k}_\mathrm{T}$ denote the reflected and the transmitted ones, then their tangential components are conserved:

$$\mathbf{k}' = \mathbf{k}'_\mathrm{R} = \mathbf{k}'_\mathrm{T}\,,$$

in agreement with the relations (2.22) of the section 2.1.3 for two homogeneous sub-domains $\mathcal{O}^-$ and $\mathcal{O}^+$.

A particular case of the above example is defined by a phase and an amplitude $S(t,\mathbf{x})/\varepsilon = \omega(S'(\mathbf{x}) - t)$ and $\mathbf{A}_\varepsilon(t,\mathbf{x}) = \mathbf{A}'_\omega(\mathbf{x})$ that do not depend on time, so that $\mathbf{u}_\varepsilon$ has the following form:

$$\mathbf{u}_\varepsilon(t,\mathbf{x}) = \mathbf{A}'_\omega(\mathbf{x})\,\mathrm{e}^{\,\mathrm{i}\,\omega(S'(\mathbf{x})-t)}\,, \quad \omega \equiv \varepsilon^{-1}\,. \tag{2.46}$$

It corresponds to a time-harmonic WKB expansion. If one considers the scalar wave equation (2.9), one obtains an equivalent form for the pressure field p_ε as:

$$\omega^2 p_\varepsilon(t,\mathbf{x}) + \frac{1}{\kappa(\mathbf{x})}\boldsymbol{\nabla}_\mathbf{x}\cdot\left(\frac{1}{\rho_0(\mathbf{x})}p_\varepsilon(t,\,\mathbf{x})\right) = 0\,, \quad t>0\,, \quad \mathbf{x}\in\mathcal{O}\,. \tag{2.47}$$

Owing to the relation between the velocity and the pressure fields $\rho_0(\mathbf{x})\partial_t\mathbf{u}_\varepsilon = -\boldsymbol{\nabla}_\mathbf{x} p_\varepsilon$, we seek an approximation $\mathbf{u}_\varepsilon$ with an amplitude $\mathbf{A}'_\omega$ with a zeroth-order term of the form $\mathbf{A}'_0 = A'_0\boldsymbol{\nabla}_\mathbf{x} S'$. The eikonal and transport equations obtained in that case read [13, Eqs. (2.4.6) and (2.4.11)]:

$$\begin{aligned} |\boldsymbol{\nabla}_\mathbf{x} S'| &= \frac{1}{c(\mathbf{x})}\,,\\ 2\boldsymbol{\nabla}_\mathbf{x} S'\cdot\boldsymbol{\nabla}_\mathbf{x}\left(\sqrt{\rho_0}A'_0\right) + \sqrt{\rho_0}A'_0\nabla\cdot\left(|\boldsymbol{\nabla}_\mathbf{x} S'|^2\boldsymbol{\nabla}_\mathbf{x} S'\right) &= 0\,, \end{aligned} \tag{2.48}$$

respectively. This system of equations can then be solved by the method of ray tracing, as Eq. (2.36) and Eq. (2.37). We refer to [18] for a complete description of that issue. Note, that the directions of propagation are given by $\boldsymbol{\nabla}_\mathbf{x} S'$ and are independent of t, as well as the difference of phase between two points. Thus the shape of the rays and the directions of propagation, which are constant in time, only depend on $S'(\mathbf{x})$. We now derive the boundary conditions for an acoustic wave with the latter form.

Boundary conditions for acoustic waves

As done in the case of harmonic plane waves, it is also possible to give a precise form of the interface conditions for approximations of HF waves of the form (2.33). Before we give the relations between the incident, reflected and transmitted amplitudes in the particular case of acoustic waves, we consider the case where the approximation $\mathbf{u}_\varepsilon$ of the velocity field is given by (2.46) to the zeroth order. The associated pressure field p_ε is then derived from the continuity equation (2.8) by $\partial_t p_\varepsilon = -\frac{1}{\kappa}\,\mathrm{div}_\mathbf{x}\,\mathbf{u}_\varepsilon$. We then observe that at an interface $\mathcal{I}$, the continuity conditions for the pressure and the normal component of the velocity at $\mathcal{I}$ read as:

$$\begin{aligned} \frac{1}{\kappa^-}\left(\mathrm{div}_\mathbf{x}\left(\mathbf{A}'_0(\mathbf{x})\,\mathrm{e}^{\,\mathrm{i}\,\omega S'(\mathbf{x})}\right) + \mathrm{R}^-\,\mathrm{div}_\mathbf{x}\left(\mathbf{A}'_{0\mathrm{R}}(\mathbf{x})\,\mathrm{e}^{\,\mathrm{i}\,\omega S'_\mathrm{R}(\mathbf{x})}\right)\right) &= \frac{1}{\kappa^+}\mathrm{T}^-\,\mathrm{div}_\mathbf{x}\left(\mathbf{A}'_{0\mathrm{T}}(\mathbf{x})\,\mathrm{e}^{\,\mathrm{i}\,\omega S'_\mathrm{T}(\mathbf{x})}\right)\,,\\ (\mathbf{A}'_0\cdot\mathbf{n})\,\mathrm{e}^{\,\mathrm{i}\,\omega S'(\mathbf{x})} + \mathrm{R}^-(\mathbf{A}'_{0\mathrm{R}}\cdot\mathbf{n})\,\mathrm{e}^{\,\mathrm{i}\,\omega S'_\mathrm{R}(\mathbf{x})} &= \mathrm{T}^-(\mathbf{A}'_{0\mathrm{T}}\cdot\mathbf{n})\,\mathrm{e}^{\,\mathrm{i}\,\omega S'_\mathrm{T}(\mathbf{x})}\,, \end{aligned} \tag{2.49}$$

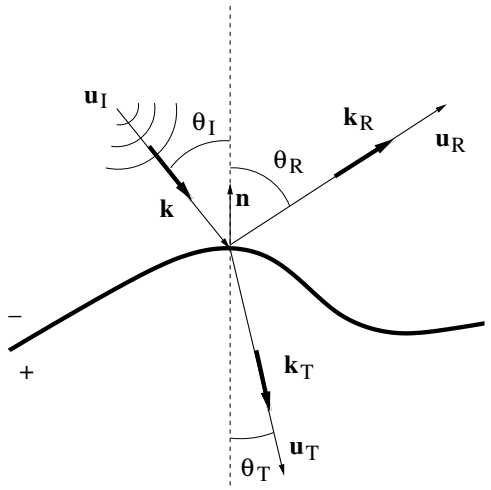

Figure 2.3: Reflected and transmitted vectors $\mathbf{k}_\mathrm{R}$ and $\mathbf{k}_\mathrm{T}$ at a point $\mathbf{x}$ of a curved interface with local unit normal $\mathbf{n}(\mathbf{x})$.

with:

$$\mathrm{div}_\mathbf{x}\left(\mathbf{A}'_0(\mathbf{x})\,\mathrm{e}^{\mathrm{i}\,\omega S'(\mathbf{x})}\right) = (\mathrm{i}\,\omega\mathbf{A}'_0(\mathbf{x})\cdot\boldsymbol{\nabla}_\mathbf{x}S' + \mathrm{div}_\mathbf{x}\,\mathbf{A}'_0(\mathbf{x}))\,\mathrm{e}^{\mathrm{i}\,\omega S'(\mathbf{x})}\,,$$

and equivalent results for the reflected and transmitted components. The differentiation terms in the above line are of two types, the terms of the form $\boldsymbol{\nabla}_\mathbf{x}\cdot\mathbf{A}'_0$ and the terms of the form $\mathrm{i}\,\omega\mathbf{A}'_0(\mathbf{x})\cdot\boldsymbol{\nabla}_\mathbf{x}S'$. where the functions $\mathbf{A}'_0(\mathbf{x})$ and $S'(\mathbf{x})$ are supposed to variate slowly in space. We may suppose for instance that $\boldsymbol{\nabla}_\mathbf{x}S'$ and $\boldsymbol{\nabla}_\mathbf{x}\cdot\mathbf{A}'_0$ are bounded on $\mathcal{O}$, satisfying $\sup_{\mathbf{x}\in\mathcal{O}}|\boldsymbol{\nabla}_\mathbf{x}S'|\ll\omega$, $\sup_{\mathbf{x}\in\mathcal{O}}|\boldsymbol{\nabla}_\mathbf{x}\cdot\mathbf{A}'_0|\ll\omega$. Note that these assumptions imply that in a region about $\mathbf{x}$ the wave front is regular. In the case of an acoustic wave, the amplitude is equal to $\kappa^{-1}(\mathbf{x})$, such that the regularity of $\mathbf{A}'_0$ actually depends on the regularity of κ (or ρ and c). At last in the high-frequency regime we can assume that $\omega\gg\frac{c}{L}$. We can then neglect the first terms in comparison to the second ones, and rewrite the above relations as for harmonic plane waves, with $\mathbf{k}=\boldsymbol{\nabla}_\mathbf{x}S'$, $\mathbf{k}_\mathrm{R}=\boldsymbol{\nabla}_\mathbf{x}S'_\mathrm{R}$ and $\mathbf{k}_\mathrm{T}=\boldsymbol{\nabla}_\mathbf{x}S'_\mathrm{T}$. It can be deduced from (2.49), that along $\mathcal{I}$, the phase terms are equal, since the reflected and transmitted amplitude should not depend on the frequency ω (see [13] where these arguments are detailed precisely). We obtain that the expressions of the amplitude and power flow reflection/transmission coefficients are the same as the ones obtained for an harmonic plane wave, see the Eq. (2.25). The relations between the normal components remains also valid at $\mathcal{I}$. Note that in the case of constant speeds on each side of $\mathcal{I}$, it can be shown that these results still hold for waves of the form (2.33). This is proved with the help of the mathematical tools presented in the following section and under certain assumptions on the initial conditions (we refer to [52], see also [6] for details about the propagation of high-frequency signals).

In the case of a curved interface $\mathcal{I}$, we use the same notations as for a straight one to denote the incident, reflected and transmitted wave vector. If the wave is time-harmonic with the form (2.46), we make the same assumptions concerning the variations of $\mathbf{A}'_0$, S' and their first derivatives in the neighborhood of $\mathcal{I}$. To this we add that at each point $\mathbf{x}$ on $\mathcal{I}$, the principal radii of curvature $R(\mathbf{x})$ and $R'(\mathbf{x})$ satisfy:

$$\varepsilon L\ll R(\mathbf{x})\,,\ \ \varepsilon L\ll R'(\mathbf{x})\,,$$

so that $\mathcal{I}$ may be approximated locally by its tangent plane at $\mathbf{x}$. In the following, we denote by $\mathbf{x}$ the point of incidence on $\mathcal{I}$, and in order to adapt the reflection/transmission laws, we introduce a local unit normal vector $\mathbf{n}(\mathbf{x})$ and the local tangent vector $\mathbf{k}'(\mathbf{x})$ located in the plane of incidence defined by $\mathbf{n}(\mathbf{x})$ and $\boldsymbol{\nabla}_\mathbf{x}S'(\mathbf{x})$, such that $\mathbf{k}'(\mathbf{x})=(\mathbf{I}_d-\mathbf{n}(\mathbf{x})\otimes\mathbf{n}(\mathbf{x}))\boldsymbol{\nabla}_\mathbf{x}S'$. The intersection between $\mathcal{I}$ and the plane of incidence is then approximated by its tangent line $(\mathbf{x},\hat{\mathbf{k}}'(\mathbf{x}))$, such that the description of reflection and transmission reduces to the case of a straight line; see the figure 2.3. This allows us to write the expressions of the normal and tangential components of the reflected and transmitted wave vectors in the

local basis defined above in the same manner as for a straight interface, section 2.1.3. They are obtained by using the formula (2.23) with the vectors $\mathbf{k} = \boldsymbol{\nabla}_{\mathbf{x}} S'$, $\mathbf{k}_{\mathrm{R}} = \boldsymbol{\nabla}_{\mathbf{x}} S'_{\mathrm{R}}$ and $\mathbf{k}_{\mathrm{T}} = \boldsymbol{\nabla}_{\mathbf{x}} S'_{\mathrm{T}}$ given in the local basis $(\mathbf{n}, \hat{\mathbf{k}}')$ by $\mathbf{k}'(\mathbf{x}) = \mathbf{k}'_{\mathrm{R}}(\mathbf{x}) = \mathbf{k}'_{\mathrm{T}}(\mathbf{x})$ and:

$$\begin{aligned} -\mathbf{k}(\mathbf{x}) \cdot \mathbf{n}(\mathbf{x}) = \mathbf{k}_{\mathrm{R}}(\mathbf{x}) \cdot \mathbf{n}(\mathbf{x}) = \sqrt{|\mathbf{k}(\mathbf{x})|^2 - |\mathbf{k}'(\mathbf{x})|^2}\,, \\ -\mathbf{k}_{\mathrm{T}}(\mathbf{x}) \cdot \mathbf{n}(\mathbf{x}) = \sqrt{\left(\frac{c^-}{c^+}|\mathbf{k}(\mathbf{x})|\right)^2 - |\mathbf{k}'(\mathbf{x})|^2}\,, \end{aligned} \tag{2.50}$$

with the same condition on $|\mathbf{k}'(\mathbf{x})|$ as in the case of a straight interface for the criticality of the incidence. The critical normal incidence is now defined pointwise on the interface. Likewise, the amplitude reflection and transmission coefficients are computed by $\mathrm{R}^-(\mathbf{k}'(\mathbf{x}))$, $\mathrm{T}^-(\mathbf{k}'(\mathbf{x}))$ for reflection/transmission from $\mathcal{O}^-$ to $\mathcal{O}^+$, and $\mathrm{R}^+(\mathbf{k}'(\mathbf{x}))$, $\mathrm{T}^+(\mathbf{k}'(\mathbf{x}))$ for reflection/transmission from $\mathcal{O}^+$ to $\mathcal{O}^-$, with similar expressions for $\mathrm{R}^\pm$ and $\mathrm{T}^\pm$ as those given by Eq. (2.25). The corresponding power flow reflection/transmission coefficients take the form $\mathcal{R}^\pm(\mathbf{k}'(\mathbf{x}))$ and $\mathcal{T}^\pm(\mathbf{k}'(\mathbf{x}))$, where $\mathcal{R}^\pm$ and $\mathcal{T}^\pm$ are given by Eq. (2.26) for a straight interface. We assume that these results still hold for more general WKB approximations of the form (2.33), in agreement with the rigorous results derived by *e.g.* Akian *et al.* [4, 5] or Miller [52].

Boundary conditions for elastic waves

It can be shown that the same kind of computations and approximations can be carried on in the case of elastic P and S waves, and that the boundary conditions for harmonic plane waves between two homogeneous media can be adapted to HF waves of the form (2.46). We refer to [13] for details of the derivation.

Diffraction phenomena and modelization of caustics

Some phenomena occuring at an interface, typically the outbreak of surface waves, cannot be taken into account by the WKB method, which is restricted by the regularity of the amplitude and phase functions. Indeed the eikonal equation leads to a single-valued solution for the phase, such that intersections of rays cannot be represented by this approach. The resolution of the eikonal equation requires further developments to obtain multi-valued solutions (see [18] in case of a time-harmonic approach), which may otherwise be derived directly by other models. We mention here the case of refraction of waves at an interface for tangential or critical incidence (see the definition (2.24)), which generate surface waves along that interface. We also mention the case of caustics, which are envelop curves for the rays that arise in heterogeneous or piecewise homogeneous media. There the rays may stack and the amplitude/polarization function $\mathbf{A}_\varepsilon$ of the waves (2.33) gets unbounded. In these cases higher order terms in this expansion of $\mathbf{u}_\varepsilon$ in powers of the wave number, or other types of expansions must be used to explain the behavior of $\mathbf{A}_\varepsilon$ in the vicinity of the caustics. Most of the authors choose a time-harmonic approach, and seek solutions of the Helmholtz equation for large ω of the form (2.46).

We recall that in the resolution of the eikonal and transport equation by the ray method, the rays are defined as the projection in the physical space-time domain of the bicharacteristic curves of the wave equation. The rays impinging at an interface $\mathcal{I}$ with a tangent incidence or with a critical incidence (at the limit of total reflection on the fast side) generate a surface wave. It propagates along the surface and diffracts energy on its path in the media on both sides of $\mathcal{I}$. This phenomenon can be characterized by a diffraction coefficient, which defines the part of the incident wave that is converted to a surface wave, and an attenuation coefficient, which accounts for the leakage of the surface wave along its path into bulk waves propagating away from the interface. Diffraction is described by several authors, *e.g.* Keller [35], Ludwig *et al.* [41, 47] or Mukhina [53], among others.

More generally rays in heterogeneous or piecewise homogeneous media may form envelopes called caustics. The latter are curves to which the rays are tangent, and where the amplitude of the approximate WKB solution has a singularity. The formation of caustics is a recurrent phenomenon that arises even for the simplest structures, see [13]. It may be observed for example in optics, at the reflection of a plane wave on curved mirrors, or at the refraction of rays at an interface. An illustration of caustic is given on the figure 2.4. We also refer to [47] and [11] for more details about caustics. We present here an example

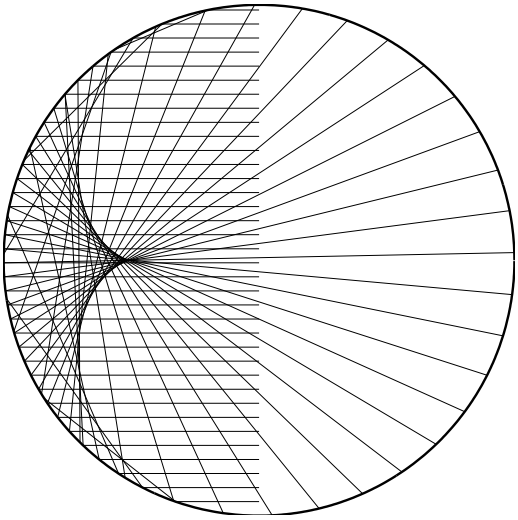

Figure 2.4: Example of a caustic curve (inner curve of the dark zone) obtained by reflection of a set of rays impinging on a circle.

of caustics in two dimensions introduced by Buchal & Keller in this last reference.

We suppose that the rays that define the caustic curve are given by their distance to the origin denoted by $\delta(\phi)$, where ϕ is the angle of the ray (straight line) with the horizontal x-axis in polar coordinates (r, ϕ) (see the figure 2.5). Along the rays the solution p_ε of the Helmholtz equation (2.47) satisfies the Sommerfeld radiation condition at infinity:

$$\lim_{r\to\infty}\left[\frac{1}{2\,\mathrm{i}\,k}\,\mathrm{e}^{-\,\mathrm{i}\,kr}\,\sqrt{r}\left(\mathrm{i}\,kp_\varepsilon-\frac{\partial p_\varepsilon}{\partial r}\right)\right]=\mathrm{I}(\phi)\,\mathrm{e}^{\,\mathrm{i}\,k\mathrm{a}(\phi)}\,, \tag{2.51}$$

where k denotes the wave number, $\mathrm{I}(\phi)$ is a 2π-periodic function, and $\mathrm{a}(\phi)$ is a continuous function. They define the amplitude and the phase, respectively, of the radiated field. Then it can be shown that the

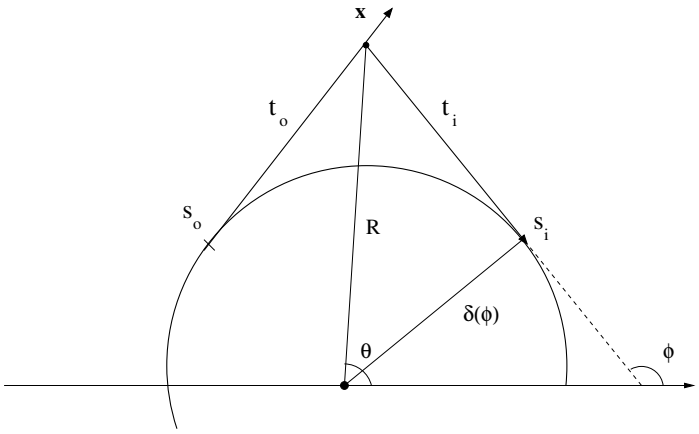

Figure 2.5: Superposition of rays at a smooth caustic and comparison between polar and caustic coordinates.

caustics can be defined properly by the Sommerfeld condition; we refer to the Appendix B for a detailed description of their shape. Let us seek a solution to the ray equations in the caustic coordinates (s, t), where s defines the arclength along the caustic curve, and t defines the arclength along the rays (see

also the figure C.1 in the Appendix C). As we will see, a classical WKB expansion in powers of the wave number is no longer valid at caustics, since the amplitude of the solution becomes infinite there. This means that another type of expansion than (2.33) must be used. Moreover, as rays impinge on the caustic and go out of it, we suppose that at each point $\mathbf{x}$ the solution p_ε is double-valued and reads as a sum of two terms, corresponding to an incoming and an outgoing ray; we refer to the Figure 2.5 for an illustration, where the arclength t_i stands for the incoming ray, and the arclength t_o stands for the outgoing one. Let us first note that the resolution of the eikonal equation of the Helmholtz equation (2.47) shows that for each ray, the phase S is an arclength parametrization since $\boldsymbol{\nabla}_{\mathbf{x}} S \cdot \frac{\mathrm{d}\mathbf{x}}{\mathrm{d}t} = 1$. This means that on a ray the arclength is related to the travel time t, so that if that arclength is denoted by s on the caustics, the following relation holds:

$$S = s + t\,. \tag{2.52}$$

A solution to the Helmholtz equation is thus sought in the form:

$$p_\varepsilon \simeq \mathrm{e}^{\mathrm{i}\,k(s_\mathrm{i}+t_\mathrm{i})}\,\mathrm{v_i}(s_\mathrm{i},t_\mathrm{i}) + \mathrm{e}^{\mathrm{i}\,k(s_\mathrm{o}+t_\mathrm{o})}\,\mathrm{v_o}(s_\mathrm{o},t_\mathrm{o})\,,\quad k \equiv \varepsilon^{-1}\,, \tag{2.53}$$

where the subscript i stands for the impinging ray, and the subscript o stands for the outgoing one. The amplitudes $\mathrm{v_i}$ and $\mathrm{v_o}$ are determined by solving the transport equation of (2.48) along the rays in terms of the arclength (see [18] or [41, Sect. 1]). To determine an expression of the amplitudes at a point $\mathbf{x}$ in a neighborhood of the caustic, the transport equation of (2.48) is written in the caustic coordinates (t,s):

$$\left[\mathrm{i}\,k\left(2\partial_t + \frac{1}{t}\right) + \frac{1}{t}\partial_t(t\partial_t) + \frac{\mathrm{a}}{t}(\partial_s - \partial_t)\frac{\mathrm{a}}{t}(\partial_s - \partial_t)\right]\mathrm{v} = 0\,, \tag{2.54}$$

where a denotes the radius of curvature at the point (t,s) on the caustics. If the incoming and outgoing amplitudes are expanded in powers of the wave number $k \equiv \varepsilon^{-1}$ in order to take into account the high-frequency ($\varepsilon \to 0$) feature of the solution:

$$p_\varepsilon \simeq \mathrm{e}^{\mathrm{i}\,k(s_\mathrm{i}+t_\mathrm{i})}\,\mathrm{h_i}(k)\sum_{n=0}^{\infty} k^{-n}\mathrm{v}_{\mathrm{i},n}(s_\mathrm{i},t_\mathrm{i}) + \mathrm{e}^{\mathrm{i}\,k(s_\mathrm{o}+t_\mathrm{o})}\,\mathrm{h_o}(k)\sum_{n=0}^{\infty} k^{-n}\mathrm{v}_{\mathrm{o},n}(s_\mathrm{o},t_\mathrm{o})\,, \tag{2.55}$$

a system of equations between $\mathrm{v}_{\mathrm{i},n}$ and $\mathrm{v}_{\mathrm{i},n-1}$ (respectively $\mathrm{v}_{\mathrm{o},n}$ and $\mathrm{v}_{\mathrm{o},n-1}$) is obtained from (2.54). The computation is detailed in the Appendix C (see (C.3)). This analysis leads to the following expression for the zeroth-order amplitude of the incoming ray:

$$\mathrm{v}_{\mathrm{i},0}(s_\mathrm{i},t_\mathrm{i}) = \mathrm{G_i}(s_\mathrm{i})\sqrt{-t_\mathrm{i}}\,. \tag{2.56}$$

The use of the Sommerfeld condition at infinity allows to find $\mathrm{h_i}(k) = 1$ and $\mathrm{G_i}(s_\mathrm{i}) = \mathrm{I}(\theta(s_\mathrm{i}))$. The same form of the solution is obtained for the outgoing ray replacing $-t_\mathrm{i}$ by t_o, but the constants are determined further (see the appendix C.2 for the details of the computations). One may observe here that $\mathrm{v}_{\mathrm{i},0}$ (resp. $\mathrm{v}_{\mathrm{o},0}$) is unbounded in a neighborhood of the caustics, so that this solution is no longer valid, in this neighborhood. For this reason, and in order to account for the high-frequency feature of the solution of Eq. (2.54), we make the assumption that the relevant variable along a ray in this neighborhood is the rescaled arclength $\tau = k^\alpha t$, $\alpha > 0$. In this boundary layer, p_ε satisfies a modified transport equation, which with the help of the variable τ reads :

$$\begin{aligned}\mathrm{i}\,k^{\alpha+1}\left(2\partial_\tau p_\varepsilon + \frac{p_\varepsilon}{\tau}\right) + k^{4\alpha}\frac{\mathrm{a}}{\tau}\left(\frac{\mathrm{a}}{\tau}\partial_\tau p_\varepsilon\right) - k^{3\alpha}\frac{\mathrm{a}}{\tau}\left[\partial_\tau\left(\frac{\mathrm{a}}{\tau}\partial_s p_\varepsilon\right) + \partial_s\left(\frac{\mathrm{a}}{\tau}\partial_\tau p_\varepsilon\right)\right]\\ + k^{2\alpha}\frac{1}{\tau}\left[\partial_\tau(\tau\partial_\tau p_\varepsilon) + \mathrm{a}\partial_s\left(\frac{\mathrm{a}}{\tau}\partial_s p_\varepsilon\right)\right] = 0\,.\end{aligned} \tag{2.57}$$

Typically α is chosen to be equal to $\frac{1}{3}$. We seek a solution of this equation as a second expansion of p_ε in the form:

$$p_\varepsilon \simeq \mathrm{e}^{\mathrm{i}\,k(s_\mathrm{i}+t_\mathrm{i})}\,\mathrm{H_i}(k)\sum_{n=0}^{\infty} k^{-n/3}\mathrm{V}_{\mathrm{i},n}(s_\mathrm{i},t_\mathrm{i}) + \mathrm{e}^{\mathrm{i}\,k(s_\mathrm{o}+t_\mathrm{o})}\,\mathrm{H_o}(k)\sum_{n=0}^{\infty} k^{-n/3}\mathrm{V}_{\mathrm{o},n}(s_\mathrm{o},t_\mathrm{o})\,. \tag{2.58}$$

Plugging the above expansion into Eq. (2.57), we may determine the form of $\mathrm{V}_{\mathrm{i},0}$ (resp. $\mathrm{V}_{\mathrm{o},0}$) as a linear combination of the functions $\mathcal{L}(s,\,t)$ and $\mathcal{M}(s,\,t)$ defined by (C.10). The comparison of the two expansions Eq. (2.55) and Eq. (2.58) outside and inside the boundary layer, enables to determine the zeroth-order term for the incoming ray:

$$\mathrm{V}_{\mathrm{i},0}(s_{\mathrm{i}},t_{\mathrm{i}}) = \mathrm{I}\left(\theta(s_{\mathrm{i}})\right)\sqrt{\pi}2^{\frac{5}{6}}\mathrm{a}^{-\frac{1}{3}}\exp\left(\frac{\mathrm{i}\,\pi}{12}-\frac{\mathrm{i}\,\tau_{\mathrm{i}}^3}{3\mathrm{a}^2}\right)\mathrm{Ai}\left(-\frac{\mathrm{a}}{2}^{\frac{2}{3}}\frac{\tau_{\mathrm{i}}^2}{\mathrm{a}^2}\,\mathrm{e}^{-\frac{2\,\mathrm{i}\,\pi}{3}}\right),$$

where $\mathrm{Ai}(x)$ stands for the Airy function, and $\tau_{\mathrm{i}} = k^{\frac{1}{3}}t_{\mathrm{i}}$ denotes the rescaled arclength along the incoming ray. The same kind of considerations for the outgoing ray leads to the following form of the solution:

$$\mathrm{v}_{\mathrm{o},0}(s_{\mathrm{o}},t_{\mathrm{o}}) = \frac{\mathrm{G}_{\mathrm{o}}(s_{\mathrm{o}})}{\sqrt{t_{\mathrm{o}}}},$$

and:

$$\mathrm{V}_{\mathrm{o},0}(s_{\mathrm{o}},t_{\mathrm{o}}) = \mathrm{G}_{\mathrm{o}}(s_{\mathrm{o}})\sqrt{\pi}2^{\frac{5}{6}}\mathrm{a}^{-\frac{1}{3}}\exp\left(-\frac{\mathrm{i}\,\pi}{12}-\frac{\mathrm{i}\,\tau_{\mathrm{o}}^3}{3\mathrm{a}^2}\right)\mathrm{Ai}\left(-\frac{\mathrm{a}}{2}^{\frac{2}{3}}\frac{\tau_{\mathrm{o}}^2}{\mathrm{a}^2}\,\mathrm{e}^{\frac{2\,\mathrm{i}\,\pi}{3}}\right),$$

where $\tau_{\mathrm{o}} = k^{\frac{1}{3}}t_{\mathrm{o}}$ denotes the arclength along the outgoing ray. The constant G_{o} and h_{o} are determined for the outgoing ray by a comparison of the boundary layer expansion with an expansion inside of the caustic. The gathered results can finally be written as follows. Outside of an area bounded by the curve C_1, p_ε admits the following expansion:

$$p_\varepsilon \simeq \frac{\mathrm{I}\left(\theta(s_{\mathrm{i}})\right)}{\sqrt{-t_{\mathrm{i}}}}\,\mathrm{e}^{\mathrm{i}\,k(s_{\mathrm{i}}+t_{\mathrm{i}})} + \frac{\mathrm{I}\left(\theta(s_{\mathrm{o}})\right)}{\sqrt{t_{\mathrm{o}}}}\,\mathrm{e}^{\mathrm{i}\left(k(s_{\mathrm{o}}+t_{\mathrm{o}})-\frac{\pi}{2}\right)}, \tag{2.59}$$

while inside of the boundary layer defined between the curves C_1 and C_2 an approximation for p_ε is given by:

$$p_\varepsilon \simeq k^{\frac{1}{6}}\mathrm{I}\left(\theta(\underline{s})\right)\sqrt{\pi}2^{-\frac{5}{6}}\mathrm{a}^{-\frac{1}{3}}\,\mathrm{e}^{\mathrm{i}(k\underline{s}-\frac{\pi}{4})}\,\mathrm{Ai}\left(-\left(\frac{2}{\mathrm{a}}\right)^{\frac{1}{3}}\bar{\mathrm{n}}\right). \tag{2.60}$$

In the above $\bar{\mathrm{n}} = \mathrm{n}k^{\frac{2}{3}}$ is proportional to the arclength n along the normal at the caustic, $\underline{s}$ denotes the value of s at the point where the normal meets the caustic, and the curves C_1 and C_2 are defined by the relations $t = k^{-\frac{1}{6}}$ and $\mathrm{n} = -k^{-\frac{1}{3}}$, respectively; see the figure 2.6 bellow for an illustration. The details of the computations are given in the Appendix C, to which we refer. The solution finally presents an expansion for p_ε valid outside of the boundary layer, and inside the boundary layer, and we obtain an expression of p_ε valid in a neighborhood around the caustic. We observe that the width of the boundary layer depends on the wave number, and goes to zero as ω goes to infinity.

Other types of models for caustics, which rely on an asymptotic expansion of the solution of the Helmholtz equation in powers of k can be used. We refer particularly to [41], where a model of caustics that describes precisely the propagation of surface waves (creeping waves) on the caustic surface is proposed. It gives an expression of the diffraction and attenuation coefficients in terms of the geometry of the caustic, and of the physical parameters of the medium. As previously, it allows to define a solution to the Helmholtz equation valid in a neighborhood around the caustic. This is useful in order to take the phenomena of diffraction into account for a wave, that propagates in an heterogeneous medium. We refer for instance to [31], where an expression of these diffraction coefficients is derived, to define numerical schemes, that take diffraction into account. The above developments show how to define a solution to the Helmholtz equation, in a neighborhood around the caustic. This is not possible with a simple WKB expansion. In that case a two rays expansion is necessary to describe the phenomenon, near the caustic. This implies the definition of a boundary layer around the caustic, where different expansions of the solution p_ε are given, and of which width depends on the frequency (or wave number). It shows, that it is possible to compute particular solutions to the Helmholtz equation inside (2.60) and outside (2.59) the boundary layer, as presented here above. This type of model allows a description of the caustic, in terms of diffraction and attenuation coefficients, and it allows to some extent to take the diffraction phenomena into account in a proper way.

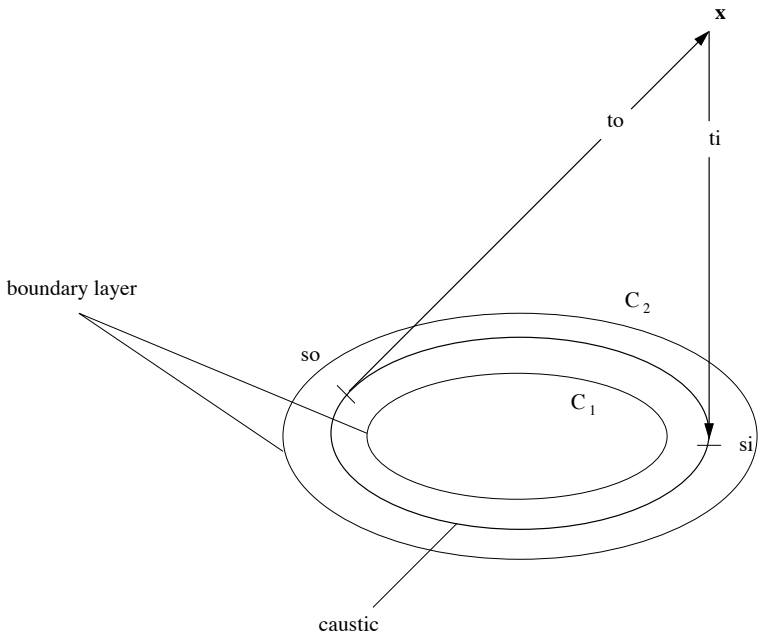

Figure 2.6: Caustic coordinates and boundary layer

2.2.4 Limitations of the WKB approach

The WKB method presents some drawbacks despite its relative simplicity and well-established developments. The first one is related to the non-linearity of the eikonal equation, which implies that the method fails at caustics, or more generally in regions where the rays intersect. In these regions, the solution must be modeled by multi-valued phase functions. In addition the amplitude of the approximate WKB solution becomes infinite there. This phenomenon cannot be modeled by the expansion (2.33), but requires other expansions in powers of ε, which correct this unboundedness of $\mathbf{A}_\varepsilon$. An other drawback is that the WKB method requires a rather strong regularity of the initial conditions. The phase and the amplitude functions must be smooth enough, not only to ensure convergence of the WKB form to the solution (see [65, Prop. 2.1]), but also to obtain a satisfactory behavior of the HF solutions at interfaces. This behavior can be well approximated by the one of plane waves, under the assumption that the initial conditions for $\mathbf{u}_\varepsilon$ are regular enough. Indeed, the interface conditions strongly depend on the WKB initial conditions of the problem, which restricts the range of applications that can be addressed by this method. To overcome the shortcomings of the WKB method, another approach that proposes larger possibilities concerning the modeling of the high-frequency problem considered here is presented in the next section.

2.3 Kinetic modeling of high-frequency waves

We present here an alternative approach to the WKB method for the characterization of high-frequency solutions of Eq. (2.10) or Eq. (2.13), which relies on the use of the so-called Wigner transform of two wave fields. The latter is defined as the spatial (or space-time) Fourier Transform of field-field correlations. It satisfies a kinetic evolution equation in the corresponding phase space. This tool is naturally best suited for high-frequency initial conditions and high-frequency wave propagation phenomena. It is useful in many micro-local analysis problems as illustrated in *e.g.* [9] and references therein. The consideration of a Wigner transform for wave fields is intrinsically based on an energetic approach of wave propagation phenomena. It allows to subsequently derive the asymptotics of the waves energy density at the limit when the relative wavelength ε goes to 0. Contrary to the WKB method, it is able to account for the superposition of different phases. Also its definition (see Eq. (2.61)) as a distribution on the phase space $\mathbb{R}^d \times \mathbb{R}^d$ requires less regularity of the initial conditions of the wave system. It is therefore adapted

to the consideration of multi-valued solutions for the phase, and even unbounded solutions of evolution equations. In this respect tricky phenomena such as the superposition of phases or the concentration at caustics may be addressed by this approach; see [65].

In this section we first give the definition and some properties of the Wigner transform of a function, and then turn to an illustration of its interest in the computation of semi-classical limits of families of highly oscillatory (high frequency) initial conditions of the form of Eq. (2.32). We then present its interest for the analysis of first-order hyperbolic systems (wave equations or linear conservation laws for example) for this type of data. In particular, we show how it can be used to determine the phase-space energy densities associated to the problems (2.10) or (2.13) with initial data (2.32) in the high-frequency limit $\varepsilon \to 0$. These observables are obtained by solving transport equations for the components of the so-called Wigner measure, the high-frequency limit of the Wigner transform of wave fields, in its decomposition on the basis formed by the eigenvectors of the Christoffel tensor. We conclude with the form of the transport equations thus obtained, and the boundary conditions satisfied by the Wigner measure.

2.3.1 Wigner transform of a function

Let $\mathbf{f}$ be a bounded function of $L^2(\mathbb{R}^d, \mathbb{C}^m)$, with $m \in \mathbb{N}^*$ and $\mathbb{C}$ standing for the set of complex numbers. The Wigner transform of $\mathbf{f}$ is defined by the following formula:

$$\mathbf{W}[\mathbf{f}](\mathbf{x}, \mathbf{k}) = \frac{1}{(2\pi)^d} \int_{\mathbb{R}^d} \mathrm{e}^{\mathrm{i}\,\mathbf{k}\cdot\mathbf{y}}\, \mathbf{f}\left(\mathbf{x} - \frac{\mathbf{y}}{2}\right) \otimes \overline{\mathbf{f}\left(\mathbf{x} + \frac{\mathbf{y}}{2}\right)} \mathrm{d}\mathbf{y}\,, \tag{2.61}$$

where $\bar{\mathbf{f}}$ stands for the complex conjugate of $\mathbf{f}$. $\mathbf{Wf}$ takes its values in $\mathcal{S}'(\mathbb{R}^d \times \mathbb{R}^d)^{m\times m}$ in the general case, where $\mathcal{S}$ denotes the Schwartz space of $\mathcal{C}^\infty$ functions which are rapidly decreasing at infinity as well as all their derivatives, and $\mathcal{S}'$ is the set of tempered distributions. The Wigner transform is Hermitian, which is verified by considering its complex conjugate of it, and it can also be checked that:

$$\int_{\mathbb{R}^d} \mathbf{W}[\mathbf{f}](\mathbf{x}, \mathbf{k}) \mathrm{d}\mathbf{k} = \mathbf{f}(\mathbf{x}) \otimes \overline{\mathbf{f}(\mathbf{x})}\,, \quad \forall \mathbf{x} \in \mathbb{R}^d\,. \tag{2.62}$$

As an example, when $m = 1$, we obtain that $\mathbf{W}[\mathbf{f}]$ is real valued, and that the above zeroth-order momentum is equal to $|\mathbf{f}(\mathbf{x})|^2$. As it also allows to recover higher order momenta of the functions $\mathbf{f}$, $\mathbf{W}[\mathbf{f}](\mathbf{x}, \mathbf{k})$ may be interpreted as a local energy density in phase space $\mathbb{R}^d \times \mathbb{R}^d \ni (\mathbf{x}, \mathbf{k})$. These properties make it an interesting tool in the asymptotic analysis of the solutions of linear partial differential equations; see the earlier works of Tartar [71], Gérard *et al.* [22], Papanicolaou *et al.* [61].

More generally, one may define the Wigner transform of a family of uniformly bounded functions $(\mathbf{f}_\varepsilon)_\varepsilon$ of $L^2(\mathbb{R}^d, \mathbb{C}^m)$ of which scale or variation is of order ε, where ε is a small parameter. One may observe first that the definition (2.61) is no longer adapted to the scale of variations of these functions. This can be verified for the highly oscillatory (WKB) plane wave $\mathbf{f}_\varepsilon(\mathbf{x}) = \mathrm{e}^{\mathrm{i}\,\mathbf{k}_0\cdot\mathbf{x}/\varepsilon}$ for instance, of which classical Wigner transform is given by $\mathbf{W}[\mathbf{f}](\mathbf{x}, \mathbf{k}) = \delta\left(\mathbf{k} - \frac{\mathbf{k}_0}{\varepsilon}\right)$, where δ denotes the Dirac distribution. We thus observe that its limit as ε goes to 0 cannot be defined. It is thus necessary to introduce a rescaled definition of the Wigner transform, which takes the form:

$$\mathbf{W}_\varepsilon[\mathbf{f}_\varepsilon](\mathbf{x}, \mathbf{k}) = \varepsilon^{-d}\mathbf{W}[\mathbf{f}_\varepsilon]\left(\mathbf{x}, \frac{\mathbf{k}}{\varepsilon}\right) = \frac{1}{(2\pi)^d} \int_{\mathbb{R}^d} \mathrm{e}^{\mathrm{i}\,\mathbf{k}\cdot\mathbf{y}}\, \mathbf{f}_\varepsilon\left(\mathbf{x} - \frac{\varepsilon\mathbf{y}}{2}\right) \otimes \overline{\mathbf{f}_\varepsilon\left(\mathbf{x} + \frac{\varepsilon\mathbf{y}}{2}\right)} \mathrm{d}\mathbf{y}\,. \tag{2.63}$$

On the contrary, the second definition (2.63) of the rescaled Wigner transform leads to $\mathbf{W}_\varepsilon[\mathbf{f}_\varepsilon](\mathbf{x}, \mathbf{k}) = \delta(\mathbf{k} - \mathbf{k}_0)$ for the WKB plane wave. This shows that it is adapted to the study of the variations of order 1 of functions oscillating at a scale $\varepsilon \ll 1$. This rescaling, which is similar to the one performed on high-frequency initial data (see the section 2.1.4), is a way to take into account the fast variations at the small scale. Thus the Wigner transform of a family of functions $(\mathbf{f}_\varepsilon)_\varepsilon$ may have a limit as ε tends to 0. In fact, if that sequence is at least in $L^2(\mathbb{R}^d)^m$ (in particular if it belongs to $\mathcal{S}(\mathbb{R}^d)^m$), the sequence $(\mathbf{W}_\varepsilon[\mathbf{f}_\varepsilon])_\varepsilon$ converges weakly in $\mathcal{S}'(\mathbb{R}^d \times \mathbb{R}^d)^{m\times m}$ (see the section 3 of [9]). The limit is called the semi-classical or the Wigner measure of the sequence $(\mathbf{f}_\varepsilon)_\varepsilon$ as ε goes to 0.

Now for the analysis of the high-frequency solutions of hyperbolic systems by considering their Wigner transforms it is necessary to precise the type of initial conditions to be used. Two types of properties

may be required, that we present hereafter. A first property concerns the scale of variations of a sequence $(\mathbf{f}_\varepsilon)_\varepsilon$, which controls the oscillation scale. It reads as follows: the sequence $(\mathbf{f}_\varepsilon)_\varepsilon$ is said to be ε-oscillatory if for every smooth, compactly supported function ϕ

$$\limsup_{\varepsilon\to 0}\int_{|\mathbf{k}|\geq\frac{R}{\varepsilon}}|\widehat{\phi\mathbf{f}_\varepsilon}(\mathbf{k})|^2\mathrm{d}\mathbf{k}\to 0\,,\quad R\to+\infty\,,$$

where $\widehat{\mathbf{f}}$ stands for the Fourier transform of $\mathbf{f}$. This property characterizes the scale of oscillations of the family $(\mathbf{f}_\varepsilon)_\varepsilon$. A second property, which insures that the density $|\mathbf{f}_\varepsilon|^2$ (corresponding to the local energy density in the applications) is localized in space is the following. The sequence $(\mathbf{f}_\varepsilon)_\varepsilon$ is said to be compact at infinity if:

$$\limsup_{\varepsilon\to 0}\int_{|\mathbf{x}|\geq R}|\mathbf{f}_\varepsilon(\mathbf{x})|^2\mathrm{d}\mathbf{x}\to 0\,,\quad R\to+\infty\,.$$

These properties are important conditions which will be useful to insure the weak convergence of energy observables in terms of the Wigner measure for certain Cauchy problems, as explained in the subsequent sections.

2.3.2 Evolution of the Wigner measure

We present here the evolution properties of the Wigner transform and its high-frequency limit associated to the solutions of Cauchy problems as (2.10) or (2.13) supplemented with initial conditions of the form (2.32). Contrary to the WKB method which is used to obtain approximate solutions of wave equations, the Wigner Transform is used here to perform an analysis of the energy density associated to the solution of first-order hyperbolic systems, from which (2.10) for acoustic waves or (2.13)for elastic waves proceed. The approach is rather based on an asymptotic expansion of the Wigner transform in powers of the wavelength ε, and leads to a system of equations for the expansion terms. We first consider propagation problems far from the possible interfaces.

Wave equation in the form of a first-order hyperbolic system

We start with the case of acoustic waves. If we use the same notations as in Sect. 2.1.1, the pressure field $p_\varepsilon(t,\mathbf{x})$ and the velocity field $\mathbf{u}_\varepsilon(t,\mathbf{x})$ in $\mathcal{O}$ satisfy a system of two equations, namely the continuity equation (2.8) and the conservation of momentum (2.3). p_ε and $\mathbf{u}_\varepsilon$ are supposed to have the same regularity as before, though they are indexed by ε since the initial data depend on this parameter. For $t>0$ and $\mathbf{x}\in\mathcal{O}$ one has:

$$\begin{cases}\partial_t\mathbf{u}_\varepsilon(t,\mathbf{x})+\dfrac{1}{\rho_0(\mathbf{x})}\boldsymbol{\nabla}_{\mathbf{x}}p_\varepsilon(t,\mathbf{x})=\mathbf{0}\,,\\ \partial_t p_\varepsilon(t,\,\mathbf{x})+\dfrac{1}{\kappa(\mathbf{x})}\boldsymbol{\nabla}_{\mathbf{x}}\cdot\mathbf{u}_\varepsilon(t,\mathbf{x})=0\,,\end{cases}\tag{2.64}$$

with ε-oscillatory initial conditions for the pressure and velocity fields $p_\varepsilon(0,\mathbf{x})=p_\varepsilon^0(\mathbf{x})$ and $\mathbf{u}_\varepsilon(0,\mathbf{x})=\mathbf{u}_\varepsilon^0(\mathbf{x})$, $\mathbf{x}\in\mathcal{O}$. The coupled equations of (2.64) have the form of a first-order linear hyperbolic system:

$$\mathbf{A}(\mathbf{x})\partial_t\mathbf{w}_\varepsilon+\mathbf{D}_j\partial_{x_j}\mathbf{w}_\varepsilon=\mathbf{0}\,,\tag{2.65}$$

where $\mathbf{w}_\varepsilon$ is the state vector defined by $\mathbf{w}_\varepsilon=(\mathbf{u}_\varepsilon^{\mathsf{T}},p_\varepsilon)^{\mathsf{T}}$. We use the Einstein convention of summation over repeated indices. The matrix $\mathbf{A}$ is a positive definite, symmetric matrix depending on the position $\mathbf{x}\in\mathcal{O}$, whereas $\mathbf{D}_j$, $1\leq j\leq d$, are symmetric constant matrices. One can identify the following expressions for $d=3$:

$$\mathbf{A}(\mathbf{x})=\mathrm{diag}(\rho_0(\mathbf{x})\mathbf{I}_3,\kappa(\mathbf{x}))\,,\quad \mathbf{D}_1=\mathbf{e}_1\otimes_s\mathbf{e}_4\,,\quad \mathbf{D}_2=\mathbf{e}_2\otimes_s\mathbf{e}_4\,,\quad \mathbf{D}_3=\mathbf{e}_3\otimes_s\mathbf{e}_4\,,$$

$(\mathbf{e}_1,\mathbf{e}_2,\mathbf{e}_3,\mathbf{e}_4)$ being the natural basis of $\mathbb{R}^4$. The form (2.65) is generic since other wave problems as the Schrödinger equation for quantum waves, the Maxwell equations for electromagnetic waves, or the Navier equation for elastic waves can be put in the same form. Moreover, it allows to express the energy density

carried by acoustic waves $\mathcal{E}_\varepsilon(t,\mathbf{x}) = \frac{1}{2}\rho_0(\mathbf{x})|\mathbf{u}_\varepsilon(t,\mathbf{x})|^2 + \frac{1}{2}\kappa(\mathbf{x})p_\varepsilon(t,\mathbf{x})^2$ and the energy flux density, or acoustic intensity $\mathbf{F}_\varepsilon(t,\mathbf{x}) = p_\varepsilon(t,\mathbf{x})\mathbf{u}_\varepsilon(t,\mathbf{x})$ in terms of the new variable $\mathbf{w}_\varepsilon$:

$$\mathcal{E}_\varepsilon = \frac{1}{2}(\mathbf{A}\mathbf{w}_\varepsilon, \mathbf{w}_\varepsilon)\,, \quad \mathbf{F}_\varepsilon \cdot \mathbf{e}_j = \frac{1}{2}(\mathbf{D}_j\mathbf{w}_\varepsilon, \mathbf{w}_\varepsilon)\,.$$

One may check that these quantities satisfy the following equation for $\varepsilon > 0$:

$$\partial_t \mathcal{E}_\varepsilon(t,\mathbf{x}) + \boldsymbol{\nabla}_\mathbf{x} \cdot \mathbf{F}_\varepsilon(t,\mathbf{x}) = 0\,, \tag{2.66}$$

which is a conservation law for the energy deduced from the scalar product of Eq. (2.65) with $\mathbf{w}_\varepsilon$.

The corresponding approach for elastic waves may be summarized as follows. As for acoustics the equation of motion (2.13) can be written as an hyperbolic system of the form (2.65):

$$\begin{cases} \rho\partial_t \mathbf{v}_\varepsilon - \boldsymbol{\nabla}_\mathbf{x} p_\varepsilon - \boldsymbol{\nabla}_\mathbf{x} \cdot \boldsymbol{\tau}_\varepsilon = \mathbf{0}\,, \\ \partial_t \boldsymbol{\tau}_\varepsilon - 2\mu(\mathbf{x})\boldsymbol{\nabla}_\mathbf{x} \otimes_s \mathbf{v}_\varepsilon = \mathbf{0}\,, \\ \partial_t p_\varepsilon - \lambda(\mathbf{x})\boldsymbol{\nabla}_\mathbf{x} \cdot \mathbf{v}_\varepsilon = 0\,, \end{cases} \tag{2.67}$$

where the new unknowns p_ε, $\boldsymbol{\tau}_\varepsilon$ and $\mathbf{v}_\varepsilon$ are defined by $p_\varepsilon = \lambda\boldsymbol{\nabla}_\mathbf{x} \cdot \mathbf{u}_\varepsilon$, $\boldsymbol{\tau}_\varepsilon = 2\mu\boldsymbol{\nabla}_\mathbf{x} \otimes_s \mathbf{u}_\varepsilon$, and $\mathbf{v}_\varepsilon = \partial_t \mathbf{u}_\varepsilon$. Their initial conditions can be deduced from the initial conditions (2.32) for $\mathbf{u}_\varepsilon$ and $\partial_t\mathbf{u}_\varepsilon$. Sorting the previous variables in a vector $\mathbf{w}_\varepsilon = \left(\mathbf{v}_\varepsilon^\mathsf{T}, \tau_{\varepsilon,11}, \tau_{\varepsilon,22}, \tau_{\varepsilon,33}, \tau_{\varepsilon,23}, \tau_{\varepsilon,13}, \tau_{\varepsilon,12}, p_\varepsilon\right)$, the equations (2.67) above read as an hyperbolic system of the form (2.65), where $\mathbf{A}(\mathbf{x})$ is the diagonal matrix given by:

$$\mathbf{A}(\mathbf{x}) = \operatorname{diag}\left(\rho(\mathbf{x})\mathbf{I}_3, \frac{1}{2\mu(\mathbf{x})}\mathbf{I}_3, \frac{1}{\mu(\mathbf{x})}\mathbf{I}_3, \frac{1}{\lambda(\mathbf{x})}\right)\,, \tag{2.68}$$

and $\mathbf{D}_j$ are symmetric matrices whose entries are 0 or -1. For a detailed expression of these matrices, we refer to the Appendix E. Finally, the definitions of the elastic energy density $\mathcal{E}_\varepsilon$ and flux density $\mathbf{F}_\varepsilon$:

$$\begin{aligned} \mathcal{E}_\varepsilon(t,\mathbf{x}) &= \frac{1}{2}\rho(\mathbf{x})|\mathbf{u}_\varepsilon(t,\mathbf{x})|^2 + \frac{1}{2\lambda(\mathbf{x})}p_\varepsilon(t,\mathbf{x})^2 + \frac{1}{4\mu(\mathbf{x})}\operatorname{Tr}(\boldsymbol{\tau}_\varepsilon(t,\mathbf{x})^2)\,, \\ \mathbf{F}_\varepsilon(t,\mathbf{x}) &= -p_\varepsilon(t,\mathbf{x})\mathbf{v}_\varepsilon(t,\mathbf{x}) - \boldsymbol{\tau}_\varepsilon(t,\mathbf{x})\mathbf{v}_\varepsilon(t,\mathbf{x})\,, \end{aligned}$$

lead to the same conservation equation (2.66) as for acoustics. The latter is detailed in the following section for the general case of a first-order linear hyperbolic system (2.65).

Liouville equation

The previous general hyperbolic system in $\mathbb{R}^n$, with for example $n = 4$ for acoustic waves or $n = 10$ for elastic waves, is the starting point for the characterization of high-frequency solutions of the wave equations (2.10) and (2.13), among others. This may be achieved by making use of the Wigner transform of $\mathbf{w}_\varepsilon$, which may depend explicitly on the small parameter through some rescaling $\mathbf{w}_\varepsilon(t,\mathbf{x}) = \mathbf{w}(\frac{t}{\varepsilon}, \frac{\mathbf{x}}{\varepsilon})$, or implicitly through its initial conditions:

$$\mathbf{w}_\varepsilon(0,\mathbf{x}) = \mathbf{w}_\varepsilon^0(\mathbf{x}) \quad \text{or} \quad \mathbf{w}_\varepsilon^0\left(\mathbf{x}, \frac{\mathbf{x}}{\varepsilon}\right)\,. \tag{2.69}$$

The derivation of the equation verified by the Wigner transform of $\mathbf{w}_\varepsilon$, which is a distribution in $\mathcal{S}'(\mathbb{R}, \mathbb{R}^d \times \mathbb{R}^d)$, is performed as follows. It is first assumed that the initial conditions $\mathbf{w}_\varepsilon^0$, the matrix $\mathbf{A}$, and the matrices $\mathbf{D}_j$, $1 \le j \le d$ satisfy the following properties. The family $(\mathbf{w}_\varepsilon^0)_\varepsilon$ is compact at infinity and ε-oscillatory, $\mathbf{A}(\mathbf{x})$ is a smooth positive definite matrix, and the matrices $\mathbf{D}_j$ do not depend on t or $\mathbf{x}$. Provided that the sequence $(\mathbf{w}_\varepsilon)_\varepsilon$ remains uniformly bounded in $L^2(\mathbb{R}^d)$, its Wigner transform $\mathbf{W}_\varepsilon(t,\mathbf{x},\mathbf{k})$ admits a non-negative weak limit as ε goes to 0 denoted by $\mathbf{W}_0(t,\mathbf{x},\mathbf{k})$, and we may characterize the high-frequency solutions of an hyperbolic system of the form (2.65) with the help of $\mathbf{W}_0$. We refer to [3, 9, 22] for a proof of the following results. Applying the definition of the Wigner Transform to the previous system (2.65), and using its properties leads to the following evolution equation for $\mathbf{W}_\varepsilon(t,\mathbf{x},\mathbf{k})$ with some initial conditions given by the Wigner transform of the family $(\mathbf{w}_\varepsilon^0)_\varepsilon$ [61, Eq. (3.13)]:

$$\partial_t \mathbf{W}_\varepsilon + \mathrm{Q}_1^\varepsilon \mathbf{W}_\varepsilon + \frac{1}{\varepsilon}\mathrm{Q}_2^\varepsilon \mathbf{W}_\varepsilon = 0\,, \quad \mathbf{W}_\varepsilon(0,\mathbf{x},\mathbf{k}) = \mathbf{W}_\varepsilon^0(\mathbf{x},\mathbf{k})\,. \tag{2.70}$$

The operators Q_1^ε and Q_2^ε are given by:

$$\begin{aligned}\mathrm{Q}_1^\varepsilon \mathbf{W}_\varepsilon &= \frac{1}{2}\int_{\mathbb{R}^d} \mathrm{e}^{-\,\mathrm{i}\,\mathbf{p}\cdot\mathbf{x}} \Big[\widehat{\mathbf{A}^{-1}}(\mathbf{p})\mathbf{D}_j\partial_{x_j}\mathbf{W}_\varepsilon\Big(t,\mathbf{x},\mathbf{k}+\frac{\varepsilon\mathbf{p}}{2}\Big) + \partial_{x_j}\mathbf{W}_\varepsilon\Big(t,\mathbf{x},\mathbf{k}-\frac{\varepsilon\mathbf{p}}{2}\Big)\mathbf{D}_j\widehat{\mathbf{A}^{-1}}(\mathbf{p}) \\ &\quad + \widehat{\mathbf{A}^{-1}}(\mathbf{p})\,\mathrm{i}\,p_j\mathbf{D}_j\mathbf{W}_\varepsilon\Big(t,\mathbf{x},\mathbf{k}+\frac{\varepsilon\mathbf{p}}{2}\Big) + \mathbf{W}_\varepsilon\Big(t,\mathbf{x},\mathbf{k}-\frac{\varepsilon\mathbf{p}}{2}\Big)\,\mathrm{i}\,p_j\mathbf{D}_j\widehat{\mathbf{A}^{-1}}(\mathbf{p})\Big]\,\mathrm{d}\mathbf{p}\,, \\ \mathrm{Q}_2^\varepsilon \mathbf{W}_\varepsilon &= \int_{\mathbb{R}^d} \mathrm{e}^{-\,\mathrm{i}\,\mathbf{p}\cdot\mathbf{x}} \Big[\widehat{\mathbf{A}^{-1}}(\mathbf{p})\,\mathrm{i}\,k_j\mathbf{D}_j\mathbf{W}_\varepsilon\Big(t,\mathbf{x},\mathbf{k}+\frac{\varepsilon\mathbf{p}}{2}\Big) - \mathbf{W}_\varepsilon\Big(t,\mathbf{x},\mathbf{k}-\frac{\varepsilon\mathbf{p}}{2}\Big)\,\mathrm{i}\,k_j\mathbf{D}_j\widehat{\mathbf{A}^{-1}}(\mathbf{p})\Big]\,.\end{aligned}$$

The hat denotes the Fourier transform. The high-frequency feature of $\mathbf{w}_\varepsilon$ suggests to seek an expansion of its Wigner transform $\mathbf{W}_\varepsilon$ in powers of ε. We thus make the assumption that $\mathbf{W}_\varepsilon$ can be expanded as:

$$\mathbf{W}_\varepsilon = \mathbf{W}_0 + \varepsilon\mathbf{W}_1 + \mathrm{O}(\varepsilon^2)\,. \tag{2.71}$$

As one may notice, the highest-order term $\mathrm{O}(\varepsilon^{-1})$ obtained by plugging the expansion (2.71) into (2.70) shows that the high-frequency limit of the Wigner transform $\mathbf{W}_\varepsilon$ must be in the kernel of Q_2, the limit operator of Q_2^ε as ε goes to 0. The next order term reads in the form of a transport equation depending on the operators Q_{21} and Q_1, obtained as the zeroth-order terms of the limit operators of $\frac{1}{\varepsilon}\mathrm{Q}_2^\varepsilon$ and Q_1^ε as ε goes to 0:

$$\begin{aligned}&\mathrm{Q}_2\mathbf{W}_0 = \mathbf{0}\,,\\ &\mathrm{Q}_2\mathbf{W}_1 = -\partial_t\mathbf{W}_0 - (\mathrm{Q}_{21}+\mathrm{Q}_1)\mathbf{W}_0\,.\end{aligned} \tag{2.72}$$

The first equation defines the eigenvalues and the eigenvectors of the matrix Wigner measure $\mathbf{W}_0$, which belongs to the kernel of the operator $\mathrm{Q}_2\mathbf{Z} = \mathrm{i}\,\mathbf{L}\mathbf{Z} - \mathrm{i}\,\mathbf{Z}\mathbf{L}^*$ with the $n\times n$ dispersion matrix:

$$\mathbf{L}(\mathbf{x},\mathbf{k}) = \mathbf{A}^{-1}(\mathbf{x})k_j\mathbf{D}_j\,. \tag{2.73}$$

The second equation in (2.72) is a transport equation, which defines the components of $\mathbf{W}_0$ in its decomposition on each eigenspace of $\mathbf{L}$, called specific intensities or coherence matrices. We study the system of equations above from an algebraic point of view in order to give an explicit expression of $\mathbf{W}_0$, as summarized hereafter along the same lines as in [61]. The operators Q_{21} and Q_1 are defined by:

$$\begin{aligned}\mathrm{Q}_1\mathbf{Z}(\mathbf{x},\,\mathbf{k}) &= \frac{1}{2}\mathbf{A}^{-1}\mathbf{D}_j(\partial_{x_j}\mathbf{Z}) + \frac{1}{2}(\partial_{x_j}\mathbf{Z})\mathbf{D}_j\mathbf{A}^{-1} - \frac{1}{2}(\partial_{x_j}\mathbf{A}^{-1})\mathbf{D}_j\mathbf{Z} - \frac{1}{2}\mathbf{Z}\mathbf{D}_j(\partial_{x_j}\mathbf{A}^{-1})\,,\\ \mathrm{Q}_{21}\mathbf{Z}(\mathbf{x},\,\mathbf{k}) &= -\frac{1}{2}(\partial_{x_i}\mathbf{A}^{-1})k_j\mathbf{D}_j(\partial_{k_j}\mathbf{Z}) - \frac{1}{2}(\partial_{k_i}\mathbf{Z})k_j\mathbf{D}_j(\partial_{x_i}\mathbf{A}^{-1})\,.\end{aligned}$$

It can be verified that the dispersion matrix $\mathbf{L}(\mathbf{x},\mathbf{k})$ of the hyperbolic system is self-adjoint for the scalar product $(\mathbf{w}_1,\mathbf{w}_2)_{\mathbf{A}} = (\mathbf{A}(\mathbf{x})\mathbf{w}_1,\mathbf{w}_2)$. Its eigenvalues $(\omega_\tau(\mathbf{x},\mathbf{k}))_\tau$ are thus real valued. As $\mathbf{W}_0$ lies in the kernel of the operator Q_2, it satisfies $\mathbf{L}\mathbf{W}_0 = \mathbf{W}_0\mathbf{L}$ and thus reads:

$$\mathbf{W}_0 = \sum_{\tau=1}^{n}\mathbf{W}_\tau\,,\quad \mathbf{W}_\tau = \sum_{i,j}\mathrm{a}_\tau^{ij}\mathbf{b}_\tau^i\otimes\mathbf{b}_\tau^j\,,$$

where $(\mathbf{b}_\tau^j)_{1\le j\le r_\tau}$ denotes the eigenvectors of $\mathbf{L}$ for the eigenvalue τ with multiplicity r_τ. The solvability condition $(\mathrm{Im}^{\perp}(\mathrm{Q}_2) = \mathrm{Ker}(\mathrm{Q}_2^*))$ reads:

$$\langle\langle\partial_t\mathbf{W}_0 + (\mathrm{Q}_{21}+\mathrm{Q}_1)\mathbf{W}_0, \mathbf{b}_\tau^i\otimes\mathbf{b}_\tau^j\rangle\rangle = 0\,,\quad 1\le\tau\le n\,,\quad 1\le i,j\le r_\tau\,,$$

where $\langle\langle\mathbf{X},\mathbf{Y}\rangle\rangle = \mathrm{Tr}(\mathbf{A}\mathbf{X}^*\mathbf{A}\mathbf{Y})$, leading to the following Liouville transport equation for the coherence matrices $\mathbf{W}_\tau$:

$$\partial_t\mathbf{W}_\tau + \boldsymbol{\nabla}_{\mathbf{k}}\omega_\tau\cdot\boldsymbol{\nabla}_{\mathbf{x}}\mathbf{W}_\tau - \boldsymbol{\nabla}_{\mathbf{x}}\omega_\tau\cdot\boldsymbol{\nabla}_{\mathbf{k}}\mathbf{W}_\tau + \mathbf{W}_\tau\mathbf{N}_\tau - \mathbf{N}_\tau\mathbf{W}_\tau = \mathbf{0}\,. \tag{2.74}$$

The skew-symmetric matrices $\mathbf{N}_\tau$ are given by:

$$N_{\tau,lm}(\mathbf{x},\mathbf{k}) = (\mathbf{b}_\tau^m,\mathbf{D}_i\partial_{x_i}\mathbf{b}_\tau^l) - \partial_{x_i}\omega_\tau\left(\mathbf{b}_\tau^m,\partial_{k_i}\mathbf{b}_\tau^l\right)_{\mathbf{A}} - \frac{1}{2}(\boldsymbol{\nabla}_{\mathbf{x}}\cdot\boldsymbol{\nabla}_{\mathbf{k}}\omega_\tau)\delta_{lm}\,.$$

We refer to [3,5,22,61] for further details about this result. Note that in the particular case when all the eigenvalues of $\mathbf{L}$ are simple, the coherence matrices are scalar coefficients a_τ called specific intensities. They satisfy scalar Liouville equations, the last two terms in the left-hand side above canceling each others. In the general case, the coherence matrices have a dimension greater than 1, and they satisfy the vector Liouville equations (2.74).

In the case of acoustics, $\mathbf{L}(\mathbf{x},\,\mathbf{k})$ has only simple eigenvalues at any point $(\mathbf{x},\mathbf{k})$, so that the scalar Liouville equations must be considered in order to determine $\mathbf{W}_0$, and then compute the high-frequency limit energy density denoted by $\mathcal{E}$ and flux density denoted by $\mathbf{F}$:

$$\mathcal{E}(t,\mathbf{x}) = \lim_{\varepsilon\to 0} \mathcal{E}_\varepsilon(t,\mathbf{x})\,, \quad \mathbf{F}(t,\mathbf{x}) = \lim_{\varepsilon\to 0} \mathbf{F}_\varepsilon(t,\mathbf{x})\,.$$

In the case of elastodynamics, coherence matrices must be introduced since although the eigenspaces of $\mathbf{L}(\mathbf{x},\mathbf{k})$ for each couple $(\mathbf{x},\mathbf{k})$ have the same structure, some of them have a dimension strictly greater than 1 (see the following paragraphs). The theoretical results above can however be applied directly to both cases, so as to determine the dispersion matrix, the Liouville equations, and the form of the specific intensities and/or coherence matrices.

Application to acoustic waves

In the acoustic case ($n=4$), the dispersion matrix $\mathbf{L}$ can be computed following the definition (2.73) given above and is obtained as:

$$\mathbf{L}(\mathbf{x},\mathbf{k}) = \frac{1}{\kappa(\mathbf{x})}\mathbf{e}_4\otimes\mathbf{k}_4 + \frac{1}{\rho(\mathbf{x})}\mathbf{k}_4\otimes\mathbf{e}_4\,,$$

where $\mathbf{e}_4 = (0,0,0,1)^\mathsf{T}$ and $\mathbf{k}_4 = (\mathbf{k}^\mathsf{T},0)^\mathsf{T}$. The eigenvalues ω_τ of the dispersion matrix are given in terms of the wave number $|\mathbf{k}|$ and the sound speed $c(\mathbf{x})$ by:

$$\begin{array}{ll} \omega_0(\mathbf{x},\mathbf{k}) = 0 & \text{with multiplicity } 2\,, \\ \omega^\pm(\mathbf{x},\mathbf{k}) = \pm c(\mathbf{x})|\mathbf{k}| & \text{each with multiplicity } 1\,. \end{array} \tag{2.75}$$

We denote the corresponding eigenvectors by $\mathbf{b}_0^i$, $i=1,2$, and $\mathbf{b}_\pm$, where:

$$\begin{aligned} \mathbf{b}_0^1(\mathbf{x},\mathbf{k}) &= \frac{1}{\sqrt{2\rho(\mathbf{x})}}\left(0,\frac{k_3}{|\mathbf{k}|},-\frac{k_2}{|\mathbf{k}|},0\right)^\mathsf{T}, \\ \mathbf{b}_0^2(\mathbf{x},\mathbf{k}) &= \frac{1}{\sqrt{2\rho(\mathbf{x})}}\left(\frac{k_2}{|\mathbf{k}|},-\frac{k_1}{|\mathbf{k}|},0,0\right)^\mathsf{T}, \\ \mathbf{b}^\pm(\mathbf{x},\mathbf{k}) &= \left(\frac{\hat{\mathbf{k}}}{\sqrt{2\rho(\mathbf{x})}},\frac{\pm 1}{\sqrt{2\kappa(\mathbf{x})}}\right)^\mathsf{T}. \end{aligned} \tag{2.76}$$

These eigenvectors are orthonormal with respect to the scalar product $(,)_\mathbf{A}$. The corresponding specific intensities are denoted by a_0^i, $i=1,2$, and $\mathrm{a}^\pm$. As explained in [61], from a physical point of view the a_0^i's describe the energy associated to transverse advection modes that do not propagate, while a^+ and a^- describe compressional waves that propagate forward and backward, respectively, with the celerity $c(\mathbf{x})$. The explicit expressions of the eigenvectors are useful to compute the specific intensities $\mathrm{a}^\pm(t,\mathbf{x},\mathbf{k})$, that satisfy the scalar Liouville equations (2.74). They read:

$$\mathrm{a}^\pm(t,\mathbf{x},\mathbf{k}) = \frac{1}{8\pi^3}\int_{\mathbb{R}^3} \mathrm{e}^{\mathrm{i}\,\mathbf{k}\cdot\mathbf{y}}\, f^\pm\left(t,\mathbf{x},\mathbf{x}-\frac{\mathbf{y}}{2},\mathbf{k}\right)\overline{f^\pm\left(t,\mathbf{x},\mathbf{x}+\frac{\mathbf{y}}{2},\mathbf{k}\right)}\mathrm{d}\mathbf{y}\,, \tag{2.77}$$

where

$$f^\pm(t,\mathbf{x},\mathbf{z},\mathbf{k}) = (\mathbf{w}(t,\mathbf{z}),\mathbf{b}\pm(\mathbf{x},\mathbf{k}))_\mathbf{A} = \sqrt{\frac{\rho(\mathbf{x})}{2}}(\mathbf{u}(t,\mathbf{z})\cdot\hat{\mathbf{k}}) \pm \sqrt{\frac{\kappa(\mathbf{x})}{2}}p(t,\mathbf{z})\,.$$

The above expressions show that $\mathrm{a}^+(t,\mathbf{x},\mathbf{k}) = \mathrm{a}^-(t,\mathbf{x},-\mathbf{k})$. Moreover they are especially interesting in order to express the HF energy density $\mathcal{E}$ and flux density $\mathbf{F}$. Indeed the latter can be computed in terms of the a_0^i's and a^+ as [61]:

$$\begin{aligned}\mathcal{E}(t,\mathbf{x}) &= \int_{\mathbb{R}^3} \mathrm{a}^+(t,\mathbf{x},\mathbf{k})\mathrm{d}\mathbf{k} + \frac{1}{2}\int_{\mathbb{R}^3} \left(\mathrm{a}_0^1(\mathbf{x},\mathbf{k}) + \mathrm{a}_0^2(\mathbf{x},\mathbf{k})\right)\mathrm{d}\mathbf{k}\,,\\ \mathbf{F}(t,\mathbf{x}) &= \int_{\mathbb{R}^3} \mathrm{a}^+(t,\mathbf{x},\mathbf{k})c(\mathbf{x})\hat{\mathbf{k}}\mathrm{d}\mathbf{k}\,,\end{aligned} \tag{2.78}$$

so that we only need to solve the Liouville equation associated with the eigenvalue $\omega+$ in order to access to the densities $\mathcal{E}(t,\mathbf{x})$ and $\mathbf{F}(t,\mathbf{x})$. The a_0^i's for the advection modes are determined by the initial conditions solely.

Application to elastic waves

In the elastic case ($n = 10$), the eigenvalues ω_τ of the 10×10 dispersion matrix $\mathbf{L}$ are given by:

$$\begin{array}{ll}\omega_0(\mathbf{x},\mathbf{k}) = 0 & \text{with multiplicity } 4\,,\\ \omega_{\mathrm{P}}^{\pm}(\mathbf{x},\mathbf{k}) = \pm c_{\mathrm{P}}(\mathbf{x})|\mathbf{k}| & \text{each with multiplicity } 1\,,\\ \omega_{\mathrm{S}}^{\pm}(\mathbf{x},\mathbf{k}) = \pm c_{\mathrm{S}}(\mathbf{x})|\mathbf{k}| & \text{each with multiplicity } 2\,.\end{array} \tag{2.79}$$

The corresponding eigenvectors are denoted by $\mathbf{b}_0^j$, $1\le j\le 4$, $\mathbf{b}_{\mathrm{P}}^{\pm}$, and $\mathbf{b}_{\mathrm{S}j}^{\pm}$, $j=1,2$, respectively. Their explicit expressions as functions of $(\mathbf{x},\mathbf{k})$ are given in the Appendix E. It is useful to compute the specific intensities $\mathrm{a}_{\mathrm{P}}^{\pm}$ and coherence matrices $\mathbf{W}_{\mathrm{S}}^{\pm}$ that appear in the Liouville equation using the Wigner transform. They read as follows:

$$\mathrm{a}_{\mathrm{P}}^{\pm}(t,\mathbf{x},\mathbf{k}) = \frac{1}{8\pi^3}\int_{\mathbb{R}^3} \mathrm{e}^{\mathrm{i}\,\mathbf{k}\cdot\mathbf{y}}\, f_{\mathrm{P}}^{\pm}\left(t,\mathbf{x},\mathbf{x}-\frac{\mathbf{y}}{2},\mathbf{k}\right)\overline{f_{\mathrm{P}}^{\pm}\left(t,\mathbf{x},\mathbf{x}+\frac{\mathbf{y}}{2},\mathbf{k}\right)}\mathrm{d}\mathbf{y}$$

where $f_{\mathrm{P}}^{\pm}(t,\mathbf{x},\mathbf{z},\mathbf{k}) = (\mathbf{w}(t,\mathbf{z}),\mathbf{b}_{\mathrm{P}}^{\pm})_{\mathbf{A}}$ for the longitudinal modes $\tau=\mathrm{P}$, while:

$$[W_{\mathrm{S}}^{\pm}(t,\mathbf{x},\mathbf{k})]_{ij} = \frac{1}{8\pi^3}\int_{\mathbb{R}^3} \mathrm{e}^{\mathrm{i}\,\mathbf{k}\cdot\mathbf{y}}\, f_{\mathrm{S}i}^{\pm}\left(t,\mathbf{x},\mathbf{x}-\frac{\mathbf{y}}{2},\mathbf{k}\right)\overline{f_{\mathrm{S}j}^{\pm}\left(t,\mathbf{x},\mathbf{x}+\frac{\mathbf{y}}{2},\mathbf{k}\right)}\mathrm{d}\mathbf{y}\,,$$

where $f_{\mathrm{S}i}^{\pm}(t,\mathbf{x},\mathbf{z},\mathbf{k}) = (\mathbf{w}(t,\mathbf{z}),\mathbf{b}_{\mathrm{S}i}^{\pm}(\mathbf{x},\mathbf{k}))_{\mathbf{A}}$, $i=1,2$, for the transverse shear modes $\tau=\mathrm{S}$. At last the components of the 4×4 coherence matrix $\mathbf{W}_{00}$ for the non propagating modes are given by:

$$[W_{00}(\mathbf{x},\mathbf{k})]_{ij} = \frac{1}{8\pi^3}\int_{\mathbb{R}^3} \mathrm{e}^{\mathrm{i}\,\mathbf{k}\cdot\mathbf{y}}\, f_0^i\left(\mathbf{x},\mathbf{x}-\frac{\mathbf{y}}{2},\mathbf{k}\right)\overline{f_0^j\left(\mathbf{x},\mathbf{x}+\frac{\mathbf{y}}{2},\mathbf{k}\right)}\mathrm{d}\mathbf{y}\,,$$

where $f_0^i(\mathbf{x},\mathbf{z},\mathbf{k}) = (\mathbf{w}(0,\mathbf{z}),\mathbf{b}_0^i(\mathbf{x},\mathbf{k}))_{\mathbf{A}}$. Similar relations as the ones obtained in the acoustic case link the specific intensities $\mathrm{a}_{\mathrm{P}}^+$ and $\mathrm{a}_{\mathrm{P}}^-$ of the forward and backward longitudinal modes, respectively, and the coherence matrices $\mathbf{W}_{\mathrm{S}}^+$ and $\mathbf{W}_{\mathrm{S}}^-$ of the forward and backward shear modes, respectively:

$$\mathrm{a}_{\mathrm{P}}^+(t,\mathbf{x},\mathbf{k}) = \mathrm{a}_{\mathrm{P}}^-(t,\mathbf{x},-\mathbf{k})\,,\quad \mathrm{Tr}\,\mathbf{W}_{\mathrm{S}}^+(t,\mathbf{x},\mathbf{k}) = \mathrm{Tr}\,\mathbf{W}_{\mathrm{S}}^-(t,\mathbf{x},-\mathbf{k})\,.$$

The energy density and the flux energy density of the elastic waves can then be expressed in terms of the previous quantities by:

$$\mathcal{E}(t,\mathbf{x}) = \int_{\mathbb{R}^3}\left(\mathrm{a}_{\mathrm{P}}^+(t,\mathbf{x},\mathbf{k}) + \mathrm{Tr}\,\mathbf{W}_{\mathrm{S}}^+(t,\mathbf{x},\mathbf{k})\right)\mathrm{d}\mathbf{k} + \frac{1}{2}\int_{\mathbb{R}^3}\mathrm{Tr}\,\mathbf{W}_{00}(\mathbf{x},\,\mathbf{k})\mathrm{d}\mathbf{k}\,, \tag{2.80}$$

and:

$$\mathbf{F}(t,\mathbf{x}) = \int_{\mathbb{R}^3}\left(c_{\mathrm{P}}(\mathbf{x})\mathrm{a}_{\mathrm{P}}^+(t,\mathbf{x},\mathbf{k}) + c_{\mathrm{S}}(\mathbf{x})\,\mathrm{Tr}\,\mathbf{W}_{\mathrm{S}}^+(t,\mathbf{x},\mathbf{k})\right)\hat{\mathbf{k}}\mathrm{d}\mathbf{k}\,. \tag{2.81}$$

The resolution of the Liouville equations allows again to obtain $\mathcal{E}$ and $\mathbf{F}$ from the specific intensities and/or coherence matrices.

2.3.3 WKB methods versus Wigner measures

The solution of the Liouville equations presented above is well described when the physical parameters of the medium are regular functions of the variable $\mathbf{x}$ ($\mathbf{A}(\mathbf{x})$ must be a non-singular smooth matrix). The problem can be solved for example in an homogeneous sub-domain of $\mathcal{O}$. In that case, it is possible to draw a parallel between the two approaches presented above, by comparing the WKB approximate solution of (2.10) and the Wigner measure for the same problem. Let us consider a WKB initial condition $\mathbf{w}_\varepsilon^0$ of the form (2.32) in $\mathbb{R}^n$, $\mathbf{w}_\varepsilon^0(\mathbf{x}) = \mathbf{A}_0(\mathbf{x})\,\mathrm{e}^{\mathrm{i}\,S_0(\mathbf{x})/\varepsilon}$, where $\mathbf{A}_0(\mathbf{x})$ and $S_0(\mathbf{x})$ are regular functions at least in $\mathcal{C}^2(\mathcal{O})$, and $\mathbf{A}_0(\mathbf{x})$ is compactly supported in $\mathcal{O}$. It is possible to show that the (semi-classical) limit of the Wigner transform of these initial conditions is then given by:

$$\lim_{\varepsilon\to 0} \mathbf{W}_\varepsilon[\mathbf{w}_\varepsilon^0](\mathbf{x},\mathbf{k}) = |\mathbf{A}_0(\mathbf{x})|^2 \delta(\mathbf{k} - \boldsymbol{\nabla}_{\mathbf{x}} S_0(\mathbf{x}))\,. \tag{2.82}$$

Indeed, as we may project the Wigner transform on an orthonormal basis of $\mathbb{R}^n$ ($m \in \mathbb{N}^*$), we restrict ourselves to the case $n = 1$ and carry the following computation. Let $\phi(\mathbf{x},\mathbf{k})$ be a smooth function of $\mathcal{S}(\mathbb{R}^d \times \mathbb{R}^d)$, we have:

$$\begin{aligned}
\langle \phi, \mathbf{W}_\varepsilon[w_\varepsilon^0]\rangle_{\mathcal{S},\mathcal{S}'} &= \iint_{\mathbb{R}^d\times\mathbb{R}^d} \left(\int_{\mathbb{R}^d} \mathrm{e}^{\mathrm{i}\,\mathbf{k}\cdot\mathbf{y}}\, A_0\left(\mathbf{x} - \frac{\varepsilon\mathbf{y}}{2}\right) \overline{A_0\left(\mathbf{x} + \frac{\varepsilon\mathbf{y}}{2}\right)}\, \mathrm{e}^{\mathrm{i}[S_0(\mathbf{x}-\frac{\varepsilon\mathbf{y}}{2}) - S_0(\mathbf{x}+\frac{\varepsilon\mathbf{y}}{2})]/\varepsilon}\, \frac{\mathrm{d}\mathbf{y}}{(2\pi)^d} \right) \phi(\mathbf{x},\mathbf{k})\mathrm{d}\mathbf{x}\mathrm{d}\mathbf{k} \\
&= \iint_{\mathbb{R}^d\times\mathbb{R}^d} \left(|A_0(\mathbf{x})|^2\, \mathrm{e}^{-\,\mathrm{i}\,\mathbf{y}\cdot\boldsymbol{\nabla}_{\mathbf{x}} S_0(\mathbf{x})} + \mathrm{O}(\varepsilon) \right) \hat{\phi}(\mathbf{x},\mathbf{y})\mathrm{d}\mathbf{x}\mathrm{d}\mathbf{y} \\
&= \int_{\mathbb{R}^d} |A_0(\mathbf{x})|^2 \phi(\mathbf{x}, \boldsymbol{\nabla}_{\mathbf{x}} S_0)\mathrm{d}\mathbf{x} + \mathrm{O}(\varepsilon)\,.
\end{aligned}$$

In the above $\hat{\phi}(\mathbf{x},\mathbf{y})$ denotes the inverse Fourier transform of the function ϕ with respect to the second variable, and belongs to $L^1(\mathbb{R}^d \times \mathbb{R}^d)$. $A_0(\mathbf{x})$ being bounded on $\mathbb{R}^d$, the theorem of dominated convergence allows to take the limit as ε goes to 0 (note that we may only require that $\hat{\phi}(\mathbf{x},\mathbf{y})$ satisfies $\int_{\mathbb{R}^d} \sup_{\mathbf{x}} |\hat{\phi}(\mathbf{x},\mathbf{y})|\mathrm{d}\mathbf{y} < \infty$, since A_0 belongs to $L^1(\mathbb{R}^d \times \mathbb{R}^d)$). Thus (2.82) is satisfied at the limit when ε goes to 0. This result shows that the Wigner transform is adapted to high-frequency oscillations of the phase S_0 for a variation scale of order ε. This is no longer true for functions that oscillate on a larger or a lower scale than ε. We refer to [9] for examples that show what may happen on different scales ($\sqrt{\varepsilon}$, ε^2 ...), and for details about the properties of the Wigner transform. It is then deduced from the previous convergence theorem (as the initial conditions used are compact at infinity and ε-oscillatory) on the one hand, and from above computations on the other hand, that the specific intensity solving the scalar Liouville equation reads in terms of the initial conditions:

$$\mathrm{a}^+(0,\mathbf{x},\mathbf{k}) = |A_0(\mathbf{x})|^2 \delta(\mathbf{k} - \boldsymbol{\nabla}_{\mathbf{x}} S_0(\mathbf{x}))\,, \tag{2.83}$$

and that for any time t before any interface is reached we have the form $\mathrm{a}^+(t,\mathbf{x},\mathbf{k}) = |A(t,\mathbf{x})|^2 \delta(\mathbf{k} - \boldsymbol{\nabla}_{\mathbf{x}} S(t,\mathbf{x}))$. Therefore the Wigner transform can be used to compute the energy density of the solution of evolution problems with WKB initial conditions, by the resolution of a Liouville equation.

2.3.4 Boundary conditions for Wigner measures

Difficulties arise when the specific intensities reach the boundaries $\partial\mathcal{O}$ of the domain or an interface $\mathcal{I}$ corresponding to a discontinuity of some physical parameter, for example. It is then necessary to describe the behavior of the specific intensities or coherence matrices at $\partial\mathcal{O}$ or $\mathcal{I}$. As already mentioned in the section 2.2.3, the boundary conditions for high-frequency initial conditions are described for the Schrödinger equation and the scalar wave equation by Miller in [52], for the case of inhomogeneous sub-domains separated by a straight (or curved) interface. The Wigner transform turns out to be also interesting in that case for the consideration of boundary conditions in terms of coherence matrices or specific intensities. They are described in [4, 52] for the Wigner measure of a family of solutions of a scalar wave equation (2.9), and in [5] for the Wigner measure of a family of solutions of a vector wave equation (2.13). These results may be summarized as follows.

Recalling the definition (2.35) of the dispersion matrix of a wave equation, the latter reads:

$$\mathbf{H}_\varepsilon(t,\mathbf{x},\mathrm{i}\,\varepsilon\partial_t,\mathrm{i}\,\varepsilon\boldsymbol{\nabla}_\mathbf{x})\mathbf{u}_\varepsilon=\mathbf{0}\,,\quad (t,\mathbf{x})\in\mathbb{R}_t\times\mathcal{O}\,,$$

where $\mathbf{H}_\varepsilon(t,\mathbf{x},\omega,\mathbf{k})=\mathbf{H}(t,\mathbf{x},\omega,\mathbf{k})+\mathrm{i}\,\varepsilon\mathbf{H}_1(\mathbf{x},\mathbf{k})$, and $\mathbf{H}_1(\mathbf{x},\mathbf{k})$ is a first-order polynomial in $\mathbf{k}$ of which matrix coefficients are the gradients of the parameters of the medium. Hence $\mathbf{H}_1(\mathbf{x},\mathrm{i}\,\varepsilon\boldsymbol{\nabla}_\mathbf{x})$ is a first-order partial differential operator, and $\mathbf{H}_1=\mathbf{0}$ in an homogeneous medium. Multiplying the above equation by $\overline{\mathbf{u}}_\varepsilon$ and then taking its spatio-temporal Wigner transform as done in *e.g.* [5, 8], one obtains at the leading order for $\varepsilon\to 0$:

$$\mathbf{H}(\mathbf{s},\boldsymbol{\xi})\mathbf{W}_0(\mathbf{s},\boldsymbol{\xi})=\mathbf{0}\,,\quad (\mathbf{s},\boldsymbol{\xi})\in\mathbb{R}_t\times\mathcal{O}_\mathbf{x}\times\mathbb{R}_\omega\times\mathbb{R}^d_\mathbf{k}$$

in the sense of distributions, where $\mathbf{W}_0$ is now the spatio-temporal Wigner measure of the sequence $(\mathbf{u}_\varepsilon)_\varepsilon$. Hence its support in phase space is characterized by the condition $\mathcal{H}=\det\mathbf{H}=0$, which from the structure of the Christoffel tensor reads:

$$\prod_{\tau=1}^{d}\mathcal{H}_\tau(\mathbf{s},\boldsymbol{\xi})=0\,,\quad \mathcal{H}_\tau(\mathbf{s},\boldsymbol{\xi})=\rho(\mathbf{x})\left(\omega_\tau^2(\mathbf{x},\mathbf{k})-\omega^2\right)\,. \tag{2.84}$$

In the above $(\omega_\tau^2)_{1\leq\tau\leq d}$ are the eigenvalues of the Christoffel tensor, which are the square of the eigenvalues (2.75) and (2.79) of the propagating modes of the dispersion matrix for the acoustic and elastic wave equations written in the form of first-order hyperbolic systems. The condition (2.84) has yet to be satisfied on the boundary $\partial\mathcal{O}$ or a discontinuity front possibly moving within the medium, that is a time-dependent interface $\mathcal{I}_D$ in phase space:

$$\mathcal{I}_D=\{(\mathbf{s},\boldsymbol{\xi})\in T^*(\mathbb{R}\times\mathcal{O});\,\Sigma(\mathbf{s},\boldsymbol{\xi})=0\}\,.$$

Thus boundary conditions for the Wigner measure of a wave field have to be determined for $(\mathbf{s},\boldsymbol{\xi})\in\mathcal{I}_D\cap(\cup_{\tau=1}^d\mathcal{X}_\tau)$, where:

$$\mathcal{X}_\tau=\{(\mathbf{s},\boldsymbol{\xi})\in T^*(\mathbb{R}\times\mathcal{O})\setminus\{\mathbf{k}=\mathbf{0}\};\,\mathcal{H}_\tau(\mathbf{s},\boldsymbol{\xi})=0\}\,.$$

Recalling the notations introduced in the section 2.1.3, one then has:

$$\mathcal{H}_\tau(\mathbf{s},\boldsymbol{\xi})=b_\tau(\mathbf{x})k_\mathbf{n}^2+\mathcal{H}_\tau(\mathbf{s},\boldsymbol{\xi}')=0\,,\quad 1\leq\tau\leq d\,, \tag{2.85}$$

isolating the normal component $k_\mathbf{n}=\mathbf{k}\cdot\mathbf{n}$ of the wave vector on the unit normal $\mathbf{n}$ to the interface or the boundary; also $\boldsymbol{\xi}'=(\omega,\mathbf{k}')$ with $\mathbf{k}'=\mathbf{k}-k_\mathbf{n}\mathbf{n}$, and b_τ is a positive coefficient. Eq. (2.85) is a simple quadratic equation for $k_\mathbf{n}$ parameterized by $\mathbf{k}'$, which has real or purely imaginary solutions for either $\mathcal{H}_\tau(\mathbf{s},\boldsymbol{\xi}')<0$ or $\mathcal{H}_\tau(\mathbf{s},\boldsymbol{\xi}')>0$. Thus the cotangent bundle to the boundary $T^*(\mathbb{R}\times\partial\mathcal{O})$ splits as $T^*(\mathbb{R}\times\partial\mathcal{O})=\mathscr{H}_\tau\cup\mathscr{E}_\tau\cup\mathscr{G}_\tau$ (for all modes τ), where the different diffraction regions on $\mathbb{R}\times\partial\mathcal{O}$ are defined by:

$$\begin{aligned}
\mathscr{H}_\tau&=\{(\mathbf{s},\boldsymbol{\xi}')\in T^*(\mathbb{R}\times\partial\mathcal{O});\,\mathcal{H}_\tau(\mathbf{s},\boldsymbol{\xi}')<0\}\quad\text{(hyperbolic)}\,,\\
\mathscr{E}_\tau&=\{(\mathbf{s},\boldsymbol{\xi}')\in T^*(\mathbb{R}\times\partial\mathcal{O});\,\mathcal{H}_\tau(\mathbf{s},\boldsymbol{\xi}')>0\}\quad\text{(elliptic)}\,,\\
\mathscr{G}_\tau&=\{(\mathbf{s},\boldsymbol{\xi}')\in T^*(\mathbb{R}\times\partial\mathcal{O});\,\mathcal{H}_\tau(\mathbf{s},\boldsymbol{\xi}')=0\}\quad\text{(tangent)}\,.
\end{aligned}$$

The first one corresponds to the transverse rays (below critical incidence) for which $k_\mathbf{n}$ is real, the second one corresponds to the totally reflected rays (above critical incidence) for which $k_\mathbf{n}$ is purely imaginary, and the third one corresponds to the tangent rays (critical or tangential incidence) for which $k_\mathbf{n}=0$ in the local frame of the tangent plane to the boundary at $\mathbf{s}$. As for an interface, these definitions have to be extended on both sides since the Christoffel tensor, and thus its eigenvalues, are *a priori* different; the cotangent bundle is then the union of all these regions [52], but the latter are not necessarily disjoint.

Mode conversions $\tau\leftrightarrow\upsilon$ in $\mathscr{H}_\tau\cap\mathscr{H}_\upsilon$ or $\mathscr{H}_\tau\cap\mathscr{E}_\upsilon$ are driven by the condition that the circular frequency ω remains constant in this scattering process, as outlined in [61]. It enforces the conservation of the Hamiltonian on the bi-characteristics $t\mapsto(\mathbf{x}(t),\mathbf{k}(t))$ solving (2.39), that is $\omega_\tau(\mathbf{x}(t_0^-),\mathbf{k}(t_0^-))=\omega_\upsilon(\mathbf{x}(t_0^+),\mathbf{k}(t_0^+))$ on any discontinuity front $\mathcal{I}_D$ of the measure $\mathrm{Tr}\,\mathbf{W}_0$, where therefore $t_0>0$ is such

that $\Sigma(\mathbf{s}(t_0), \boldsymbol{\xi}(t_0)) = 0$. Besides, the Rankine-Hugoniot condition on $\mathcal{I}_D \cap (\cup_{\tau=1}^{d} \mathcal{X}_\tau)$ is for the Liouville equation:

$$[\![\{\mathcal{H}, \Sigma\} \operatorname{Tr} \mathbf{W}_0]\!] = 0\,,$$

where $[\![f]\!] = f(\tau_0^+) - f(\tau_0^-)$ stands for the jump of f on the front. This condition expresses the conservation of the normal energy flux on the discontinuity, but it does not describe *a priori* how the energy density is distributed among the different modes by the reflections and transmissions on a fixed (independent of time) interface for example. In fact the outgoing Wigner measures in the elliptic and hyperbolic regions can be expressed in terms of the incoming one by considering the power flow reflexion and transmission coefficients obtained for harmonic plane waves in the section 2.1.3. This issue is addressed in [4, 5, 52] for both the acoustic and elastic cases. These results allow to compute numerically the solutions of reflection/transmission problems for the specific intensities solving transport equations. Moreover, they justify for smooth interfaces the expressions of the reflected and transmitted specific intensities in the hyperbolic region, using (2.83). In the other diffraction regions, it is shown in [5, 52] that the measures are totally reflected in the elliptic case, and that for the scalar wave equation no energy is lost by refraction in the glancing region $\mathscr{G}$.

It should be noted that in the case of arbitrary geometries of the boundary and interfaces, the computation of the reflected and transmitted measures do not allow to obtain closed-form solutions. The use of numerical computation is necessary to solve the Liouville equation. However the discretization of this last equation is seriously restricted by the dimension of the phase space, which covers four independent variables in two dimensions, and six independent variables in three dimensions. That is to say, the number of degrees of freedom increases as N^4 or N^6 if N stands for the number of degrees of freedom along one dimension. This issue is a major drawback of kinetic models of wave propagation phenomena for the higher frequency ranges, though they contribute to significantly reduce the demands in computational resources by smoothing out the highly oscillatory features of such waves.

2.4 Summary

Let us now summarize the setting of the high-frequency wave propagation problem which is addressed in this thesis. We aim at computing the energy density (and the energy flux density) associated to highly oscillating acoustic wave fields that obey the scalar (for the pressure field) or the vector (for the velocity field) wave equations (2.9) and (2.10), respectively. This amounts to solving the Liouville equation (2.74) for the acoustic specific intensities introduced in Eq. (2.77). However the formula (2.78) shows that we only need to compute the specific intensity $\mathrm{a}_+(t, \mathbf{x}, \mathbf{k})$ for the forward energy modes corresponding to the Hamiltonian $\omega^+(\mathbf{x}, \mathbf{k}) = +c(\mathbf{x})|\mathbf{k}|$. Thus one has to solve the following scalar Liouville equation in phase space:

$$\partial_t \mathrm{a}^+ + \boldsymbol{\nabla}_{\mathbf{k}}\omega^+ \cdot \boldsymbol{\nabla}_{\mathbf{x}}\mathrm{a}^+ - \boldsymbol{\nabla}_{\mathbf{x}}\omega^+ \cdot \boldsymbol{\nabla}_{\mathbf{k}}\mathrm{a}^+ = 0\,, \tag{2.86}$$

with some initial conditions given for $\mathrm{a}^+(0, \mathbf{x}, \mathbf{k})$. The latter are deduced from the initial conditions for the pressure field p_ε and velocity field $\mathbf{u}_\varepsilon$. For WKB highly oscillatory initial conditions of the form (2.32) for example, we obtain:

$$\mathrm{a}^+(0, \mathbf{x}, \mathbf{k}) = \mathrm{a}^-(0, \mathbf{x}, -\mathbf{k}) = \frac{1}{2}\left(\rho(\mathbf{x})|\mathbf{A}(\mathbf{x})|^2|\boldsymbol{\nabla}_{\mathbf{x}}S(\mathbf{x})|^2 + \kappa(\mathbf{x})|\mathbf{B}(\mathbf{x})|^2\right)\delta\left(\mathbf{k} - \boldsymbol{\nabla}_{\mathbf{x}}S\right)\,. \tag{2.87}$$

The boundary conditions to be applied to the measure $\mathrm{a}^+(t, \mathbf{x}, \mathbf{k})$ at an interface $\mathcal{I}$ where the sound speed c may be discontinuous are defined as follows. The geometrical setting in the same as the one considered in the section 2.1.3. In particular, the interface separates the propagation medium $\mathcal{O}$ into two subdomains $\mathcal{O}^-$ and $\mathcal{O}^+$ where the sound speed is constant and equal to c^- and c^+, respectively. For a given wave vector $\mathbf{k}$ impinging on $\mathbf{x} \in \mathcal{I}$ at time t, the incident specific intensity $\mathrm{a}^+(t, \mathbf{x}, \mathbf{k})$ is reflected and transmitted at that location following the Snell-Descartes laws (2.22). Thus if $\mathrm{a}^+_{\mathrm{R}}(t, \mathbf{x}, \mathbf{k})$ and $\mathrm{a}^+_{\mathrm{T}}(t, \mathbf{x}, \mathbf{k})$ denote the reflected and transmitted specific intensities, the following relations hold for reflection and transmission from $\mathcal{O}^-$ to $\mathcal{O}^+$:

$$\begin{aligned} \mathrm{a}^+_{\mathrm{R}}(t, \mathbf{x}, \mathbf{k}_{\mathrm{R}}) &= \mathcal{R}^-(\mathbf{k})\mathrm{a}^+(t, \mathbf{x}, \mathbf{k})\,, \\ \mathrm{a}^+_{\mathrm{T}}(t, \mathbf{x}, \mathbf{k}_{\mathrm{T}}) &= \mathcal{T}^-(\mathbf{k})\mathrm{a}^+(t, \mathbf{x}, \mathbf{k}), \end{aligned} \tag{2.88}$$

for $t \geq 0$ and $(\mathbf{x}, \mathbf{k}) \in \mathcal{I} \times \mathbb{R}^d$, where $\mathcal{R}^-$ and $\mathcal{T}^-$ are given by Eq. (2.26). Equivalent definitions are obtained for reflection and transmission from $\mathcal{O}^+$ to $\mathcal{O}^-$ by replacing $\mathcal{R}^-$ and $\mathcal{T}^-$ by $\mathcal{R}^+$ and $\mathcal{T}^+$. Finally at the boundaries of the domain $\mathcal{O}$, we use total reflection, corresponding to transmission coefficients equal to 0. It should be noted that in the case of elastic waves, an equivalent formulation of the aforementioned problem can be proposed, using the appropriate Liouville equations (2.74). We refer to [5] for some recent theoretical works on this issue.

Different numerical schemes may be implemented in order to solve the scalar Liouville equation (2.86). However they should all share the same basic features, namely (i) the ability the conserve the total energy brought by the initial conditions when it is both propagated within the medium and diffracted at interfaces, and (ii) the ability to preserve the positivity of the specific intensities in these processes. Positivity-preserving schemes need to be considered for Eq. (2.86) because it concerns quadratic (positive) observables. The issue of developing such schemes is the subject of intense research in the dedicated literature as evidenced by the recent review [74] for example (see also [58]), though it is beyond the scope of the thesis. The works presented subsequently are specifically dedicated to conservation issues, which are much less studied especially for the simulation of diffraction phenomena. Lagrangian approaches, by which the specific intensities may be reconstructed by different ray tracing and front tracking techniques in phase space, are considered in [18] and references therein. The Monte-Carlo method is also a method of choice for kinetic equations, see for example [38]. The present thesis is focused on Eulerian approaches, since much progress has been reported in recent years on such methods; see the seminal developments of Jin and co-workers in *e.g.* [27–31]. These methods are much more demanding in terms of computational resources, however they are also much more versatile than Lagrangian approaches. In particular, the subsequent chapters focuses on finite difference (FD) schemes, though finite element (FE) schemes may also be devised for kinetic equations. For example, a discontinuous finite element method has been proposed in [63] for the computation of high-frequency wave propagation phenomena in built-up structures. Contrary to FD schemes, FE schemes can handle unstructured meshes, a highly desirable feature in engineering applications. Nevertheless the former are much satisfactory for the present research. Indeed, resorting to finite differences allows us to evade several difficulties raised by the need to preserve positivity because the retained schemes ensure that positivity in phase space for the observables we are interested in.

3

Finite difference schemes for the Liouville equation in heterogeneous media

As explained in the previous chapter, we are concerned with solving the acoustic wave equation (2.9) or (2.10), or the equivalent problem (2.64), with high-frequency initial data of the form (2.32) at the limit when the relative wavelength ε goes to 0. As seen in the section 2.1.4, different types of approaches can be investigated to deal with such high-frequencies. The approach that we use follows the work of Jin & Yin [31] and the theory presented by Ryzhik, Papanicolaou & Keller in [61], where the problem (2.64) is considered in terms of the specific intensities $\mathrm{a}^+(t,\mathbf{x},\mathbf{k})$ and $\mathrm{a}^-(t,\mathbf{x},\mathbf{k})$ of acoustic waves (see Eq. (2.77)), corresponding to energy densities resolved in the phase space position $\times$ wave vector. They satisfy in addition a scalar Liouville transport equation of the form (2.86). We refer to the section 2.3.2 for some further details. The integration of these specific intensities about the wave vector $\mathbf{k}$ leads to the expression of the energy density in the medium denoted by $\mathrm{E}(t,\mathbf{x})$, and the integration of the specific intensities multiplied by the group velocities $\boldsymbol{\nabla}_{\mathbf{k}}\omega^{\pm} = \pm c\hat{\mathbf{k}}$ leads to the expression of the energy flux density $\mathbf{F}(t,\mathbf{x})$; see Eq. (2.78). They provide with a description of the behavior of the high-frequency waves in the propagation medium $\mathcal{O}$.

Our aim is thus to solve the Liouville equation numerically so as to approximate the evolution of E and $\mathbf{F}$ accurately, and thus characterize the propagation of high-frequency acoustic waves as well as their reflections and transmissions along the interfaces within $\mathcal{O}$. To this purpose, we discretize the phase-space domain on which the specific intensities are defined, and follow the numerical methods introduced by Jin and co-workers in [29, 31] for acoustics and elastodynamics (see also the related works [27, 28, 30]). For that purposes, the physical domain considered in this chapter is bounded in order to enable numerical simulations. It is denoted by $\mathcal{O}_h$ and constituted by a piecewise linear homogeneous isotropic medium. It may possibly including several interfaces, but for clarity purposes we will consider only one interface $\mathcal{I}$ in the subsequent exposition. Using these schemes one may observe that the number of variables stored at each iteration of the time in order to solve the discretized Liouville equation increases with the product of the discretization numbers along each direction x_j and k_j, $1 \leq j \leq d$, in the phase space $(\mathbf{x},\mathbf{k}) \in \mathcal{O} \times \mathbb{R}^d$. Thus the computational demand grows heavily with these average discretization numbers. This is a severe limitation in terms of computational resources, and it is relevant to solve the Liouville equation for low discretization numbers, while preserving some basic properties of the numerical solution such as positivity, stability, good convergence orders, and conservation of the total energy during the simulation. To perform this discretization, we essentially follow [31], where a positive Hamiltonian-preserving finite difference scheme for transport equations is proposed. It is based on a classical upwind flux far from $\mathcal{I}$, and the choice of specific analytical expressions for the reflected and transmitted discretized specific intensities about $\mathcal{I}$. We will mainly rely on this scheme in this chapter, and describe it in more details. Note that to overcome the difficulties raised by high-frequency problems, in particular dispersion and instability, different numerical methods have been developed, mainly finite element (FE) methods and

finite difference (FD) methods. Some classical references on this topic includes [17, 23, 40, 72, 73] among others. FD methods require less memory space for the numerical simulations than FE methods, but they use regular meshes less adapted to complicated geometries. On the contrary, FE methods allow to treat boundary problems with more versatility. Regarding some recent developments on FE and FD schemes, one may get involved in spectral element methods (see for instance [12, 16, 21, 34, 51, 60, 70]), or in high-order finite difference approximations (see for instance [46, 55, 68]) with a dedicated treatment of the interface conditions (see for instance [42, 43]).

One of the shortcomings of FD schemes is that they conserve energy and are non-dispersive only for very fine meshes. In the case of low discretization numbers the loss of energy due to the approximation of the Liouville equation by its discretized versions given in the following Eq. (3.14) of the section 3.2 can no longer be neglected. Our approach in handling this issue is to focus on energy conservation at $\mathcal{I}$. In fact, it can be shown that the classical upwind scheme combined with standard interpolations of the reflected and transmitted specific intensities at an interface does not conserve the total energy. More precisely the loss of numerical energy is due to the difficulty raised by the interpolation of the specific intensities on the mesh of the discretized wave vectors at the points located at $\mathcal{I}$. Indeed this interpolation does not always cover the whole mesh of discretized wave vectors, so that a part of the incident wave vectors may be not transmitted although it should have been. This problem is introduced properly in the section 3.4 of this chapter, and a solution is proposed in the subsequent chapter 4 (see more particularly the sections 4.3.2 and 4.3.3 for the case of a straight interface). In this work, because of the simple form of the approximation domain and of the equation solved, we basically follow [28] and [31], and restrict our choice to the FD methods presented there. We start this chapter by fixing the notations for the discretization of the geometry and phase-space variables of the problem, before introducing the presentation of the numerical discretization of the Liouville equation (2.86) itself.

3.1 Discretization of the phase space

To solve the Liouville equation (2.86) numerically, the continuous variables $\mathbf{x}$ and $\mathbf{k}$ of the phase-space, and the time t are discretized on regular grids, on which the known wave speed $c(\mathbf{x})$ and the unknown specific intensity $\mathrm{a}(t, \mathbf{x}, \mathbf{k})$, as well as their derivatives, are themselves discretized (see the next section 3.2).

3.1.1 Grids and meshes

The computational domain $\mathcal{O}_h$ is represented by a structured spatial grid denoted by $\mathcal{G}_{\mathbf{x}}$ and defined by a set of points hereafter called the grid points. They are defined as follows. Let $\boldsymbol{\delta}^j$ denote the following unit vector:

$$\delta_i^j = \begin{cases} 0 & \text{if} \quad i \neq j \\ 1 & \text{if} \quad i = j \end{cases} \qquad 1 \leq i, j \leq d\,.$$

The grid point $\mathbf{X}_{\alpha - \frac{1}{2}}$ of $\mathcal{G}_{\mathbf{x}}$ is defined for a multi-index $\alpha = (\alpha_1, \dots \alpha_d) \in \mathbb{Z}^d$ by:

$$\mathbf{X}_{\alpha - \frac{1}{2}} = \mathbf{O} + \sum_{j=1}^{d} (\alpha_j - 1)\, \Delta x_j \boldsymbol{\delta}^j\,, \quad \alpha_j \in \left\{ -M_j^-, \dots M_j^+ \right\}\,,$$

where $\mathbf{O}$ denotes the origin of the canonical frame of $\mathbb{R}^d$, $\Delta x_j > 0$ are the spatial discretization steps, M_j^- and M_j^+ are strictly positive integers, and $\left(M_j^- + M_j^+ + 1\right)$ is the number of grid points along the j-th space coordinate. The total number of grid points is then equal to $\prod_{j=1}^{d} \left(M_j^- + M_j^+ + 1\right)$. The staggered mesh points at which the discrete specific intensity is computed are defined similarly for each multi-index $\alpha = (\alpha_1, \dots \alpha_d)$ in $\mathbb{Z}^d$ by:

$$\begin{aligned} \mathbf{X}_{\alpha} &= \mathbf{X}_{\alpha - \frac{1}{2}} + \frac{1}{2} \sum_{j=1}^{d} \Delta x_j \boldsymbol{\delta}^j \\ &= \mathbf{O} + \sum_{j=1}^{d} \left(\alpha_j - \frac{1}{2} \right) \Delta x_j \boldsymbol{\delta}^j\,, \quad \alpha_j \in \left\{ -M_j^-, \dots M_j^+ - 1 \right\}\,, \end{aligned}$$

and constitute the mesh $\mathcal{M}_{\mathbf{x}}$. The number of mesh points along the j-th coordinate is thus equal to $M_j^+ + M_j^-$. This construction is illustrated on Figure 3.1 for the case $d = 2$.

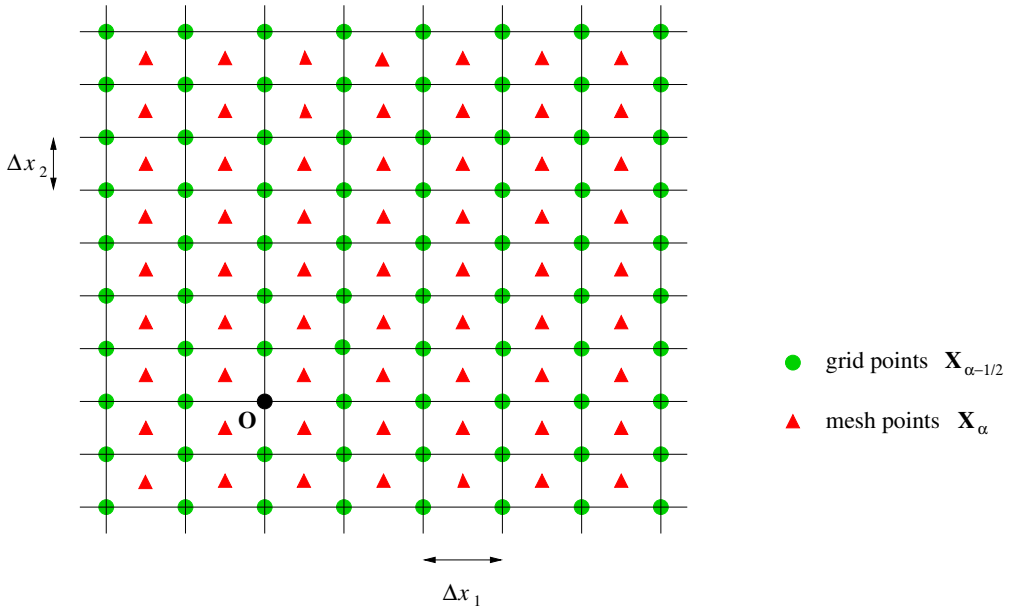

Figure 3.1: Grid points and mesh on a structured spatial grid in $d = 2$ dimensions.

As for the space coordinates, the grid of wave vectors $\mathcal{G}_{\mathbf{k}}$ is defined by a set of points $\mathbf{K}_{\beta-\frac{1}{2}}$ for $\beta = (\beta_1, \dots \beta_d) \in \mathbb{Z}^d$. Those grid points are defined by:

$$\mathbf{K}_{\beta-\frac{1}{2}} = \mathbf{O} + \sum_{j=1}^{d} (\beta_j - 1)\, \Delta k_j \boldsymbol{\delta}^j \,, \quad \beta_j \in \{-N_j, \dots N_j\} \,,$$

where $\Delta k_j > 0$ is the wave vector discretization step in the j-th direction, and $2N_j + 1$ is the number of points along that coordinate. The total number of grid points is then equal to $\prod_{j=1}^{d}(2N_j + 1)$. The wave vector mesh $\mathcal{M}_{\mathbf{k}}$ is defined as the set of staggered points $\mathbf{K}_\beta$ for $\beta = (\beta_1, \dots \beta_d) \in \mathbb{Z}^d$, as follows:

$$\begin{aligned} \mathbf{K}_\beta &= \mathbf{K}_{\beta-\frac{1}{2}} + \frac{1}{2} \sum_{j=1}^{d} \Delta k_j \boldsymbol{\delta}^j \\ &= \mathbf{O} + \sum_{j=1}^{d} \left(\beta_j - \frac{1}{2}\right) \Delta k_j \boldsymbol{\delta}^j \,, \quad \beta_j \in \{-N_j, \dots N_j - 1\} \,. \end{aligned}$$

These meshes allow to define the discrete values of the specific intensity and of the speed, and to approximate the interfaces of the problem on the cells of the mesh as presented hereafter. The cells $\mathcal{C}_\alpha$ (respectively $\mathcal{C}_\beta$) of the mesh $\mathcal{M}_{\mathbf{x}}$ (respectively $\mathcal{M}_{\mathbf{k}}$) are defined for any index $\alpha = (\alpha_1, \dots \alpha_d)$ (respectively $\beta = (\beta_1, \dots \beta_d)$) by:

$$\begin{aligned} \mathcal{C}_\alpha &= \prod_{1 \le j \le d} \left[X_{\alpha_j - \frac{1}{2}}, X_{\alpha_j + 1 - \frac{1}{2}} \right] \,, \\ \mathcal{C}_\beta &= \prod_{1 \le j \le d} \left[K_{\beta_j - \frac{1}{2}}, K_{\beta_j + 1 - \frac{1}{2}} \right] , \end{aligned}$$

where $X_{\alpha_j - \frac{1}{2}}$ denotes the components of $\mathbf{X}_{\alpha - \frac{1}{2}}$ in the canonical basis, and $K_{\beta_j - \frac{1}{2}}$ are the components of $\mathbf{K}_{\beta - \frac{1}{2}}$; see the Figure 3.2 below.

Remark: For convenience purposes, we shall also denote by $\mathcal{M}_{\mathbf{x}}$ and $\mathcal{M}_{\mathbf{k}}$ the sets of multi-indices α and β for the corresponding mesh points in phase space. These definitions will be used throughout in the following sections.

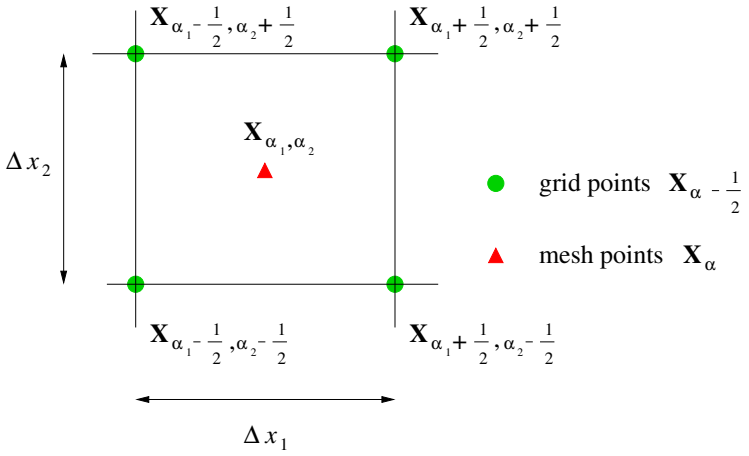

Figure 3.2: A spatial cell $\mathcal{C}_\alpha$ in $d = 2$ dimensions.

3.1.2 Interfaces

Let us first recall that for the numerical applications, we consider a bounded computational domain $\mathcal{O}_h$ with a single interface $\mathcal{I}$. Thus $\mathcal{O}_h$ is devided into two sub-domains. By convention, we choose the left side of $\mathcal{I}$ to be the slow medium denoted by $\mathcal{O}_h^-$, and the right side of $\mathcal{I}$ to be the fast one denoted by $\mathcal{O}_h^+$. This terminology follows the one introduced in the section 2.1.3, where the medium density and wave speed were denoted by $\rho\pm$ and $c^\pm$ on both sides of the interface with $c^- < c^+$. In this setting, the terminology "left" and "right" will be made clear just bellow. Also the origin $\mathbf{O}$ of the canonical frame of $\mathbb{R}^d$ is located on the interface, in order to simplify the notations. We first consider the description of a plane interface.

Straight or plane interface

In the case of a plane interface, and without loss of generality, we choose $\mathcal{I}$ to be defined by an equation of the form $x_1 = 0$, such that $\mathcal{I}$ is given by an abscissa of the grid equal to 0 by convention. A consequence is that $\mathcal{I}$ already corresponds to the edges of the cells $\mathcal{C}_\alpha$, $\alpha_1 = 0$ or $\alpha_1 = 1$, and thus does not need to be discretized on the grid. A normal vector at $\mathcal{I}$ is then defined by $\mathbf{n} = -\boldsymbol{\delta}^1$, and $\mathcal{I}$ is entirely defined by its approximation on the grid $\mathcal{G}_{\mathbf{x}}$. We refer to the Figure 3.3 for a two-dimensional illustration of a straight interface among the set of grid points $\mathcal{G}_{\mathbf{x}}$. In order to distinguish waves crossing $\mathcal{I}$ between the two subdomains $\mathcal{O}^-$ and $\mathcal{O}^+$, we introduce the following notations. We consider a wave vector $\mathbf{K}_\beta = (K_{\beta_1}, \dots K_{\beta_d})$ given on the slow side of $\mathcal{I}$. For a wave crossing $\mathcal{I}$ from $\mathcal{O}^-$ to $\mathcal{O}^+$, $\mathbf{K}_\beta$ will be said to be subcritical if:

$$K_{\beta_1} > 0 \quad \text{and} \quad K_{\beta_1} > -\xi_c\left(\mathbf{K}'_\beta\right) ,$$

where:

$$\mathbf{K}'_\beta := \sum_{j=2}^{d} K_{\beta_j} \boldsymbol{\delta}^j \tag{3.1}$$

is the tangent component of $\mathbf{K}_\beta$ to $\mathcal{I}$ in the canonical basis of $\mathbb{R}^d$, and the function $\mathbf{k}' \mapsto \xi_c(\mathbf{k}')$ has been defined by Eq. (2.24). The index $\beta_c^+ > 0$ for the first subcritical, positive normal component $K_{\beta_c^+}$ is computed by:

$$\beta_c^+ = \mathrm{Nd}^1\left(-\xi_c(\mathbf{K}'_\beta)\right) + 1 , \tag{3.2}$$

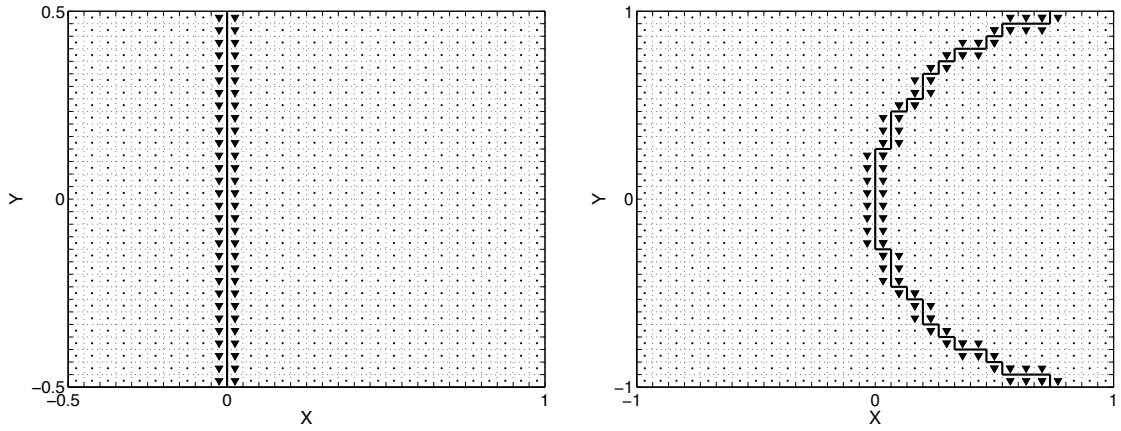

Figure 3.3: Discretization of a straight and of a semicircular interface. The centers $\mathbf{M}_j^-$ or $\mathbf{M}_j^+$ of the cells adjoining the interface are shown by triangles ▼.

where:

$$\mathrm{Nd}^j(k) = \left\lfloor \frac{k}{\Delta k_j} + \frac{1}{2} \right\rfloor , \tag{3.3}$$

for $\lfloor Y \rfloor$ being the integer part of the real number Y. The function $k \mapsto \mathrm{Nd}^j(k)$ sends the index of the j-th component of the discretized wave vector of $\mathcal{M}_{\mathbf{k}}$ which is the closest to k. For a wave crossing $\mathcal{I}$ from $\mathcal{O}^+$ to $\mathcal{O}^-$, $\mathbf{K}_\beta$ will be said to be subcritical if:

$$K_{\beta_1} < 0 \quad \text{and} \quad K_{\beta_1} < \xi_c\left(\mathbf{K}'_\beta\right) .$$

The index $\beta_c^- < 0$ for the first subcritical, negative normal component $K_{\beta_c^-}$ is computed by:

$$\beta_c^- = \mathrm{Nd}^1\left(\xi_c(\mathbf{K}'_\beta)\right) . \tag{3.4}$$

The corresponding sets of subcritical multi-indices $\mathcal{K}_c^- \subset \mathcal{K}^- = \{\beta \in \mathcal{M}_{\mathbf{k}} \mid -N_1 \leq \beta_1 \leq 0\}$, and $\mathcal{K}_c^+ \subset \mathcal{K}^+ = \{\beta \in \mathcal{M}_{\mathbf{k}} \mid 1 \leq \beta_1 \leq N_1\}$ are defined by:

$$\begin{aligned} \mathcal{K}_c^- &= \left\{\beta \in \mathcal{M}_{\mathbf{k}} \mid K_{\beta_1} < \xi_c\left(\mathbf{K}'_\beta\right)\right\} = \left\{\beta \in \mathcal{M}_{\mathbf{k}} \mid \beta_1 \leq \beta_c^-\right\} , \\ \mathcal{K}_c^+ &= \left\{\beta \in \mathcal{M}_{\mathbf{k}} \mid K_{\beta_1} > -\xi_c\left(\mathbf{K}'_\beta\right)\right\} = \left\{\beta \in \mathcal{M}_{\mathbf{k}} \mid \beta_1 \geq \beta_c^+\right\} . \end{aligned} \tag{3.5}$$

These definitions will be useful for the numerical schemes presented in the next chapter.

Curved interface

Suppose now that $\mathcal{I}$ is a curved interface. We recall that the celerity c^- on the left side of $\mathcal{I}$ is supposed to be lower than the celerity c^+ on the right side of $\mathcal{I}$. In order to approximate it on the space grid $\mathcal{G}_{\mathbf{x}}$, it is discretized as described in the section 5.2 of [31] when $d = 2$. We summarize here their approach. First let $\mathbf{n}$ be the unit normal vector at a point $\mathbf{x}$ of $\mathcal{I}$. We restrict ourselves to the case where $\mathcal{I}$ is curved in such a way that $\mathbf{n}$ satisfies either $\mathbf{n} \cdot \boldsymbol{\delta}^1 > 0$ for all point $\mathbf{x}$ on $\mathcal{I}$, or $\mathbf{n} \cdot \boldsymbol{\delta}^1 < 0$ for all points $\mathbf{x}$ on $\mathcal{I}$. In the first case $\mathcal{I}$ is said to be of type A, and in the second case it is said to be of type B; see the Figure 3.4 for an illustration. The terminology follows that of [31]. In the following, we exclusively consider interfaces of type B, provided that equivalent considerations may be deduced for interfaces of type A. Thus the construction below may be adapted to the case of an interface of type A. To construct the approximation of $\mathcal{I}$ on the space grid, we first construct for each multi-index α and each set of multi-indices $J_j = \left\{\alpha' \in \mathbb{Z}^d \mid \alpha'_i = \alpha_i \text{ for } i \neq j\right\}$ the end points $\mathbf{P}_j^-$ and $\mathbf{P}_j^+$, $1 \leq j \leq d$, as follows. We define the multi-index $(\alpha)_j \in J_j$ by $(\alpha)_j = (\alpha_1, \ldots \alpha_{j-1}, 1, \alpha_{j+1}, \ldots \alpha_d)$ such that:

$$\mathbf{X}_{(\alpha)_j} = \mathbf{X}_\alpha - (\alpha_j - 1)\Delta x_j \boldsymbol{\delta}^j ,$$

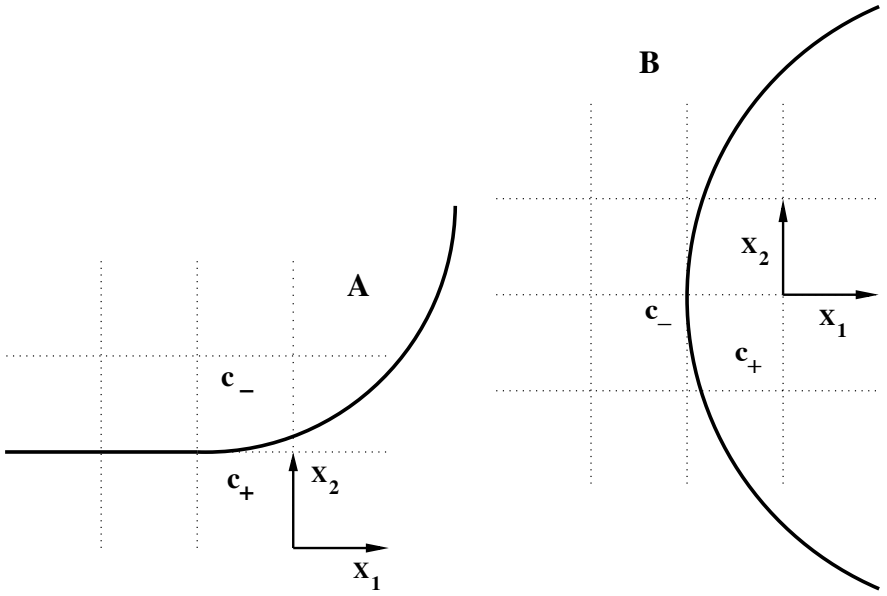

Figure 3.4: Semicircular interface on a regular two-dimensional grid: an interface of type A is displayed on the left sketch, and an interface of type B is displayed on the right sketch.

and the end-points $\mathbf{P}_j^-$ and $\mathbf{P}_j^+$ are such that:

$$\mathbf{P}_j^- = \mathbf{X}_{(\alpha)_j} - (M_j^- + 1)\Delta x_j \boldsymbol{\delta}^j \,,$$
$$\mathbf{P}_j^+ = \mathbf{X}_{(\alpha)_j} + (M_j^+ - 2)\Delta x_j \boldsymbol{\delta}^j \,.$$

The approximation of $\mathcal{I}$ on the grid is then performed as described hereafter for $1 \leq j \leq d$.

- For each index or multi-index $(\alpha)_j$ go through the segment line $[\mathbf{P}_j^-, \mathbf{P}_j^+]$. If there is an index α_j, such that one of the two cells marked off by the abscissa X_{α_j} or X_{α_j+1} on the previous segment is located in $\mathcal{O}_h^-$, while the other is located in $\mathcal{O}_h^+$, mark with $\mathbf{M}_j^-$ (respectively with $\mathbf{M}_j^+$) the center of the cell located in $\mathcal{O}_h^-$ (respectively in $\mathcal{O}_h^+$).
- For each index or multi-index $(\alpha)_j$ the approximated interface $\mathcal{I}$ is defined between $\mathbf{M}_j^-$ and $\mathbf{M}_j^+$ by the segment ($d = 2$) or by the rectangle ($d = 3$) belonging to the grid and crossed by the segment $[\mathbf{M}_j^-, \mathbf{M}_j^+]$ in its middle.

We refer to the Figure 3.3 for an example of a semicircular interface discretized on $\mathcal{G}_\mathbf{x}$ for $d = 2$, and to the Figure 3.5 for an illustration of the method. Now in order to mark more precisely the cells that surround the approximation of $\mathcal{I}$ on the grid $\mathcal{G}_\mathbf{x}$, the following notations are introduced. We denote by $\mathcal{M}^-$ the subset of $\mathcal{M}_\mathbf{x}$ constituted by the points $\mathbf{M}_j^-$ and $\mathcal{M}^+$ the subset of $\mathcal{M}_\mathbf{x}$ constituted by the points $\mathbf{M}_j^+$ constructed as above. If we consider interfaces of type B for instance, we suppose that for all index j in $\{1, \dots d\}$:

- if $j = 1$ there exists at most one multi-index α such that $\mathbf{X}_\alpha \in \mathcal{M}^-$ and $\mathbf{X}_\alpha + \Delta x_1 \boldsymbol{\delta}^1 \in \mathcal{M}^+$,
- if $j > 1$ there exists at most one multi-index α such that $\mathbf{X}_\alpha \in \mathcal{M}^-$ and $\mathbf{X}_\alpha + \Delta x_j \boldsymbol{\delta}^j \in \mathcal{M}^+$, and at most one multi-index α such that $\mathbf{X}_\alpha \in \mathcal{M}^-$ and $\mathbf{X}_\alpha - \Delta x_j \boldsymbol{\delta}^j \in \mathcal{M}^+$.

The subsets J_1^1 and J_j^1, J_j^2 for $j \geq 2$ are then defined as follows:

$$J_1^1 = \left\{ (\alpha)_1 \mid \mathbf{X}_\alpha \in \mathcal{M}^- \,,\, \mathbf{X}_\alpha + \Delta x_1 \boldsymbol{\delta}^1 \in \mathcal{M}^+ \right\} \,,$$

and:

$$J_j^1 = \left\{ (\alpha)_j \mid \mathbf{X}_\alpha \in \mathcal{M}^- \,,\, \mathbf{X}_\alpha + \Delta x_j \boldsymbol{\delta}^j \in \mathcal{M}^+ \right\} \,,$$
$$J_j^2 = \left\{ (\alpha)_j \mid \mathbf{X}_\alpha \in \mathcal{M}^- \,,\, \mathbf{X}_\alpha - \Delta x_j \boldsymbol{\delta}^j \in \mathcal{M}^+ \right\} \,.$$

The points $\mathbf{M}_j^-$ (as the points $\mathbf{M}_j^+$) of the mesh obtained by the above construction can be defined for all $1 \leq j \leq d$ by their abscissa α_j^1 and α_j^2 along the j-th coordinate. More precisely, if $j = 1$ and if J_1^1 is not empty (it contains a multi-index α), $\mathbf{M}_1^-$ is given by the following relation:

$$\mathbf{M}_1^- = \mathbf{X}_{(\alpha)_1} + (\alpha_1^1 - 1)\Delta x_1 \boldsymbol{\delta}^1 \,,$$

while if $j > 1$ and J_j^1 (respectively J_j^2) is not empty $\mathbf{M}_j^-$ is given in J_j^1 (resp. J_j^2) by:

$$\mathbf{M}_j^- = \mathbf{X}_{(\alpha)_j} + (\alpha_j^1 - 1)\Delta x_j \boldsymbol{\delta}^j \quad \Big(\text{resp.} \quad \mathbf{M}_j^- = \mathbf{X}_{(\alpha)_j} + (\alpha_j^2 - 1)\Delta x_j \boldsymbol{\delta}^j\Big) \,. \tag{3.6}$$

We refer again to the Figure 3.5 for an illustration of the construction of the points $\mathbf{M}_j^-$ and $\mathbf{M}_j^+$ defined above in the case of a two-dimensional problem. For $j \geq 2$, the set J_j^1 corresponds to the multi-indices $(\alpha)_j$ with $\alpha_j = 1$ for which the points $\mathbf{M}_j^-$ are "below" the interface, while set J_j^2 corresponds to that multi-indices for which the points $\mathbf{M}_j^-$ are "above" the interface. These notations will be useful for

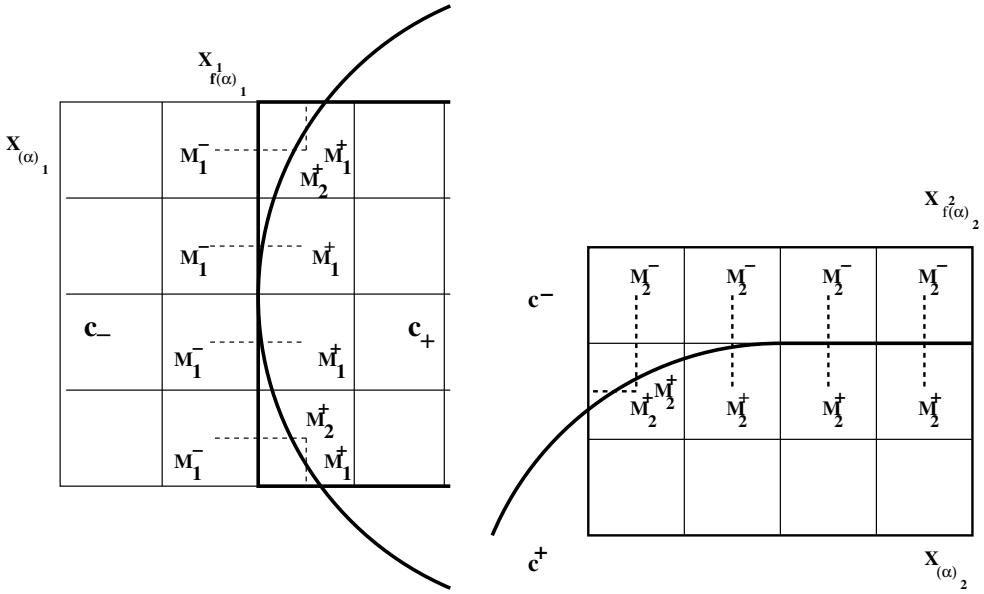

Figure 3.5: Illustration of the discretization of a curved interface on a uniform grid and construction of a couple of points $\mathbf{M}_1^-$, $\mathbf{M}_1^+$ and $\mathbf{M}_2^-$, $\mathbf{M}_2^+$.

handling curved interfaces in the subsequent parts of the thesis.

In this context, we introduce two additional definitions to describe waves crossing $\mathcal{I}$ from $\mathcal{O}^-$ to $\mathcal{O}^+$ or the other way around. Let $\mathbf{M}_j^-$ and $\mathbf{M}_j^+$ be two points of the mesh located on each side of $\mathcal{I}$, as the ones defined above, and $\mathbf{x}$ be the intersection of $\mathcal{I}$ with the segment $[\mathbf{M}_j^-, \mathbf{M}_j^+]$. A discretized wave vector $\mathbf{K}_\beta$ given on the slow side of $\mathcal{I}$ by its normal and tangential components will be said to be subcritical if:

$$\mathbf{K}_\beta \cdot \mathbf{n} < 0 \quad \text{and} \quad \mathbf{K}_\beta \cdot \mathbf{n} < \xi_c\left(\mathbf{K}'_\beta\right) \,. \tag{3.7}$$

The wave with wave vector $\mathbf{K}_\beta$ is thus crossing $\mathcal{I}$ from $\mathcal{O}^-$ to $\mathcal{O}^+$. Here:

$$\mathbf{K}'_\beta := \mathbf{K}_\beta - (\mathbf{K}_\beta \cdot \mathbf{n})\mathbf{n} \tag{3.8}$$

is the tangent component of $\mathbf{K}_\beta$ to $\mathcal{I}$, and $\xi_c(\mathbf{K}'_\beta)$ is again the critical incidence that has been defined previously by Eq. (2.24). For a wave crossing $\mathcal{I}$ from $\mathcal{O}^+$ to $\mathcal{O}^-$, $\mathbf{K}_\beta$ is subcritical if:

$$\mathbf{K}_\beta \cdot \mathbf{n} > 0 \quad \text{and} \quad \mathbf{K}_\beta \cdot \mathbf{n} > -\xi_c\left(\mathbf{K}'_\beta\right) \,. \tag{3.9}$$

The corresponding subsets of multi-indices $\mathcal{K}_c^-(\mathbf{n})$ of $\mathcal{K}^-(\mathbf{n}) = \left\{\beta \in \mathbb{Z}^d \mid \mathbf{K}_\beta \cdot \mathbf{n} > 0\right\}$ and $\mathcal{K}_c^+(\mathbf{n})$ of $\mathcal{K}^+(\mathbf{n}) = \left\{\beta \in \mathbb{Z}^d \mid \mathbf{K}_\beta \cdot \mathbf{n} < 0\right\}$ are defined by:

$$\begin{aligned} \mathcal{K}_c^-(\mathbf{n}) &= \left\{\beta \in \mathbb{Z}^d \mid \mathbf{K}_\beta \cdot \mathbf{n} > -\xi_c\left(\mathbf{K}'_\beta\right)\right\}, \\ \mathcal{K}_c^+(\mathbf{n}) &= \left\{\beta \in \mathbb{Z}^d \mid \mathbf{K}_\beta \cdot \mathbf{n} < \xi_c\left(\mathbf{K}'_\beta\right)\right\}. \end{aligned} \tag{3.10}$$

3.2 Discretization of the Liouville equation

The previous discretizations concern the phase-space variables of the problem and constitute a first step to defining discrete quantities used in the numerical schemes introduced further, such as the wave celerities and the specific intensities. They will be used to construct the discretized version of the Liouville transport equation (2.86) together with the reflection and transmission conditions (2.88) at an interface, which is expounded now. We first consider the finite difference scheme adopted for the discretization of wave transport away from the interfaces, and then detail the upwind fluxes implemented for the reflection/transmission phenomena.

3.2.1 Finite difference scheme for wave transport

The sound speeds and the specific intensities are discretized on the spatial and wave vector meshes $\mathcal{M}_{\mathbf{x}}$ and $\mathcal{M}_{\mathbf{k}}$, respectively, and the corresponding discrete values are denoted by:

$$c_\alpha = c(\mathbf{X}_\alpha), \quad \alpha = (\alpha_1, \dots \alpha_d) \in \prod_{j=1}^{d} \left\{-M_j^-, \dots M_j^+ - 1\right\}$$

and:

$$\mathrm{a}_{\alpha\beta}^n = \mathrm{a}(t_n, \mathbf{X}_\alpha, \mathbf{K}_\beta), \quad \beta = (\beta_1, \dots \beta_d) \in \prod_{j=1}^{d} \left\{-N_j, \dots N_j - 1\right\},$$

where $n \in \mathbb{N}^*$ is the index for time discretization. With the notations defined previously one has $\mathbf{X}_\alpha = (X_{\alpha_1}, \dots X_{\alpha_d})$ and $\mathbf{K}_\beta = (K_{\beta_1}, \dots K_{\beta_d})$. In order to define the numerical scheme that will allow to compute the set of values $\{\mathrm{a}_{\alpha\beta}^{n+1}\}_{\alpha\beta}$ for the time increment $t_{n+1} = t_n + \Delta t$, $n \in \mathbb{N}^*$ and $\Delta t > 0$, we introduce the following notations. If α is a given multi-index and $1 \leq j \leq d$, we denote by $\mathrm{a}_{\alpha\pm\frac{j}{2},\beta}^n$ the specific intensity values at the two face centers of the cell $\mathcal{C}_\alpha$, located respectively at the grid abscissa $X_{\alpha_j - \frac{1}{2}}$ and $X_{\alpha_j + \frac{1}{2}}$:

$$\mathrm{a}_{\alpha\pm\frac{j}{2},\beta}^n := \mathrm{a}\left(t_n, \mathbf{X}_\alpha \pm \frac{1}{2}\Delta x_j \boldsymbol{\delta}^j, \mathbf{K}_\beta\right). \tag{3.11}$$

Likewise, if β is a given multi-index and again $1 \leq j \leq d$, we denote by $\mathrm{a}_{\alpha,\beta\pm\frac{j}{2}}^n$ the specific intensity values at the two faces centers of the cell $\mathcal{C}_\beta$, located respectively at the grid abscissa $K_{\beta_j - \frac{1}{2}}$ and $K_{\beta_j + \frac{1}{2}}$:

$$\mathrm{a}_{\alpha,\beta\pm\frac{j}{2}}^n := \mathrm{a}\left(t_n, \mathbf{X}_\alpha, \mathbf{K}_\beta \pm \frac{1}{2}\Delta k_j \boldsymbol{\delta}^j\right). \tag{3.12}$$

We straightforwardly extend these notations to $\mathrm{a}_{\alpha\pm j,\beta}^n$ or $\mathrm{a}_{\alpha,\beta\pm j}^n$ defined by:

$$\begin{aligned} \mathrm{a}_{\alpha\pm j,\beta}^n &:= \mathrm{a}\left(t_n, \mathbf{X}_\alpha \pm \Delta x_j \boldsymbol{\delta}^j, \mathbf{K}_\beta\right), \\ \mathrm{a}_{\alpha,\beta\pm j}^n &:= \mathrm{a}\left(t_n, \mathbf{X}_\alpha, \mathbf{K}_\beta \pm \Delta k_j \boldsymbol{\delta}^j\right), \end{aligned} \tag{3.13}$$

respectively.

The time-incremented discretized specific intensity $\mathrm{a}_{\alpha\beta}^{n+1}$ is then computed using the following discretization of the Liouville equation:

$$\frac{\mathrm{a}_{\alpha\beta}^{n+1} - \mathrm{a}_{\alpha\beta}^n}{\Delta t} + c_\alpha \sum_{j=1}^{d} \left[\frac{K_{\beta_j}}{|\mathbf{K}_\beta|}\left(\frac{\mathrm{a}_{\alpha+\frac{j}{2},\beta}^n - \mathrm{a}_{\alpha-\frac{j}{2},\beta}^n}{\Delta x_j}\right) - |\mathbf{K}_\beta|\left(\frac{c_{\alpha+\frac{j}{2}} - c_{\alpha-\frac{j}{2}}}{\Delta x_j}\right)\left(\frac{\mathrm{a}_{\alpha,\beta+\frac{j}{2}}^n - \mathrm{a}_{\alpha,\beta-\frac{j}{2}}^n}{\Delta k_j}\right)\right] = 0, \tag{3.14}$$

where:

$$|\mathbf{K}_\beta| = \sqrt{\sum_{j=1}^{d} K_{\beta_j}^2}\,.$$

Note that in the case of a piecewise homogeneous medium, the sound speed is piecewise constant, and the third term of the above equation (3.14) vanishes. The latter thus reduces to:

$$\mathrm{a}_{\alpha\beta}^{n+1} = \mathrm{a}_{\alpha\beta}^{n} - \sum_{j=1}^{d} \frac{c_\alpha \Delta t}{\Delta x_j} \frac{K_{\beta_j}}{|\mathbf{K}_\beta|} \left(\mathrm{a}_{\alpha+\frac{j}{2},\beta}^{n} - \mathrm{a}_{\alpha-\frac{j}{2},\beta}^{n} \right) . \tag{3.15}$$

In each cell, $\mathrm{a}_{\alpha\pm\frac{j}{2},\beta}^{n}$ is defined for a given index β from the values $\mathrm{a}_{\alpha\beta}^{n}$ and $\mathrm{a}_{\alpha\pm j,\beta}^{n}$ of the discretized specific intensity in the cells $\mathcal{C}_{\alpha\pm\boldsymbol{\delta}^j}$ adjoining the cell $\mathcal{C}_\alpha$. Likewise, $\mathrm{a}_{\alpha,\beta\pm\frac{j}{2}}^{n}$ is defined for a given index α from the values $\mathrm{a}_{\alpha\,\beta}^{n}$ and $\mathrm{a}_{\alpha,\beta\pm j}^{n}$ in the wave vector cells $\mathcal{C}_{\beta\pm\boldsymbol{\delta}^j}$ adjoining the cell $\mathcal{C}_\beta$. Away from the interface, which means in cells that have no common edge with $\mathcal{I}$, these four values are given by the following upwind scheme:

$$\begin{aligned} &\mathrm{a}_{\alpha+\frac{j}{2},\beta}^{n} = \mathrm{a}_{\alpha\beta}^{n}\,, \quad \mathrm{a}_{\alpha-\frac{j}{2},\beta}^{n} = \mathrm{a}_{\alpha-j,\beta}^{n} \quad \text{if} \quad K_{\beta_j} > 0\,, \quad 1 \le j \le d\,, \\ &\mathrm{a}_{\alpha+\frac{j}{2},\beta}^{n} = \mathrm{a}_{\alpha+j,\beta}^{n}\,, \quad \mathrm{a}_{\alpha-\frac{j}{2},\beta}^{n} = \mathrm{a}_{\alpha\beta}^{n} \quad \text{if} \quad K_{\beta_j} < 0\,, \quad 1 \le j \le d\,, \end{aligned} \tag{3.16}$$

which supplements the fully discretized transport equation (3.15) in each homogeneous subdomain of $\mathcal{O}_h$. If we now treat the case of the interface, the laws (2.88) that rule the behavior of the specific intensities at $\mathcal{I}$ are used, so as to extend the above upwind scheme to the cells that have a common edge with $\mathcal{I}$. As the case of a straight interface is much easier to handle, and for better understanding, we first present this case below before considering the more general case of a curved interface.

3.2.2 Upwind fluxes for a straight interface

We first recall that if $\mathcal{I}$ is a straight interface, it is assumed to belong to the grid without loss of generality. We choose for example $\mathbf{n} = -\boldsymbol{\delta}_1$ to be a unit normal vector at $\mathcal{I}$. The abscissa index that marks $\mathcal{I}$ on the grid (see the section 3.1) is $\alpha_1 = 1$. Let $\mathbf{K}_\beta \in \mathcal{M}_\mathbf{k}$ be a discretized wave vector for a high-frequency wave located on one side of $\mathcal{I}$ and propagating away from it. Then the Snell-Descartes laws for reflection and transmission (see the section 2.1.3) are invoked in order to determine the "transmitted" and "reflected" wave vectors $\mathbf{k}_\beta^{\mathrm{T}}$ and $\mathbf{k}_\beta^{\mathrm{R}}$, respectively, that correspond to high-frequency waves that are transmitted and reflected in the direction of the actual outgoing wave vector $\mathbf{K}_\beta$ when they impinge the interface $\mathcal{I}$. Conservation of the "reflected" and "transmitted" tangential coordinates $k_{\beta_j}^{\mathrm{R}}$ and $k_{\beta_j}^{\mathrm{T}}$, $2 \le j \le d$, is expressed by (2.22), which reads in a discrete setting:

$$k_{\beta_j}^{\mathrm{R}} = k_{\beta_j}^{\mathrm{T}} = K_{\beta_j}\,, \quad 2 \le j \le d\,, \tag{3.17}$$

so that the "reflected" and "transmitted" wave vectors may be denoted simply by $\mathbf{k}_\beta^{\mathrm{R}} = (k_{\beta_1}^{\mathrm{R}}, \mathbf{K}'_\beta)$ and $\mathbf{k}_\beta^{\mathrm{T}} = (k_{\beta_1}^{\mathrm{T}}, \mathbf{K}'_\beta)$, where $\mathbf{K}'_\beta$ is the tangent component of $\mathbf{K}_\beta$ (see Eq. (3.1)).

Remark: We point out here that we adopt the following approach, which consists in computing the "transmitted" wave vector from the outgoing one initially chosen on the mesh $\mathcal{M}_\mathbf{k}$ by backward transmission, so that this "transmitted" wave vector is denoted by $\mathbf{k}_\beta^{\mathrm{T}}$ when the former is some $\mathbf{K}_\beta \in \mathcal{M}_\mathbf{k}$. The same consideration applies for the "reflected" wave vector $\mathbf{k}_\beta^{\mathrm{R}}$, which is computed by backward reflection of that $\mathbf{K}_\beta$. This point of view is imposed by the fact that an upwind flux is used in order to account for the reflection/transmission phenomena at the interface.

The "reflected" and "transmitted" normal components, respectively, are given by the Eq. (2.23):

$$k_{\beta_1}^{\mathrm{R}} = -K_{\beta_1}\,, \quad k_{\beta_1}^{\mathrm{T}} = \begin{cases} f(K_{\beta_1}, \mathbf{K}'_\beta) & \text{if} \quad K_{\beta_1} > 0 \\ g(K_{\beta_1}, \mathbf{K}'_\beta) & \text{if} \quad K_{\beta_1} < \xi_c(\mathbf{K}'_\beta) \end{cases}\,, \tag{3.18}$$

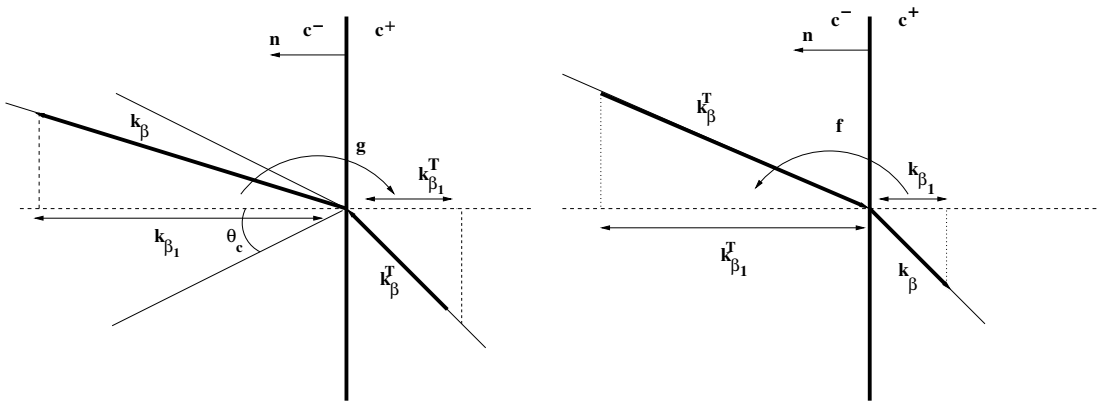

Figure 3.6: "Incident" wave vectors constructed by backward transmission of the discretized wave vector $\mathbf{k}_\beta$ on the mesh. Left figure: transmission from the slow to the fast medium; right figure: transmission from the fast to the slow medium.

where f and g are defined by:

$$\begin{aligned} f(k_{\mathbf{n}}, \mathbf{k}') &= \sqrt{\nu^2 k_{\mathbf{n}}^2 + (\nu^2 - 1)|\mathbf{k}'|^2}\,, \\ g(k_{\mathbf{n}}, \mathbf{k}') &= -\frac{1}{\nu}\sqrt{k_{\mathbf{n}}^2 + (1 - \nu^2)|\mathbf{k}'|^2}\,, \end{aligned} \tag{3.19}$$

with $\nu = \frac{c^+}{c^-} > 1$, and ξ_c is defined by Eq. (2.24). This construction is illustrated on the Figure 3.6 below. Let $\alpha = (0, \alpha_2, \dots \alpha_d)$ mark a cell adjoining $\mathcal{I}$ from the left. We define the discrete specific intensities at the cell $\mathcal{C}_\alpha$ and $\mathcal{C}_{\alpha+1}$, for waves crossing $\mathcal{I}$ from the slow to the fast medium by the following expressions:

$$\begin{cases} \mathrm{a}^n_{\alpha+\frac{1}{2},\beta} = \mathrm{a}^n_{\alpha\beta}\,, \\ \mathrm{a}^n_{\alpha+1-\frac{1}{2},\beta} = \mathcal{R}^+(k^{\mathrm{R}}_{\beta_1}, \mathbf{K}'_\beta)\tilde{\mathrm{a}}^n(\mathbf{X}_\alpha + \Delta x_1 \boldsymbol{\delta}^1, \mathbf{k}^{\mathrm{R}}_\beta) + \mathrm{b}^n_{\alpha\beta}\,, \end{cases} \quad \text{if} \quad K_{\beta_1} > 0\,, \tag{3.20}$$

while the corresponding discrete specific intensities at the cell $\mathcal{C}_{\alpha+\boldsymbol{\delta}^1}$ for waves crossing $\mathcal{I}$ from the fast to the slow medium are given by:

$$\begin{cases} \mathrm{a}^n_{\alpha+1-\frac{1}{2},\beta} = \mathrm{a}^n_{\alpha+1,\beta}\,, \\ \mathrm{a}^n_{\alpha-\frac{1}{2},\beta} = \mathcal{R}^-(k^{\mathrm{R}}_{\beta_1}, \mathbf{K}'_\beta)\tilde{\mathrm{a}}^n(\mathbf{X}_\alpha, \mathbf{k}^{\mathrm{R}}_\beta) + \mathrm{b}^n_{\alpha+1,\beta}\,, \end{cases} \quad \text{if} \quad K_{\beta_1} < 0\,. \tag{3.21}$$

In the above $\mathcal{R}^\pm(k^{\mathrm{R}}_{\beta_1}, \mathbf{K}'_\beta)$ are power flow reflection coefficients of which precise expressions are given by Eq. (2.26). The corrective quantities $\mathrm{b}^n_{\alpha\beta}$ and $\mathrm{b}^n_{\alpha+1,\beta}$ that correspond to transmitted specific intensities respectively from the slow to the fast, and from the fast to the slow medium, have the following form:

$$\begin{aligned} \mathrm{b}^n_{\alpha\beta} &= \mu^-_\beta \tilde{\mathrm{a}}^n(\mathbf{X}_\alpha, \mathbf{k}^{\mathrm{T}}_\beta)\,, \\ \mathrm{b}^n_{\alpha+1,\beta} &= \mu^+_\beta \tilde{\mathrm{a}}^n(\mathbf{X}_\alpha + \Delta x_1 \boldsymbol{\delta}^1, \mathbf{k}^{\mathrm{T}}_\beta)\,, \end{aligned} \tag{3.22}$$

where μ^-_β and μ^+_β are coefficients depending on the numerical scheme. They are given as linear functions of the power flow transmission coefficients $\mathcal{T}^\pm(k^{\mathrm{T}}_{\beta_1}, \mathbf{K}'_\beta)$ and $\mathcal{T}^\pm(k^{\mathrm{T}}_{\beta_1-1}, \mathbf{K}'_\beta)$ of Eq. (2.26). Finally $\tilde{\mathrm{a}}^n(\mathbf{X}_\alpha, \mathbf{k}^{\mathrm{R}}_\beta)$, $\tilde{\mathrm{a}}^n(\mathbf{X}_\alpha + \Delta x_1 \boldsymbol{\delta}^1, \mathbf{k}^{\mathrm{R}}_\beta)$ and $\tilde{\mathrm{a}}^n(\mathbf{X}_\alpha, \mathbf{k}^{\mathrm{T}}_\beta)$, $\tilde{\mathrm{a}}^n(\mathbf{X}_\alpha + \Delta x_1 \boldsymbol{\delta}^1, \mathbf{k}^{\mathrm{T}}_\beta)$ represent linearly interpolated, discretized specific intensities obtained by backward reflection and transmission, respectively. They have the following expressions:

$$\begin{aligned} \tilde{\mathrm{a}}^n(\mathbf{X}_\alpha, \mathbf{k}^{\mathrm{T}}_\beta) &= C^-_0\, \mathrm{a}^n_{\alpha\beta^{\mathrm{T}}} + C^-_1\, \mathrm{a}^n_{\alpha,\beta^{\mathrm{T}}+1}\,, \\ \tilde{\mathrm{a}}^n(\mathbf{X}_\alpha + \Delta x_1 \boldsymbol{\delta}^1, \mathbf{k}^{\mathrm{R}}_\beta) &= \frac{K_{\beta^{\mathrm{R}}_1+1} - k^{\mathrm{R}}_{\beta_1}}{\Delta k_1}\mathrm{a}^n_{\alpha+1,\beta^{\mathrm{R}}} + \frac{k^{\mathrm{R}}_{\beta_1} - K_{\beta^{\mathrm{R}}_1}}{\Delta k_1}\mathrm{a}^n_{\alpha+1,\beta^{\mathrm{R}}+1}\,, \end{aligned} \tag{3.23}$$

as regards transmission from the slow to the fast medium ($K_{\beta_1} > 0$), and:

$$\begin{aligned} \tilde{\mathrm{a}}^n(\mathbf{X}_\alpha + \Delta x_1 \boldsymbol{\delta}_1, \mathbf{k}^{\mathrm{T}}_\beta) &= C_0^+ \mathrm{a}^n_{\alpha+1,\beta^{\mathrm{T}}} + C_1^+ \mathrm{a}^n_{\alpha+1,\beta^{\mathrm{T}}+1}\,, \\ \tilde{\mathrm{a}}^n(\mathbf{X}_\alpha, \mathbf{k}^{\mathrm{R}}_\beta) &= \frac{K_{\beta_1^{\mathrm{R}}+1} - k^{\mathrm{R}}_{\beta_1}}{\Delta k_1} \mathrm{a}^n_{\alpha\beta^{\mathrm{R}}} + \frac{k^{\mathrm{R}}_{\beta_1} - K_{\beta_1^{\mathrm{R}}}}{\Delta k_1} \mathrm{a}^n_{\alpha,\beta^{\mathrm{R}}+1}\,, \end{aligned} \tag{3.24}$$

as regards transmission from the fast to the slow medium ($K_{\beta_1} < 0$). In the above $C_0^\pm$ and $C_1^\pm$ are positive coefficients that, again, depend on the numerical scheme, and β^{R} and β^{T} denote the following multi-indices:

$$\begin{aligned} \beta^{\mathrm{R}} &= (\beta)_1 + \left(\mathrm{Nd}^1\left(k^{\mathrm{R}}_{\beta_1}\right) - 1\right)\boldsymbol{\delta}^1\,, \\ \beta^{\mathrm{T}} &= (\beta)_1 + \left(\mathrm{Nd}^1\left(k^{\mathrm{T}}_{\beta_1}\right) - 1\right)\boldsymbol{\delta}^1\,. \end{aligned}$$

We observe that $\mathbf{k}^{\mathrm{T}}_\beta$ is interpolated on the mesh $\mathcal{M}_{\mathbf{k}}$ between the two discretized vectors $\mathbf{K}_{\beta^{\mathrm{T}}}$ and $\mathbf{K}_{\beta^{\mathrm{T}}+1}$, because it does not belong to the mesh *a priori*. On the contrary the normal component $k^{\mathrm{R}}_{\beta_1}$ of the reflected vector does, as one can verify it with the definition (3.18) and the symmetry of the set $\{K_{\beta_1}\}_{-N_1 \le \beta_1 \le N_1 - 1}$ about 0. More precisely for a given vector $\mathbf{K}_\beta = (K_{\beta_1}, \dots K_{\beta_d})$, one can verify that its image by specular reflection on $\mathcal{I}$ reads:

$$\mathbf{k}^{\mathrm{R}}_\beta = \left(k^{\mathrm{R}}_{\beta_1}, \mathbf{K}'_\beta\right) \quad \text{with} \quad k^{\mathrm{R}}_{\beta_1} = K_{-\beta_1+1}\,, \tag{3.25}$$

which means that $\mathbf{k}^{\mathrm{R}}_\beta = \mathbf{K}_{\beta^{\mathrm{R}}}$ for $\beta^{\mathrm{R}} = (-\beta_1 + 1, \beta_2, \dots \beta_d)$. In the particular case of a straight interface, this allows to give an equivalent definition of the discretized specific intensities obtained by reflection:

$$\tilde{\mathrm{a}}^n(\mathbf{X}_\alpha, \mathbf{k}^{\mathrm{R}}_\beta) = \mathrm{a}^n_{\alpha\beta^{\mathrm{R}}}\,, \tag{3.26}$$

for α neighboring the interface $\mathcal{I}$, such that $\alpha_1 = 0$ or $\alpha_1 = 1$.

3.2.3 Upwind fluxes for a curved interface

We now suppose that $\mathcal{I}$ is a curved interface, that has been discretized on the regular space grid $\mathcal{G}_{\mathbf{x}}$ as described in the previous section 3.1.2. We make the assumption that Snell-Descartes laws can be applied at a point $\mathbf{x}$ of $\mathcal{I}$ by approximating $\mathcal{I}$ by its tangent plane defined by the unit normal $\mathbf{n}$ at that point, as introduced above in the section 3.1.2 (see also the figure 3.7 below for an illustration). The previous expressions (2.22) and (2.23) used in the case of a straight interface to determine the normal and tangent components of the "reflected" and "transmitted" wave vectors in Eq. (3.18) are replaced here by the expressions (2.50) as follows. Let $\mathbf{K}_\beta$ be an "incident" wave vector (for a high-frequency wave propagating away from the interface), we denote by $\mathbf{K}_\beta \cdot \mathbf{n}$ its normal component and by $\mathbf{K}'_\beta$ its tangential one, as in Eq. (3.8). Then the corresponding "reflected" and "transmitted" wave vectors denoted by $\mathbf{k}^{\mathrm{R}}_\beta$ and $\mathbf{k}^{\mathrm{T}}_\beta$, respectively, are given by their tangential and normal components as:

$$\begin{aligned} (\mathbf{I} - \mathbf{n}\otimes\mathbf{n})\mathbf{k}^{\mathrm{R}}_\beta = (\mathbf{I} - \mathbf{n}\otimes\mathbf{n})\mathbf{k}^{\mathrm{T}}_\beta &= \mathbf{K}'_\beta\,, \\ \mathbf{k}^{\mathrm{R}}_\beta \cdot \mathbf{n} &= -\mathbf{K}_\beta \cdot \mathbf{n}\,, \\ \mathbf{k}^{\mathrm{T}}_\beta \cdot \mathbf{n} &= -f(\mathbf{K}_\beta \cdot \mathbf{n},\, \mathbf{K}'_\beta) \quad \text{if} \quad \mathbf{K}_\beta \cdot \mathbf{n} < 0 \end{aligned} \tag{3.27}$$

for transmission from the slow to the fast medium ($\mathbf{K}_\beta$ corresponds to a wave propagating on the fast side of $\mathcal{I}$), and by:

$$\begin{aligned} (\mathbf{I} - \mathbf{n}\otimes\mathbf{n})\mathbf{k}^{\mathrm{R}}_\beta = (\mathbf{I} - \mathbf{n}\otimes\mathbf{n})\mathbf{k}^{\mathrm{T}}_\beta &= \mathbf{K}'_\beta\,, \\ \mathbf{k}^{\mathrm{R}}_\beta \cdot \mathbf{n} &= -\mathbf{K}_\beta \cdot \mathbf{n}\,, \\ \mathbf{k}^{\mathrm{T}}_\beta \cdot \mathbf{n} &= -g(\mathbf{K}_\beta \cdot \mathbf{n},\, \mathbf{K}'_\beta) \quad \text{if} \quad \mathbf{K}_\beta \cdot \mathbf{n} > -\xi_c\left(\mathbf{K}'_\beta\right)\,, \end{aligned} \tag{3.28}$$

for transmission from the fast to the slow medium ($\mathbf{K}_\beta$ corresponds to a wave propagating on the slow side of $\mathcal{I}$). Again $\xi_c(\mathbf{K}'_\beta)$ denotes the critical incidence defined by (2.24). Then the coordinates of $\mathbf{k}^{\mathrm{R}}_\beta$ and

$\mathbf{k}_\beta^{\mathrm{T}}$ in the canonical basis of $\mathbb{R}^d$ can be computed from the above expressions. Indeed, the correspondence between the coordinates of any vector $\mathbf{K}_\beta$ in this very basis and its coordinates in the local tangent plane is given by:

$$\begin{pmatrix} K_{\beta_1} \\ \vdots \\ K_{\beta_d} \end{pmatrix} = Q \begin{pmatrix} \mathbf{K}_\beta \cdot \mathbf{n} \\ \mathbf{K}'_\beta \end{pmatrix},$$

where Q is the rotation matrix of which columns are given by the coordinates of $\mathbf{n}$ and the tangent vectors to the interface $\mathcal{I}$ in the canonical basis of $\mathbb{R}^d$.

An expression of the specific intensity for the cells below the interface: $(\alpha)_j \in J_j^1$

We recall that only interfaces of type B are considered here, such that for all $\mathbf{x}$ on $\mathcal{I}$, $\mathbf{n}(\mathbf{x}) \cdot \boldsymbol{\delta}^1 < 0$. Let

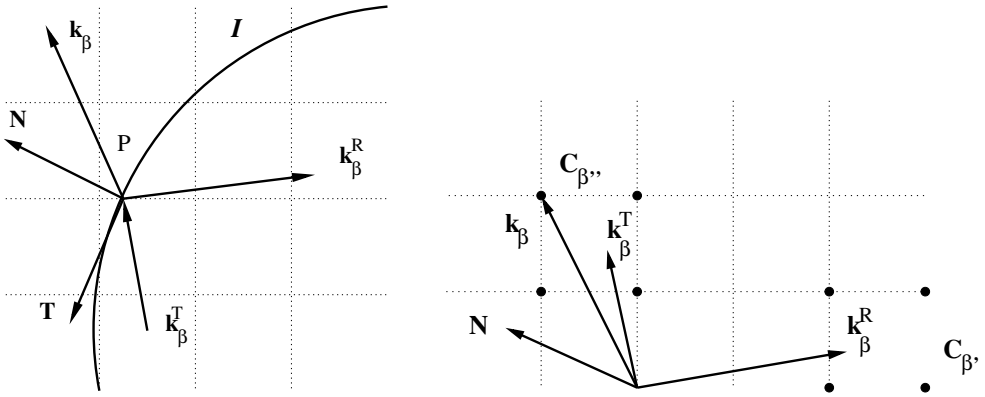

Figure 3.7: "Reflected" and "transmitted" wave vectors at a curved interface $\mathcal{I}$ and their interpolation on the mesh of discretized wave vectors.

then α be a multi-index, we adopt the notations defined in the section 2.1.3 and suppose that $(\alpha)_j \in J_j^1$, so that we can introduce $\alpha' = (\alpha)_j + \alpha_j^1 \boldsymbol{\delta}^j$ for $1 \leq j \leq d$, which is defined in such a way that the segment line or the rectangle defined by the set of points:

$$\left\{ \mathbf{X}_{\alpha'+\frac{1}{2}} + \frac{1}{2} \left(\Delta x_j \boldsymbol{\delta}^j + \sum_{l=1,\, l\neq j}^{d} (-1)^{r_l} \Delta x_l \boldsymbol{\delta}^l \right),\ r_l \in \{0,1\} \right\}$$

belongs to the grid. The discrete specific intensities $\mathrm{a}^n_{\alpha'+\frac{j}{2},\beta}$ and $\mathrm{a}^n_{\alpha'+j-\frac{j}{2},\beta}$ are defined to take into account the reflection and transmission phenomena as described below. The specific intensities defined for the cells that have a common edge with $\mathcal{I}$ are given by:

$$\begin{cases} \mathrm{a}^n_{\alpha'+\frac{j}{2},\beta} = \mathrm{a}^n_{\alpha'\beta} \\ \mathrm{a}^n_{\alpha'+j-\frac{j}{2},\beta} = \mathcal{R}^+(\mathbf{K}_\beta \cdot \mathbf{n}, \mathbf{K}'_\beta) \tilde{\mathrm{a}}^n(\mathbf{X}_{\alpha'} + \Delta x_j \boldsymbol{\delta}^j, \mathbf{k}^{\mathrm{R}}_\beta) + \mathrm{b}^n_{\alpha'\beta} \end{cases} \quad \text{if} \quad \mathbf{K}_\beta \cdot \mathbf{n} < 0 \tag{3.29}$$

for the waves crossing $\mathcal{I}$ from the slow to the fast medium, while equivalent expressions for transmission from the fast to the slow medium are given by:

$$\begin{cases} \mathrm{a}^n_{\alpha'+\frac{j}{2},\beta} = \mathcal{R}^-(\mathbf{K}_\beta \cdot \mathbf{n}, \mathbf{K}'_\beta) \tilde{\mathrm{a}}^n(\mathbf{X}_{\alpha'}, \mathbf{k}^{\mathrm{R}}_\beta) + \mathrm{b}^n_{\alpha'+j,\beta} \\ \mathrm{a}^n_{\alpha'+j-\frac{j}{2},\beta} = \mathrm{a}^n_{\alpha'+j,\beta} \end{cases} \quad \text{if} \quad \mathbf{K}_\beta \cdot \mathbf{n} > 0\,. \tag{3.30}$$

$\mathbf{k}^{\mathrm{R}}_\beta$ above as well as $\mathbf{k}^{\mathrm{T}}_\beta$ denote the "reflected" and the "transmitted" wave vectors, respectively, that have just been defined by their tangential and normal components in the local basis $(\mathbf{n}, \mathbf{t}_j, j \geq 2)$ in

Eqs. (3.27)–(3.28). The corrective quantities $\mathrm{b}^n_{\alpha'\beta}$ and $\mathrm{b}^n_{\alpha'+j,\beta}$, which represent the contribution to the specific intensities $\mathrm{a}^n_{\alpha'\pm\frac{j}{2},\beta}$ arising from transmission, depend on the numerical scheme and have the following form:

$$\begin{aligned} \mathrm{b}^n_{\alpha'\beta} &= \mu^-_\beta \tilde{\mathrm{a}}^n(\mathbf{X}_{\alpha'}, \mathbf{k}^{\mathrm{T}}_\beta)\,, \\ \mathrm{b}^n_{\alpha'+j,\beta} &= \mu^+_\beta \tilde{\mathrm{a}}^n(\mathbf{X}_{\alpha'} + \Delta x_j \boldsymbol{\delta}^j, \mathbf{k}^{\mathrm{T}}_\beta)\,, \end{aligned} \tag{3.31}$$

where μ^-_β and μ^+_β are weighting functions depending on the power flow transmission coefficients $\mathcal{T}^-(f(\mathbf{K}_\beta \cdot \mathbf{n}, \mathbf{K}'_\beta), \mathbf{K}'_\beta)$ and $\mathcal{T}^+(g(\mathbf{K}_\beta \cdot \mathbf{n}, \mathbf{K}'_\beta), \mathbf{K}'_\beta)$. The reflection and transmission coefficients $\mathcal{T}^\pm$ and $\mathcal{R}^\pm$ used above follow easily from the previous results of the section 2.1.3. The quantities $\tilde{\mathrm{a}}^n(\mathbf{X}_{\alpha'}, \mathbf{k}^{\mathrm{R}}_\beta)$ and $\tilde{\mathrm{a}}^n(\mathbf{X}_{\alpha'} + \Delta x_j \boldsymbol{\delta}^j, \mathbf{k}^{\mathrm{R}}_\beta)$, or $\tilde{\mathrm{a}}^n(\mathbf{X}_{\alpha'}, \mathbf{k}^{\mathrm{T}}_\beta)$ and $\tilde{\mathrm{a}}^n(\mathbf{X}_{\alpha'} + \Delta x_j \boldsymbol{\delta}^j, \mathbf{k}^{\mathrm{T}}_\beta)$, are discretized specific intensities obtained by backward reflection and transmission. They are interpolated on the wave vector mesh $\mathcal{M}_{\mathbf{k}}$ as follows. Let the multi-indices β^{R} and β^{T} be defined by their components:

$$\begin{aligned} \beta^{\mathrm{R}}_j &= \mathrm{Nd}^j\left(k^{\mathrm{R}}_{\beta_j}\right)\,, \\ \beta^{\mathrm{T}}_j &= \mathrm{Nd}^j\left(k^{\mathrm{T}}_{\beta_j}\right)\,, \end{aligned} \tag{3.32}$$

for $1 \le j \le d$. In both cases $\mathbf{K}_\beta \cdot \mathbf{n} \lesseqgtr 0$, the "reflected" discretized specific intensities obtained by backward reflection are given by:

$$\begin{aligned} \tilde{\mathrm{a}}^n(\mathbf{X}_{\alpha'}, \mathbf{k}^{\mathrm{R}}_\beta) &= \sum_{u\in\{0,1\}^d} C^-_{\beta^{\mathrm{R}}+\boldsymbol{\delta}^u} \mathrm{a}^n_{\alpha',\beta^{\mathrm{R}}+\boldsymbol{\delta}^u} \quad \text{if} \quad \mathbf{K}_\beta \cdot \mathbf{n} > 0\,, \\ \tilde{\mathrm{a}}^n(\mathbf{X}_{\alpha'} + \Delta x_j \boldsymbol{\delta}^j, \mathbf{k}^{\mathrm{R}}_\beta) &= \sum_{u\in\{0,1\}^d} C^+_{\beta^{\mathrm{R}}+\boldsymbol{\delta}^u} \mathrm{a}^n_{\alpha'+j,\beta^{\mathrm{R}}+\boldsymbol{\delta}^u} \quad \text{if} \quad \mathbf{K}_\beta \cdot \mathbf{n} < 0\,, \end{aligned} \tag{3.33}$$

where $\boldsymbol{\delta}^u = \sum_{j=1}^d u_j \boldsymbol{\delta}^j$. This means that they are interpolated on the edges of the wave vector cell $\mathcal{C}_{\beta^{\mathrm{R}}}$ to which $\mathbf{k}^{\mathrm{R}}_\beta$ belongs (see the Figure 3.7 for an illustration). In the above the constants $C^\pm_{\beta^{\mathrm{R}}+\boldsymbol{\delta}^u}$ for $u \in \{0,1\}^d$ are positive interpolation coefficients depending on the numerical scheme. Finally, $\tilde{\mathrm{a}}^n(\mathbf{X}_{\alpha'}, \mathbf{k}^{\mathrm{T}}_\beta)$ and $\tilde{\mathrm{a}}^n(\mathbf{X}_{\alpha'} + \Delta x_j \boldsymbol{\delta}^j, \mathbf{k}^{\mathrm{T}}_\beta)$ represent "transmitted" discretized specific intensities obtained by backward transmission. They are interpolated on the edges of the cell $\mathcal{C}_{\beta^{\mathrm{T}}}$ in the same manner as the ones obtained by reflection:

$$\begin{aligned} \tilde{\mathrm{a}}^n(\mathbf{X}_{\alpha'}, \mathbf{k}^{\mathrm{T}}_\beta) &= \sum_{u\in\{0,1\}^d} \Gamma^-_{\beta^{\mathrm{T}}+\boldsymbol{\delta}^u} \mathrm{a}^n_{\alpha',\beta^{\mathrm{T}}+\boldsymbol{\delta}^u} \quad \text{if} \quad \mathbf{K}_\beta \cdot \mathbf{n} < 0\,, \\ \tilde{\mathrm{a}}^n(\mathbf{X}_{\alpha'} + \Delta x_j \boldsymbol{\delta}^j, \mathbf{k}^{\mathrm{T}}_\beta) &= \sum_{u\in\{0,1\}^d} \Gamma^+_{\beta^{\mathrm{T}}+\boldsymbol{\delta}^u} \mathrm{a}^n_{\alpha'+j,\beta^{\mathrm{T}}+\boldsymbol{\delta}^u} \quad \text{if} \quad \mathbf{K}_\beta \cdot \mathbf{n} > 0\,, \end{aligned} \tag{3.34}$$

where the coefficients $\Gamma^\pm_{\beta^{\mathrm{T}}+\boldsymbol{\delta}^u}$, $u \in \{0,1\}^d$, are positive and depend on the numerical scheme.

An expression of the specific intensities for the cells above the interface: $(\alpha)_j \in J^2_j$

Similarly if we consider now that $(\alpha)_j \in J^2_j$ for $2 \le j \le d$, we can introduce $\alpha'' = (\alpha)_j + \alpha^2_j \boldsymbol{\delta}^j$, which is defined in such a way that the segment line or the rectangle defined by the following set of points:

$$\left\{ \mathbf{X}_{\alpha''-\frac{1}{2}} + \frac{1}{2}\left(-\Delta x_j \boldsymbol{\delta}^j + \sum_{l=1, l\neq j}^{d} (-1)^{r_l} \Delta x_l \boldsymbol{\delta}^l \right)\,,\ r_l \in \{0,1\} \right\}$$

belongs to the grid. The quantities:

$$\mathrm{a}^n_{\alpha''-j+\frac{j}{2},\beta}\,, \quad \mathrm{a}^n_{\alpha''-\frac{j}{2},\beta}\,,$$

are defined to take into account the reflection and transmission phenomena as described here. Let β^{R} and β^{T} be defined by their components exactly as above, Eq. (3.32), the discrete specific intensities defined

for cells that have a common edge with $\mathcal{I}$ are given for transmission from the slow to the fast medium by:

$$\begin{cases} \mathrm{a}^n_{\alpha''-j+\frac{j}{2},\beta} = \mathcal{R}^+(\mathbf{K}_\beta\cdot\mathbf{n},\mathbf{K}'_\beta)\tilde{\mathrm{a}}^n(\mathbf{X}_{\alpha''}-\Delta x_j\boldsymbol{\delta}^j,\mathbf{k}^{\mathrm{R}}_\beta)+\mathrm{b}^n_{\alpha''\beta}\,, \\ \mathrm{a}^n_{\alpha''-\frac{j}{2},\beta} = \mathrm{a}^n_{\alpha''\beta}\,, \end{cases} \quad \text{if} \quad \mathbf{K}_\beta\cdot\mathbf{n}<0 \tag{3.35}$$

and for transmission from the fast to the slow medium by:

$$\begin{cases} \mathrm{a}^n_{\alpha''-\frac{j}{2},\beta} = \mathcal{R}^-(\mathbf{K}_\beta\cdot\mathbf{n},\mathbf{K}'_\beta)\tilde{\mathrm{a}}^n(\mathbf{X}_{\alpha'},\mathbf{k}^{\mathrm{R}}_\beta)+\mathrm{b}^n_{\alpha''-j,\beta}\,, \\ \mathrm{a}^n_{\alpha''-j+\frac{j}{2},\beta} = \mathrm{a}^n_{\alpha''-j,\beta}\,, \end{cases} \quad \text{if} \quad \mathbf{K}_\beta\cdot\mathbf{n}>0\,, \tag{3.36}$$

where $\mathbf{k}^{\mathrm{R}}_\beta$, $\mathbf{k}^{\mathrm{T}}_\beta$ and $\mathbf{K}_\beta$ still denote the "reflected", "transmitted" and "incident" (actual) discrete wave vectors, respectively. The corrective discrete specific intensities $\mathrm{b}^n_{\alpha''\beta}$ and $\mathrm{b}^n_{\alpha''-j,\beta}$ obtained by backward transmission depend on the numerical scheme, and have the following form:

$$\begin{aligned} \mathrm{b}^n_{\alpha''-j,\beta} &= \mu^+_\beta\tilde{\mathrm{a}}^n(\mathbf{X}_{\alpha''}-\Delta x_j\boldsymbol{\delta}^j,\,\mathbf{k}^{\mathrm{T}}_\beta)\,, \\ \mathrm{b}^n_{\alpha''\beta} &= \mu^-_\beta\tilde{\mathrm{a}}^n(\mathbf{X}_{\alpha''},\,\mathbf{k}^{\mathrm{T}}_\beta)\,, \end{aligned}$$

where μ^-_β and μ^+_β denote again linear functions of the power flow transmission coefficients $\mathcal{T}^-(f(\mathbf{K}_\beta\cdot\mathbf{n},\mathbf{K}'_\beta),\mathbf{K}'_\beta)$ and $\mathcal{T}^+(g(\mathbf{K}_\beta\cdot\mathbf{n},\mathbf{K}'_\beta),\mathbf{K}'_\beta)$. Now when $(\alpha'')_j\in J^2_j$, the same approach as the one outlined in the foregoing paragraph can be used in order to define the interpolations of $\tilde{\mathrm{a}}^n(\mathbf{X}_{\alpha''}-\Delta x_j\boldsymbol{\delta}^j,\mathbf{k}^{\mathrm{T}}_\beta)$ and $\tilde{\mathrm{a}}^n(\mathbf{X}_{\alpha''},\mathbf{k}^{\mathrm{T}}_\beta)$ on the wave vector mesh $\mathcal{M}_{\mathbf{k}}$, see Eq. (3.33) and Eq. (3.34). It will however not be detailed here.

3.2.4 Outcome on the upwind fluxes

Now the previous equations (3.20) and (3.21) for a straight interface or (3.29) and (3.30) for a curved interface define the general form of the numerical schemes that will be used throughout in the remaining of this thesis. The following chapter presents in particular the different numerical methods that have been implemented in order to correct the difficulties raised at the beginning of this chapter. They are discussed in detail in the following section 3.4 for the case of a straight interface. The corrective schemes basically focus on the construction of the various interpolating coefficients introduced above, such as μ^-_β and μ^+_β, $C^\pm_0$ and $C^\pm_1$, $C^\pm_{\beta^{\mathrm{R}}+\boldsymbol{\delta}^u}$ and $\Gamma^\pm_{\beta^{\mathrm{T}}+\boldsymbol{\delta}^u}$, so as to conserve the energy propagated by the underlying FD scheme. In the next section though we first recall the order of convergence of the method, which is illustrated by the numerical examples of the chapter 5.

3.3 Error and order of convergence of the FD scheme

As illustrated in the next chapters, it is possible to compute the exact solution to the problem (2.86) with initial conditions (2.87), in case of reflection and transmission on a straight interface (see the Appendix H). This allows to compare the approximated numerical solutions obtained to the exact ones, and to estimate the L^2 error of the numerical solution. The results obtained by numerical simulations with the scheme introduced above show that the error remains relatively important. More precisely, it can be shown that the L^1 error (and thus the L^2 error) of the FD method presented above for solving a first-order Liouville equation, is of order $\mathrm{O}(\sqrt{\Delta x})$ in the space variable, where Δx is the typical space step, when the solution is discontinuous. We refer to the theory established by Kuznetsov [69]. Note that in the case of regular initial conditions, and far from the interface, the scheme is of order 1 in the space and time variable (we have a first order approximation of the derivatives by the numerical scheme, which means that the error is linear in the space and time variables). We refer for instance to [44]. Besides, the influence of boundary conditions on the convergence and stability properties is analyzed in *e.g.* [24, 25, 56, 57].

3.4 Discussion about the transmission of waves between a fast and a slow medium

Numerical simulations of the propagation of an acoustic wave in a piecewise homogeneous sub-domain of $\mathcal{O}_h$ by the high-frequency model considered in this work can be summarized as follows. The evolution of the associated specific intensity $\mathrm{a}^+(t,\mathbf{x},\mathbf{k})$ discretized on a uniform grid of wave vectors, is given by the discretized Liouville equation (3.15) in each homogeneous sub-domain of $\mathcal{O}_h$. At an interface $\mathcal{I}$, the reflection and transmission phenomena arising from the difference of speeds between both sub-domains on both sides must be taken into account in the derivation of the numerical schemes, as outlined before. The evolution of the specific intensity is then given by Snell-Descartes laws, that describe the relations between the incident, reflected and transmitted wave vectors at an interface. They correspond to the relations (2.23) and (2.50) of the previous chapter. They underline the fact that the difference of speed between the slow and the fast medium induces two scales of distributions among the wave vectors on each side of $\mathcal{I}$. This difference of distribution raises the question of the interpolation of the specific intensity on the mesh of the discretized wave vectors when it is transmitted through $\mathcal{I}$; see the sections 3.2.2 and 3.2.3. We illustrate this approach in the next paragraph from a discrete point of view. For purposes of simplification, the discussion is limited to the case of a straight interface $\mathcal{I}$ where the unit normal vector is given by $\mathbf{n}=-\boldsymbol{\delta}^1$, though the subsequent analysis applies to curved interfaces as well without any loss of generality.

3.4.1 Transmission from the slow to the fast medium

Let us consider at first the transmission from $\mathcal{O}_h^-$ to $\mathcal{O}_h^+$. As in the section 3.2.2, $\mathbf{K}_\beta \in \mathcal{M}_{\mathbf{k}}$ is the discretized wave vector for a high-frequency wave located on the fast side of $\mathcal{I}$ and propagating away from it ($K_{\beta_1}>0$). The relation between the "transmitted" and "incident" wave vectors $\mathbf{k}_\beta^{\mathrm{T}}$ and $\mathbf{K}_\beta$, respectively, is given by the second line of (2.23), and reads:

$$\left(\frac{k_{\beta_1}^{\mathrm{T}}}{c^+}\right)^2=\left(\frac{K_{\beta_1}}{c^-}\right)^2+\left[\left(\frac{1}{c^-}\right)^2-\left(\frac{1}{c^+}\right)^2\right]|\mathbf{K}'_\beta|^2\,,$$

where $|\mathbf{K}'_\beta|^2=\sum_{j=2}^d K_{\beta_j}^2$, which shows that the scale of variation of $k_{\beta_1}^{\mathrm{T}}$ on the slow side of $\mathcal{I}$ is c^+, while the scale of variation of K_{β_1} on the fast side of $\mathcal{I}$ is c^-. Another way to formulate this observation is the following. For f defined by Eq. (3.19), consider the set:

$$\mathcal{F}_\beta^{\mathrm{T}}=\left\{\mathbf{k}_\beta^{\mathrm{T}}=(f(\mathbf{K}_{(\beta)_1}+(\beta'_1-1)\Delta k_1\boldsymbol{\delta}^1),\mathbf{K}'_\beta)\mid 1\le\beta'_1\le N_1\right\}$$

of subcritical "transmitted" wave vectors computed by backward transmission through $\mathcal{I}$ of $\mathbf{K}_\beta$ on the mesh $\mathcal{M}_{\mathbf{k}}$ of discretized wave vectors. The former are represented by triangles ▲ on the Figure 3.8, while the latter correspond to the dots · on this plot. It is observed that the "transmitted" wave vectors do not belong to the mesh $\mathcal{M}_{\mathbf{k}}$. Thus the discretized specific intensities $\tilde{\mathrm{a}}^n(\mathbf{X}_{\alpha'},\mathbf{k}_\beta^{\mathrm{T}})$ of Eq. (3.23) or Eq. (3.34) may be constructed with the help of a two-point interpolation as follows. Let β'_1 be defined by $\beta'_1=\mathrm{Nd}^1\left(f(\mathbf{K}_\beta)\right)$ where Nd^1 is given by Eq. (3.3), the specific intensity $\tilde{\mathrm{a}}^n(\mathbf{X}_{\alpha'},\mathbf{k}_\beta^{\mathrm{T}})$ is interpolated on $\mathcal{M}_{\mathbf{k}}$ between the two points:

$$\mathbf{K}_{(\beta)_1}+(\beta'_1-1)\Delta k_1\boldsymbol{\delta}^1\quad\text{and}\quad\mathbf{K}_{(\beta)_1}+\beta'_1\Delta k_1\boldsymbol{\delta}^1\,,\tag{3.37}$$

with the form of interpolation given by Eq. (3.23) or Eq. (3.34). These interpolation wave vectors correspond to both circles ∘ that frame each "transmitted" wave vector mentioned previously on the Figure 3.8. Now it is seen on this plot that the discretized wave vectors used for the interpolation do not map the whole mesh of discretized subcritical wave vectors, so that the upwind flux of Eq. (3.23) does not consider any of the discretized wave vectors which are not circled on the Figure 3.8. Introducing the sets of multi-indices:

$$\begin{aligned}J^+&=\left\{\beta\in\mathcal{M}_{\mathbf{k}}\mid\beta_1=\mathrm{Nd}^1\left(f(\mathbf{K}_{(\beta)_1}+(\beta'_1-1)\Delta k_1\boldsymbol{\delta}^1)\right),\,1\le\beta'_1\le N_1\right\}\,,\\ J^{+1}&=J^+\cup\left\{\beta\in\mathcal{M}_{\mathbf{k}}\mid\beta_1=1+\mathrm{Nd}^1\left(f(\mathbf{K}_{(\beta)_1}+(\beta'_1-1)\Delta k_1\boldsymbol{\delta}^1)\right),\,1\le\beta'_1\le N_1\right\}\,,\end{aligned}\tag{3.38}$$

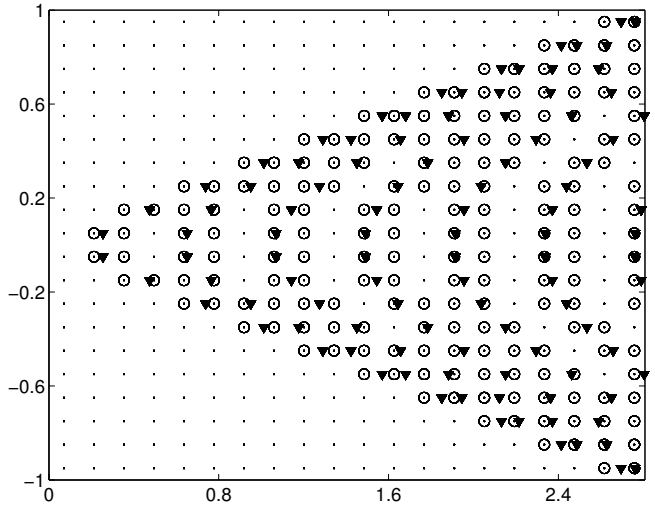

Figure 3.8: Repartition of "transmitted" wave vectors (represented by triangles ▼) computed from the discretized wave vectors by backward transmission from a slow medium $c^- = 1.0$ to a fast medium $c^+ = 3.0$, among their interpolation vectors (represented by circles o) on a regular mesh (represented by the dots ·).

then J^{+1} is nothing but the set of the multi-indices for the discretized wave vectors used by the two-points interpolation. However it may happen that when the ratio $\nu = \frac{c^+}{c^-}$ becomes too large, this set does not cover all possible indices for discretized "transmitted" wave vectors. That is, one may have:

$$J^{+1} \neq \mathcal{K}_c^+ \,,$$

where $\mathcal{K}_c^+$ has been defined above by Eq. (3.5). This particular case is again illustrated by the Figure 3.8, on which the set of subcritical wave vectors $\mathcal{F}_\beta^{\mathrm{T}}$ is displayed for $(\beta_2, \dots \beta_d) \in \prod_{j=2}^d \{-N_j, \dots N_j\}$ together with their interpolation points. We observe that the distribution of wave vectors imaged by the function f is not regular enough among the discretized transmitted wave vectors, such that a two-point interpolation of $\mathrm{b}^n_{\alpha'\beta}$ and $\mathrm{b}^n_{\alpha'+j,\beta}$ (see Eq. (3.22) for a straight interface or Eq. (3.31) for a curved interface) may be unadapted.

3.4.2 Transmission from the fast to the slow medium

Let us now consider the situation of transmission from the domain $\mathcal{O}_h^+$ to the domain $\mathcal{O}_h^-$. The difference of scale in the distribution of "transmitted" wave vectors is rather an advantage in terms of interpolation in this case. Again, $\mathbf{K}_\beta \in \mathcal{M}_{\mathbf{k}}$ is the discretized, subcritical wave vector for a high-frequency wave located on the slow side of $\mathcal{I}$ and propagating away from it ($K_{\beta_1} < \xi_c(\mathbf{K}'_\beta)$). We consider the set of "transmitted" wave vectors obtained by backward transmission:

$$\mathcal{G}_\beta^{\mathrm{T}} = \left\{ \mathbf{k}_\beta^{\mathrm{T}} = (g(\mathbf{K}_{(\beta)_1} + (\beta'_1 - 1)\Delta k_1 \boldsymbol{\delta}^1), \mathbf{K}'_\beta) \mid K_{\beta'_1} < \xi_c(\mathbf{K}'_\beta) \right\} ,$$

where g is given in Eq. (3.19). A short study shows that for all $\beta''_1 \leq \beta_c^-$ where β_c^- is given by Eq. (3.4), the following inequality holds:

$$|g(\mathbf{K}_{(\beta)_1} + (\beta''_1 - 1)\Delta k_1 \boldsymbol{\delta}^1) - g(\mathbf{K}_{(\beta)_1} + \beta''_1 \Delta k_1 \boldsymbol{\delta}^1)| < \Delta k_1 \,,$$

since the gradient of g is lower than 1 on this set of coordinates. In fact, one observes that $k \mapsto g(k)$ has an asymptotic direction $k \mapsto \frac{k}{\nu}$ as k goes to $-\infty$ whenever $\nu > 1$. The above condition is thus a sufficient condition for a two-point interpolation to be appropriate. This can be interpretated as follows. Let then

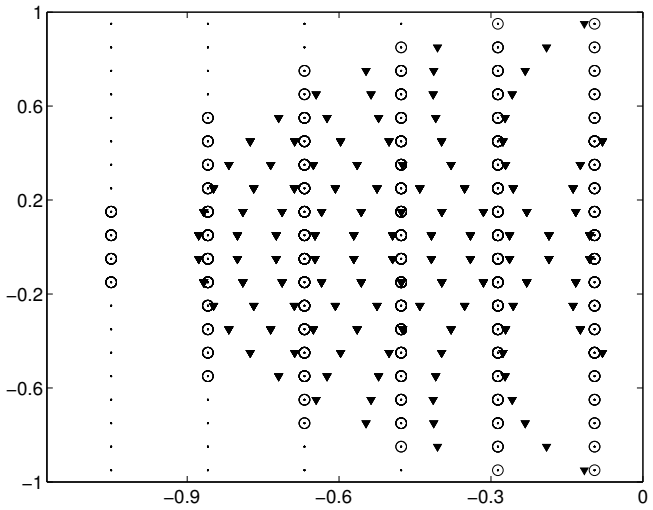

Figure 3.9: Repartition of "transmitted" wave vectors (represented by triangles ▼) computed from the discretized wave vectors by backward transmission from a fast medium $c^+ = 2.5$ to a slow medium $c^- = 1.0$, among their interpolation vectors (represented by circles o) on a regular mesh (represented by the dots ·).

the sets of indices J^- and J^{-1} be defined by:

$$\begin{aligned} J^- &= \left\{\beta \in \mathcal{M}_{\mathbf{k}} \mid \beta_1 = \mathrm{Nd}^1\left(g(\mathbf{K}_{(\beta)_1} + (\beta_1'' - 1)\Delta k_1 \boldsymbol{\delta}^1)\right),\ \beta_1'' \leq \beta_c^-\right\}, \\ J^{-1} &= J^- \cup \left\{\beta \in \mathcal{M}_{\mathbf{k}} \mid \beta_1 = 1 + \mathrm{Nd}^1\left(g(\mathbf{K}_{(\beta)_1} + (\beta_1'' - 1)\Delta k_1 \boldsymbol{\delta}^1)\right),\ \beta_1'' \leq \beta_c^-\right\}, \end{aligned} \tag{3.39}$$

respectively. The above inequality shows that the set J^{-1} defined above forms a sequence of consecutive integers of $\{-N_1, \ldots 0\}$, so that a two-point interpolation may be appropriate in most cases as illustrated on the Figure 3.9. However, we see that the distribution of $\mathcal{G}_\beta^{\mathrm{T}}$ among the mesh points $\mathcal{M}_{\mathbf{k}}$ is quite irregular, which underlines the importance of a proper interpolation of the specific intensities at $\mathcal{I}$.

3.5 Conclusions

The previous remark raises the question of the accuracy of the solution obtained, as well as the question of the conservation of the total energy during numerical simulation, since an obvious shortcoming for the interpolation of the numerical specific intensity crossing the interface $\mathcal{I}$ has been pointed out. The main issue of our work is to find methods for overcoming this problem while conserving the existing properties of the numerical schemes (typically their positivity, ℓ^1–contraction, or ℓ^∞–boundedness). Two approaches will be mainly detailed in the next chapter for this purpose. A first approach is based on the interpolations (3.23)–(3.24) (straight interface) and (3.33)–(3.34) (curved interface) above and consists in a discretization of the wave vector normal coordinates, while introducing a correction of the loss of energy for each "transmitted" wave vector. A second approach is based on a global change of variables, considering the difference of scales for the variations of $\mathbf{k}$ on each side of $\mathcal{I}$. It consists in discretizing the frequency variable $c^\pm\mathbf{k}$ on each side of the interface $\mathcal{I}$ rather than the wave vector $\mathbf{k}$ solely, and to correct the loss of energy at that interface with this modified discretization. Both approaches are considered for a straight interface and for a curved interface alike. They will be shown to give satisfactory results in terms of energy conservation. Their basic feature consists in computing precisely the total numerical energy, and then using interpolation coefficients chosen to insure its conservation in the simulation of its transmission at $\mathcal{I}$. Numerical results will be presented in the chapter 5 in order to illustrate the different strategies developed in this thesis.

4

Conservative upwind fluxes for acoustic waves at a straight and curved interface

In this chapter, we present several numerical schemes defined in order to correct the loss of energy due to the jump of sound speeds at the interfaces of the computational domain $\mathcal{O}_h$. The proposed remedy is to impose the conservation of the total energy and energy fluxes at the interfaces in the construction of the numerical fluxes. The starting point is the computation of the discretized total energy in the computational domain $\mathcal{O}_h$ at all times, which is presented in the next section 4.1. Based on this derivation, we compute in a subsequent section 4.2 the increments of the discretized total energy between two time steps. They are shown to depend on the jumps of the discretized specific intensities at the interfaces solely, as expected with the chosen numerical fluxes (3.16). Therefore our approach of constructing conservative numerical schemes consists in adapting those jumps in order to cancel the increments of the discretized total energy arising from the reflection/transmission processes at the interfaces. The latter are explicitly taken into account in the definitions of the upwind fluxes adapted to them, namely Eq. (3.20) and Eq. (3.21) for straight interfaces or Eq. (3.29) and Eq. (3.30) for curved interfaces. In these definitions, the contributions of the transmitted specific intensities to the numerical fluxes are evaluated by linear interpolations on the "transmitted" wave vector mesh, by picking up by backward transmission or reflection the "transmitted" and "reflected" wave vectors corresponding to the actual discretized wave vector. This procedure leaves some gaps in the "transmitted" wave vector mesh as explained in the section 3.4, in such a way that the computed total energy may be not conserved. The purpose of this chapter is to refine the aforementioned interpolations so as to erase this unwanted effect.

We first consider conservative numerical schemes for a straight interface in the section 4.3. The classical scheme used by Jin and co-workers in *e.g.* [27–31] is first recalled in the section 4.3.1, where it is argued that this approach potentially lacks the property of conserving the computed total energy. A first corrective scheme (FCS) is proposed in the section 4.3.2, which relies on a proper interpolation of the "transmitted" discretized specific intensities so as to avoid any loss of energy in the transmission process. A second corrective scheme (CKS) is subsequently proposed in the section 4.3.3, which consists in a global mesh adaptation to account for the variation of scales of the sound speed on each side of an interface. In this approach the discretization of the frequency variable $c^{\pm}\mathbf{k}$ is privileged over the discretization of the wave vector $\mathbf{k}$, since the norm of the former (the Hamiltonian) is conserved in the reflection/transmission processes considered in this work. Two different meshes are defined on both sides of the interface, where the discretized specific intensities are evaluated. Conservative numerical schemes are deduced from this setting by imposing either the conservation of the normal energy flux, or canceling the increments of the computed total energy.

We then consider conservative numerical schemes for a curved interface in the section 4.4. We first recall the classical scheme developed by Jin & Yin [31] based on a two-point interpolation of the "transmitted" discretized specific intensity. Then we show how the CKS approach of mesh adaptation to the variation of scales of the sound speed on each side of the interface extends to the curved case in the section 4.4.2. Here we discuss how the wave vector grid and mesh points are redistributed thanks to

the mesh adaptation strategy, and derive interpolation coefficients for the "reflected" and "transmitted" discretized specific intensities that conserve the energy by either imposing the continuity of the normal energy flux, or canceling the increments of the computed total energy.

4.1 Computation of the discretized total energy

Let $n \in \mathbb{N}^*$, our aim is to express the discretized total energy denoted by $\mathcal{E}^n$ at the time step t_n of the numerical simulation from the general definition (2.78) of the energy density. The discretized specific intensity a^n is computed using the discretized Liouville equation (3.15). As seen in the discussion of the section 2.1.3, the tangent component of the wave vector is conserved by transmission and reflection along an interface $\mathcal{I}$; see Eq. (2.22). This means that for the case of a straight interface, the set of discretized wave vector coordinates $\{K_{\beta_j} \mid -N_j \leq \beta_j \leq N_j - 1\}$ for $j \geq 2$ is conserved through transmission, while the set $\{K_{\beta_1} \mid -N_1 \leq \beta_1 \leq N_1 - 1\}$ is not conserved through transmission, because of Snell-Descartes laws; see also Eq. (2.23) of this very section. However, it is globally conserved through reflection as we have seen. This is why the first wave vector coordinate k_1 plays a crucial role in our schemes for straight interfaces. For the case of a curved interface, the previous sets are not conserved at all by reflection and transmission through $\mathcal{I}$ because of the various forms of the interface edges, so that all the wave vector coordinates need be re-evaluated in the discretization of their reflection and transmission images.

As discussed in the section 3.4, Snell-Descartes laws indicate in addition that the distribution of wave vector mesh points $\{\mathbf{K}_\beta\}_\beta$ does not vary on the same scale as its image through backward transmission. It is thus important to compute the energy associated to both distributions of points on each side of $\mathcal{I}$ in order to account for that difference of scales, so that the discretization steps may be adapted to these distributions. In the case of a straight interface, as the tangential component of an impinging wave vector is not modified through transmission, there is no need to adapt the discretization steps Δk_j for $j \geq 2$, so they are taken to be constant over the whole computational domain. On the contrary, the discretization step Δk_1 may depend on the cells $\mathcal{C}_\alpha$ where the specific intensity is evaluated on both sides of an interface. Therefore it has the form $\Delta k_1 = \Delta k_1(\alpha)$ in the most general case, in order to take into account both variation scales. In addition, for the case of a straight or plane vertical interface $\mathcal{I}$, Δk_1 may only depend on the first space coordinate α_1 (with the conventions set in the section 3.1). However for the case of a curved interface, the discretization steps Δk_j may all depend on the spatial cells $\mathcal{C}_\alpha$ and are thus functions of α. These situations shall be encountered in the subsequent sections 4.3.3 and 4.4.2, where corrective schemes for the upwind fluxes are described in order to address the aforementioned difference of scales on either side of $\mathcal{I}$. We shall adopt specific notations for the Δk_j's there.

For the present, we shall stick to general notations without any reference to this particularity and introduce:

$$\Delta\mathbf{x} = \prod_{j=1}^{d} \Delta x_j \,, \quad \Delta\mathbf{k} = \prod_{j=1}^{d} \Delta k_j \,.$$

Owing to these definitions and Eq. (2.78), the discretized total energy $\mathcal{E}^n$ at the n-th time step t_n is computed by either:

$$\mathcal{E}^n = \sum_\alpha \sum_\beta \mathrm{a}^n_{\alpha\beta} \Delta\mathbf{x}\Delta\mathbf{k} \,, \tag{4.1}$$

or:

$$\mathcal{E}^n = \frac{1}{2^d} \sum_\alpha \sum_\beta \sum_{u\in\{0,1\}^d} \mathrm{a}^n_{\alpha,\beta+\boldsymbol{\delta}^u} \Delta\mathbf{x}\Delta\mathbf{k} \,, \tag{4.2}$$

where $\boldsymbol{\delta}^u = \sum_{j=1}^d u_j \boldsymbol{\delta}^j$, and $\boldsymbol{\delta}^0 = \mathbf{0}$ by convention. In the first form, the specific intensity $\mathbf{k} \to \mathrm{a}(t_n, \mathbf{X}_\alpha, \mathbf{k})$ is approximated in each cell $\mathcal{C}_\alpha$ by a step function in each variable k_j, which belongs to the set $[-N_j\Delta k_j, N_j\Delta k_j]$. This corresponds to an approximation of the integral of the specific intensity with respect to the wave vector by rectangles. In the second form, it is approximated in each cell $\mathcal{C}_\alpha$ by a piecewise linear function of k_j, with the convention that the definition of $\mathrm{a}^n_{\alpha\beta}$ is extended to the index $N_j + 1$ by $\mathrm{a}^n_{\alpha,(\beta)_j+(N_j+1)\boldsymbol{\delta}^j} = 0$. This corresponds to an approximation of the integral of specific intensity with respect to the wave vector by trapezoids. Using the discretized Liouville equation (3.15) and the

upwind fluxes (3.16), the first definition of the discretized total energy given above leads to the following expression of the total energy jump $\mathcal{E}^{n+1} - \mathcal{E}^n$:

$$\mathcal{E}^n - \mathcal{E}^{n+1} = \sum_{j=1}^{d} \sum_{\alpha} \sum_{\beta} \frac{c_\alpha \Delta t}{\Delta x_j} \hat{K}_{\beta_j} \left(\mathrm{a}^n_{\alpha+\frac{j}{2},\beta} - \mathrm{a}^n_{\alpha-\frac{j}{2},\beta} \right) \Delta \mathbf{x} \Delta \mathbf{k} \,, \tag{4.3}$$

where:

$$\hat{K}_{\beta_j} = \frac{K_{\beta_j}}{|\mathbf{K}_\beta|} \,, \quad |\mathbf{K}_\beta| = \sqrt{\sum_{j=1}^{d} K^2_{\beta_j}} \,.$$

In the above one uses the notation introduced in Eq. (3.11) for the discretized specific intensities at the face centers of the cells. The second definition of the discretized total energy (when it is computed with linear interpolations) yields:

$$\mathcal{E}^n - \mathcal{E}^{n+1} = \frac{1}{2^d} \sum_{j=1}^{d} \sum_{\alpha} \sum_{\beta} \frac{c_\alpha \Delta t}{\Delta x_j} \hat{K}_{\beta_j} \sum_{u \in \{0,1\}^d} \left(\mathrm{a}^n_{\alpha+\frac{j}{2},\beta+\boldsymbol{\delta}^u} - \mathrm{a}^n_{\alpha-\frac{j}{2},\beta+\boldsymbol{\delta}^u} \right) \Delta \mathbf{x} \Delta \mathbf{k} \,.$$

The above expressions for the variations of $\mathcal{E}^n$ between two successive time steps are used to estimate the loss of energy for each proposed scheme, that is, for each proposed numerical flux for the consideration of reflection/transmission of the discretized specific intensities at the interface. By minimizing, indeed canceling these energy increments, one derives the various interpolation coefficients $C_0^\pm$, $C_1^\pm$, $C^\pm_{\beta^{\mathrm{R}}+\boldsymbol{\delta}^u}$ or $\Gamma^\pm_{\beta^{\mathrm{T}}+\boldsymbol{\delta}^u}$ introduced in the construction of the upwind schemes (3.20) and (3.21) (straight interface) or (3.29) and (3.30) (curved interface).

4.2 Increments of the discretized total energy

Before we consider the computation of the interpolation coefficients themselves, we start by describing how the increments of the numerical total energy of our problem are effectively computed for both definitions of $\mathcal{E}^n$ given by Eq. (4.1) and Eq. (4.2).

4.2.1 Approximation of the energy by step functions

Let us first define the partial sum $S^n_{(\alpha)_j\beta}$:

$$S^n_{(\alpha)_j\beta} = \frac{\Delta t \Delta k_j}{\Delta x_j} \hat{K}_{\beta_j} \sum_{\alpha_j=-M_j^-}^{M_j^+} c_\alpha \left(\mathrm{a}^n_{(\alpha)_j+\alpha_j+\frac{j}{2},\beta} - \mathrm{a}^n_{(\alpha)_j+\alpha_j-\frac{j}{2},\beta} \right) , \tag{4.4}$$

that appear in the computation of $\mathcal{E}^n - \mathcal{E}^{n+1}$ by Eq. (4.3). Since an upwind scheme is used, the latter also reads:

$$S^n_{(\alpha)_1\beta} = \frac{\Delta t \Delta k_1}{\Delta x_1} \hat{K}_{\beta_1} \left(c^- \mathrm{a}^n_{(\alpha)_1+(\alpha_1^1+\frac{1}{2})\boldsymbol{\delta}^1,\beta} - c^+ \mathrm{a}^n_{(\alpha)_1+(\alpha_1^1+1-\frac{1}{2})\boldsymbol{\delta}^1,\beta} \right)$$

if $j = 1$ (including the case of a straight interface), or:

$$\begin{aligned} S^n_{(\alpha)_j\beta} = \frac{\Delta t \Delta k_j}{\Delta x_j} \hat{K}_{\beta_j} \Big(& c^- \mathrm{a}^n_{(\alpha)_j+(\alpha_j^1+\frac{1}{2})\boldsymbol{\delta}^j,\beta} - c^+ \mathrm{a}^n_{(\alpha)_j+(\alpha_j^1+1-\frac{1}{2})\boldsymbol{\delta}^j,\beta} \\ & - c^- \mathrm{a}^n_{(\alpha)_j+(\alpha_j^2-\frac{1}{2})\boldsymbol{\delta}^j,\beta} + c^+ \mathrm{a}^n_{(\alpha)_j+(\alpha_j^2-1+\frac{1}{2})\boldsymbol{\delta}^j,\beta} \Big) \end{aligned}$$

if $j > 1$ (curved interface). In the above, the multi-indices $(\alpha)_j + (\alpha_j^1 + \frac{1}{2})\boldsymbol{\delta}^j$ and $(\alpha)_j + (\alpha_j^1 + 1 - \frac{1}{2})\boldsymbol{\delta}^j$ run through the cells adjoining the interface $\mathcal{I}$ from both sides when the slow side $\mathcal{O}_h^-$ is "below" $\mathcal{I}$ and the fast side $\mathcal{O}_h^+$ is "above" it; see the section 3.1.2. Likewise, the multi-indices $(\alpha)_j + (\alpha_j^2 - \frac{1}{2})\boldsymbol{\delta}^j$ and

$(\alpha)_j + (\alpha_j^2 - 1 + \frac{1}{2})\boldsymbol{\delta}^j$ run through the cells adjoining $\mathcal{I}$ from both sides when the slow side is "above" $\mathcal{I}$ and the fast side is "below" it. At last, one has considered the fact that:

$$\begin{aligned} c_{\alpha_j} &= c^- \quad \text{if} \quad \alpha_j \leq \alpha_j^1 \quad \text{or} \quad \alpha_j \geq \alpha_j^2 \,, \\ c_{\alpha_j} &= c^+ \quad \text{if} \quad \alpha_j^1 \leq \alpha_j \leq \alpha_j^2 \,. \end{aligned}$$

These expressions show that the discretized total energy shall be obtained in terms of the jumps of the discretized specific intensities at that interface solely, as expected from an upwind flux scheme. For all time steps t_n and indices α and β, we have assumed that:

$$\mathrm{a}^n_{(\alpha)_j + (M_j^+ - 1)\boldsymbol{\delta}^j, \beta} = \mathrm{a}^n_{(\alpha)_j - M_j^- \boldsymbol{\delta}^j, \beta} = \mathrm{a}^n_{(\alpha)_j + M_j^+ \boldsymbol{\delta}^j, \beta} = \mathrm{a}^n_{(\alpha)_j - (M_j^- + 1)\boldsymbol{\delta}^i j, \beta} = 0 \,,$$

because the boundaries of the computational physical domain $\mathcal{O}_h$ are chosen such that they will never be reached during the simulation. In addition the values of the discretized specific intensities outside $\mathcal{O}_h$, namely $\mathrm{a}^n_{(\alpha)_j + M_j^+ \boldsymbol{\delta}^j, \beta}$ and $\mathrm{a}^n_{(\alpha)_j - (M_j^- + 1)\boldsymbol{\delta}^j, \beta}$, are conventionally set to zero. The increment:

$$\mathcal{E}^n - \mathcal{E}^{n+1} := S^n \Delta \mathbf{x}$$

of the discretized total energy finally reads:

$$\begin{aligned} S^n = &\sum_{j=1}^{d} \sum_{(\alpha)_j} \sum_{\beta} \frac{\Delta t \Delta \mathbf{k}}{\Delta x_j} \hat{K}_{\beta_j} \left(c^- \mathrm{a}^n_{(\alpha)_j + (\alpha_j^1 + \frac{1}{2})\boldsymbol{\delta}^j, \beta} - c^+ \mathrm{a}^n_{(\alpha)_j + (\alpha_j^1 + 1 - \frac{1}{2})\boldsymbol{\delta}^j, \beta} \right) \\ &+ \sum_{j=2}^{d} \sum_{(\alpha)_j} \sum_{\beta} \frac{\Delta t \Delta \mathbf{k}}{\Delta x_j} \hat{K}_{\beta_j} \left(c^+ \mathrm{a}^n_{(\alpha)_j + (\alpha_j^2 - 1 + \frac{1}{2})\boldsymbol{\delta}^j, \beta} - c^- \mathrm{a}^n_{(\alpha)_j + (\alpha_j^2 - \frac{1}{2})\boldsymbol{\delta}^j, \beta} \right) . \end{aligned}$$

In order to compute this difference accurately, the sum S^n may be reordered accounting for the fact that $\forall \beta_j \leq 0$, $(K)_{\beta_j} \leq 0$ and $\forall \beta_j \geq 1$, $(K)_{\beta_j} \geq 0$. Its first term for instance reads:

$$\begin{aligned} S^n = \sum_{j=1}^{d} \sum_{(\alpha)_j} \frac{\Delta t \Delta \mathbf{k}}{\Delta x_j} \Bigg[&\sum_{\beta \in \mathcal{K}^-(\mathbf{n})} \hat{K}_{\beta_j} \left(c^- \mathrm{a}^n_{(\alpha)_j + (\alpha_j^1 + \frac{1}{2})\boldsymbol{\delta}^j, \beta} - c^+ \mathrm{a}^n_{(\alpha)_j + (\alpha_j^1 + 1 - \frac{1}{2})\boldsymbol{\delta}^j, \beta} \right) \\ &+ \sum_{\beta \in \mathcal{K}^+(\mathbf{n})} \hat{K}_{\beta_j} \left(c^- \mathrm{a}^n_{(\alpha)_j + (\alpha_j^1 + \frac{1}{2})\boldsymbol{\delta}^j, \beta} - c^+ \mathrm{a}^n_{(\alpha)_j + (\alpha_j^1 + 1 - \frac{1}{2})\boldsymbol{\delta}^j, \beta} \right) \Bigg] + \cdots \,, \end{aligned} \tag{4.5}$$

etc., where the sets $\mathcal{K}^{\pm}(\mathbf{n})$ of multi-indices have been defined with Eq. (3.10). Now in the above, the discretized specific intensities have to be interpolated on the wave vector mesh for both cases of a straight and a curved interface. In the former case, reflection leaves the set of discretized wave vectors invariant for their components which are tangent to the interface, whereas their normal components are simply reversed. This means that the wave vector mesh contains its image through reflection, and the "reflected" specific intensities do not actually need to be interpolated. This is the reason why Eq. (3.26) holds, where we also refer to Eq. (3.25) for the expression of the image of a given vector $\mathbf{K}_\beta$ by reflection in the case of a straight interface. Introducing:

$$\alpha^- := (\alpha)_1 + \alpha_1^1 \boldsymbol{\delta}^1 \,, \quad \alpha^+ := (\alpha)_1 + (\alpha_1^1 + 1)\boldsymbol{\delta}^1 \tag{4.6}$$

for the multi-indices running through the spatial cells $\mathcal{C}_{\alpha^-}$ and $\mathcal{C}_{\alpha^+}$ adjoining a straight interface on the slow and fast sides, respectively, one has therefore:

$$\begin{aligned} \tilde{\mathrm{a}}^n \left(\mathbf{X}_{\alpha^-}, \mathbf{k}^{\mathrm{R}}_\beta \right) &= \mathrm{a}^n_{\alpha^- \beta^{\mathrm{R}}} \,, \\ \tilde{\mathrm{a}}^n \left(\mathbf{X}_{\alpha^+}, \mathbf{k}^{\mathrm{R}}_\beta \right) &= \mathrm{a}^n_{\alpha^+ \beta^{\mathrm{R}}} \,, \end{aligned}$$

with $\beta_1^{\mathrm{R}} = -\beta_1 + 1$ and $\beta^{\mathrm{R}} = (\beta_1^{\mathrm{R}}, \beta_2, \dots \beta_d) = -\beta_1 \boldsymbol{\delta}^1 + (\beta)_1$. In the case of a straight interface, this leads to an increment $\mathcal{E}^n - \mathcal{E}^{n+1}$ that can finally be merged into $\mathcal{E}^n - \mathcal{E}^{n+1} = (S_1^n + S_2^n) \prod_{j=2}^d \Delta k_j$ where:

$$\begin{aligned} S_1^n &= \frac{\Delta t \Delta k_1}{\Delta x_1} \sum_{(\alpha)_1} \sum_{\beta \in \mathcal{K}^-} \hat{K}_{\beta_1} \left(c^- \mathrm{b}^n_{\alpha^+\beta} - c^+ (1 - \mathcal{R}^+(\mathbf{K}_\beta)) \mathrm{a}^n_{\alpha^+\beta} \right) , \\ S_2^n &= \frac{\Delta t \Delta k_1}{\Delta x_1} \sum_{(\alpha)_1} \sum_{\beta \in \mathcal{K}^+} \hat{K}_{\beta_1} \left(c^- (1 - \mathcal{R}^-(\mathbf{K}_\beta)) \mathrm{a}^n_{\alpha^-\beta} - c^+ \mathrm{b}^n_{\alpha^-\beta} \right) , \end{aligned} \tag{4.7}$$

where the sets $\mathcal{K}^\pm$ of multi-indices have been defined with Eq. (3.5). The scalars $\mathrm{b}^n_{\alpha^-\beta}$ and $\mathrm{b}^n_{\alpha^+\beta}$ have been defined in the section 3.2 by the equations (3.20), (3.21), (3.23) and (3.24). The exact values of $\mathrm{b}^n_{\alpha^-\beta}$ and $\mathrm{b}^n_{\alpha^+\beta}$ are established further on, since they depend on the numerical method chosen to cancel the increments of the discretized total energy within the medium.

4.2.2 Transmission from the slow to the fast medium

In the case of transmission from the slow to the fast medium, we suppose that no wave impinges the interface from the right so that one can check that S_1^n above is null. In order to insure the conservation of energy in that case, the term S_2^n has thus to be set to zero through a proper choice of the scalar $\mathrm{b}^n_{\alpha^-\beta}$.

4.2.3 Transmission from the fast to the slow medium

In the case of transmission from the fast to the slow medium, we suppose that no wave impinges the interface from the left so that one can check that S_2^n above is null. In order to insure the conservation of energy in that case, the term S_1^n has thus to be set to zero through a proper choice of the scalar $\mathrm{b}^n_{\alpha^+\beta}$.

4.2.4 Approximation by piecewise linear functions

We derive here the increments of the discretized total energy when it is computed by using linear functions to approximate the specific intensities along the first coordinate of the wave vectors, as defined by Eq. (4.2). In comparison to the approximation by step functions, we make the additional assumption that for all indexes $(\alpha)_1 \in \{0\} \times \prod_{j=2}^d \{-M_j^-, \dots M_j^+\}$, $(\beta)_1 \in \{0\} \times \prod_{j=2}^d \{-N_j, \dots N_j\}$ and $\alpha_1 \in \{-M_1, \dots 0\}$, we have $\mathrm{a}^0_{\alpha,(\beta)_1+\boldsymbol{\delta}^1} = \mathrm{a}^0_{\alpha,(\beta)_1+N_1\boldsymbol{\delta}^1} = 0$, and consider that during the whole simulation the propagation of the initial condition does not reach the boundaries of the domain $\mathcal{O}_h$. Then using the notations introduced previously, the increment of energy between two time steps reads:

$$\begin{aligned} \mathcal{E}^n - \mathcal{E}^{n+1} = {} & \frac{1}{2^d} \sum_{j=1}^d \sum_{(\alpha)_j} \sum_{\beta} \frac{\Delta t}{\Delta x_j} \hat{K}_{\beta_j} \sum_{u \in \{0,1\}^d} \left(c^- \mathrm{a}^n_{(\alpha)_j + (\alpha_j^1 + \frac{1}{2})\boldsymbol{\delta}^j, \beta + \boldsymbol{\delta}^u} - c^+ \mathrm{a}^n_{(\alpha)_j + (\alpha_j^1 + 1 - \frac{1}{2})\boldsymbol{\delta}^j, \beta + \boldsymbol{\delta}^u} \right) \Delta \mathbf{x} \Delta \mathbf{k} \\ & + \frac{1}{2^d} \sum_{j=2}^d \sum_{(\alpha)_j} \sum_{\beta} \frac{\Delta t}{\Delta x_j} \hat{K}_{\beta_j} \sum_{u \in \{0,1\}^d} \left(c^+ \mathrm{a}^n_{(\alpha)_j + (\alpha_j^2 - 1 + \frac{1}{2})\boldsymbol{\delta}^j, \beta + \boldsymbol{\delta}^u} - c^- \mathrm{a}^n_{(\alpha)_j + (\alpha_j^2 - \frac{1}{2})\boldsymbol{\delta}^j, \beta + \boldsymbol{\delta}^u} \right) \Delta \mathbf{x} \Delta \mathbf{k} \, . \end{aligned}$$

After several simplifications, we obtain for the first term for instance:

$$\mathcal{E}^n - \mathcal{E}^{n+1} = \frac{1}{2^d} \sum_{(\alpha)_1} \sum_{\beta} \frac{\Delta t}{\Delta x_1} \hat{K}_{\beta_1} \sum_{u \in \{0,1\}^d} \left(c^- \mathrm{a}^n_{\alpha^- + \frac{1}{2}, \beta + \boldsymbol{\delta}^u} - c^+ \mathrm{a}^n_{\alpha^+ - \frac{1}{2}, \beta + \boldsymbol{\delta}^u} \right) \Delta \mathbf{x} \Delta \mathbf{k} + \dots$$

The increments of discretized total energy are derived in terms of the jumps of the discretized specific intensities at the interface solely, as expected. Then the corresponding sums S_1^n and S_2^n defined by Eq. (4.7) read in the case of a straight interface:

$$\begin{aligned} S_1^n &= \frac{\Delta t \Delta k_1}{\Delta x_1} \sum_{(\alpha)_1} \sum_{\beta \in \mathcal{K}^-} \hat{K}_{\beta_1} \left(c^- \mathrm{b}^n_{\alpha^+\beta} - c^+ (1 - \mathcal{R}^+(\mathbf{K}_\beta)) \mathrm{a}^n_{\alpha^+\beta} \right) , \\ S_2^n &= \frac{\Delta t \Delta k_1}{\Delta x_1} \sum_{(\alpha)_1} \sum_{\beta \in \mathcal{K}^+} \hat{K}_{\beta_1} \left(c^- (1 - \mathcal{R}^-(\mathbf{K}_\beta)) \mathrm{a}^n_{\alpha^-\beta} - c^+ \mathrm{b}^n_{\alpha^-\beta} \right) , \end{aligned} \tag{4.8}$$

assuming that the boundaries of the computational domain have not been reached. Thus the same expressions as Eq. (4.7) are recovered in this case. This result will be useful for the construction of the numerical schemes below.

4.3 Numerical schemes for a straight interface

4.3.1 Classical upwind fluxes by two-point interpolations

The previous definitions established in the general case $d = 2$ or $d = 3$ are used to introduce the classical numerical scheme that can be found in [27–31]. The discretization of the domain $\mathcal{O}_h$ is the one outlined in the section 3.1, and that scheme has the general form given in the section 3.2 for the case of a straight interface. As for the upwind fluxes, the scalars $\mathrm{b}^n_{\alpha^-\beta}$ and $\mathrm{b}^n_{\alpha^+\beta}$ are defined by the equations (3.23) and (3.24), where the interpolation coefficients $C_0^\pm$ and $C_1^\pm$ are typically given in [31] by:

$$C_0^\pm = \frac{K_{\beta_1^{\mathrm{T}}} + \Delta k_1 - k^{\mathrm{T}}_{\beta_1}}{\Delta k_1}\,, \quad C_1^\pm = \frac{k^{\mathrm{T}}_{\beta_1} - K_{\beta_1^{\mathrm{T}}}}{\Delta k_1}\,, \tag{4.9}$$

for both cases of transmission from the slow to the fast medium and from the fast to the slow medium. We recall that $\beta_1^{\mathrm{T}} = \mathrm{Nd}^1(k^{\mathrm{T}}_{\beta_1})$ and $\beta^{\mathrm{T}} = (\beta)_1 + (\beta_1^{\mathrm{T}} - 1)\boldsymbol{\delta}^1$. The "reflected" and "transmitted" components $k^{\mathrm{R}}_{\beta_1}$ and $k^{\mathrm{T}}_{\beta_1}$ are defined by the formula (3.18) (we also refer to Eq. (3.20) and Eq. (3.21), respectively, and to the related formulas for the complete construction of the upwind fluxes in [31]). From the above definition, one can compute the corresponding expressions for S_1^n and S_2^n of the definition (4.7). In the case of transmission from the fast to the slow medium, the sum S_1^n reads:

$$\begin{aligned} S_1^n = \frac{\Delta t \Delta k_1}{\Delta x_1} \sum_{(\alpha)_1} \Bigg[& \sum_{\beta \in \mathcal{K}^-} -c^+ \hat{K}_{\beta_1} (1 - \mathcal{R}^+(\mathbf{K}_\beta)) \mathrm{a}^n_{\alpha^+\beta} \\ & + \sum_{\beta' \in \mathcal{K}^-} \sum_{K_{\beta_1'} \le k^{\mathrm{T}}_{\beta_1} < K_{\beta_1'+1}} c^- \hat{K}_{\beta_1} \left(\frac{k^{\mathrm{T}}_{\beta_1} - K_{\beta_1'}}{\Delta k_1} \right) \mathcal{T}^+(k^{\mathrm{T}}_{\beta_1}, \mathbf{K}'_\beta) \mathrm{a}^n_{\alpha^+\beta'} \\ & + \sum_{(\beta'-1) \in \mathcal{K}^-} \sum_{K_{\beta_1'-1} \le k^{\mathrm{T}}_{\beta_1} < K_{\beta_1'}} c^- \hat{K}_{\beta_1} \left(\frac{K_{\beta_1'} - k^{\mathrm{T}}_{\beta_1}}{\Delta k_1} \right) \mathcal{T}^+(k^{\mathrm{T}}_{\beta_1}, \mathbf{K}'_\beta) \mathrm{a}^n_{\alpha^+\beta'} \Bigg], \end{aligned} \tag{4.10}$$

where $k^{\mathrm{T}}_{\beta_1} = g(\mathbf{K}_\beta)$ and g is defined by Eq. (3.19). Also the set $\mathcal{K}^-$ has been defined with Eq. (3.5). The above expression shows that the discretized total energy between t_n and t_{n+1} is not necessarily conserved *a priori*, since the sum S_1^n is not necessarily equal to zero. Examples of the chapter 5 show that the loss of energy may even be important in that case.

In the case of transmission from the slow to the fast medium, the sum S_2^n can be computed similarly as:

$$\begin{aligned} S_2^n = \frac{\Delta t \Delta k_1}{\Delta x_1} \sum_{(\alpha)_1} \Bigg[& \sum_{\beta \in \mathcal{K}_c^+} c^- \hat{K}_{\beta_1} (1 - \mathcal{R}^-(\mathbf{K}_\beta)) \mathrm{a}^n_{\alpha^-\beta} \\ & - \sum_{\beta' \in \mathcal{K}_c^+} \sum_{K_{\beta_1'} \le k^{\mathrm{T}}_{\beta_1} < K_{\beta_1'+1}} c^+ \hat{K}_{\beta_1} \left(\frac{k^{\mathrm{T}}_{\beta_1} - K_{\beta_1'}}{\Delta k_1} \right) \mathcal{T}^-(k^{\mathrm{T}}_{\beta_1}, \mathbf{K}'_\beta) \mathrm{a}^n_{\alpha^-\beta'} \\ & - \sum_{\beta' \in \mathcal{K}_c^+} \sum_{K_{\beta_1'-1} \le k^{\mathrm{T}}_{\beta_1} < K_{\beta_1'}} c^+ \hat{K}_{\beta_1} \left(\frac{K_{\beta_1'} - k^{\mathrm{T}}_{\beta_1}}{\Delta k_1} \right) \mathcal{T}^-(k^{\mathrm{T}}_{\beta_1}, \mathbf{K}'_\beta) \mathrm{a}^n_{\alpha^-\beta'} \Bigg], \end{aligned} \tag{4.11}$$

where $k^{\mathrm{T}}_\beta = f(\mathbf{K}_\beta)$ and f is defined by Eq. (3.19). Also the set $\mathcal{K}_c^+$ has been defined by Eq. (3.5). For all indices $1 \le \beta_1 \le \beta_c^+ - 1$, where β_c^+ is the index of the first positive normal component on the wave

vector mesh which is above the critical normal incidence (as defined by Eq. (3.2)), $\mathbf{K}_\beta$ is totally reflected which means that:

$$\mathcal{R}^-(\mathbf{K}_\beta) = 1 \tag{4.12}$$

in this case. This explains the form of the first sum in the right-hand side above and why the corresponding terms vanish. Here again, the energy increment for transmission from the slow to the fast medium represented by S_2^n does not necessarily vanish. As pointed out in the next chapter through different numerical illustrations, the loss of energy can even be important in that case. In the subsequent sections it is explained that these issues, of which importance increases as the phase-space discretization gets coarser, may be corrected by particular choices of the upwind fluxes. We introduce two of them in the following sections 4.3.2 and 4.3.3. The first scheme (called hereafter FCS scheme) is based on the computation of the sums S_1^n and S_2^n in order to fix the problems related to the conservation of the normal fluxes at an interface $\mathcal{I}$. The second scheme (called hereafter CKS) is based on a reformulation of the discretization of the wave vector distribution at that interface for refined meshes.

4.3.2 First corrective scheme (FCS)

We first consider the sum S_1^n for transmission from the fast to the slow medium. As already explained, one may observe that the gthe function $g(k)$ of Eq. (3.19) has an asymptotic direction $k \mapsto \frac{k}{\nu}$ as k goes to $-\infty$ (see the section 3.4). This means that its slopes are lower than 1 on a subset of $]-\infty, \xi_c(\mathbf{K}'_\beta)]$, and implies that the the set J^{-1} (see Eq. (3.39) in the section 3.4) is equal to a subset of consecutive integers of $\{-N_1, \dots 0\}$. On this subset, a two-point interpolation of the form:

$$\begin{aligned} \mathrm{b}^n_{\alpha^+\beta} &= \mu^+_\beta \tilde{\mathrm{a}}^n(\mathbf{X}_{\alpha^+}, \mathbf{k}^{\mathrm{T}}_\beta)\,, \\ \tilde{\mathrm{a}}^n(\mathbf{X}_{\alpha^+}, \mathbf{k}^{\mathrm{T}}_\beta) &= C^+_0 \mathrm{a}^n_{\alpha^+\beta'} + C^+_1 \mathrm{a}^n_{\alpha^+,\beta'+1}\,, \end{aligned} \tag{4.13}$$

where $\alpha^+ = (\alpha)_1 + (\alpha^1_1 + 1)\boldsymbol{\delta}^1$ (see Eq. (4.6)), is thus sufficient in order to cover all the set of "transmitted" wave vectors (obtained by backward transmission). In the above, μ^+_β is equal to $\mathcal{T}^+(\mathbf{k}^{\mathrm{T}}_\beta)$ and $\tilde{\mathrm{a}}^n(\mathbf{X}_{\alpha^+}, \mathbf{k}^{\mathrm{T}}_\beta)$ is the specific intensity that is transmitted by the upwind flux. Also we recall our notations (3.13). If we insert these expressions in the sum S_1^n of Eq. (4.10), canceling it for each index $-N_1 \leq \beta'_1 \leq 0$, one obtains the following interpolation coefficients:

$$\begin{aligned} C^+_0 &= \frac{\nu \hat{K}_{\beta'_1} \mathcal{T}^+(K_{\beta'_1}, \mathbf{K}'_\beta)}{2 \sum_{K_{\beta'_1} \leq k^{\mathrm{T}}_{\beta_1} < K_{\beta'_1+1}} \hat{K}_{\beta_1} \mathcal{T}^+(k^{\mathrm{T}}_{\beta_1}, \mathbf{K}'_\beta)}\,, \\ C^+_1 &= \frac{\nu \hat{K}_{\beta'_1} \mathcal{T}^+(K_{\beta'_1}, \mathbf{K}'_\beta)}{2 \sum_{K_{\beta'_1-1} \leq k^{\mathrm{T}}_{\beta_1} < K_{\beta'_1}} \hat{K}_{\beta_1} \mathcal{T}^+(k^{\mathrm{T}}_{\beta_1}, \mathbf{K}'_\beta)}\,, \end{aligned}$$

where $\nu = \frac{c^+}{c^-}$. This choice provides the desired conservative numerical scheme, which means that the discrete energy flux density is conserved at the straight interface $\mathcal{I}$. Outside the set , a more than two-point interpolation may be necessary, but we do not consider this case here. We refer to [66] for further details. This situation is explained hereafter, though, for the case of transmission from the slow to the fast medium.

In case of transmission from the slow to the fast medium, one may observe that for all indices $\beta_1 \geq \mathrm{Nd}^1(|\mathbf{K}'_\beta|/\nu)$, the gradient of f is greater than 1. Thus it may happen that the set J^{+1} of Eq. (3.38) does not necessarily covers all the indices of the set $\mathcal{K}^+_c$ of Eq. (3.5). In that case, one may split the sum S_2^n as follows:

$$\begin{aligned} S^n_2 = \frac{\Delta t \Delta k_1}{\Delta x_1} \sum_{(\alpha)_1} \Bigg[& \sum_{\substack{\beta \in \mathcal{K}^+_c \\ \beta^+_c \leq \beta_1 \leq \beta'_1}} \hat{K}_{\beta_1} \left(c^-(1 - \mathcal{R}^-(\mathbf{K}_\beta)) \mathrm{a}^n_{\alpha^-\beta} - c^+ \mathrm{b}^n_{\alpha^-\beta} \right) \\ & + \sum_{\substack{\beta \in \mathcal{K}^+_c \\ \beta'_1 + 1 \leq \beta_1 \leq N_1}} \hat{K}_{\beta_1} \left(c^-(1 - \mathcal{R}^-(\mathbf{K}_\beta)) \mathrm{a}^n_{\alpha^-\beta} - c^+ \mathrm{b}^n_{\alpha^-\beta} \right) \Bigg], \end{aligned}$$

where $1 \leq \beta_1' \leq N_1$ satisfies the following. For all the indices $\beta_1 \leq \beta_1'$, the set of the multi-indices of the discrete wave vectors obtained by backward transmission of $(K_{\beta_1}, \mathbf{K}'_\beta)$ is a subset of $\mathcal{K}_c^+$ with consecutive integers along the first direction. A two-point interpolation of the transmitted discretized specific intensity is then sufficient to take all the "transmitted" wave vectors into account. The transmitted discretized specific intensity takes the form:

$$\begin{aligned} \mathrm{b}^n_{\alpha^- \beta} &= \mu^-_\beta \tilde{\mathrm{a}}^n(\mathbf{X}_{\alpha^-}, \mathbf{k}^{\mathrm{T}}_\beta)\,, \\ \tilde{\mathrm{a}}^n(\mathbf{X}_{\alpha^-}, \mathbf{k}^{\mathrm{T}}_\beta) &= C^-_0\, \mathrm{a}^n_{\alpha^- \beta} + C^-_1\, \mathrm{a}^n_{\alpha^-, \beta+1}\,, \end{aligned} \tag{4.14}$$

where $\alpha^- = (\alpha)_1 + \alpha^1_1 \boldsymbol{\delta}^1$ (see Eq. (4.6)). The expression of C^-_0 and C^-_1 is then similar to the ones obtained above. However for indices β_1 greater than β_1', the gradient of f is greater than 1 and the set of indices of the discrete wave vectors obtained by backward transmission of $(K_{\beta_1}, \mathbf{K}'_\beta)$ is not constituted by consecutive integers along the first direction. A two-point interpolation is no longer sufficient to catch all the "transmitted" wave vectors. This implies that the transmitted discretized specific intensity is now chosen in the form:

$$\begin{aligned} \mathrm{b}^n_{\alpha^- \beta} &= \mu^-_\beta \tilde{\mathrm{a}}^n(\mathbf{X}_{\alpha^-}, \mathbf{k}^{\mathrm{T}}_\beta)\,, \\ \tilde{\mathrm{a}}^n(\mathbf{X}_{\alpha^-}, \mathbf{k}^{\mathrm{T}}_\beta) &= \sum_{\beta_i = \beta_m}^{\beta_M} \gamma^-_i\, \mathrm{a}^n_{\alpha^- \beta_i}\,, \end{aligned} \tag{4.15}$$

where β_m and β_M are multi-indices within $\mathcal{K}_c^+$ that define the above interpolation, and μ^-_β is chosen as the transmission coefficient $\mathcal{T}^-(\mathbf{k}^{\mathrm{T}}_\beta)$. Plugging this expansion in S^n_2, one may deduce an explicit expression for the coefficients γ^-_i given by:

$$\gamma^-_i = \frac{\hat{K}_{\beta_{i1}} \mathcal{T}^-(K_{\beta_{i1}}, \mathbf{K}'_\beta)}{\nu \hat{K}_{\beta_1} \mathcal{T}^-(k^{\mathrm{T}}_{\beta_1}, \mathbf{K}'_\beta)}\,,$$

for all $\beta_i = \beta_m, \ldots \beta_M$, where the latter multi-indices may depend on β. This choice of interpolation coefficients for each β_1 within $\{1, \ldots N_1\}$ defines a conservative numerical scheme at the straight interface $\mathcal{I}$ for any choice of the discretization numbers N_j, $1 \leq j \leq d$.

4.3.3 Second corrective scheme (CKS)

It is mentionned in the section 3.4, that two different methods are employed in order to correct the non conservative classical scheme defined in the section 4.3.1. Particularly, the interpolation of the "transmitted" wave vectors at an interface $\mathcal{I}$ raises difficulties owing to the irregularity of the distribution of their images by the functions f and g. We present here the second method used to correct these problems. A first form is based on the correction of the difference of variation scales between the "incident" and "transmitted" wave vectors in each medium toward the wave vector coordinate k_1. A second form completes the first form, by the choice of specific interpolation coefficients in order to correct the loss of energy observed. Both are described in the following subsection. The description of the first form in the case of a straight interface $\mathcal{I}$ is presented in the next paragraph.

General form of the numerical scheme

We start this section by introducing our choice of discretization, motivated by the property (3.17) which states that the tangent component $\mathbf{K}'_\beta$ of an "transmitted" wave vector $\mathbf{k}^{\mathrm{T}}_\beta$ toward $\mathcal{I}$ is conserved through transmission, *i.e.* are equal to the tangent component of the actual wave vector $\mathbf{K}_\beta$. Furthermore, the formula (3.19) shows that the variation scale of $k^{\mathrm{T}}_{\beta_1}$ depends on the values of the celerity on each side of $\mathcal{I}$.

We thus propose to discretize the normal coordinates $c^- k_1$ in the slow medium and $c^+ k_1$ in the fast one, so as to correct the difference of scale on each side of $\mathcal{I}$. In this respect we start by fixing the discretization number N_1 as well as the discretization step Δk^-_1 in the slow medium, so that the wave

vector grid and mesh points are defined on the slow side, with the notations introduced in the section 3.1. The corresponding wave vector discretization step Δk_1^+ in the fast medium is defined by:

$$\Delta k_1^- = \nu \Delta k_1^+ .$$

These new wave vector steps define the grid and mesh points in each subdomain of $\mathcal{O}_h$ for the above discretization. We introduce hereafter the notations that will complete the ones introduced in the section 3.1. They will be used for both descriptions of transmission from the fast to the slow medium, and from the slow to the fast medium. We denote by $\mathrm{g}_{\mathbf{k}}^-$ and $\mathrm{g}_{\mathbf{k}}^+$ the wave vector grids considered in the subdomains $\mathcal{O}_h^-$ and $\mathcal{O}_h^+$, respectively, defined by:

$$\mathrm{g}_{\mathbf{k}}^{\pm} = \left\{ \mathbf{k}_{\beta-\frac{1}{2}}^{\pm} \mid \beta = (\beta_1, \dots \beta_d) \in \prod_{j=1}^{d} \{-N_j, \dots N_j\} \right\} ,$$

where the normal components of $\mathbf{k}_{\beta-\frac{1}{2}}^{\pm}$ are given by:

$$k_{\beta_1-\frac{1}{2}}^{\pm} = (\beta_1 - 1)\Delta k_1^{\pm} ,$$

and their tangential components for $j \geq 2$ are given by:

$$k_{\beta_j-\frac{1}{2}}^{\pm} = (\beta_j - 1)\Delta k_j ,$$

for Δk_j being the wave vector discretization step along the j-th coordinate. Note that the tangential components are not modified as compared to the discretization defined in the section 3.1. Likewise, the meshes $\mathrm{m}_{\mathbf{k}}^-$ and $\mathrm{m}_{\mathbf{k}}^+$ are defined by the coordinates:

$$\mathrm{m}_{\mathbf{k}}^{\pm} = \left\{ \mathbf{k}_{\beta}^{\pm} \mid \beta = (\beta_1, \dots \beta_d) \in \prod_{j=1}^{d} \{-N_j, \dots N_j - 1\} \right\} ,$$

where the normal components of $\mathbf{k}_{\beta}^{\pm}$ are given by:

$$k_{\beta_1}^{\pm} = k_{\beta_1-\frac{1}{2}}^{\pm} + \frac{\Delta k_1^{\pm}}{2} ,$$

while their tangential components for $j \geq 2$ are given by:

$$k_{\beta_j}^{\pm} = k_{\beta_j-\frac{1}{2}}^{\pm} + \frac{\Delta k_j}{2} .$$

These notations enable to rewrite the sums S_1^n and S_2^n defined in the previous section 4.2.1 (see Eq. (4.7)) with the latter discretization, and with the help of an interpolation formula for $\mathrm{b}_{\alpha^{\pm}\beta}^n$ defined by the equations (3.23) and (3.24). With these notations, S_1^n reads :

$$S_1^n = \frac{\Delta t}{\Delta x_1} \sum_{(\alpha)_1} \sum_{\beta' \in \mathcal{K}^-} \left[-c^+ \hat{k}_{\beta_1'}^+ \Delta k_1^+ \mathcal{T}^+(\mathbf{k}_{\beta'}^+) + c^- \Delta k_1^- \mu_{\beta'}^+ \left(\sum_{k_{\beta_1'-1}^+ \leq k_{\beta_1}^{\mathrm{T}} < k_{\beta_1'}^+} \hat{k}_{\beta_1}^- C_0^+ + \sum_{k_{\beta_1'}^+ \leq k_{\beta_1}^{\mathrm{T}} < k_{\beta_1'+1}^+} \hat{k}_{\beta_1}^- C_1^+ \right) \right] \mathrm{a}_{\alpha^+\beta'}^n , \tag{4.16}$$

where $k_{\beta_1}^{\mathrm{T}} = g(\mathbf{k}_{\beta}^-)$, while S_2^n reads:

$$S_2^n = \frac{\Delta t}{\Delta x_1} \sum_{(\alpha)_1} \sum_{\beta' \in \mathcal{K}_c^+} \left[c^- \hat{k}_{\beta_1'}^- \Delta k_1^- \mathcal{T}^-(\mathbf{k}_{\beta'}^-) - c^+ \Delta k_1^+ \mu_{\beta'}^- \left(\sum_{k_{\beta_1'}^- \leq k_{\beta_1}^{\mathrm{T}} < k_{\beta_1'+1}^-} \hat{k}_{\beta_1}^+ C_0^- + \sum_{k_{\beta_1'-1}^- \leq k_{\beta_1}^{\mathrm{T}} < k_{\beta_1'}^-} \hat{k}_{\beta_1}^+ C_1^- \right) \right] \mathrm{a}_{\alpha^-\beta'}^n , \tag{4.17}$$

where $k^{\mathrm{T}}_{\beta_1} = f(\mathbf{k}^+_\beta)$. In the above $\mu^\pm_\beta$, $C^\pm_0$ and $C^\pm_1$ are positive coefficients depending on the numerical scheme chosen to cancel the sums above. For example, the latter coefficients may be defined in a simple way as for the two-point interpolation by:

$$C^\pm_0 = \frac{k^{\mathrm{T}}_{\beta_1} - k^\pm_{\beta'_1}}{\Delta k^\pm_1}\,, \quad C^\pm_1 = \frac{k^\pm_{\beta'_1} + \Delta k^\pm_1 - k^{\mathrm{T}}_{\beta_1}}{\Delta k^\pm_1}\,, \tag{4.18}$$

as illustrated in the numerical applications. In this case the coefficients $\mu^\pm_\beta$ may be defined such that the discretized normal energy flux at the interface is kept constant, as elaborated in a subsequent paragraph. Another solution shall be to fix them, and then determine the interpolation coefficients $C^\pm_0$ and $C^\pm_1$ so that the sums above cancel, as done for the FCS scheme in the section 4.3.2.

Remarks: A first remark concerning the influence of the choice of different grids on each side of $\mathcal{I}$, is that it modifies the computation of the energy increments S^n_1 and S^n_2 between two time steps by the form of the weights in front of the specific intensities. A second remark concerns the influence of that discretization on the distribution of the coordinates $k^{\mathrm{T}}_{\beta_1} = g(\mathbf{k}^-_\beta)$ for $\beta \in \mathcal{K}^-_c$ (transmission from the fast to the slow medium) and $k^{\mathrm{T}}_{\beta_1} = f(\mathbf{k}^+_\beta)$ with $\beta \in \mathcal{K}^+$ (transmission from the slow to the fast medium) picking up the normal components of the "transmitted" wave vectors among the set of discretized wave vectors as obtained by backward transmission. This issue is first discussed in the following paragraph.

Distribution of the interpolation points

We describe here the distribution of the interpolation points and discuss the relevance of the discretization approach introduced above, along the same lines as the question raised in the section 3.4 regarding the distribution of the normal components of the interpolated "transmitted" wave vectors among the set of discretized vectors, with a reference to the Figure 3.8. For transmission from the slow to the fast medium, one can show that the interpolation of the normal component distribution $\{k^{\mathrm{T}}_{\beta_1}\}_{\beta\in\mathcal{K}^+}$ introduced in the previous paragraph covers all the set of discretized normal components $\{k^-_{\beta_1}\}_{-N_1\le\beta_1\le 0}$. For that purpose, we introduce the following sets which are the counterparts of the sets of Eq. (3.38) for the discretization defined above:

$$\begin{aligned} J^+_+ &= \left\{\beta \in \mathcal{M}_{\mathbf{k}} \mid \beta_1 = \mathrm{Nd}^1\left(f\left(\mathbf{k}^+_{(\beta)_1} + (\beta'_1-1)\Delta k^+_1 \boldsymbol{\delta}^1\right)\right),\ 1 \le \beta'_1 \le N_1\right\}, \\ J^{+1}_+ &= J^+ \cup \left\{\beta \in \mathcal{M}_{\mathbf{k}} \mid \beta_1 = 1 + \mathrm{Nd}^1\left(f\left(\mathbf{k}^+_{(\beta)_1} + (\beta'_1-1)\Delta k^+_1 \boldsymbol{\delta}^1\right)\right),\ 1 \le \beta'_1 \le N_1\right\}, \end{aligned} \tag{4.19}$$

where f is defined by the formula (3.19). For transmission from the fast to the slow medium, the counterparts of Eq. (3.39) are:

$$\begin{aligned} J^-_- &= \left\{\beta \in \mathcal{M}_{\mathbf{k}} \mid \beta_1 = \mathrm{Nd}^1\left(g\left(\mathbf{k}^-_{(\beta)_1} + (\beta''_1-1)\Delta k^-_1 \boldsymbol{\delta}^1\right)\right),\ \beta''_1 \le \beta^-_c\right\}, \\ J^{-1}_- &= J^- \cup \left\{\beta \in \mathcal{M}_{\mathbf{k}} \mid \beta_1 = 1 + \mathrm{Nd}^1\left(g\left(\mathbf{k}^-_{(\beta)_1} + (\beta''_1-1)\Delta k^-_1 \boldsymbol{\delta}^1\right)\right),\ \beta''_1 \le \beta^-_c\right\}. \end{aligned} \tag{4.20}$$

where g is defined by the same formula (3.19), and β^-_c by Eq. (3.4). The indices of the coordinates intercepted by a two-point interpolation defines the set J^{+1}_+ in the case of transmission from the slow to the fast medium, and the set J^{-1}_- in the case of transmission from the fast to the slow medium. Let us show that they fully cover the set of indices $\mathcal{K}^+_c$ in the first case, and a subset of consecutive indices of $\{1,\dots N_1\}$ in the second case, corresponding to subcritical discretized wave vectors.

Let $\beta \in \mathcal{K}^+$, the "transmitted" wave vector $(f(k^+_{\beta_1}, \mathbf{K}'_\beta), \mathbf{K}'_\beta)$ associated to the actual one $\mathbf{k}^+_\beta$ in case of transmission from the slow to the fast medium is denoted by $\mathbf{k}^{\mathrm{T}}_\beta = (k^{\mathrm{T}}_{\beta_1}, \mathbf{K}'_\beta)$. The definition of f yields:

$$\begin{aligned} \left(k^{\mathrm{T}}_{\beta_1}\right)^2 &= \nu^2 (k^+_{\beta_1})^2 + \xi_c \left(\mathbf{K}'_\beta\right)^2 \\ &= (k^-_{\beta_1})^2 + \xi_c \left(\mathbf{K}'_\beta\right)^2 . \end{aligned}$$

Likewise, let $\beta \in \mathcal{K}_c^-$, the "transmitted" wave vector $(g(k_{\beta_1}^-, \mathbf{K}'_\beta), \mathbf{K}'_\beta)$ associated to the actual one $\mathbf{k}_\beta^-$ in case of transmission from the fast to the slow medium is also denoted by $\mathbf{k}_\beta^{\mathrm{T}} = (k_{\beta_1}^{\mathrm{T}}, \mathbf{K}'_\beta)$. The definition of g yields:

$$\begin{aligned}\left(k_{\beta_1}^{\mathrm{T}}\right)^2 &= \nu^{-2}(k_{\beta_1}^-)^2 - \nu^{-2}\xi_c\left(\mathbf{K}'_\beta\right)^2 \\ &= (k_{\beta_1}^+)^2 - \nu^{-2}\xi_c\left(\mathbf{K}'_\beta\right)^2 .\end{aligned}$$

Now we can show that for both cases of transmission a two-point interpolation is sufficient in most situations. To this purpose, we consider the difference between two consecutive normal coordinates $k_{\beta_1}^{\mathrm{T}}$ and $k_{\beta_1+1}^{\mathrm{T}}$. It reads:

$$k_{\beta_1+1}^{\mathrm{T}} - k_{\beta_1}^{\mathrm{T}} = \sqrt{(k_{\beta_1}^{\mp} + \Delta k_1^{\mp})^2 \pm \left(\frac{c^\pm}{c^+}\right)^2 \xi_c(\mathbf{K}'_\beta)^2} - \sqrt{{k_{\beta_1}^{\mp}}^2 \pm \left(\frac{c^\pm}{c^+}\right)^2 \xi_c(\mathbf{K}'_\beta)^2} .$$

One can check that the function $k \mapsto (k^2 + \xi_c(\mathbf{K}'_\beta)^2)^{\frac{1}{2}}$ has a positive derivative, that is also lower than 1 on $\mathbb{R}_+^*$ so that in case of transmission from the slow to the fast medium:

$$k_{\beta_1+1}^{\mathrm{T}} - k_{\beta_1}^{\mathrm{T}} \leq \Delta k_1^- . \tag{4.21}$$

Moreover in that case, the "transmitted" coordinates are given respectively by:

$$\begin{aligned}k_1^{\mathrm{T}} &= \sqrt{\left(k_1^-\right)^2 + \xi_c(\mathbf{K}'_\beta)^2} , \\ k_{N_1}^{\mathrm{T}} &= \sqrt{\left(k_{N_1}^-\right)^2 + \xi_c(\mathbf{K}'_\beta)^2} > k_{N_1}^- ,\end{aligned}$$

where $k_1^- \in \{\frac{\Delta k_1^-}{2}, \Delta k_1^-\}$ depends on whether N_1 is even or odd, so that the following inequalities hold:

$$\begin{aligned}-\xi_c(\mathbf{K}'_\beta) \leq k_1^{\mathrm{T}} &\leq -\xi_c(\mathbf{K}'_\beta) + \Delta k_1^- , \\ -\xi_c(\mathbf{K}'_\beta) < k_{\beta_c^+}^- &\leq -\xi_c(\mathbf{K}'_\beta) + \Delta k_1^- .\end{aligned}$$

The three lines above show that:

$$k_1^{\mathrm{T}} \in [k_{\beta_c^+}^- - \Delta k_1^-, k_{\beta_c^+}^- + \Delta k_1^-] ,$$

thus we see that the upper and lower bounds of J_+^{+1} frame $\{\beta_c^+, \dots N_1\}$. As Eq. (4.21) shows that this former set is made of consecutive integers, we conclude that it covers all the indices of the latter one.

In case of transmission from the fast to the slow medium, one may verify that the function $k \mapsto (k^2 - \nu^{-2}\xi_c(\mathbf{K}'_\beta)^2)^{\frac{1}{2}}$ has an asymptotic direction $k \mapsto k$ as k goes to $-\infty$, and that its derivative goes to 1. This implies that there exists an index β_1' such that for all $k \leq k_{\beta_1'}$ its derivative is lower than 2. This means that for all $k_{\beta_1} \leq k_{\beta_1'}$:

$$k_{\beta_1+1}^{\mathrm{T}} - k_{\beta_1}^{\mathrm{T}} \leq 2\Delta k_1^+ , \tag{4.22}$$

and that a two-point interpolation is sufficient. On $[k_{\beta_1'}, \xi_c(\mathbf{K}'_\beta)]$ a more than two-point interpolation may be necessary, but this case is not considered here. We refer to [66], where similar considerations are made. We assume that a two-point interpolation is sufficient for most of the cases.

An example of the distribution of the "transmitted" wave vectors from the fine mesh among the discretized vectors of the coarse mesh is plotted on the Figure 4.1. As one can see, the interpolation points do frame each "transmitted" wave vector computed by backward transmission. In that sense, the proposed numerical scheme is satisfactory.

Defining the upwind fluxes by imposing the continuity of the discretized normal energy flux

Having introduced the modified meshes for the discretization of the wave vectors, one may complete the definition of the numerical fluxes given by Eq. (3.23) for transmission from the slow to the fast medium, and by Eq. (3.24) for transmission from the fast to the slow medium. The discretized specific

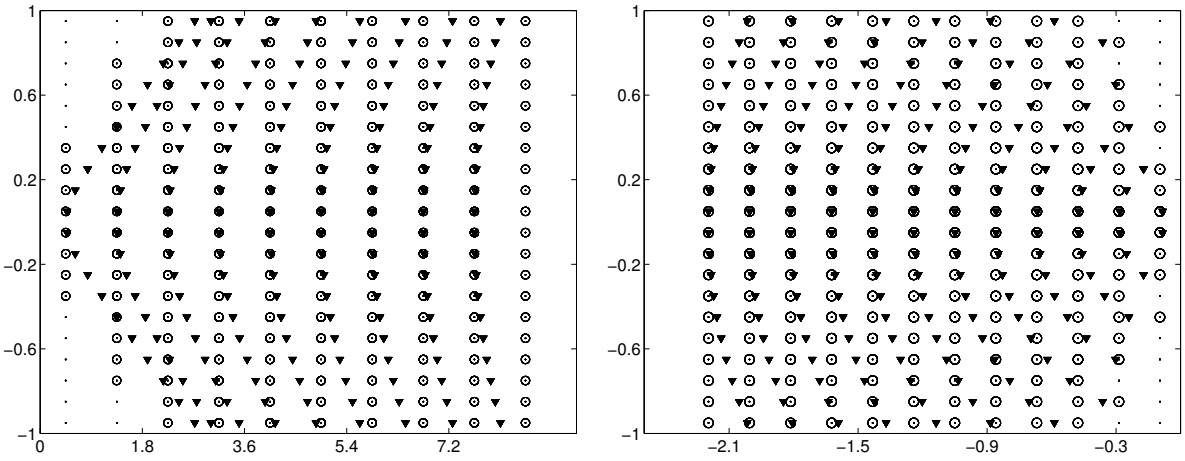

Figure 4.1: Distribution of "transmitted" wave vectors (represented by triangles ▼) computed by backward transmission among their interpolation wave vectors (represented by circles o) on a regular mesh (represented by the dots ·) of $c\,k_1$ with the discretization steps $\Delta k_1^- = \nu \Delta k_1^+$ (CKS scheme). Left figure: transmission from the slow to the fast medium (see the Figure 3.8); right figure: transmission from the fast to the slow medium (see the Figure 3.9).

intensities $\tilde{\mathrm{a}}^n(\mathbf{X}_\alpha, \mathbf{k}_\beta^{\mathrm{T}})$ and $\tilde{\mathrm{a}}^n(\mathbf{X}_\alpha + \Delta x_1 \boldsymbol{\delta}^1, \mathbf{k}_\beta^{\mathrm{T}})$ are constructed in the same way as for the classical scheme described in the section 4.3.1, by a linear interpolation of $\mathrm{a}^n_{\alpha\beta'}$ and $\mathrm{a}^n_{\alpha,\beta'+1}$, and $\mathrm{a}^n_{\alpha+1,\beta'}$ and $\mathrm{a}^n_{\alpha+1,\beta'+1}$ with interpolation coefficients $C_0^\pm$ and $C_1^\pm$ given by Eq. (4.18) (see also Eq. (3.20), Eq. (3.21) and the related formulas) leading to the following form of the interpolation. As for transmission from the slow to the fast medium one has:

$$\tilde{\mathrm{a}}^n(\mathbf{X}_\alpha, \mathbf{k}_\beta^{\mathrm{T}}) = \frac{k^-_{\beta'_1} + \Delta k_1^- - k^{\mathrm{T}}_{\beta_1}}{\Delta k_1^-} \mathrm{a}^n_{\alpha\beta'} + \frac{k^{\mathrm{T}}_{\beta_1} - k^-_{\beta'_1}}{\Delta k_1^-} \mathrm{a}^n_{\alpha,\beta'+1}\,, \tag{4.23}$$

where the index β'_1 is given by $\beta'_1 := \mathrm{Nd}^1_-(k^{\mathrm{T}}_{\beta_1}) = \lfloor \frac{k^{\mathrm{T}}_{\beta_1}}{\Delta k_1^-} + \frac{1}{2} \rfloor$ for $\lfloor Y \rfloor$ being the integer part of Y; as for transmission from the fast to the slow medium one has:

$$\tilde{\mathrm{a}}^n(\mathbf{X}_\alpha + \Delta x_1 \boldsymbol{\delta}^1, \mathbf{k}_\beta^{\mathrm{T}}) = \frac{k^+_{\beta'_1} + \Delta k_1^+ - k^{\mathrm{T}}_{\beta_1}}{\Delta k_1^+} \mathrm{a}^n_{\alpha+1,\beta'} + \frac{k^{\mathrm{T}}_{\beta_1} - k^+_{\beta'_1}}{\Delta k_1^+} \mathrm{a}^n_{\alpha+1,\beta'+1},$$

where $\beta'_1 := \mathrm{Nd}^1_+(k^{\mathrm{T}}_{\beta_1}) = \lfloor \frac{k^{\mathrm{T}}_{\beta_1}}{\Delta k_1^+} + \frac{1}{2} \rfloor$.

In a second step we have to describe how the corrective quantities $\{\mathrm{b}^n_{\alpha^\pm\beta}\}_\beta$ of the numerical fluxes (3.20) and (3.21) are defined in order to avoid an important loss of energy when the specific intensities cross the interface $\mathcal{I}$. As already mentioned, this is done in this work by choosing interpolation coefficients in a form that sets S_1^n or S_2^n (previously defined by Eq. (4.16) and Eq. (4.17)) to zero, and is precisely described in the next subsection. An alternative approach may be to impose the conservation of the normal energy flux density at the interface $\mathcal{I}$. Using the change of grids defined above, the latter reads:

$$\sum_{\beta\in\mathcal{K}^+} (c^+ \hat{\mathbf{k}}^+_\beta \cdot \mathbf{n}) \Delta k_1^+ \mathrm{b}^n_{\alpha^-\beta} = \sum_{\beta\in\mathcal{K}^+} (c^- \hat{\mathbf{k}}^{\mathrm{T}}_\beta \cdot \mathbf{n}) c_\beta \Delta k_1^+ \mathcal{T}^-(\mathbf{k}^{\mathrm{T}}_\beta) \tilde{\mathrm{a}}^n \left(\mathbf{X}_{\alpha^-}, \mathbf{k}^{\mathrm{T}}_\beta\right)$$

for transmission from the slow to the fast medium, and:

$$\sum_{\beta\in\mathcal{K}_c^-} (c^- \hat{\mathbf{k}}^-_\beta \cdot \mathbf{n}) \Delta k_1^- \mathrm{b}^n_{\alpha^+\beta} = \sum_{\beta\in\mathcal{K}_c^-} (c^+ \hat{\mathbf{k}}^{\mathrm{T}}_\beta \cdot \mathbf{n}) c_\beta \Delta k_1^- \mathcal{T}^+(\mathbf{k}^{\mathrm{T}}_\beta) \tilde{\mathrm{a}}^n \left(\mathbf{X}_{\alpha^+}, \mathbf{k}^{\mathrm{T}}_\beta\right)\,,$$

for transmission from the fast to the slow medium, using the notations introduced above. Also:

$$\hat{\mathbf{k}}^\pm_\beta = \frac{\mathbf{k}^\pm_\beta}{|\mathbf{k}^\pm_\beta|}\,, \quad \hat{\mathbf{k}}^{\mathrm{T}}_\beta = \frac{\mathbf{k}^{\mathrm{T}}_\beta}{|\mathbf{k}^{\mathrm{T}}_\beta|}\,,$$

and the c_β's are coefficients chosen in order to correct for the change of discretization steps between the slow and fast media. One may consider for example one of the two formula below:

$$c_\beta = \frac{\partial f}{\partial k_{\mathbf{n}}}(\mathbf{k}_\beta^+ \cdot \mathbf{n}, \mathbf{K}'_\beta)\,, \quad c_\beta = \frac{k^{\mathrm{T}}_{\beta_1+1} - k^{\mathrm{T}}_{\beta_1}}{\Delta k_1^+}\,, \tag{4.24}$$

for transmission from the slow to the fast medium, and one of the two formula below:

$$c_\beta = -\frac{\partial g}{\partial k_{\mathbf{n}}}(\mathbf{k}_\beta^- \cdot \mathbf{n}, \mathbf{K}'_\beta)\,, \quad c_\beta = \frac{k^{\mathrm{T}}_{\beta_1} - k^{\mathrm{T}}_{\beta_1+1}}{\Delta k_1^-}\,, \tag{4.25}$$

for transmission from the fast to the slow medium. A way to construct $\mathrm{b}^n_{\alpha^-\beta}$ and $\mathrm{b}^n_{\alpha^+\beta}$ suggested by the above equalities is as follows. Let $\beta \in \mathcal{K}^+$, taking into account the fact that for a straight interface $\mathbf{n} = -\boldsymbol{\delta}_1$, we obtain:

$$\begin{aligned} \mathrm{b}^n_{\alpha^-\beta} &= \mu_\beta^- \tilde{\mathrm{a}}^n\left(\mathbf{X}_{\alpha^-}, \mathbf{k}^{\mathrm{T}}_\beta\right)\,, \\ \mu_\beta^- &= \frac{c_\beta \hat{k}^{\mathrm{T}}_{\beta_1}}{\nu \hat{k}^+_{\beta_1}} \mathcal{T}^-(\mathbf{k}^{\mathrm{T}}_\beta)\,. \end{aligned} \tag{4.26}$$

Note that μ_β^- may be reduced to $\mu_\beta^- = \mathcal{T}^-(\mathbf{k}^{\mathrm{T}}_\beta)$ if c_β is chosen as $c_\beta = -\frac{\partial g}{\partial k_{\mathbf{n}}}(\mathbf{k}_\beta^- \cdot \mathbf{n}, \mathbf{K}'_\beta)$. The definition (4.26) of $\mathrm{b}^n_{\alpha^-\beta}$ completes the upwind fluxes (3.20) of the CKS numerical scheme for transmission from the slow to the fast medium. Indeed the discretization of the "reflected" specific intensities do not require any change of grid, since both grids have the same discretization following the coordinates β_j for $j \geq 2$, by the construction of the meshes $\mathrm{m}^\pm_{\mathbf{k}}$ at the beginning of this section. In other words, the "reflected" discretized specific intensities are given by the expressions used for the classical numerical scheme, which means that they are given by the formula (3.26):

$$\tilde{\mathrm{a}}^n(\mathbf{X}_{\alpha^+}, \mathbf{k}^{\mathrm{R}}_\beta) = \mathrm{a}^n_{\alpha^+\beta^{\mathrm{R}}}$$

for $\beta^{\mathrm{R}} = (-\beta_1 + 1, \beta_2, \ldots \beta_d)$. Therefore the specific intensities at cells located close to $\mathcal{I}$ are entirely defined in the case of transmission from the slow to the fast medium ; see again Eq. (3.20).

Now let $\beta \in \mathcal{K}_c^-$, the same type of computation as above gives the following expression of $\mathrm{b}^n_{\alpha^+\beta}$ on the fast side of $\mathcal{I}$:

$$\begin{aligned} \mathrm{b}^n_{\alpha^+\beta} &= \mu_\beta^+ \tilde{\mathrm{a}}^n\left(\mathbf{X}_{\alpha^+}, \mathbf{k}^{\mathrm{T}}_\beta\right)\,, \\ \mu_\beta^+ &= \frac{\nu c_\beta \hat{k}^{\mathrm{T}}_{\beta_1}}{\hat{k}^-_{\beta_1}} \mathcal{T}^+(\mathbf{k}^{\mathrm{T}}_\beta)\,. \end{aligned} \tag{4.27}$$

Likewise, the upwind fluxes of the CKS numerical scheme are now completed by the above definition of the corrective factor $\mathrm{b}^n_{\alpha^+\beta}$, that describes transmission from the fast to the slow medium ; see Eq. (3.21). Numerical simulations that compare the classical numerical scheme introduced in the section 4.3.1 to the CKS scheme outlined here are presented in the following chapter 5.

The loss of energy at the interface induced by the upwind fluxes constructed just above is estimated by computing the sums S_1^n and S_2^n defined by Eq. (4.16) and Eq. (4.17), together with the interpolation coefficients of Eq. (4.18). The same remarks as the ones for the classical scheme defined in the section 4.3.1 can be made. In the following chapter that presents the numerical applications of the schemes introduced here, some results illustrating the present approach are presented. This scheme is again compared through numerical examples to the classical one.

We conclude this paragraph by mentioning that the above construction was carried on for a piecewise constant approximation (4.1) of the discretized total energy within the computational domain. The same construction for a piecewise linear approximation (4.2) of that energy is detailed in the appendix F.

Defining the upwind fluxes by imposing the conservation of the discretized energy

We now adopt the strategy outlined in the section 4.3.2 defining the FCS scheme, by seeking some positive parameters $C_0^{\pm}$ and $C_1^{\pm}$ such that sums S_1^n and S_2^n defined by Eq. (4.16) and Eq. (4.17), respectively, cancel. The parameters $\mu_\beta^{\pm}$ are defined by:

$$\mu_\beta^{\pm} = \mathcal{T}^{\pm}(\mathbf{k}_\beta^{\mathrm{T}})\,.$$

It should be noticed that the above expression corresponds to Eq. (4.26) and Eq. (4.27), where the parameter c_β is taken equal to $c_\beta = \nu^{\pm 1}(\hat{k}_{\beta_1}^{\mp}/\hat{k}_{\beta_1}^{\mathrm{T}})$, which corresponds to the left side of the equations (4.24) and (4.25).

Let us first compute S_2^n with this general form of interpolation. The corrective quantity $\mathrm{b}_{\alpha^-\beta}^n$ corresponding to a "transmitted" discretized specific intensity in the upwind fluxes (3.20) is:

$$\mathrm{b}_{\alpha^-\beta}^n = \mathcal{T}^-(\mathbf{k}_\beta^{\mathrm{T}})\tilde{\mathrm{a}}^n(\mathbf{X}_{\alpha^-}, \mathbf{k}_\beta^{\mathrm{T}})\,. \tag{4.28}$$

Now we insert the above expression of $\mathrm{b}_{\alpha^-\beta}^n$ into the expression (4.17) of the sum S_2^n, yields:

$$S_2^n = \frac{c^-\Delta k_1^-\Delta t}{\Delta x_1}\sum_{(\alpha)_1}\sum_{\beta'\in\mathcal{K}_c^+}\left[\hat{k}_{\beta'_1}^-\mathcal{T}^-(\mathbf{k}_{\beta'}^-)\right.$$
$$\left. -\left(\sum_{k_{\beta'_1}^-\le k_{\beta_1}^{\mathrm{T}}<k_{\beta'_1+1}^-}\hat{k}_{\beta_1}^+\mathcal{T}^-(\mathbf{k}_\beta^{\mathrm{T}})C_0^- + \sum_{k_{\beta'_1-1}^-\le k_{\beta_1}^{\mathrm{T}}<k_{\beta'_1}^-}\hat{k}_{\beta_1}^+\mathcal{T}^-(\mathbf{k}_\beta^{\mathrm{T}})C_1^-\right)\right]\mathrm{a}_{\alpha^-\beta'}^n\,.$$

In order to simplify the expression above, the coefficients C_0^- and C_1^- are supposed to depend only on the index $\beta'_1 = \mathrm{Nd}_-^1(k_{\beta_1}^{\mathrm{T}})$, where:

$$\mathrm{Nd}_{\pm}^j(k) = \left\lfloor \frac{k}{\Delta k_j^{\pm}} + \frac{1}{2}\right\rfloor\,. \tag{4.29}$$

Then it is easy to deduce expressions for C_0^- and C_1^- that cancel the sum S_2^n, that is:

$$\begin{aligned} C_0^- &= \frac{\hat{k}_{\beta'_1}^-\mathcal{T}^-(\mathbf{k}_{\beta'}^-)}{2\sum_{k_{\beta'_1}^-\le k_{\beta_1}^{\mathrm{T}}<k_{\beta'_1+1}^-}\hat{k}_{\beta_1}^+\mathcal{T}^-(\mathbf{k}\mathrm{T}_\beta)}\,,\\ C_1^- &= \frac{\hat{k}_{\beta'_1}^-\mathcal{T}^-(\mathbf{k}_{\beta'}^-)}{2\sum_{k_{\beta'_1-1}^-\le k_{\beta_1}^{\mathrm{T}}<k_{\beta'_1}^-}\hat{k}_{\beta_1}^+\mathcal{T}^-(\mathbf{k}_\beta^{\mathrm{T}})}\,. \end{aligned} \tag{4.30}$$

In case of transmission from the fast to the slow medium, the corrective specific intensity is given by:

$$\mathrm{b}_{\alpha^+\beta}^n = \mathcal{T}^+(\mathbf{k}_\beta^{\mathrm{T}})\tilde{\mathrm{a}}^n(\mathbf{X}_{\alpha^+}, \mathbf{k}_\beta^{\mathrm{T}})\,. \tag{4.31}$$

Inserting this expression into Eq. (4.16) and canceling S_1^n, one obtains equivalently the coefficients:

$$\begin{aligned} C_0^+ &= \frac{\hat{k}_{\beta'_1}^+\mathcal{T}^+(\mathbf{k}_{\beta'}^+)}{2\sum_{k_{\beta'_1}^+\le k_{\beta_1}^{\mathrm{T}}<k_{\beta'_1+1}^+}\hat{k}_{\beta_1}^-\mathcal{T}^+(\mathbf{k}_\beta^{\mathrm{T}})}\,,\\ C_1^+ &= \frac{\hat{k}_{\beta'_1}^+\mathcal{T}^+(\mathbf{k}_{\beta'}^-)}{2\sum_{k_{\beta'_1-1}^+\le k_{\beta_1}^{\mathrm{T}}<k_{\beta'_1}^+}\hat{k}_{\beta_1}^-\mathcal{T}^+(\mathbf{k}_\beta^{\mathrm{T}})}\,. \end{aligned} \tag{4.32}$$

The choices above guarantee that for an initial condition compactly supported in $\mathcal{O}_h^-$ or $\mathcal{O}_h^+$ and propagating toward the interface $\mathcal{I}$, no numerical energy is lost because of the crossing of that interface. This can be expressed by saying that the proposed numerical scheme is ℓ^1-preserving, and one may check that it is also positive. Examples that compare the scheme developed above to the classical one (section 4.3.1), and to the adapted classical schemes presented previously, show that it is satisfying compared to the other methods. They are detailed in the subsequent chapter 5.

4.4 Numerical schemes for a curved interface

In the case of a curved interface, the one-dimensional feature of the problem observed in case of a straight interface is lost. This means that the special role played by the first wave vector coordinate no longer holds, or is fully reduced. The upwind scheme is defined by the formulas (3.29) and (3.30), or (3.35) and (3.36) introduced in the section 3.2.3, that give the "reflected" and "transmitted" discretized specific intensities at $\mathcal{I}$. We recall the notations introduced there for the multi-indices of the spatial cells $\mathcal{C}_{\alpha'}$ and $\mathcal{C}_{\alpha''}$ of the slow medium $\mathcal{O}_h^-$ which are "below" and "above" the interface, respectively:

$$\alpha' = (\alpha)_j + \alpha_j^1 \boldsymbol{\delta}^j \,, \quad \alpha'' = (\alpha)_j + \alpha_j^2 \boldsymbol{\delta}^j \,, \tag{4.33}$$

for $2 \leq j \leq d$, and α_j^1 and α_j^2 are defined through Eq. (3.6). The corrective quantities $\mathrm{b}^n_{\alpha'\beta}$ and $\mathrm{b}^n_{\alpha'+j,\beta}$, or $\mathrm{b}^n_{\alpha''\beta}$ and $\mathrm{b}^n_{\alpha''-j,\beta}$ (which are proportional to the "transmitted" discretized specific intensities), and the "reflected" discretized specific intensities $\tilde{\mathrm{a}}^n(\mathbf{X}_{\alpha'}, \mathbf{k}^{\mathrm{R}}_\beta)$ and $\tilde{\mathrm{a}}^n(\mathbf{X}_{\alpha'} + \Delta x_j \boldsymbol{\delta}^j, \mathbf{k}^{\mathrm{R}}_\beta)$, or $\tilde{\mathrm{a}}^n(\mathbf{X}_{\alpha''}, \mathbf{k}^{\mathrm{R}}_\beta)$ and $\tilde{\mathrm{a}}^n(\mathbf{X}_{\alpha''} - \Delta x_j \boldsymbol{\delta}^j, \mathbf{k}^{\mathrm{R}}_\beta)$, are this time interpolated on the whole wave vector mesh rather than the sole normal coordinate, as this was done for a straight interface.

4.4.1 Classical upwind fluxes by two-point interpolations

For the classical upwind fluxes proposed by Jin & Yin in [31, Sect. 5.1] for curved interfaces, the upwind fluxes are completely defined by the interpolation coefficients $\{C^{\pm}_{\beta^{\mathrm{R}}+\boldsymbol{\delta}^u}\}_{u\in\{0,1\}^d}$ and $\{\Gamma^{\pm}_{\beta^{\mathrm{T}}+\boldsymbol{\delta}^u}\}_{u\in\{0,1\}^d}$, which replace the one-dimensional interpolation coefficients $C_0^{\pm}$ and $C_1^{\pm}$ of Eq. (4.9). For instance, they are given in the two-dimensional case $d = 2$ by:

$$\begin{aligned}
\Gamma^{\pm}_{\beta^{\mathrm{T}}} &= \frac{k^{\mathrm{T}}_{\beta_1} - K_{\beta_1^{\mathrm{T}}}}{\Delta k_1} \frac{k^{\mathrm{T}}_{\beta_2} - K_{\beta_2^{\mathrm{T}}}}{\Delta k_2} \,, \\
\Gamma^{\pm}_{\beta^{\mathrm{T}}+\boldsymbol{\delta}^1} &= \frac{K_{\beta_1^{\mathrm{T}}+1} - k^{\mathrm{T}}_{\beta_1}}{\Delta k_1} \frac{k^{\mathrm{T}}_{\beta_2} - K_{\beta_2^{\mathrm{T}}}}{\Delta k_2} \,, \\
\Gamma^{\pm}_{\beta^{\mathrm{T}}+\boldsymbol{\delta}^2} &= \frac{k^{\mathrm{T}}_{\beta_1} - K_{\beta_1^{\mathrm{T}}}}{\Delta k_1} \frac{K_{\beta_2^{\mathrm{T}}+1} - k^{\mathrm{T}}_{\beta_2}}{\Delta k_2} \,, \\
\Gamma^{\pm}_{\beta^{\mathrm{T}}+\boldsymbol{\delta}^1+\boldsymbol{\delta}^2} &= \frac{K_{\beta_1^{\mathrm{T}}+1} - k^{\mathrm{T}}_{\beta_1}}{\Delta k_1} \frac{K_{\beta_2^{\mathrm{T}}+1} - k^{\mathrm{T}}_{\beta_2}}{\Delta k_2} \,,
\end{aligned}$$

for backward transmission (from the slow or the fast medium), and by:

$$\begin{aligned}
C^{\pm}_{\beta^{\mathrm{R}}} &= \frac{k^{\mathrm{R}}_{\beta_1} - K_{\beta_1^{\mathrm{R}}}}{\Delta k_1} \frac{k^{\mathrm{R}}_{\beta_2} - K_{\beta_2^{\mathrm{R}}}}{\Delta k_2} \,, \\
C^{\pm}_{\beta^{\mathrm{R}}+\boldsymbol{\delta}^1} &= \frac{K_{\beta_1^{\mathrm{R}}+1} - k^{\mathrm{R}}_{\beta_1}}{\Delta k_1} \frac{k^{\mathrm{R}}_{\beta_2} - K_{\beta_2^{\mathrm{R}}}}{\Delta k_2} \,, \\
C^{\pm}_{\beta^{\mathrm{R}}+\boldsymbol{\delta}^2} &= \frac{k^{\mathrm{R}}_{\beta_1} - K_{\beta_1^{\mathrm{R}}}}{\Delta k_1} \frac{K_{\beta_2^{\mathrm{R}}+1} - k^{\mathrm{R}}_{\beta_2}}{\Delta k_2} \,, \\
C^{\pm}_{\beta^{\mathrm{R}}+\boldsymbol{\delta}^1+\boldsymbol{\delta}^2} &= \frac{K_{\beta_1^{\mathrm{R}}+1} - k^{\mathrm{R}}_{\beta_1}}{\Delta k_1} \frac{K_{\beta_2^{\mathrm{R}}+1} - k^{\mathrm{R}}_{\beta_2}}{\Delta k_2} \,,
\end{aligned}$$

for backward reflection (from the slow or the fast medium). Here we recall Eq. (3.32):

$$\beta_j^{\mathrm{R}} = \mathrm{Nd}^j\left(k^{\mathrm{R}}_{\beta_j}\right) \,, \quad \beta_j^{\mathrm{T}} = \mathrm{Nd}^j\left(k^{\mathrm{T}}_{\beta_j}\right) \,,$$

for $1 \leq j \leq d$, and the "reflected" and "transmitted" wave vectors $\mathbf{k}^{\mathrm{R}}_\beta$ and $\mathbf{k}^{\mathrm{T}}_\beta$ are defined by their components in the local basis $(\mathbf{n}, \mathbf{t}_j, j \geq 2)$; see Eqs.(3.27)–(3.28).

As in the case of a straight interface, the difference of celerities (sound speeds) between the fast and the slow medium induces two scales of distributions of the wave vectors. This inhomogeneity raises the question of the relevance of the interpolation for the discretized specific intensity at the interface $\mathcal{I}$, and

the question of energy conservation as already discussed in the section 3.4. One may notice at first that the two- (or three-) dimensional character of the geometry induces some changes in the treatment of these issues. One may verify again that the sums S^n that express the difference of energy between two successive time steps t_n and t_{n+1} (of which computation is detailed afterwards in the section 4.4.2) do not necessarily cancel. This means that the discretized total energy is not necessarily conserved by the numerical schemes. The loss of energy at $\mathcal{I}$ may even be important in certain cases, as illustrated in some examples of the chapter 5. It may however be corrected as explained previously for the case of a straight interface by different types of numerical upwind fluxes, detailed in the subsequent section. The presentation is restricted to the counterpart of the CKS scheme of the section 4.3 for the present case of a curved interface. That scheme relies on a correction of the difference of scales between the fast and the slow medium, and enables to conserve the numerical normal energy fluxes at $\mathcal{I}$. It is illustrated at the end of the chapter 5 for different discretization numbers.

4.4.2 Second corrective scheme (CKS)

Thus we consider here a corrective method similar to the one adopted in the section 4.3.3. It is developed in order to correct the loss of discretized total energy of the classical scheme outlined above. The approach consists in the correction of the difference of scales between the wave vectors distributions in the slow and in the fast medium. A first form is based on a global correction of this difference. A second form is based on the computation of the loss of energy between two time steps, and the choice of dedicated interpolation coefficients in order to correct it. The proposed upwind fluxes are less easy to implement than in the case of a straight interface, that is why they are presented with some details in the next paragraphs. We consider the first form of correction below.

General form of the numerical scheme

The difference of variation scales of the normal components $k_{\mathbf{n}}$ and $k_{\mathbf{n}}^{\mathrm{T}}$ of the actual and "transmitted" wave vectors suggests to use different discretization on both sides of $\mathcal{I}$. The dissymmetry of the problem in the case of a curved interface requires to use a global discretization. More precisely we consider for each component $j \in \{1, \dots d\}$, $d = 2$ or $d = 3$, the discretization of the quantities $c^- k_j$ in the slow medium, and $c^+ k_j$ in the fast medium, which is defined as follows. If Δk_j^- stands for the discretization step in the slow medium, the following relation holds:

$$\Delta k_j^- = \nu \Delta k_j^+ , \quad 1 \leq j \leq d ,$$

where Δk_j^+ stands for the discretization step in the fast medium. As in the case of a straight interface, we introduce here additional notations that complete the notations introduced in the section 3.1. We define the grids and meshes in each subdomain $\mathcal{O}_h^-$ and $\mathcal{O}_h^+$ as follows. The grids $\mathcal{G}_{\mathbf{k}}^-$ and $\mathcal{G}_{\mathbf{k}}^+$ are defined by:

$$\mathcal{G}_{\mathbf{k}}^{\pm} = \left\{ \mathbf{K}_{\beta - \frac{1}{2}}^{\pm} \ | \ \beta = (\beta_1, \dots \beta_d) \in \prod_{j=1}^{d} \{-N_j, \dots N_j\} \right\} ,$$

where the components $K_{\beta_j - \frac{1}{2}}^{\pm}$ for $1 \leq j \leq d$ are defined by:

$$K_{\beta_j - \frac{1}{2}}^{\pm} = (\beta_j - 1) \Delta k_j^{\pm} .$$

In a similar manner, the meshes are defined in the slow and in the fast medium as follows:

$$\mathcal{M}_{\mathbf{k}}^{\pm} = \left\{ \mathbf{K}_{\beta}^{\pm} \ | \ \beta = (\beta_1, \dots \beta_d) \in \prod_{j=1}^{d} \{-N_j, \dots N_j - 1\} \right\} ,$$

where the components for each index $1 \leq j \leq d$ are given by:

$$K_{\beta_j}^{\pm} = K_{\beta_j - \frac{1}{2}}^{\pm} + \frac{\Delta k_j^{\pm}}{2} .$$

These definitions allow to redefine the interpolation coefficients of the "reflected" and "transmitted" discretized specific intensities at the interface of $\mathcal{O}_h$. The formulas (4.18) used in the case of a straight interface are substituted by:

$$\begin{aligned}
\Gamma^{\pm}_{\beta^{\mathrm{T}}} &= \frac{k^{\mathrm{T}}_{\beta_1} - K^{\pm}_{\beta^{\mathrm{T}}_1}}{\Delta k_1}\frac{k^{\mathrm{T}}_{\beta_2} - K^{\pm}_{\beta^{\mathrm{T}}_2}}{\Delta k_2}\,,\\
\Gamma^{\pm}_{\beta^{\mathrm{T}}+\boldsymbol{\delta}^1} &= \frac{K^{\pm}_{\beta^{\mathrm{T}}_1+1} - k^{\mathrm{T}}_{\beta_1}}{\Delta k^{\pm}_1}\frac{k^{\mathrm{T}}_{\beta_2} - K^{\pm}_{\beta^{\mathrm{T}}_2}}{\Delta k^{\pm}_2}\,,\\
\Gamma^{\pm}_{\beta^{\mathrm{T}}+\boldsymbol{\delta}^2} &= \frac{k^{\mathrm{T}}_{\beta_2} - K^{\pm}_{\beta^{\mathrm{T}}_1}}{\Delta k^{\pm}_1}\frac{K^{\pm}_{\beta^{\mathrm{T}}_2+1} - k^{\mathrm{T}}_{\beta_2}}{\Delta k^{\pm}_2}\,,\\
\Gamma^{\pm}_{\beta^{\mathrm{T}}+\boldsymbol{\delta}^1+\boldsymbol{\delta}^2} &= \frac{K^{\pm}_{\beta^{\mathrm{T}}_1+1} - k^{\mathrm{T}}_{\beta_1}}{\Delta k^{\pm}_1}\frac{K^{\pm}_{\beta^{\mathrm{T}}_2+1} - k^{\mathrm{T}}_{\beta_2}}{\Delta k^{\pm}_2}\,,
\end{aligned} \tag{4.34}$$

for backward transmission, and by:

$$\begin{aligned}
C^{\pm}_{\beta^{\mathrm{R}}} &= \frac{k^{\mathrm{R}}_{\beta_1} - K^{\pm}_{\beta^{\mathrm{R}}_1}}{\Delta k^{\pm}_1}\frac{k^{\mathrm{R}}_{\beta_2} - K^{\pm}_{\beta^{\mathrm{R}}_2}}{\Delta k^{\pm}_2}\,,\\
C^{\pm}_{\beta^{\mathrm{R}}+\boldsymbol{\delta}^1} &= \frac{K^{\pm}_{\beta^{\mathrm{R}}_1+1} - k^{\mathrm{R}}_{\beta_1}}{\Delta k^{\pm}_1}\frac{k^{\mathrm{R}}_{\beta_2} - K^{\pm}_{\beta^{\mathrm{R}}_2}}{\Delta k^{\pm}_2}\\
C^{\pm}_{\beta^{\mathrm{R}}+\boldsymbol{\delta}^2} &= \frac{k^{\mathrm{R}}_{\beta_1} - K^{\pm}_{\beta^{\mathrm{R}}_1}}{\Delta k^{\pm}_1}\frac{K^{\pm}_{\beta^{\mathrm{R}}_2+1} - k^{\mathrm{R}}_{\beta_2}}{\Delta k^{\pm}_2}\,,\\
C^{\pm}_{\beta^{\mathrm{R}}+\boldsymbol{\delta}^1+\boldsymbol{\delta}^2} &= \frac{K^{\pm}_{\beta^{\mathrm{R}}_1+1} - k^{\mathrm{R}}_{\beta_1}}{\Delta k^{\pm}_1}\frac{K^{\pm}_{\beta^{\mathrm{R}}_2+1} - k^{\mathrm{R}}_{\beta_2}}{\Delta k^{\pm}_2}\,,
\end{aligned} \tag{4.35}$$

for backward reflection. Here the indices β^{R}_j and β^{T}_j, $1 \le j \le d$, are defined by:

$$\beta^{\mathrm{R}}_j = \mathrm{Nd}^j_{\pm}\left(k^{\mathrm{R}}_{\beta_j}\right)\,, \quad \beta^{\mathrm{T}}_j = \mathrm{Nd}^j_{\pm}\left(k^{\mathrm{T}}_{\beta_j}\right)\,,$$

with the notation of Eq. (4.29), and the "reflected" and "transmitted" wave vectors $\mathbf{k}^{\mathrm{R}}_{\beta}$ and $\mathbf{k}^{\mathrm{T}}_{\beta}$ are defined by their components in the local basis $(\mathbf{n}, \mathbf{t}_j, j \ge 2)$ as described in the section 3.2.3; see again Eqs. (3.27)–(3.28).

This change of grids and meshes modifies the expression of the total energy increment between two time steps, as well as the wave vector distribution. One may observe though that this new distribution is better adapted to the problem of transmission. Its interest is discussed in the next paragraph for the case of transmission from the slow to the fast medium. The case of transmission from the fast to the slow medium may be treated in the same manner, though some difficulties arise that are also outlined in the subsequent paragraphs.

Distribution of the interpolation points

We consider here the distribution of discrete wave vectors obtained by backward transmission in the case of a curved interface. The unit normal vector to that interface is denoted by $\mathbf{n}$. As compared to the discussion about such a distribution for a straight interface, the normal wave vector coordinate k_1 is replaced by the normal wave vector coordinate $k_{\mathbf{n}} = \mathbf{k}\cdot\mathbf{n}$. Then one may discuss the variations of the normal coordinates $k^{\mathrm{T}}_{\mathbf{n}}$ of two "transmitted" wave vectors obtained by backward transmission from the fast to the slow medium of two close wave vectors belonging to the meshes $\mathcal{M}^+_{\mathbf{k}}$, say $\mathbf{K}^+_{\beta}$ and $\mathbf{K}^+_{\beta+\boldsymbol{\delta}^j}$. The analysis below is done in order to characterize the distribution of such points obtained with the change of meshes defined above. Thus let $\mathbf{k}^{\mathrm{T}}_{\beta}$ and $\mathbf{k}^{\mathrm{T}}_{\beta+\boldsymbol{\delta}^j}$ be defined by Eq. (3.27), one is interested in estimating the difference $|\mathbf{k}^{\mathrm{T}}_{\beta} - \mathbf{k}^{\mathrm{T}}_{\beta+\boldsymbol{\delta}^j}|$. It may be decomposed as:

$$\left|\mathbf{k}^{\mathrm{T}}_{\beta} - \mathbf{k}^{\mathrm{T}}_{\beta+\boldsymbol{\delta}^j}\right|^2 = \left|\sqrt{|f(\mathbf{K}^+_{\beta})|^2} - \sqrt{|f(\mathbf{K}^+_{\beta+\boldsymbol{\delta}^j})|^2}\right|^2 + |\Delta k^+_j|^2\,,$$

where the function $f(\mathbf{k})$ is defined by Eq. (3.19). The difference above can then be majorized as follows:

$$\begin{aligned}\left|\sqrt{|f(\mathbf{K}_\beta^+)|^2}-\sqrt{|f(\mathbf{K}_{\beta+\boldsymbol{\delta}^j}^+)|^2}\right| &= \frac{\left||f(\mathbf{K}_\beta^+)|^2-|f(\mathbf{K}_{\beta+\boldsymbol{\delta}^j}^+)|^2\right|}{|f(\mathbf{K}_\beta^+)|+|f(\mathbf{K}_{\beta+\boldsymbol{\delta}^j}^+)|}\\ &= \frac{\left|\Delta k_j^-(\boldsymbol{\delta}^j\cdot\mathbf{n})(\mathbf{K}_\beta^-\cdot\mathbf{n}+\mathbf{K}_{\beta+\boldsymbol{\delta}^j}^-\cdot\mathbf{n})+\eta^2\Delta k_j^-\boldsymbol{\delta}^j\cdot(\mathbf{K}'_\beta+\mathbf{K}'_{\beta+\boldsymbol{\delta}^j})\right|}{|f(\mathbf{K}_\beta^+)|+|f(\mathbf{K}_{\beta+\boldsymbol{\delta}^j}^+)|}\\ &= \frac{\left|\Delta k_j^-\boldsymbol{\delta}^j\cdot\left((\mathbf{K}_\beta^-\cdot\mathbf{n})\mathbf{n}+\eta^2\mathbf{K}'_\beta+(\mathbf{K}_{\beta+\boldsymbol{\delta}^j}^-\cdot\mathbf{n})\mathbf{n}+\eta^2\mathbf{K}'_{\beta+\boldsymbol{\delta}^j}\right)\right|}{|f(\mathbf{K}_\beta^+)|+|f(\mathbf{K}_{\beta+\boldsymbol{\delta}^j}^+)|}\\ &\leq |\Delta k_j^-|\end{aligned}$$

where $\eta^2=1-(\frac{1}{\nu})^2\leq 1$, and $\mathbf{K}'_\beta$ stands for the tangential component of $\mathbf{K}_\beta^-$ as usual. We finally obtain the following estimate:

$$|\mathbf{k}_\beta^{\mathrm{T}}-\mathbf{k}_{\beta+\boldsymbol{\delta}^j}^{\mathrm{T}}|^2\leq\left(1+\frac{1}{\nu^2}\right)|\Delta k_j^-|^2$$

We have thus shown that the distance between the two points chosen above is lower than $(1+\frac{1}{\nu^2})^{\frac{1}{2}}|\Delta k_j^-|$ in the transmission area. We assume that the number of interpolation points is then sufficient. Note that this is no longer the case for transmission from the fast to the slow medium. Indeed in that case we may then use a more than four-point interpolation, when necessary. It is not treated here but could be carried out in the same manner, as done in the case of a straight interface.

Defining the upwind fluxes by imposing the continuity of the discretized normal energy flux

Having introduced the modified meshes for the discretization of the wave vectors, one may complete the definition of the numerical fluxes given by Eq. (3.29) or Eq. (3.35) for transmission from the slow to the fast medium, and by Eq. (3.30) or Eq. (3.36) for transmission from the fast to the slow medium, as introduced in the section 3.2.3. This means that, as for the case of a straight interface, we have to define the corrective quantities at a curved interface $\mathrm{b}^n_{\alpha'\beta}$, $\mathrm{b}^n_{\alpha'+j,\beta}$, $\mathrm{b}^n_{\alpha''\beta}$ and $\mathrm{b}^n_{\alpha''-j,\beta}$ as we compute the normal energy flux density at that interface and impose its continuity. Using the change of grids defined above, the latter reads:

$$\sum_{\beta\in\mathcal{K}^+(\mathbf{n})}(c^+\hat{\mathbf{K}}_\beta^+\cdot\mathbf{n})\Delta\mathbf{k}^+\mathrm{b}^n_{\alpha'\beta}=\sum_{\beta\in\mathcal{K}^+(\mathbf{n})}(c^-\hat{\mathbf{k}}_\beta^{\mathrm{T}}\cdot\mathbf{n})C_\beta\Delta\mathbf{k}^+\mathcal{T}^-(\mathbf{k}_\beta^{\mathrm{T}})\mathrm{a}^n\left(\mathbf{X}_{\alpha'},\mathbf{k}_\beta^{\mathrm{T}}\right)$$

for transmission from the slow to the fast medium, and:

$$\sum_{\beta\in\mathcal{K}_c^-(\mathbf{n})}(c^-\hat{\mathbf{K}}^-\cdot\mathbf{n})\Delta\mathbf{k}^-\mathrm{b}^n_{\alpha'+j,\beta}=\sum_{\beta\in\mathcal{K}_c^-(\mathbf{n})}(c^+\hat{\mathbf{k}}_\beta^{\mathrm{T}}\cdot\mathbf{n})C_\beta\Delta\mathbf{k}^-\mathcal{T}^+(\mathbf{k}_\beta^{\mathrm{T}})\mathrm{a}^n\left(\mathbf{X}_\alpha+\Delta x_j\boldsymbol{\delta}^j,\mathbf{k}_\beta^{\mathrm{T}}\right)$$

for transmission from the fast to the slow medium. Here we consider the normal energy flux density at the spatial cells $\mathcal{C}_{\alpha'}$ of the slow medium $\mathcal{O}_h^-$ which are "below" the interface, it being understood that the present discussion applies straightforwardly to the spatial cells $\mathcal{C}_{\alpha''}$ of $\mathcal{O}_h^-$ which are "above" the interface. Also:

$$\hat{\mathbf{K}}_\beta^\pm=\frac{\mathbf{K}_\beta^\pm}{|\mathbf{K}_\beta^\pm|},\quad \hat{\mathbf{k}}_\beta^{\mathrm{T}}=\frac{\mathbf{k}_\beta^{\mathrm{T}}}{|\mathbf{k}_\beta^{\mathrm{T}}|},$$

and the C_β's are coefficients chosen in order to correct for the change of discretization steps between the slow and fast media, as for the case of a straight interface. One may consider for example:

$$C_\beta=\frac{\partial f}{\partial k_{\mathbf{n}}}(\mathbf{K}_\beta^+\cdot\mathbf{n},\mathbf{K}'_\beta)\tag{4.36}$$

for transmission from the slow to the fast medium, and:

$$C_\beta=-\frac{\partial g}{\partial k_{\mathbf{n}}}(\mathbf{K}_\beta^-\cdot\mathbf{n},\mathbf{K}'_\beta)\tag{4.37}$$

for transmission from the fast to the slow medium. From the above equalities one may obtain the following expression of $\mathrm{b}^n_{\alpha'\beta}$:

$$\begin{aligned} \mathrm{b}^n_{\alpha'\beta} &= \mu^-_\beta \tilde{\mathrm{a}}^n \left(\mathbf{X}_{\alpha'}, \mathbf{k}^{\mathrm{T}}_\beta\right) , \\ \mu^-_\beta &= \nu^{-1} C_\beta \left(\frac{\hat{\mathbf{k}}^{\mathrm{T}}_\beta \cdot \mathbf{n}}{\hat{\mathbf{K}}^+_\beta \cdot \mathbf{n}}\right) \mathcal{T}^-(\mathbf{k}^{\mathrm{T}}_\beta) , \end{aligned} \tag{4.38}$$

for transmission from the slow to the fast medium, and recover as for a straight interface that μ^-_β reduces to $\mathcal{T}^-(\mathbf{k}^{\mathrm{T}}_\beta)$ for the above choice of C_β. One may also obtain the following expression of $\mathrm{b}^n_{\alpha'+j,\beta}$:

$$\begin{aligned} \mathrm{b}^n_{\alpha'+j,\beta} &= \mu^+_\beta \tilde{\mathrm{a}}^n(\mathbf{X}_{\alpha'} + \Delta x_j \boldsymbol{\delta}^j, \mathbf{k}^{\mathrm{T}}_\beta) , \\ \mu^+_\beta &= \nu C_\beta \left(\frac{\hat{\mathbf{k}}^{\mathrm{T}}_\beta \cdot \mathbf{n}}{\hat{\mathbf{K}}^-_\beta \cdot \mathbf{n}}\right) \mathcal{T}^+(\mathbf{k}^{\mathrm{T}}_\beta) , \end{aligned} \tag{4.39}$$

for transmission from the fast to the slow medium, and recover that μ^+_β reduces to $\mathcal{T}^+(\mathbf{k}^{\mathrm{T}}_\beta)$ for the above choice of C_β. The equations (4.38) and (4.39) define partly the upwind fluxes. The latter are supplemented with the expressions of the "reflected" discretized specific intensities, defined as an interpolation of the specific intensities $\mathrm{a}^n_{\alpha',\beta^{\mathrm{R}}+\boldsymbol{\delta}^u}$, $u \in \{0,1\}^d$, with the interpolation coefficients of Eq. (4.35); see Eq. (3.33). This completes the definition of the CKS scheme for a curved interface. An alternative approach consists in finding interpolations that cancel the increments of energy that arise from the upwind fluxes used for the numerical resolution of the Liouville equation (the counterpart of the schemes of the sections 4.3.2 and 4.3.3 for a straight interface). It is outlined in the next paragraph.

Defining the upwind fluxes by imposing the conservation of the discretized energy

Let $\Delta\mathbf{k}^\pm := \prod_{j=1}^d \Delta k^\pm_j$. To begin with, the sums for the case of a curved interface that correspond to S^n_1 and S^n_2 of Eq. (4.5) with Eq. (4.7) read as:

$$\begin{aligned} S^n_1 = \sum_{j=1}^d \sum_{(\alpha)_j} \frac{\Delta t}{\Delta x_j} \Bigg[& \sum_{\beta\in\mathcal{K}^-(\mathbf{n})} -c^+ \hat{K}^+_{\beta_j} \Delta\mathbf{k}^+ \mathrm{a}^n_{\alpha'+j,\beta} + \sum_{\beta\in\mathcal{K}^-(\mathbf{n})} c^- \hat{K}^-_{\beta_j} \Delta\mathbf{k}^- \mathrm{b}^n_{\alpha'+j,\beta} \\ & - \sum_{\beta\in\mathcal{K}^+(\mathbf{n})} c^+ \hat{K}^+_{\beta_j} \Delta\mathbf{k}^+ \mathcal{R}^+(\mathbf{K}^+_\beta) \tilde{\mathrm{a}}^n(\mathbf{X}_{\alpha'} + \Delta x_j \boldsymbol{\delta}^j, \mathbf{k}^{\mathrm{R}}_\beta) \Bigg] + \cdots \\ S^n_2 = \sum_{j=1}^d \sum_{(\alpha)_j} \frac{\Delta t}{\Delta x_j} \Bigg[& \sum_{\beta\in\mathcal{K}^+_c(\mathbf{n})} c^- \hat{K}^-_{\beta_j} \Delta\mathbf{k}^- \mathrm{a}^n_{\alpha'\beta} - \sum_{\beta\in\mathcal{K}^+_c(\mathbf{n})} c^+ \hat{K}^+_{\beta_j} \Delta\mathbf{k}^+ \mathrm{b}^n_{\alpha'\beta} \\ & + \sum_{\beta\in\mathcal{K}^-_c(\mathbf{n})} c^- \hat{K}^-_{\beta_j} \mathcal{R}^-(\mathbf{K}^-_\beta) \tilde{\mathrm{a}}^n(\mathbf{X}_{\alpha'}, \mathbf{k}^{\mathrm{R}}_\beta) \Bigg] + \cdots \end{aligned} \tag{4.40}$$

where the dots stand for the part related to the cells which are above the interface and labelled by α'' (as defined by Eq. (4.33)). Again $\tilde{\mathrm{a}}^n(\mathbf{X}_{\alpha'}, \mathbf{k}^{\mathrm{R}}_\beta)$ and $\tilde{\mathrm{a}}^n(\mathbf{X}_{\alpha'} + \Delta x_j \boldsymbol{\delta}^j, \mathbf{k}^{\mathrm{R}}_\beta)$ stands for the "reflected" discretized specific intensities at each edges that the cells $\mathcal{C}_{\alpha'}$ share with $\mathcal{I}$, as given by Eq. (3.33). One may then observes that the different terms in the sums above can be cancelled as a whole. In particular, for a given index β, the terms associated to the "reflected" and "transmitted" wave vectors may cancel the term that corresponds to the "incident" (actual) wave vector $\mathbf{K}_\beta$. One has however to consider the different cases of transmission from the slow to the fast (so as to possibly cancel S^n_2) and from the fast to the slow medium (so as to possibly cancel S^n_1). Actually it is possible to show that the sum S^n_2 can always be cancelled, except for the case of total reflection of Eq. (4.12). We thus consider this situation hereafter, taking the example of a two-dimensional ($d = 2$) physical domain. The two-point interpolation of the normal coordinate of the "transmitted" wave vectors (as obtained by backward transmission) used for a straight interface, is replaced by a four-point interpolation of the "reflected" and "transmitted" wave vectors (as

obtained by backward reflection and transmission) using four mesh points. We implicitly assume here that such a four-point interpolation is sufficient in order to cover all the set of multi- indices by backward reflection and transmission. We thus define for the actual wave vector $\mathbf{K}_\beta$, the set of discretized wave vectors (obtained by backward reflection or transmission) that shall be used in a four-point interpolation so as to cancel S_2^n. It is denoted by IC_β, such that:

$$\mathrm{IC}_\beta = \mathcal{C}_\beta \cup \mathcal{C}_{\beta-\boldsymbol{\delta}^1} \cup \mathcal{C}_{\beta-\boldsymbol{\delta}^2} \cup \mathcal{C}_{\beta-\boldsymbol{\delta}^1-\boldsymbol{\delta}^2}\,.$$

We then adopt the strategy outlined in the section 4.3.2 defining the FCS scheme for a straight interface, by seeking some positive coefficients $C^{\pm}_{\beta'+\boldsymbol{\delta}^u}$ and $\Gamma^{\pm}_{\beta''+\boldsymbol{\delta}^u}$, $u \in \{0,1\}^d$, such that the sum S_2^n of Eq. (4.40) above cancel. The parameters $\mu_\beta^\pm$ are defined by:

$$\mu_\beta^\pm = \mathcal{T}^\pm(\mathbf{k}_\beta^{\mathrm{T}})\,,$$

which corresponds to Eq. (4.38) and Eq. (4.39) where the parameter C_β is taken as in Eq. (4.36) and Eq. (4.37), respectively. For a given cell $\mathcal{C}_{\alpha'}$ of the slow medium $\mathcal{O}_h^-$ which is "below" the interface (it being understood again that the present analysis applies straightforwardly to a spatial cell $\mathcal{C}_{\alpha''}$ of $\mathcal{O}_h^-$ which is "above" the interface):

$$\begin{aligned}
\mathrm{b}^n_{\alpha'\beta} &= \mathcal{T}^-(\mathbf{k}_\beta^{\mathrm{T}})\tilde{\mathrm{a}}^n\left(\mathbf{X}_{\alpha'}, \mathbf{k}_\beta^{\mathrm{T}}\right)\,,\\
\mathrm{b}^n_{\alpha'+j,\beta} &= \mathcal{T}^+(\mathbf{k}_\beta^{\mathrm{T}})\tilde{\mathrm{a}}^n\left(\mathbf{X}_{\alpha'} + \Delta x_j \boldsymbol{\delta}^j, \mathbf{k}_\beta^{\mathrm{T}}\right)
\end{aligned}$$

where $\tilde{\mathrm{a}}^n(\mathbf{X}_{\alpha'}, \mathbf{k}_\beta^{\mathrm{T}})$ and $\tilde{\mathrm{a}}^n(\mathbf{X}_{\alpha'} + \Delta x_j\boldsymbol{\delta}^j, \mathbf{k}_\beta^{\mathrm{T}})$ are interpolated on the wave vector meshes following Eq. (3.34). Likewise, $\tilde{\mathrm{a}}^n(\mathbf{X}_{\alpha'}, \mathbf{k}_\beta^{\mathrm{R}})$ and $\tilde{\mathrm{a}}^n(\mathbf{X}_{\alpha'} + \Delta x_j\boldsymbol{\delta}^j, \mathbf{k}_\beta^{\mathrm{R}})$ are interpolated on the wave vector meshes following Eq. (3.33). The coefficients $C^-_{\beta'+\boldsymbol{\delta}^u}$ and $\Gamma^-_{\beta''+\boldsymbol{\delta}^u}$ are sought for such that they cancel the sum S_2^n, plugging these interpolations into Eq. (4.40). In doing so one may show that the latter reads as a sum on the spatial cells $\mathcal{C}_{\alpha'}$ and $\mathcal{C}_{\alpha''}$ of the slow medium $\mathcal{O}_h^-$ which are "below" and "above" the interface, respectively, as:

$$\begin{aligned}
S_2^n = &-\frac{\Delta t}{\Delta x_1}\sum_{\alpha'}\Bigg[\sum_{\beta'\in\mathcal{K}_c^+(\mathbf{n})}(c^-\hat{\mathbf{K}}^-_{\beta'}\cdot\mathbf{N})\Delta\mathbf{k}^-\mathrm{a}^n_{\alpha'\beta'} - \sum_{u\in\{0,1\}^2}\sum_{\beta\in\mathcal{K}^+(\mathbf{n})}(c^+\hat{\mathbf{K}}^+_{\beta}\cdot\mathbf{N})\Delta\mathbf{k}^+\Gamma^-_{\beta^{\mathrm{T}}+\boldsymbol{\delta}^u}\mathcal{T}^-(\mathbf{k}_\beta^{\mathrm{T}})\mathrm{a}^n_{\alpha',\beta^{\mathrm{T}}+\boldsymbol{\delta}^u}\\
&\qquad + \sum_{u\in\{0,1\}^2}\sum_{\beta\in\mathcal{K}_c^-(\mathbf{n})}(c^-\hat{\mathbf{K}}^-_{\beta}\cdot\mathbf{N})\Delta\mathbf{k}^-C^-_{\beta^{\mathrm{R}}+\boldsymbol{\delta}^u}\mathcal{R}^-(\mathbf{K}^-_\beta)\mathrm{a}^n_{\alpha',\beta^{\mathrm{R}}+\boldsymbol{\delta}^u} + \dots\Bigg]\\
&-\frac{\Delta t}{\Delta x_1}\sum_{\alpha''}\Bigg[\sum_{\beta'\in\mathcal{K}_c^+(\mathbf{n})}(c^-\hat{\mathbf{K}}^-_{\beta'}\cdot\mathbf{N})\Delta\mathbf{k}^-\mathrm{a}^n_{\alpha''\beta'} - \sum_{u\in\{0,1\}^2}\sum_{\beta\in\mathcal{K}^+(\mathbf{n})}(c^+\hat{\mathbf{K}}^+_{\beta}\cdot\mathbf{N})\Delta\mathbf{k}^+\Gamma^-_{\beta^{\mathrm{T}}+\boldsymbol{\delta}^u}\mathcal{T}^-(\mathbf{k}_\beta^{\mathrm{T}})\mathrm{a}^n_{\alpha'',\beta^{\mathrm{T}}+\boldsymbol{\delta}^u}\\
&\qquad + \sum_{u\in\{0,1\}^2}\sum_{\beta\in\mathcal{K}_c^-(\mathbf{n})}(c^-\hat{\mathbf{K}}^-_{\beta}\cdot\mathbf{N})\Delta\mathbf{k}^-C^-_{\beta^{\mathrm{R}}+\boldsymbol{\delta}^u}\mathcal{R}^-(\mathbf{K}^-_\beta)\mathrm{a}^n_{\alpha'',\beta^{\mathrm{R}}+\boldsymbol{\delta}^u} + \dots\Bigg],
\end{aligned} \tag{4.41}$$

where the discretized normal vector $\mathbf{N}$ depends on the cell and is defined as follows. For the spatial cells $\mathcal{C}_{\alpha'}$ or $\mathcal{C}_{\alpha''}$ that share one common edge with $\mathcal{I}$ one has:

$$\mathbf{N} = \begin{cases} -\boldsymbol{\delta}^1 & \text{if} \quad \alpha' = (\alpha)_1 + \alpha_1^1\boldsymbol{\delta}^1\,,\\ -\dfrac{\Delta x_1}{\Delta x_2}\boldsymbol{\delta}^2 & \text{if} \quad \alpha' = (\alpha)_2 + \alpha_2^1\boldsymbol{\delta}^2\,,\\ \dfrac{\Delta x_1}{\Delta x_2}\boldsymbol{\delta}^2 & \text{if} \quad \alpha'' = (\alpha)_2 + \alpha_2^2\boldsymbol{\delta}^2\,. \end{cases}$$

For those cells that share two common edges with $\mathcal{I}$, one has:

$$\mathbf{N} = \begin{cases} -\boldsymbol{\delta}^1 - \dfrac{\Delta x_1}{\Delta x_2}\boldsymbol{\delta}^2 & \text{if} \quad \alpha' = (\alpha)_1 + \alpha_1^1\boldsymbol{\delta}^1 = (\alpha)_2 + \alpha_2^1\boldsymbol{\delta}^2\,,\\ -\boldsymbol{\delta}^1 + \dfrac{\Delta x_1}{\Delta x_2}\boldsymbol{\delta}^2 & \text{if} \quad \alpha'' = (\alpha)_1 + \alpha_1^2\boldsymbol{\delta}^1 = (\alpha)_2 + \alpha_2^2\boldsymbol{\delta}^2\,. \end{cases}$$

This expansion is further detailed in the appendix G, see the Eq. (G.1). Note that in the above, $\Gamma^-_{\beta^{\mathrm{T}}+\boldsymbol{\delta}^u}$ and $C^-_{\beta^{\mathrm{R}}+\boldsymbol{\delta}^u}$ depend *a priori* on β. Now it is possible to show that these coefficients may be chosen in order to cancel the different terms that are made explicit in the expansion of S_2^n above. More precisely, it is possible to show that in most cases the signs of the different contributions from the "incident", "reflected" and "transmitted" terms in S_2^n above cancel each other. Further details about this analysis are again given in the appendix G.

Now the same approach used for the sum S_1^n shows that the different contributions of the "incident", "reflected" and "transmitted" terms may no longer be cancelled for each "incident" discrete wave vector $\mathbf{K}_\beta$. More specifically it is possible to show, that the projections of the "incident", "reflected" and "transmitted" discrete wave vectors on the vector $\mathbf{N}$ have signs that do not allow to cancel the corresponding contributions. This is illustrated on the Figure 4.2 below, where a counterexample is given. In that case of transmission of acoustic waves from a fast to a slow medium, it is no longer possible to define conservative numerical schemes as the ones detailed here for transmission from a slow to a fast medium. It is then necessary to adopt another approach in this situation, which is not considered further on in the subsequent chapter 5 concerning the numerical results. A possible alternative may be the following. Assume some "incident", "reflected" and "transmitted" wave vectors are given. We also consider two additional vectors $\mathbf{N}$ and $\mathbf{N}'$ that form a basis of $\mathbb{R}^2$, and that correspond to discretized normal vectors on neighboring spatial cells. An important feature is that the projections of the "incident", "reflected" and "transmitted" wave vectors have opposite signs whether they are considered along the vector $\mathbf{N}$ or along the vector $\mathbf{N}'$. It is thus possible to define interpolation coefficients that take into account the different contributions on several neighboring cells with different discretized normal vectors. They are obtained by equating to zero the terms in front of the discretized specific intensities corresponding to those different cells. This is a way to define non-conservative numerical schemes, of which efficiency may be compared to the classical and modified schemes expounded in this chapter. This applies especially for relatively important discretization numbers, in order to reduce the global loss of energy.

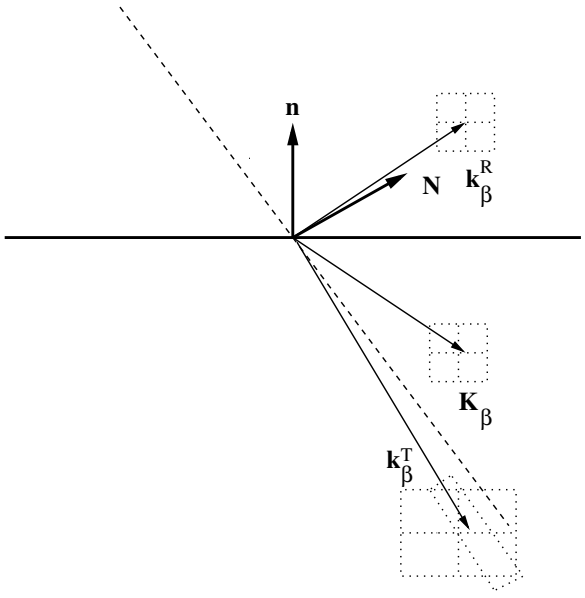

Figure 4.2: Counterexample for canceling the sum S_1^n in case of transmission from a fast to a slow medium. We observe that the projections of the "transmitted" wave vector and of the "incident" wave vector $\mathbf{K}_\beta$ along the vector $\mathbf{N}$ have opposite signs, while the projections of the "reflected" wave vector and of the "incident" wave vector along that $\mathbf{N}$ have the same sign. In that case, the components in front of the $\mathrm{a}^n_{\alpha,\beta}$'s cannot be cancelled.

4.5 Conclusions

In this chapter, we have derived several numerical upwind fluxes to be used with the finite difference scheme considered for the resolution of the kinetic equation (Liouville transport equation) chosen to describe high-frequency wave diffractions at an interface between two acoustic media with different sound speeds. They are constructed so as to conserve the discretized normal energy flux or the discretized total energy within the computational domain as the waves get reflected and transmitted by that interface. Both cases of a straight and a curved interface have been investigated. In the case of a straight interface, a classical scheme is compared to different corrective schemes, and satisfactory results are obtained in terms of the conservation of the computed total energy. In the case of a curved interface, the same results are obtained with similar methods, but they do not apply to all cases as briefly discussed at the end of the foregoing section. Thus the methods used with a straight interface can be adapted to some particular cases of curved interfaces in order to obtain the same results. They need be developed further on to obtain numerical schemes that would be efficient in all cases.

5

Numerical Results for straight and curved interfaces

In this Chapter, we consider the numerical applications of the conservative schemes defined in the previous Chapter. We recall, that the non-conservation of the energy flux density at the single interface $\mathcal{I}$ considered here, is due to the irregular distribution of the incident wave vectors mesh, which means, that all the incident wave vectors are not necessarely caught by a classical interpolation of points. This irregularity is related to the importance of the ratio $\frac{c^+}{c^-}$, which rules the distribution of wave vectors on each side of $\mathcal{I}$. A second cause is the interpolation of the incident wave vectors itself, at the interface $\mathcal{I}$, which may be fixed by a corrective scheme, that uses a specific interpolation of the incident wave vectors obtained by transmission from the slow to the fast, or from the fast to the slow medium, on the discretized mesh. These interpolations, correspond to a point by point correction of the loss of energy at the interfaces of the medium. In case of a global correction of the loss of the flux density at the interface $\mathcal{I}$, corrective schemes, that are based on the choice of different distribution of wave vectors meshes on each side of $\mathcal{I}$ are used. The latter are efficients in case of large discretization numbers of the wave vector meshes, and they enable to correct the problem in that case. They also apply for small discretization numbers, and may be completed in that case, by the first type of corrective schemes mentionned above.

In order to demonstrate the interest of the method, and of the different types of schemes presented above, we consider different examples of (WKB) initial conditions, discretized with a small number of wave vectors, and for which a theoretical solution is known (see the Example (2.87)). This allows to draw a comparison between the latter solution and the numerical solutions obtained. The theoretical solution is computed for a straight interface, which correspond to a straight line (in case of a straight interface), and to a slanted line, in case of a curved interface. These comparisons allow to estimate, the error to the exact solution.

We consider first, the case of a straight interface, and examples, that illustrate the first corrective method, and show the interest of the method. We then consider examples, that show the interest of the second corrective method. The case of a curved interface is presented in the second part of this chapter.

5.1 Straight interface

We consider in the present section, the reflexion and transmission problem through a straight interface, discretized on a regular grid of wave vectors by one of the FD schemes presented in the previous chapter.

We consider initial conditions, with a small number of incident wave vectors, which highlight the problem raised by a classical discretization presented in the Section 3.4. More precisely, the examples presented in this section, rely on different initial conditions, that illustrate the loss and increase of energy at the crossing of the interface $\mathcal{I}$ of the domain $\mathcal{O}_h$, for the standart numerical schemes denoted SNS (see the Section 4.3.1 of Chapter 4). We consider a computational domain with a single interface $\mathcal{I}$, these conditions applying for specific intensities (see Equation (2.74)) are all derived from high-frequency initial

conditions for a solution of the wave or of the Navier equation, which is described in the Section 2.4 of the Chapter 2.

The solutions obtained are compared to a theoretical one, derived in case of a straight interface by solving the formal equations on the rays, and by using the conservative numerical schemes presented in the Sections 4.3.2 and 4.3.3. The comparison between the two solutions is done computing the errors of the energy field locally and globally. Convergence results with respect to spatial discretization, are given in the following paragraphs.

5.1.1 Illustration of the problem: classical FD scheme

We first present, the solution obtained using a standart FD scheme described in the Section 4.3.1. This solution is compared to a theoretical solution, described in the Appendix H, and illustrate the loss and gain of energy. All these examples, correspond to an initial condition of the form (2.45) (WKB initial condition).

We detail here the form of these initial conditions. One may verify (see (2.87)), that for an amplitude and phase function given by the form (2.32), the following initial condition (case of acoustic waves) is obtained:

$$\mathrm{a}(0,\mathbf{x},\mathbf{k}) = \left[\frac{\rho(\mathbf{x})}{2}|A(\mathbf{x})^2||\nabla S(\mathbf{x})|^2 + \frac{1}{2\rho(\mathbf{x})c(\mathbf{x})^2}|B(\mathbf{x})|^2\right]\delta\left(\mathbf{k}-\nabla_{\mathbf{x}}S\right)\,, \tag{5.1}$$

where $\rho(\mathbf{x})$ and $c(\mathbf{x})$ denote the density and the celerity of the acoustic medium, and are functions of the position. In the subsequent examples, the amplitude and phase functions $A(\mathbf{x})$, $A(\mathbf{x})$ and $S(\mathbf{x})$ read:

$$B(\mathbf{x}) = A(\mathbf{x}) = A_0 \exp\left(-((x_1-\mathrm{u}_1)/r_1)^2 - ((x_2-\mathrm{u}_2)/r_2)^2\right)\,,$$
$$S(\mathbf{x}) = \left(\frac{x_1-\mathrm{v}_1}{r_1'}\right)^2 + \left(\frac{x_2-\mathrm{v}_2}{r_2'}\right)^2\,.$$

The parameters $\mathbf{u}$, $\mathbf{v}$ denote the characteristic vectors around which this Gaussian initial condition is centered, while the parameters r_1, r_2, r_1' and r_2' denote its characteristic widths. $B(\mathbf{x})$ has the same form as $A(\mathbf{x})$. The characteristic lengths are usually small parameters, that describe stung initial conditions, bounded in space and in the wave vector domain. The celerities and densities are taken constant, in each homogeneous subdomain of $\mathcal{O}_h$. The different parameters used in the examples presented in this Section, are summarized in the Table 5.1. The examples illustrate the loss of energy, that appears at the crossing

Parameters	*Example 1*	*Example 2*	*Example 3*
$\mathbf{v}-\mathbf{u}$	(-1.6, 0)	(-1.6, 0)	(-2.4, -0.4)
Initial position, $\mathbf{u}$	(-0.3, 0)	(-0.3, 0)	(-0.3, 0)
$x_{\mathcal{I}}$	0.25	0	0
c^-	1.0	1.0	1.0
c^+	3.0	3.0	3.0
$N_1 = N_2$	25	50	50
$M_1 = M_2$	100	100	100
r_1	0.05	0.05	0.05
r_2	0.05	0.05	0.05
r_1'	$1/\sqrt{2}$	$1/\sqrt{2}$	$1/\sqrt{2}$
r_2'	$1/\sqrt{2}$	$1/\sqrt{2}$	$1/\sqrt{2}$

Table 5.1: The different parameters for each of the three examples.

of the interface $\mathcal{I}$, due to the classical interpolation of the incident wave vectors. We observe in a first step the evolution of the total energy, for the classical scheme, during one crossing of the straight interface $\mathcal{I}$, and compare it to the analytical solution. We then draw in a second step the L^2-Error of the classical solution obtained, in order to estimate the error to the exact solution. We recall, that our examples are chosen in order to highlight the problems encountered, for an initial condition, that carries energy on a

few number of wave vectors. In this case, the interpolation method of the incident wave vectors, computed by transmission, on the mesh of discretized wave vectors, play an important role in the conservation of the flux density at the interface $\mathcal{I}$. We thus start with a classical example of transmission of an initial condition, from a slow to a fast homogeneous subdomain of $\mathcal{O}_h$. *Example 1* is defined by the following parameters. The dimensionless celerities in the slow and in the fast medium are taken respectively equal to $c^- = 1.0$ and $c^+ = 3.0$, while the dimensionless densities are both taken equal to $\rho^- = \rho^+ = 1.0$. The energy of the initial condition, is then distributed onto a small number of discretized wave vectors. More precisely, the Dirac distribution, that appears in the initial condition is discretized as follows:

$$\delta(\mathbf{k}-\mathbf{k}_0) = \frac{1}{4} \sum_{\delta_k^{1,2} \in \{0,\Delta k_{1,2}\}} \delta_0 \left(\mathbf{k} - (\mathbf{k}'_0 + \delta_k^1 \mathbf{x}_1 + \delta_k^2 \mathbf{x}_2)\right) , \tag{5.2}$$

where $\mathbf{k}_0$ belongs to the square defined by its corners $\left\{\mathbf{k}'_0 + (\delta_k^1 \mathbf{x}_1 + \delta_k^2 \mathbf{x}_2),\ \delta_k^{1,2} \in \{0, \Delta k_{1,2}\}\right\}$, and δ_0 is defined as follows:

$$\delta_0(\mathbf{k}-\mathbf{k}') = \left\{ \begin{array}{lll} 1 & \text{if} & \mathbf{k} = \mathbf{k}' , \\ 0 & \text{if} & \mathbf{k} \neq \mathbf{k}' . \end{array} \right.$$

In the numerical simulations, the term $\nabla S(\mathbf{x})$ is approximated by the vector $(2(\mathrm{u}_1 - \mathrm{v}_1)/(r'_1)^2, 2(\mathrm{u}_2 - \mathrm{v}_2)/(r'_2)^2)$, such that the initial condition is carried by four discretized wave vectors.

The main vectors of the initial condition $\mathbf{u}$ and $\mathbf{v}$ are given here by:

$$\mathbf{u} = (-0.3,\, 0)\,, \quad \mathbf{v} = (-1.9,\, 0)\,,$$

while the relative lengths are given by $r_1 = r_2 = 0.05$, and $r'_1 = r'_2 = 1/\sqrt{2}$. The wave vector domain is defined for this example, as the set $[-2.4,\, 2.4] \times [-0.6,\, 0.6]$, while $\mathcal{O}_h$ is defined as the set of points $[-0.75,\, 0.75] \times [-0.5,\, 0.5]$. The discretization numbers are respectively taken equal to $N_1 = N_2 = 25$ for the wave vector domain, and $M_1^- = M_2^- = M_2^+ = M_1^+ = 50$ for the space domain, which defines the whole discretization (see the Section 3.1 of Chapter 3, and the Figure 5.1).

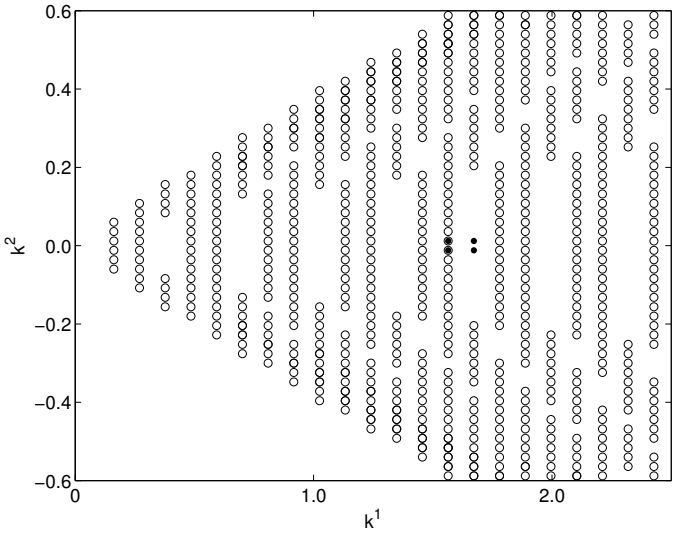

Figure 5.1: Image of the wave vectors distribution obtained by transmission represented by its interpolation points (grey rings) and corresponding incident wave vectors (black dots) for the *Example 1* (normal incidence on a straight interfantsce, $\mathbf{u} = (-0.3, 0)$, $\mathbf{v} = (-1.9,\, 0)$), with respective discretization numbers along the wave vectors variable defined by $N_1 = N_2 = 25$ (see the Section 3.4 of Chapter 3).

The energy variation for this initial condition is shown in the Figure 5.2, and the loss of energy obtained with the classical scheme is important. We observe that more than 60% of the energy of the

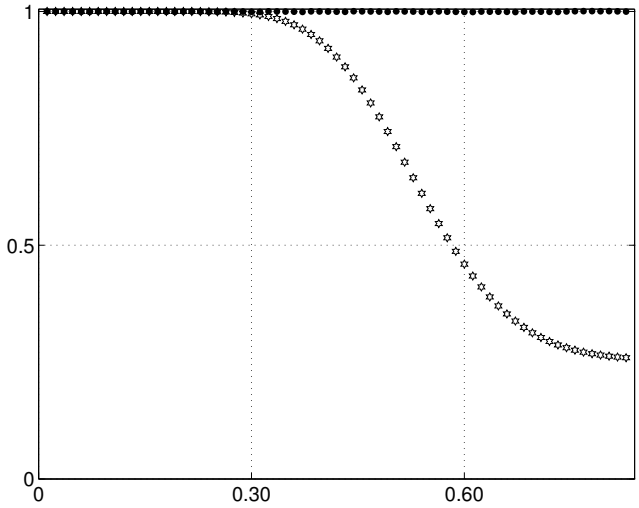

Figure 5.2: Total energy variations for the classical scheme (white stars) and for the analytical scheme (black points), as a function of time t (s), with a time step $\mathrm{d}t = 0.003\,s$ (*Example 1*, normal incidence, with parameters $\mathbf{u} = (-0.3,\, 0)$, $\mathbf{v} = (-1.9,\, 0)$, $N_1 = N_2 = 25$).

classical solution is lost during the simulation at the interface $\mathcal{I}$, in comparison to the analytical solution for which energy is conserved. This corresponds to snapshots of the Figure 5.3, where the energy density of the solutions is plotted. One observes, that a very small part of the energy density is transmitted through the straight interface in comparison to the theoretical solution. Note, that energy obtained at the end of the simulation (for a passage from the slow to the fast side of $\mathcal{I}$) corresponds almost to the reflected energy (reflection for a normal incidence with $\mathcal{R}^- = 0.25$). Hence the transmitted energy is almost totally lost. One observes, that the transmission of the incident density at $\mathcal{I}$ depends on the distribution of the incident wave vectors among the interpolation points of the wave vectors obtained by transmission through $\mathcal{I}$ (see the Figure 5.1), And on the weights of the interpolation of the transmitted density at the interface $\mathcal{I}$. More precisely, the transmission of the initial energy density depends on the distribution of the energy on the incident wave vectors, which shows the importance of the choice of the initial incident vectors for the transmission of energy through the interface $\mathcal{I}$. *Example 2* deals with the same physical domain and initial conditions as *Example 1*. Only the numerical parameters N_1 and N_2, and the interface abscissa $x_{\mathcal{I}}$ differ of the numerical solution (see the Figure 5.4).

The total energy variations for the classical scheme, show that the energy increases at the interface. One may observe that the transmitted energy is multiplied by a number of the order the ratio $\nu = \frac{c^+}{c^-}$ (see the Figure 5.5), as the initial density crosses $\mathcal{I}$. The transmitted energy density is thus multiplied by an important factor, which is confirmed by making the comparison of the classical solution with the analytical solution (see the Figure 5.6). The energy density carried by the interpolated wave vectors is thus amplified at $\mathcal{I}$, because of the difference of celerity between the slow and the fast medium. We thus observe once more on this example, that the global energy is modified at $\mathcal{I}$, and that the error of the classical solution is important for this discretization (see the Figure 5.7). One observes more precisely, that the distribution of the incident vectors is important in the transmission of energy through the interface $\mathcal{I}$.

Example 3 is given by an initial condition propagating from the slow to the fast medium, but with an incident angle of $\arctan(1/6) \approx 9.46$. Hence the initial density is centered on the following main vectors:

$$\mathbf{u} = (-0.3,\, 0.0)\,, \quad \mathbf{v} = (-2.7,\, -0.4)\,,$$

Main vectors of the initial condition are plotted in the Figure 5.8, while the energy variations of the classical scheme, and of the analytical solution are plotted in the Figure 5.9. We observe that the global variation (loss) of energy is less important than for the two other examples. This is confirmed by

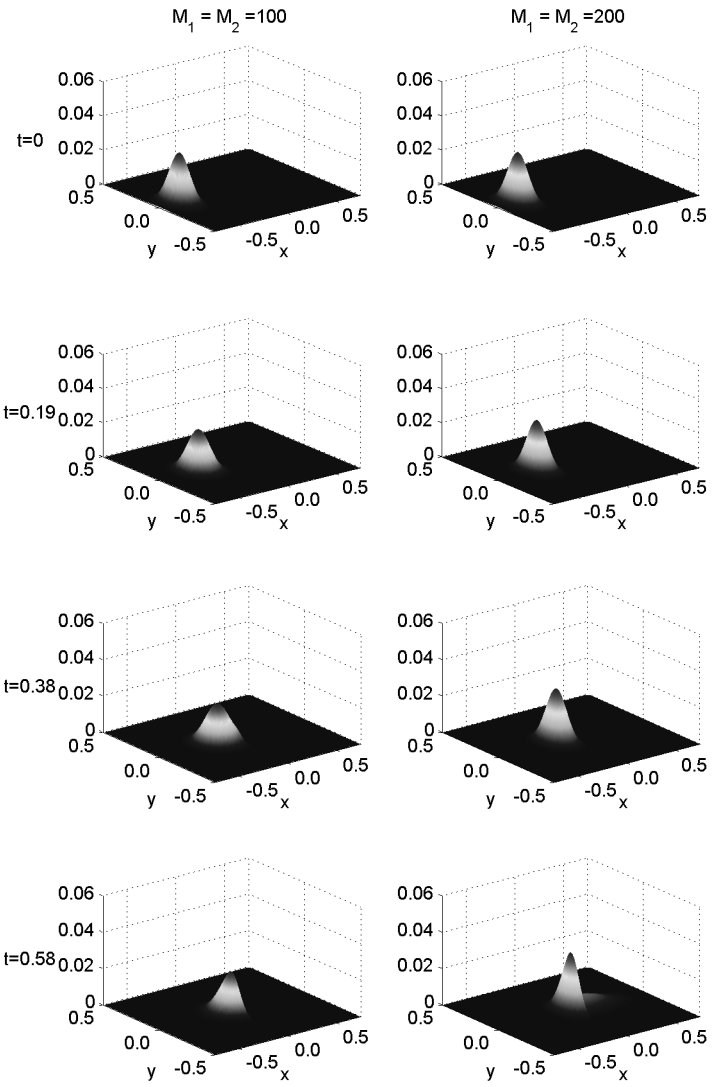

Figure 5.3: Energy density of the classical and analytical schemes for transmission from the slow to the fast medium, *Example 1* (normal incidence, with parameters $\mathbf{u} = (-0.3,\, 0)$ and $\mathbf{v} = (-1.9,\, 0)$ and discretization numbers $N_1 = N_2 = 25$). The density is plotted at time steps $t = 0\,s$, $t = 0.19\,s$, $t = 0.38\,s$, $t = 0.58\,s$, with time step $\mathrm{d}t = 0.003\,s$.

comparing the energy densities (plotted at time steps $t = 0\,s$, $t = 0.17\,s$ and $t = 0.34\,s$ and $t = 0.50\,s$) in the Figure 5.10, that corresponds to the classical and analytical solutions. The error plotted in the Figure 5.11 is also less important, than for the previous example. The solution obtained with this discretization is thus closer to the exact solution. Nevertheless, the energy variations through $\mathcal{I}$ remains important, such that this loss may be corrected. Note, that the initial conditions presented in this paragraph, are chosen in order to underline the loss of energy. In the next Section, the numerical schemes, and variations of the discretization number $M_1 = M_1^- + M_1^+$ and $M_2 = M_2^- + M_2^+$ show how to correct the approximated solutions obtained here.

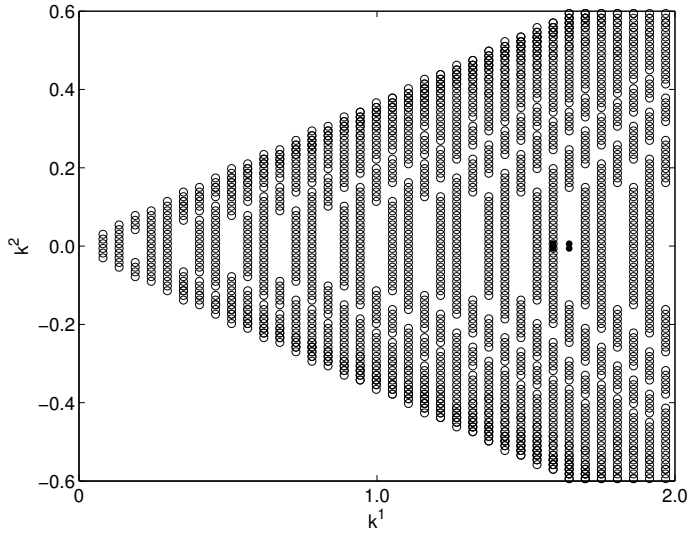

Figure 5.4: Image of the wave vectors distribution obtained by transmission represented by its interpolation points for the *Example 2* (normal incidence, with parameters $\mathbf{u} = (-0.3, 0)$ and $\mathbf{v} = (-1.9, 0)$), with a discretization number following the wave vectors coordinates N_1 and N_2 equal to $N_1 = N_2 = 50$.

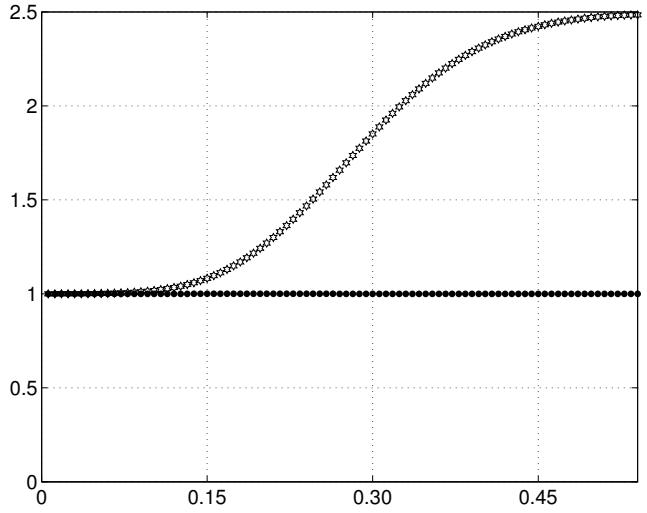

Figure 5.5: Total energy variation, for the classical and analytical solutions, as a function of time t (s), for the *Example 2* (normal incidence, with parameters $\mathbf{u} = (-0.3, 0)$, $\mathbf{v} = (-1.9, 0)$, $N_1 = N_2 = 50$), with a time step $\mathrm{d}t = 0.003\,s$.

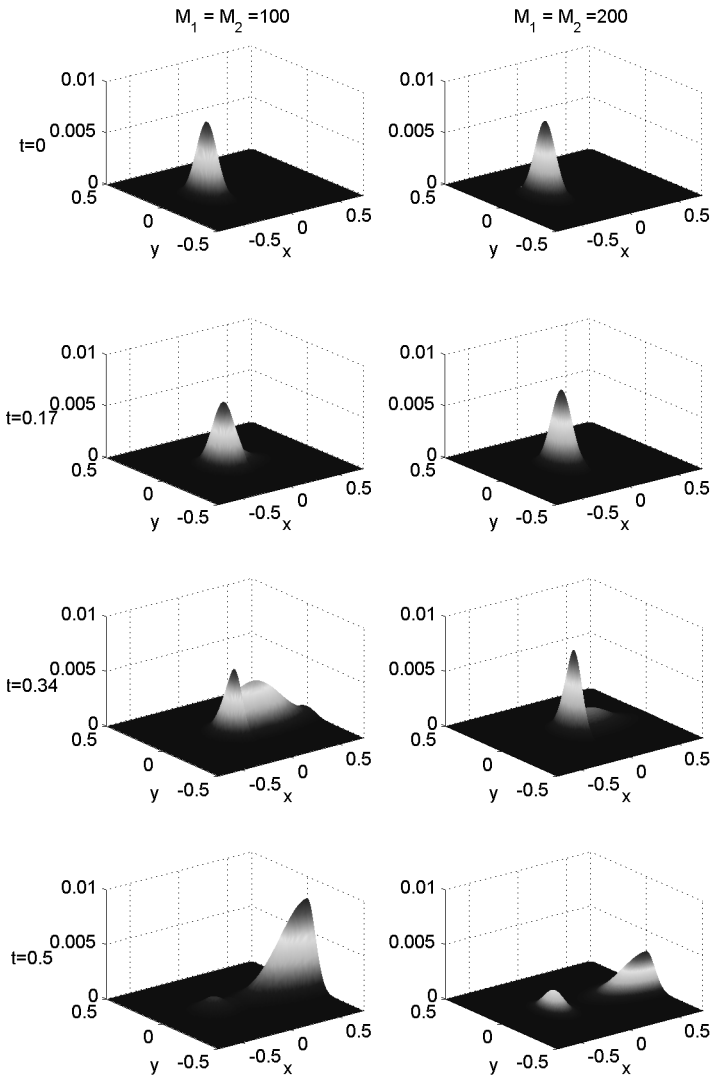

Figure 5.6: Energy density of the classical and analytical solution for the *Example 2* (normal incidence, with parameters $\mathbf{u} = (-0.3, 0)$, $\mathbf{v} = (-1.9, 0)$, $N_1 = N_2 = 50$) at the different time steps $t = 0\,s$, $t = 0.17\,s$, $t = 0.34\,s$ and $t = 0.50\,s$.

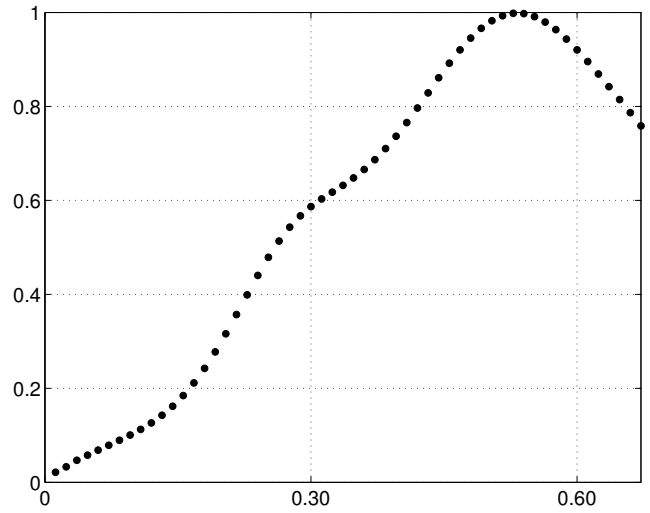

Figure 5.7: L^2-error on the standart solution during a simulation (t in seconds (s)) for the *Example 2* (normal incidence, with parameters $\mathbf{u} = (-0.3,\, 0)$, $\mathbf{v} = (-1.9,\, 0)$, $N_1 = N_2 = 50$), transmission from a slow to a fast medium, with $\mathrm{d}t = 0.003\,s$.

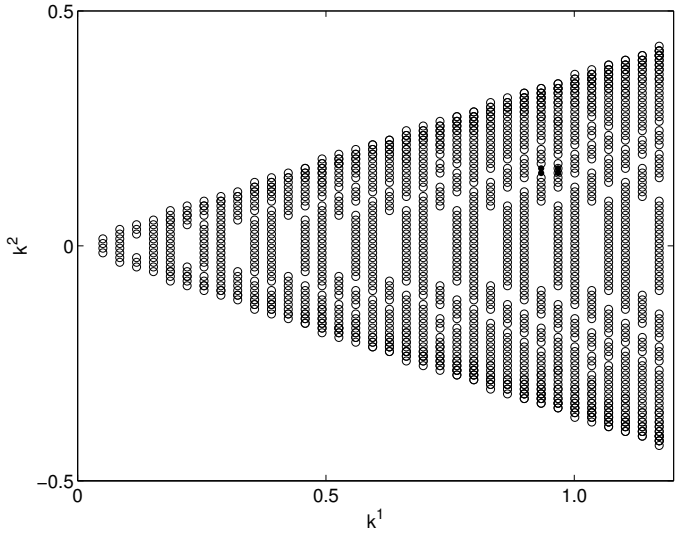

Figure 5.8: Image of the wave vectors distribution obtained by transmission represented by its interpolation points for the *Example 3* (slanted incidence with parameters $\mathbf{u} = (-0.3,\, 0)$, $\mathbf{v} = (-2.7,\, -0.4)$, and discretization steps $N_1 = N_2 = 50$) with a time step $\mathrm{d}t = 0.003\,s$.

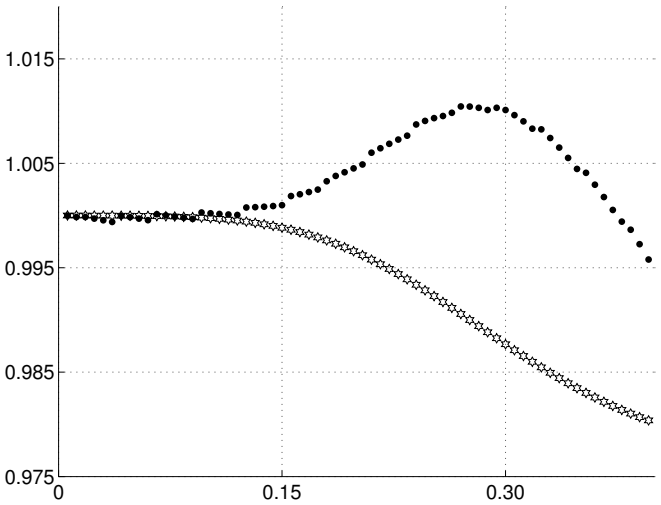

Figure 5.9: Energy variations for the classical and analytical solution of the *Example 3* as functions of the time t (s) (slanted incidence with parameters $\mathbf{u} = (-0.3,\, 0)$, $\mathbf{v} = (-2.7,\, -0.4)$, and discretization steps $N_1 = N_2 = 50$) with a time step $\mathrm{d}t = 0.003\, s$.

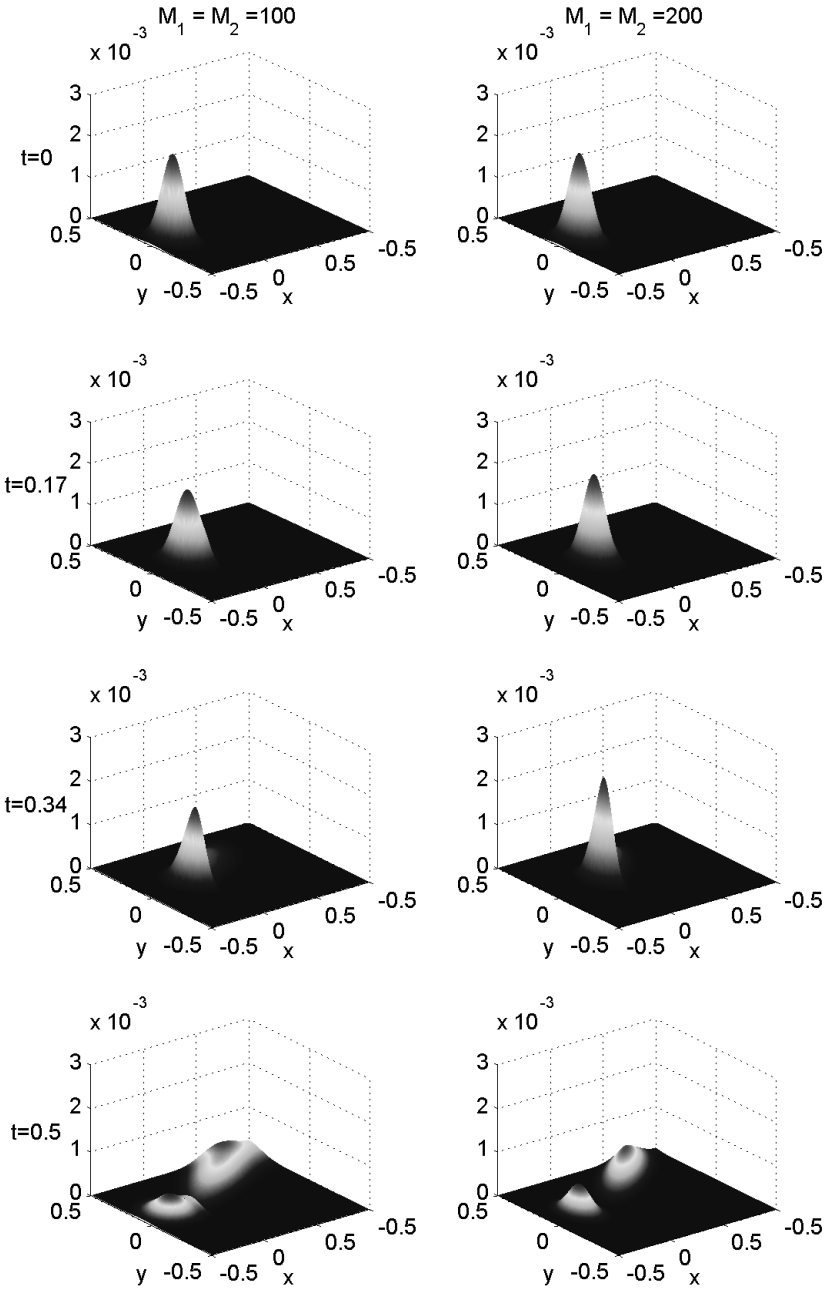

Figure 5.10: Energy density of the classical and analytical solution plotted at time steps $t = 0\,s$, $t = 0.17\,s$, $t = 0.34\,s$, $t = 0.50\,s$, for the *Example 3* presented above (slanted incidence with parameters $\mathbf{u} = (-0.3,\ 0)$, $\mathbf{v} = (-2.7,\ -0.4)$, and discretization steps $N_1 = N_2 = 50$).

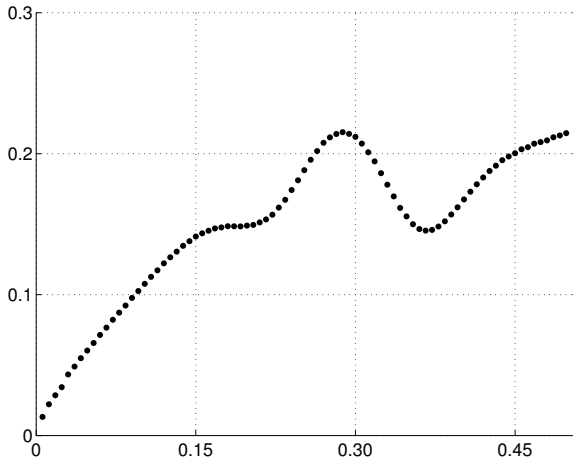

Figure 5.11: L^2-Error of the classical solution for the *Example 3* as a function of the time t (s) (slanted incidence with parameters $\mathbf{u} = (-0.3,\, 0)$, $\mathbf{v} = (-2.7,\, -0.4)$, and discretization numbers $N_1 = N_2 = 50$).

5.1.2 Discretization of k, first conservative scheme (FCS)

The three examples presented in the Section 5.1.1, are now solved using the first corrective method, presented in the previous chapter (see the Paragraph 4.3.2 of the Chapter 4). We recall, that this method consists in a FD scheme, that corrects the loss of energy of the classical scheme. We thus consider, the corrected solution, for different values of the discretization number $M_1 = M_1^- + M_1^+$ and $M_2 = M_2^- + M_2^+$, and a constant value of the discretization numbers N_1 and N_2, equal to $N_1 = N_2 = 25$ for the first example and $N_1 = N_2 = 50$ for the others. The numerical solutions preserve the total energy during the whole simulation, on homogeneous subdomains (propagation), and at the interfaces of $\mathcal{O}_h$ (reflection and transmission), and this for all values of the discretization numbers. Nevertheless, the different energy densities obtained do not fit the analytical one, and the error to the exact solution can be computed and observed for these different values. We thus observe the evolution of the energy densities and of the (L^2-)error to the exact solution, for different values of M_1 and M_2.

We consider, the energy densities for the *Example 1*, whose parameters are described in the Table 5.1, except M_1 and M_2 which varie from 50 to 200. We observe in the Figure 5.12 the reflected and transmitted energy densities for a value of $\mathcal{R}^-$ and $\mathcal{T}^-$ equal to $\mathcal{R}^- = 0.25$, and $\mathcal{T}^- = 0.75$. The curves, show that the relative total energy is constant equal to 1 all along the simulation, in comparison to the loss observed for the classical solution (see the Figure 5.13). This is true for all the numbers of discretization M_1 and M_2. However the energy density obtained is not equal to the exact solution, and depends on the number M_1 and M_2 following the x_1 coordinate and x_2 coordinate. This is observed for different values of the discretization number M_1 and M_2 in the Figure 5.12. The errors plotted in the Figure 5.14 show, that the solution computed using the corrective method tends to converge to the exact solution, as M_1 and M_2 increase. One can also notice, that the error increases almost linearly with time, in conformance with the convergence of a first order scheme in time. The convergence of the solution, is roughly inversely proportional to M_1 and M_2, as one may verify on the different curves. This example shows, that the corrected solutions, converges to the analytical solution (described hereafter), and that this convergence is linear in space and time, as observed in the Figure 5.14. One may also note, that the total energy of the initial condition is conserved all along the simulation, so that the numerical scheme is L^1-preserving.

The *Example 2* presented above, shows that the energy density plotted at the same time steps $t = 0\,s$, $t = 0.17\,s$, $t = 0.34\,s$, $t = 0.50\,s$, is corrected by the FCS. As for the *Example 1*, the main vector is given by $\mathbf{u} - \mathbf{v} = (1.6,\, 0.0)$, such that the initial peak propagates from the slow to the fast medium, in a direction normal to $\mathcal{I}$. The total energy is now well preserved, as plotted in the Figure 5.15, where one may observe the energy variations of the analytical and corrected solution. The energy densities for the FCS, are plotted in the Figure 5.16, for different values of the discretization number $M_1^- = M_1^+ = 25$, and $M_1^- = M_1^+ = 100$. The convergence of the densities to the theoretical density with $M_1 = M_1^- + M_1^+$ is obvious in this Figure. It can also be observed in the Figure 5.17, where the L^2-errors of the corrected solutions are plotted. Results in this Figure show that the point by point interpolation of the incident density, proposed by the corrective scheme can be considered as satisfactory. The error decreases down to 10% for the finer grid ($M_1 = 200$). It can also be observed in the Figure 5.17 (right), that the error scales as $(1/M)$.

The last example presents the propagation of an initial peak with a main vector $\mathbf{u} - \mathbf{v} = (2.4,\, 0.4)$, so that that the direction of propagation makes an angle, with the normal direction. The reflection and transmission through $\mathcal{I}$, happens with values of $\mathcal{R}^-$ and $\mathcal{T}^-$ equal to $\mathcal{R}^- = 0.29$, $\mathcal{T}^- = 0.71$. The total energy variation is plotted in Figure 5.18, where the FCS is compared to the analytical solution. The loss of energy for both curves is very low (the scheme is L^1-preserving). As already explained the total energy is conserved as the peak crosses $\mathcal{I}$, but the solutions obtained may have an important error in comparison to the analytical solution. One can observe in the Figure 5.19, for different values of the discretization number $M_1 = 50$ and $M_1 = 200$. It is easy to see, that the energy densities converge to the theoretical one. The L^2-errors of the corrected solutions, show that the convergence of the solution is roughly linear in the time and space variables. More precisely, the curves obtained are approximately straight lines, until the peak crosses totally the interface of the medium $\mathcal{O}_h$. And one may verify by comparing the values of the total energy for the different curves, that the convergence with the space variable is also linear.

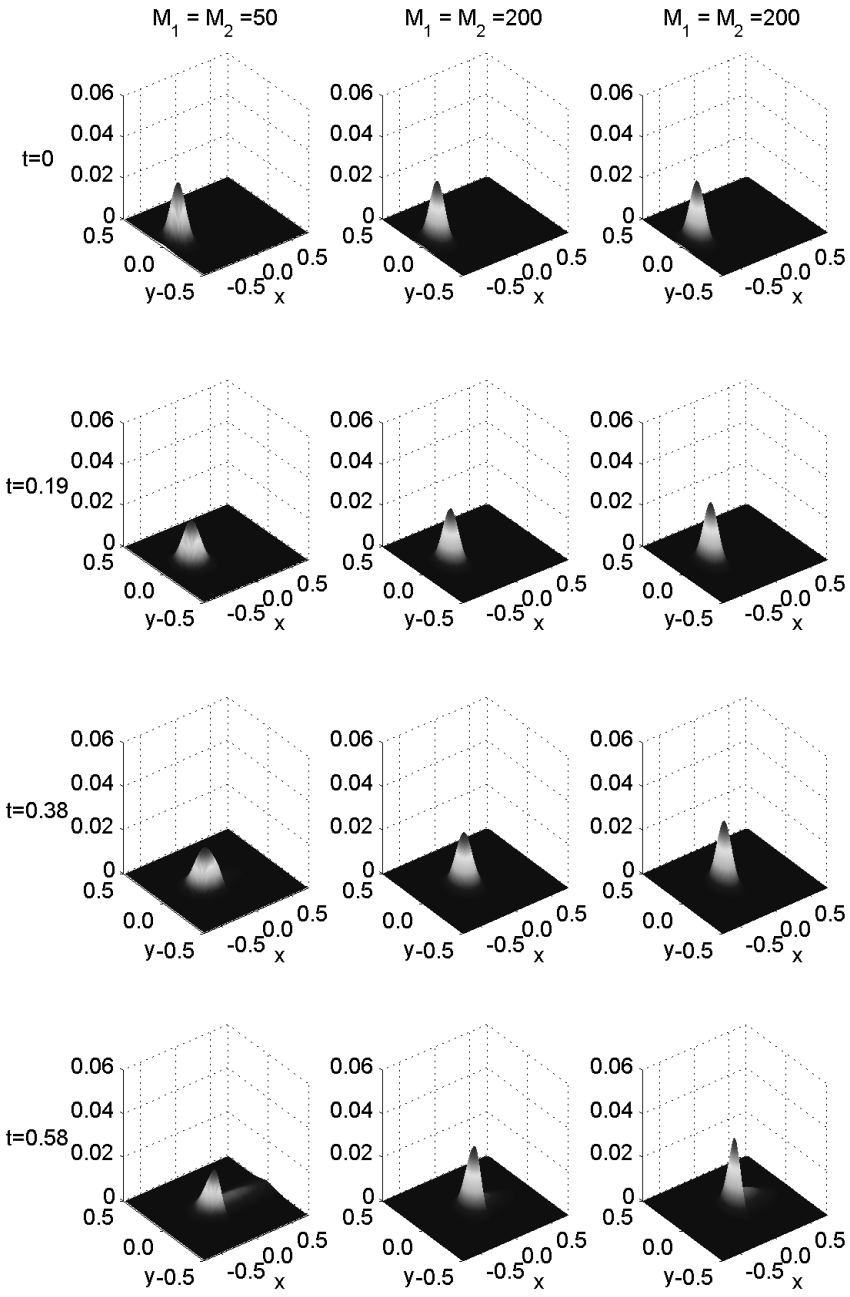

Figure 5.12: Energy density for the *Example 1*, first corrected solution, (normal incidence, $\mathbf{u} = (-0.3,\, 0)$, $\mathbf{v} = (-1.9,\, 0)$ and $N_1 = N_2 = 25$), plotted at time steps $t = 0$s, $t = 0.19$s, $t = 0.38$s and $t = 0.58$s, for the discretization numbers $M_1^- = M_2^- = M_1^+ = M_2^+ = 25$, 100 and analytical solution, for transmission from the slow to the fast medium.

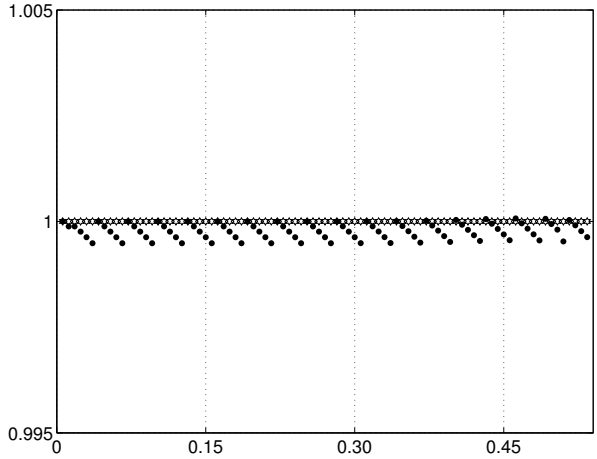

Figure 5.13: Energy variation for the analytical (black circles) and corrected (whited diamonds) solutions, as a function of the time t (s), (*Example 1*, normal incidence, $\mathbf{u} = (-0.3, 0)$, $\mathbf{v} = (-1.9, 0)$, with paramters $N_1 = N_2 = 25$). The curves that correspond to the analytical solution and the corrected one are represented by the constant line $E = 1$.

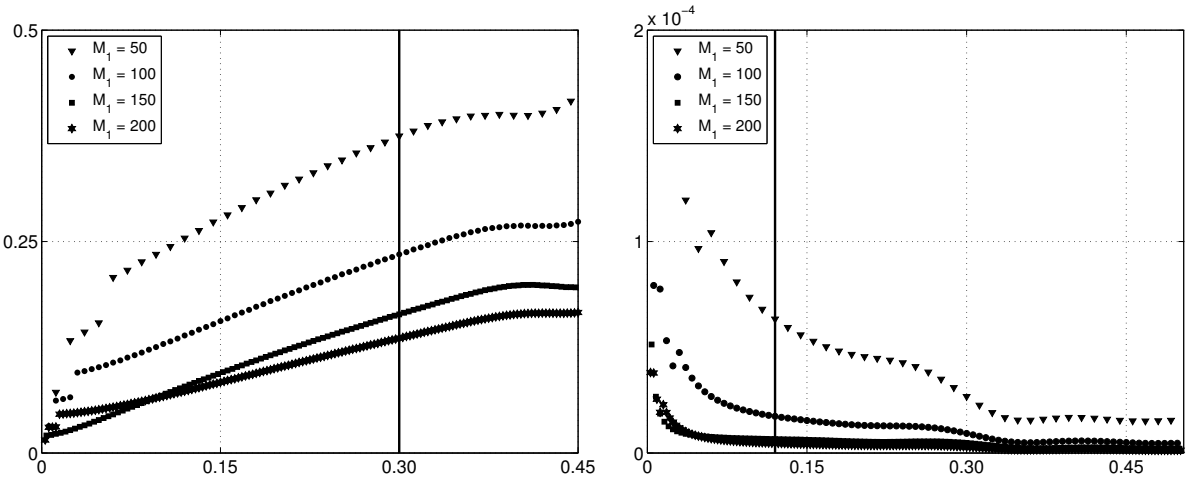

Figure 5.14: L^2-error of the corrected solutions, to the exact solution, with the parameter M_1 and M_2, that variates, from the top to the bottom, from 50 to 200 for the first example (normal incidence, $\mathbf{u} = (-0.3, 0)$, $\mathbf{v} = (-1.9, 0)$ and $N_1 = N_2 = 25$). One observes the L^2-error (left), and the L^2-error $\times \frac{1}{t}$ (right), where t denotes the time. The vertical line indicates the time at which the peak reaches the interface.

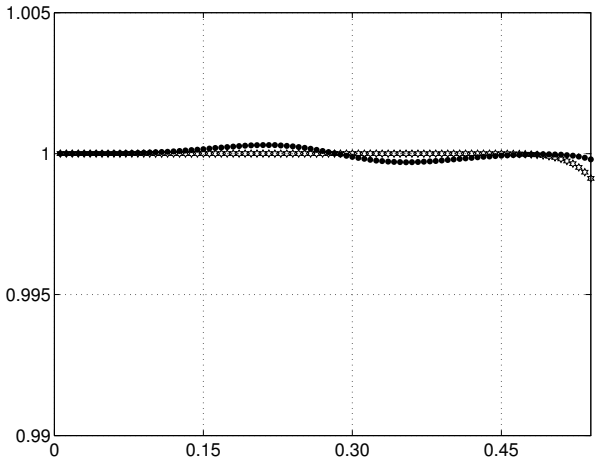

Figure 5.15: Energy variations of the corrected (white stars) and analytical solutions (black dots) for the *Example 2* (normal incidence, $\mathbf{u} = (-0.3,\, 0)$, $\mathbf{v} = (-1.9,\, 0)$ and with parameters $N_1 = N_2 = 50$).

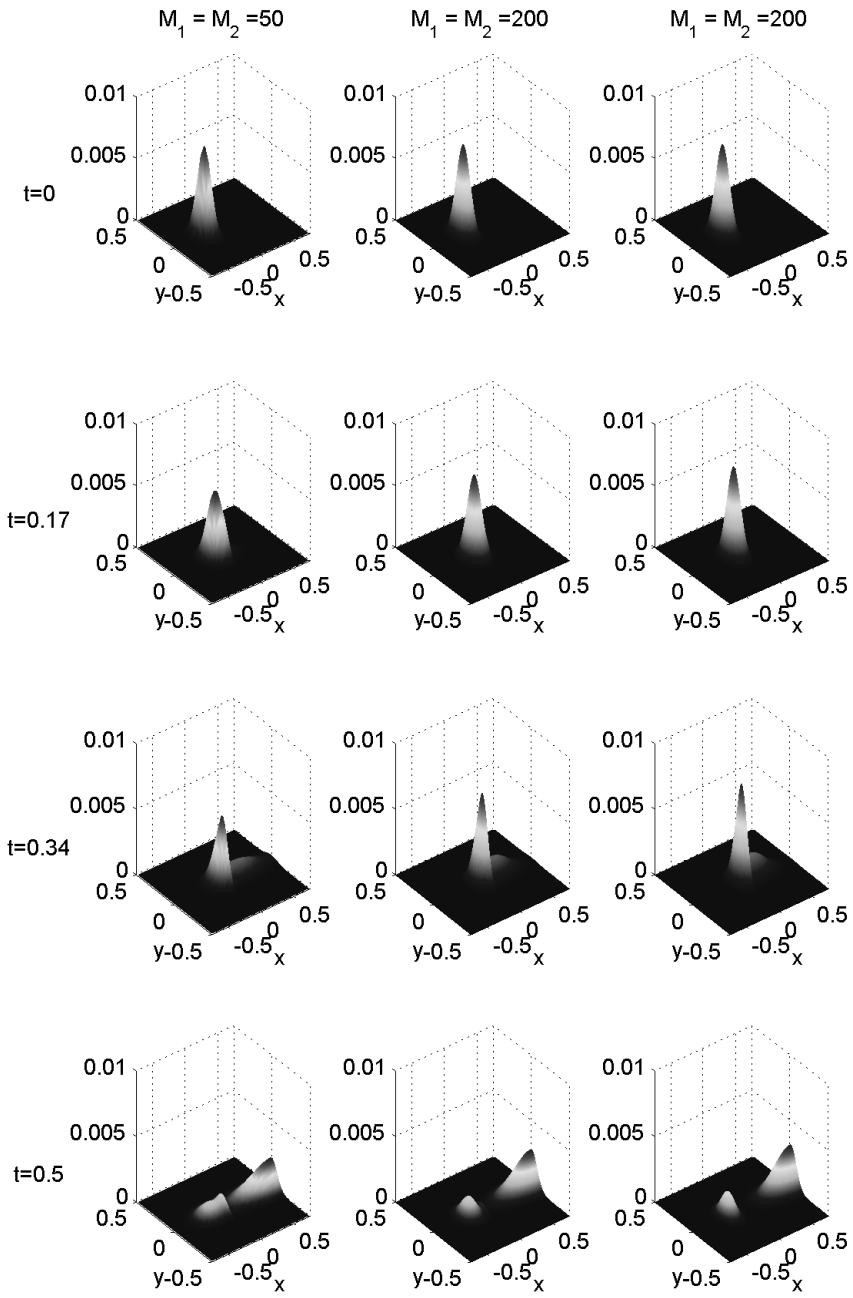

Figure 5.16: Energy densities of the corrected solutions, for the numbers $M_1 = M_2 = 50$ or 200, for the *Example 2* (normal incidence, $\mathbf{u} = (-0.3, 0)$, $\mathbf{v} = (-1.9, 0)$ and with parameters $N_1 = N_2 = 50$), plotted at time steps $t = 0$s $t = 0.17$s, $t = 0.34$s and $t = 0.50$s.

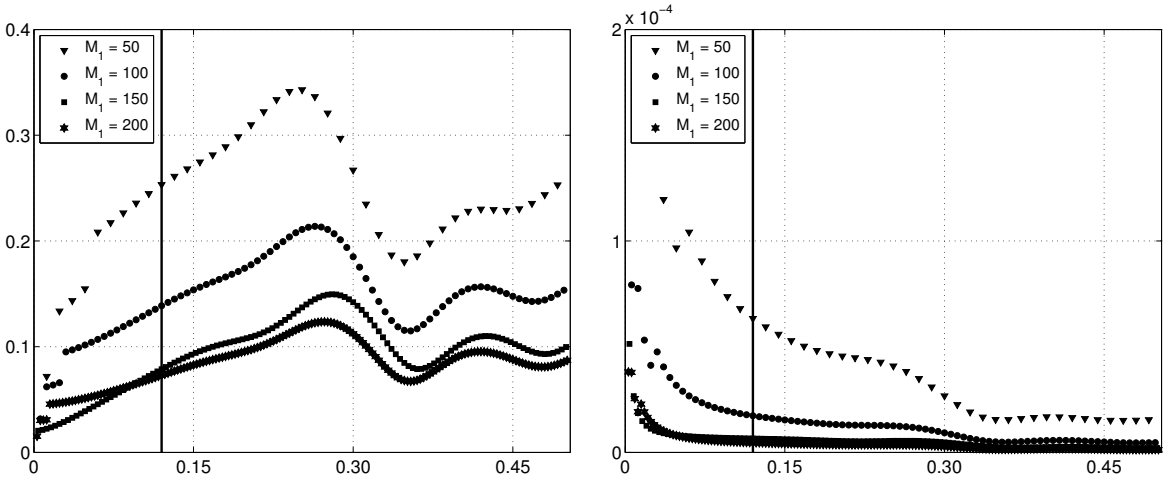

Figure 5.17: L^2-error of the classical solution as a function of the time t(s), for the *Example 2* (normal incidence, $\mathbf{u} = (-0.3, 0)$, $\mathbf{v} = (-1.9, 0)$ and with parameters $N_1 = N_2 = 50$), with the discretization numbers along the x_1 coordinate from the top to the bottom, $M_1 = M_2 = 50$ to $M_1 = M_2 = 200$. One observes the L^2-error (left), and the L^2-error $\times \frac{1}{M_1 t}$ (right), where t is the time.

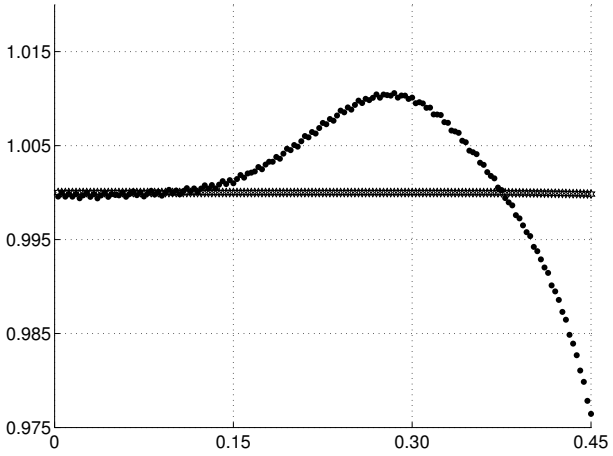

Figure 5.18: Energy variations of the corrected and analytical solutions as a function of the time t (s) for the *Example 3* (slanted incidence, with $\mathbf{u} = (-0.3, 0)$, $\mathbf{v} = (-2.7, -0.4)$, and $N_1 = N_2 = 50$).

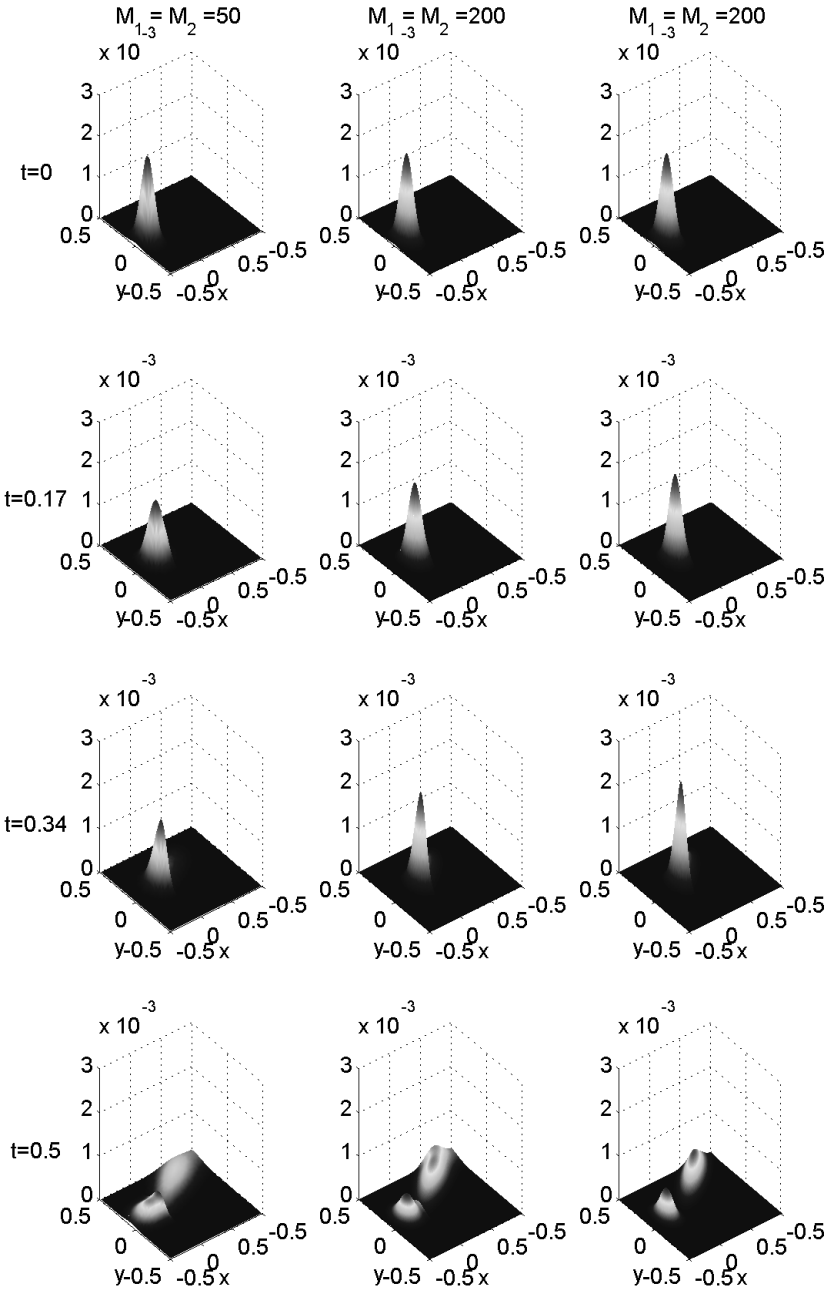

Figure 5.19: Energy densities obtained for the classical solution, with $M_1 = M_2 = 50$ or $M_1 = M_2 = 200$, for the *Example 3* (slanted incidence, with $\mathbf{u} = (-0.3, 0)$, $\mathbf{v} = (-2.7, -0.4)$, and $N_1 = N_2 = 50$), plotted at time steps $t = 0$s, $t = 0.17$s, $t = 0.34$s and $t = 0.50$s.

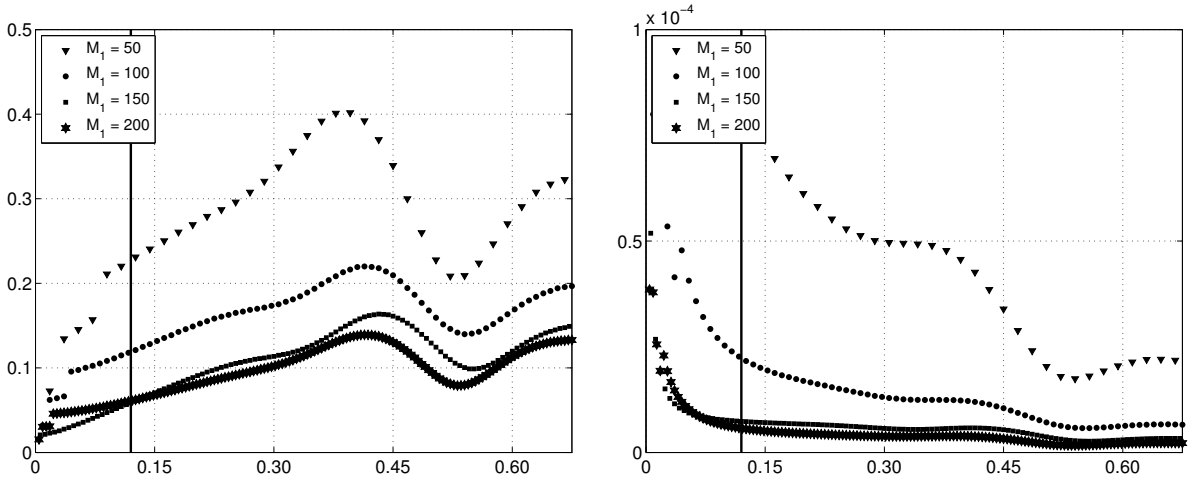

Figure 5.20: L^2-error of the corrected solution for the discretization numbers along the x_1 coordinates from the top to the bottom $M_1 = M_2 = 50$ to $M_1 = M_2 = 200$, *Example 3* (slanted incidence, with $\mathbf{u} = (-0.3,\, 0)$, $\mathbf{v} = (-2.7,\, -0.4)$, and $N_1 = N_2 = 50$). One observes the L^2-error (left), and the L^2-error $\times \frac{1}{M_1 t}$ (right), where t is the time.

5.1.3 $c \times \mathbf{k}$ scheme (CKS)

In this part, we adopt the same approach as in the previous one, but we consider the solutions of the Liouville equation obtained with the numerical schemes described in the subsection 4.3.3 of the previous chapter. These schemes rely on a different approach, that consists in taking into account the difference of celerity on each side of $\mathcal{I}$, by discretizing the variable $c(\mathbf{x}) \times \mathbf{k}$ instead of $\mathbf{k}$. It turns out to be easier to implement, and in some cases as efficient as the conservative schemes presented so far. To illustrate the method, we use the same examples as the previous ones, and the initial conditions are also the same. The wave vectors domain is thus discretized in our examples (case of a single interface) by two different grids. The wave vectors step depends on the celerity in the considered sub-domain, located on each side of the interface $\mathcal{I}$. We use the same meshes in the slow medium as the ones used in the previous examples, and adapt the discretization in the fast medium. Among the schemes presented in the previous parts (see the section 4.3.3), we present the results obtained with the classical $c \times \mathbf{k}$ scheme (adapted classical scheme). It consists in a global approach, that does not depend on the form of $\mathcal{I}$, and is easy to implement. We also consider the results obtained with the adapted corrective scheme, described at the end of the section 4.3.3, and derived from the adapted classical scheme. In that case the results obtained with both types of schemes are satisfactory. We compare them by plotting the energy variations during a whole simulation, and by considering the errors to an analytical solution based on the corrective scheme, and defined in the Appendix H. We also plot the energy densities, and observe the convergence of our solutions with the discretization number M_1 and M_2 following the space variable. At last, we plot the form of the energy densities following the x_1 abscissa, for a given x_2 coordinate (for example $x_2 = 0$), to observe the point by point convergence of the computed solutions, to the theoretical one. Note, that the adapted meshes do give good results for both schemes, despite the fact, that the initial conditions are modeled with a small number of wave vectors. The energy variations, give almost the same results for both schemes, in comparison to the schemes presented in Section 4.3.3. The curves, that draw the energy density for a given coordinate x_2, show that the convergence of the density depends mainly on the discretization number M_1 and M_2, and that the convergence is satisfactory for important discretization numbers.

Classical $c \times \mathbf{k}$ scheme

In this Section, we consider the adapted classical scheme, defined in the Chapter 4 (see the end of the Subsection 4.3.3). As already seen, it relies on the use of two grids on each side of $\mathcal{I}$, that take into account, the difference of celerity in the slow and in the fast medium. This method is another way to correct the loss and gain of energy observed with the classical scheme at $\mathcal{I}$, that have been pointed out in the previous Section. It gives satisfactory results, in terms of energy variations and approximation of the energy density. We adopt the same approach as in the first part of this Chapter, and compare the solutions obtained with an analytical solution described in the Appendix H. We observe the energy variations and the energy densities of the solutions, and the L^2-errors to the theoretical solution. To make the comparison, we consider the same examples as in the previous Section, but restrict ourselves to the last two ones, characterized by a discretization number $N_1 = N_2 = 50$.

The first example presented here is the same as the *Example 2* of the previous subsection. It is centered on $\mathbf{u} - \mathbf{v} = (1.60, 0)$, and has the parameters $c_1 = c_2 = 0.05$. The celerities in each medium are given by $c^- = 1.0$ and $c^+ = 3.0$. The domain $\mathcal{O}_h$ is the same as in the previous Subsection $[-0.75, 0.75] \times [-0.5, 0.5]$, and the discretization numbers following the first and second coordinate are given by $M_1 = M_2 = 100$. The wave vector steps are given, for a discretization number $N_1 = N_2 = 50$, by $\Delta k_1^+ = 1/3\Delta k_1^- = 0.0094$, and $\Delta k_2 = 0.01$. The two meshes in the slow and in the fast medium, are thus adapted to the scale of variation of the celerity in each sub-domain of $\mathcal{O}_h$. One may observe in Figure 5.21 for instance, that the initial peak propagates in both media, with a normal incidence toward $\mathcal{I}$, and is reflected and transmitted through $\mathcal{I}$ with the coefficients $\mathcal{R}^- = 0.25$ and $\mathcal{T}^- = 0.75$. The energy density obtained is close to the analytical solution. One observes, that this energy density converges with M_1 and M_2, as plotted in Figure 5.21. The energy densities obtained for this scheme are thus satisfying, and converge to the exact solution (see Figure 5.21). To this we may add, that the total energy variation is conserved all throughout the simulation, which means, that the total energy remains very close to 1, as plotted in the Figure 5.22. Concerning the energy density, we observe the convergence of the density with

the increasing discretization numbers M_1, M_2. The classical $c \times \mathbf{k}$-scheme gives here satisfying results, and the total energy is globally conserved.

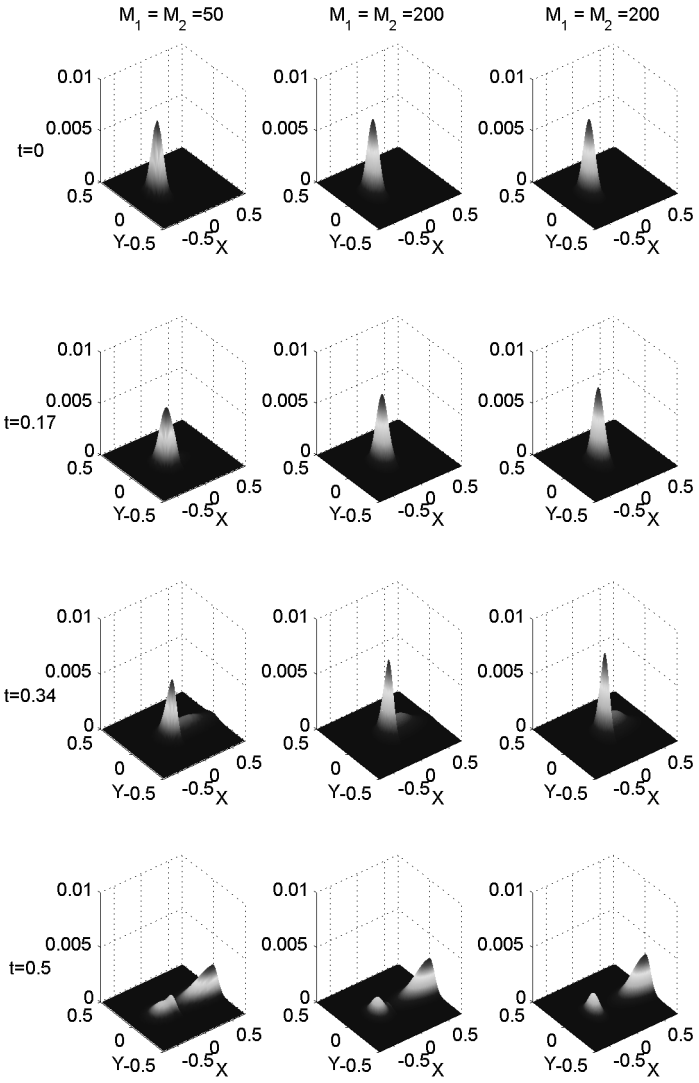

Figure 5.21: Energy density for the classical $c \times \mathbf{k}$ scheme, for the discretization numbers $M_1 = M_2 = 50$, and $M_1 = M_2 = 200$, and analytical solution, plotted at time steps $t = 0$s, $t = 0.17$s, $t = 0.34$s and $t = 0.50$s.

The second example considered here is the same as *Example 3*. It is defined by a main vector $\mathbf{u} - \mathbf{v} = (2.4, 0.4)$, the characteristic lengths $c_1 = 0.05$, $c_2 = 0.05$, and the respective velocities $c^- = 1.0$ and $c^+ = 3.0$. The computational domain is the same as for the previous example. One observes on the Figure 5.25, that the initial peak propagates in direction of $\mathcal{I}$ with a certain angle to the normal. It is reflected and transmitted through $\mathcal{I}$ with the reflection and transmission coefficients $\mathcal{R}^- = 0.29$ and $\mathcal{T}^- = 0.71$. The same parameters as for the previous example are used, to discretize the grids on each side of $\mathcal{I}$. One observes, that the loss of energy obtained for the classical scheme on the previous Subsection (see the Figure 5.24) in case of transmission from the slow to the fast medium is partly corrected. Note, that the error of the classical $c \times \mathbf{k}$ scheme may be reduced, by increasing the number of discretized wave vectors, that appear in the initial condition. The theoretical solution is not exactly conservative, but may be improved by increasing the discretization number ($M_1 = M_2 = 300$ or $M_1 = M_2 = 400$). The

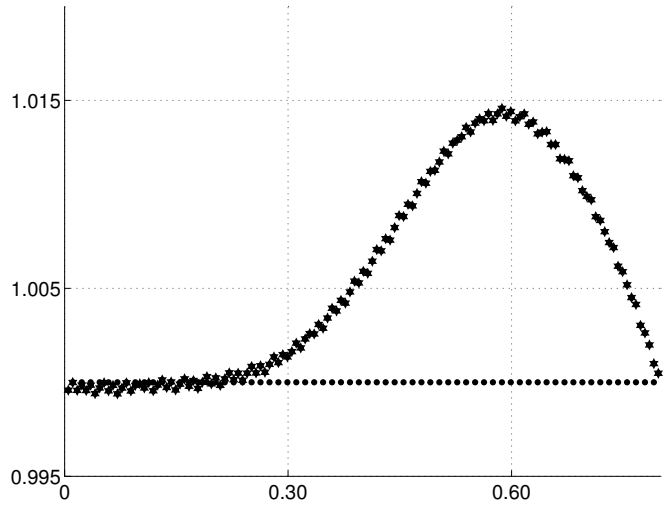

Figure 5.22: Energy variations of the classical (discretization number $M_1 = M_2 = 100$) (dots), and theoretical solutions ($c \times \mathbf{k}$ scheme) for the *Example 2*, for the discretization numbers $M_1 = M_2 = 200$ (stars).

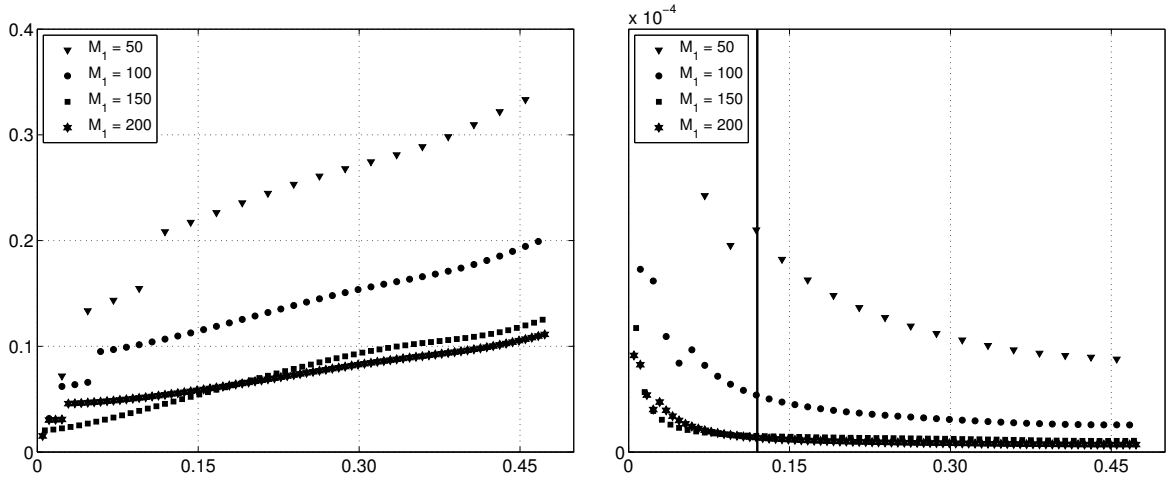

Figure 5.23: L^2-error of the corrected solution, for the discretization numbers along the x_1 coordinates $M_1 = M_2 = 50$ to $M_1 = M_2 = 200$ from the top to the bottom, *Example 2* (normal incidence, with $\mathbf{u} = (-0.3, 0)$, $\mathbf{v} = (-1.9, 0)$, and $N_1 = N_2 = 50$). One observes the L^2-error of the corrected solution (left), and the L^2-error $\times \frac{1}{M_1 t}$ (right).

energy densities obtained converge to the theoretical one, with the discretization number M_1 and M_2, as one may observe on the Figures 5.25, where the latter are plotted for the numbers $M_1 = M_2 = 50$, $M_1 = M_2 = 200$. The density obtained is satisfying, and we also observe the L^2-error of the solutions obtained to an exact solution. One observes, that the error is lower, than the errors obtained in the previous subsection, and of same order, which shows the interest of the method.

We may also observe the corresponding results for the numerical scheme presented at the end of the Subsection 4.3.3. One observes for the *Example 2*, that the energy is conserved for both schemes (classical $c \times \mathbf{k}$ and CKS scheme), and the energy densities obtained are satisfactory. The convergence of the energy density with the discretization number $M_1 = M_2$ is observed on curves, that represent the contour of the

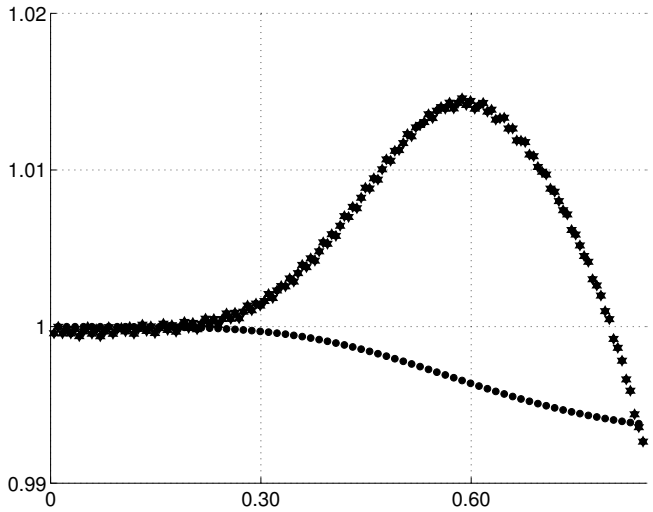

Figure 5.24: Energy variations of the theoretical solution with the time t, $M_1 = M_2 = 200$ and of a solution obtained, by a classical $c \times \mathbf{k}$ scheme, for the *Example 3*, with $M_1 = M_2 = 100$.

energy density plotted along the x_1 coordinate, for a given index x_2 ($x_2 = 0$ in the examples). These curves correspond to the point by point convergence of the energy densities obtained, to the theoretical solution, and are plotted in the Figures 5.27 and 5.28. The L^2 error is also plotted, showing convergence of the solutions obtained to the exact one. For the *Example 3*, the energy is also globally conserved for both schemes. One may notice, that the solutions could be improved, by using initial conditions, with an energy distributed on more vectors, and with a finer discretization. We also observe, the convergence of the energy density with M_1, along the x_1 coordinate, for $x_2 = 0$. The point by point convergence, and the L^2 error show the convergence of the solution. Although the results obtained, are lightly better than, those obtained in the previous Subsection, the L^2 error remains of same order (it is linear in space and time). The convergence observed on the curves of the Figures 5.27, 5.28 and 5.29, and 5.30 remains slow.

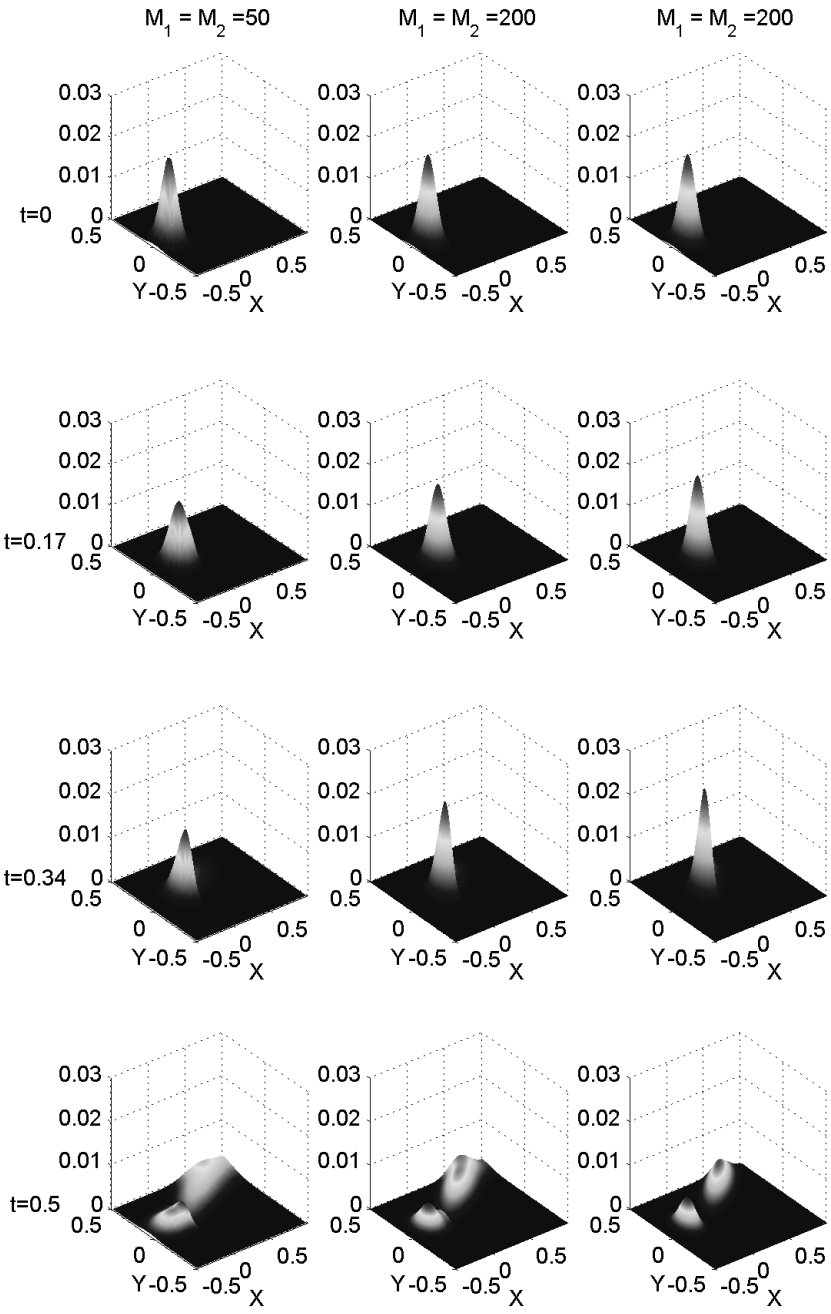

Figure 5.25: Energy density obtained by a classical $c \times \mathbf{k}$ scheme for the discretization numbers $M_1 = M_2 = 50$ and $M_1 = M_2 = 200$, and analytical solution, plotted at time steps $t = 0$s, $t = 0.17$s, $t = 0.34$s and $t = 0.50$s, for the *Example 3*.

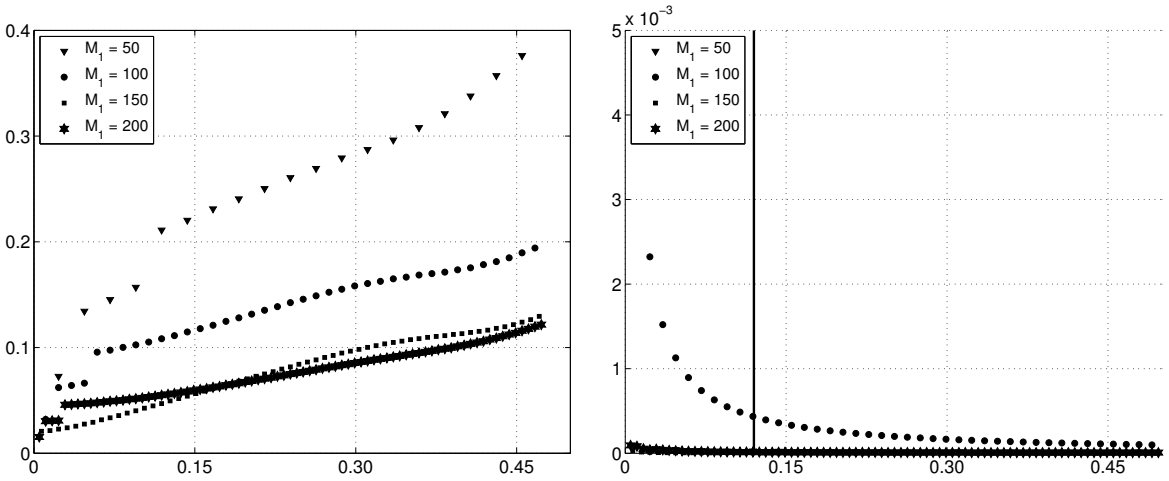

Figure 5.26: L^2-error of the corrected solution as a function of time, for the discretization numbers along the x_1 coordinates $M_1 = M_2 = 50$ to $M_1 = M_2 = 200$, from the top to the bottom, *Example 3* (slanted incidence, with $\mathbf{u} = (-0.3,\, 0)$, $\mathbf{v} = (-2.7,\, -0.4)$, and $N_1 = N_2 = 50$). L^2-error of the corrected solution, for the discretization numbers along the x_1 coordinates $M_1 = M_2 = 50$ to $M_1 = M_2 = 200$ from the top to the bottom, *Example 2* (normal incidence, with $\mathbf{u} = (-0.3,\, 0)$, $\mathbf{v} = (-1.9,\, 0)$, and $N_1 = N_2 = 50$). One observes the L^2-error of the corrected solution (left), and the L^2-error $\times \frac{1}{M_1 t}$ (right).

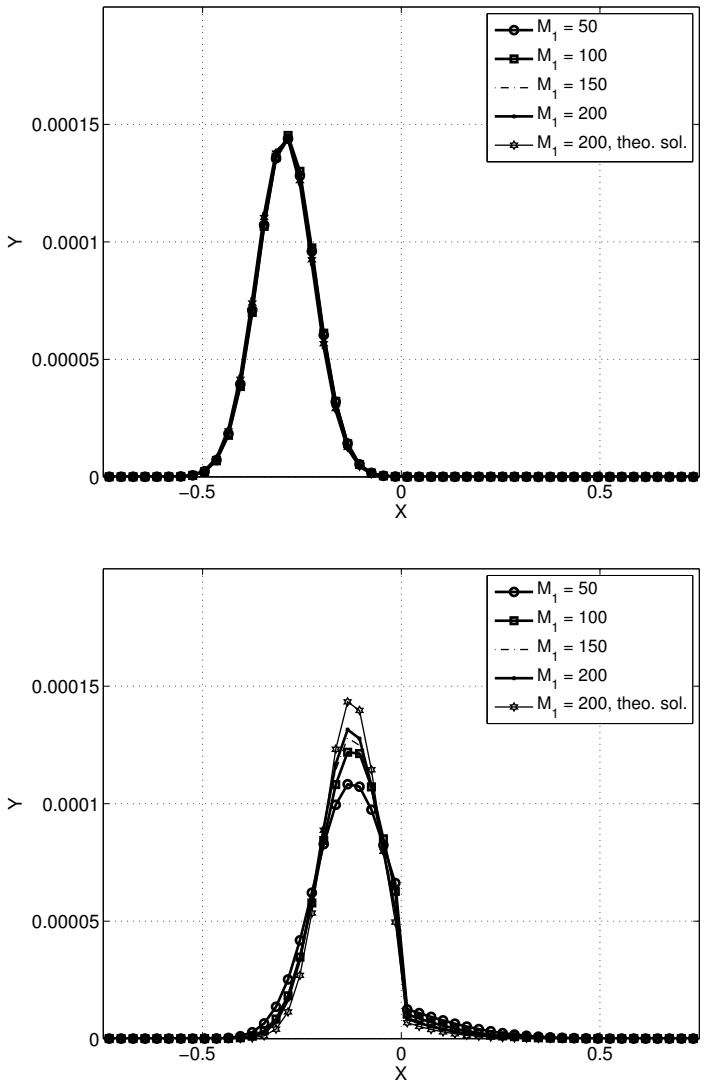

Figure 5.27: Contour of the energy densities for the second corrective scheme (*Example 2*), at the coordinate $x_2 = 0$, and at time steps, $t = 0$s and $t = 0.17$s.

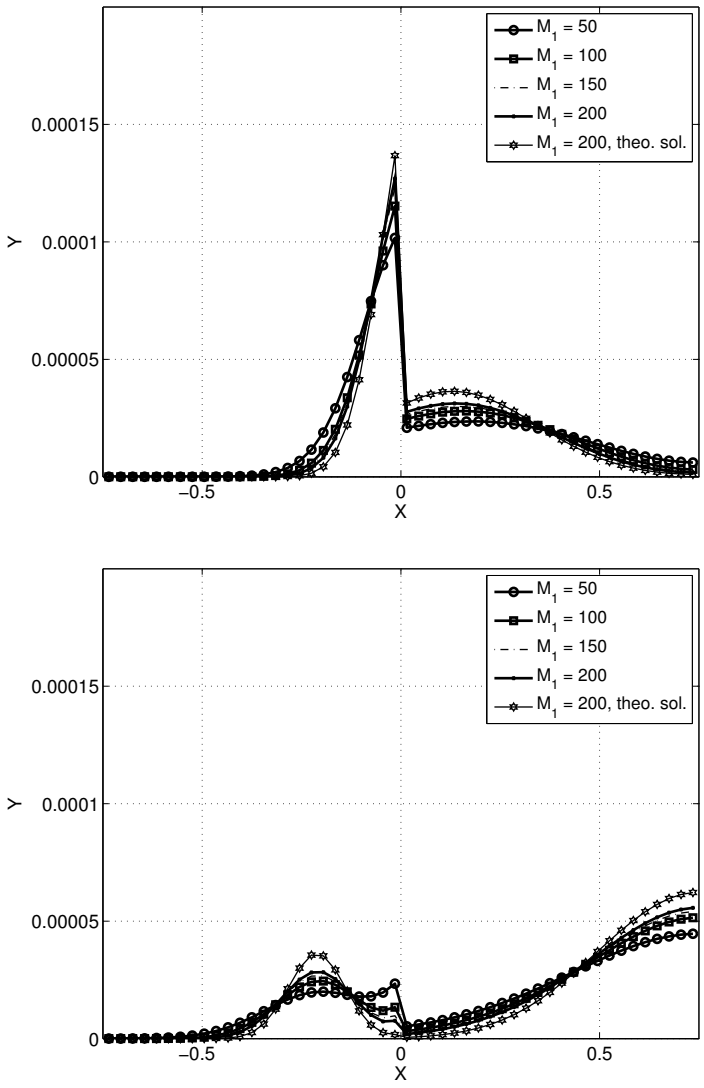

Figure 5.28: Contour of the energy densities for the second corrective scheme (*Example 2*), at the coordinate $x_2 = 0$, and at time steps, $n_t = 0.34$s and $n_t = 0.50$s.

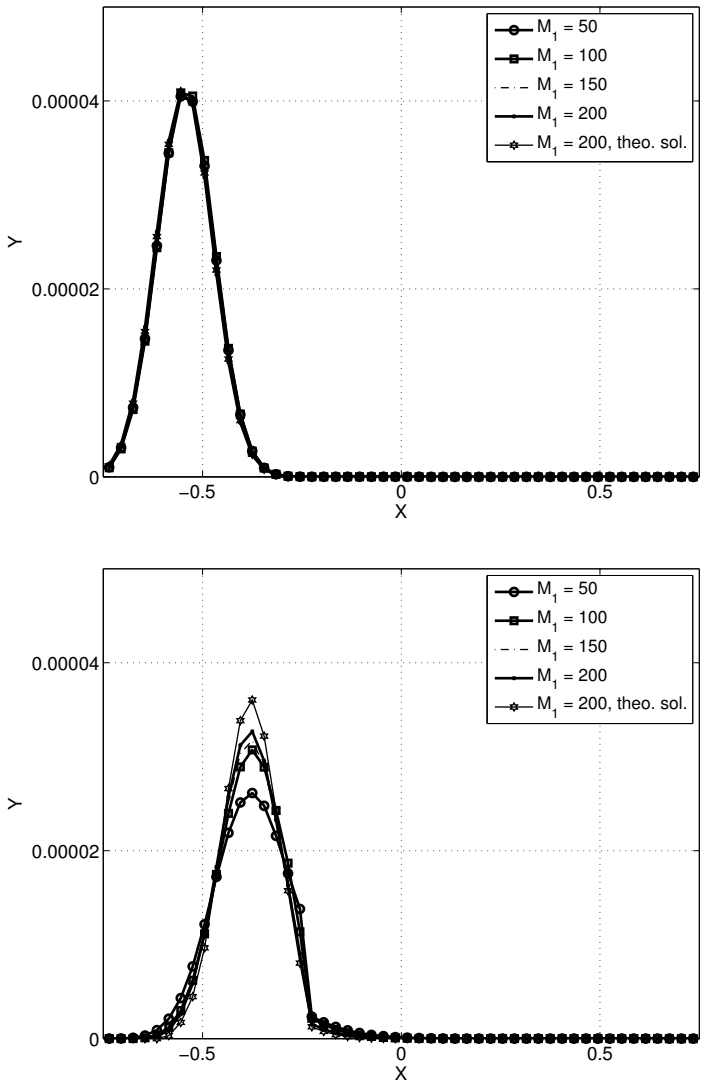

Figure 5.29: Contour of the energy densities for the second corrective scheme (*Example 3*), at the coordinate $x_2 = 0$, and at time steps, $t = 0$s and $t = 0.17$s.

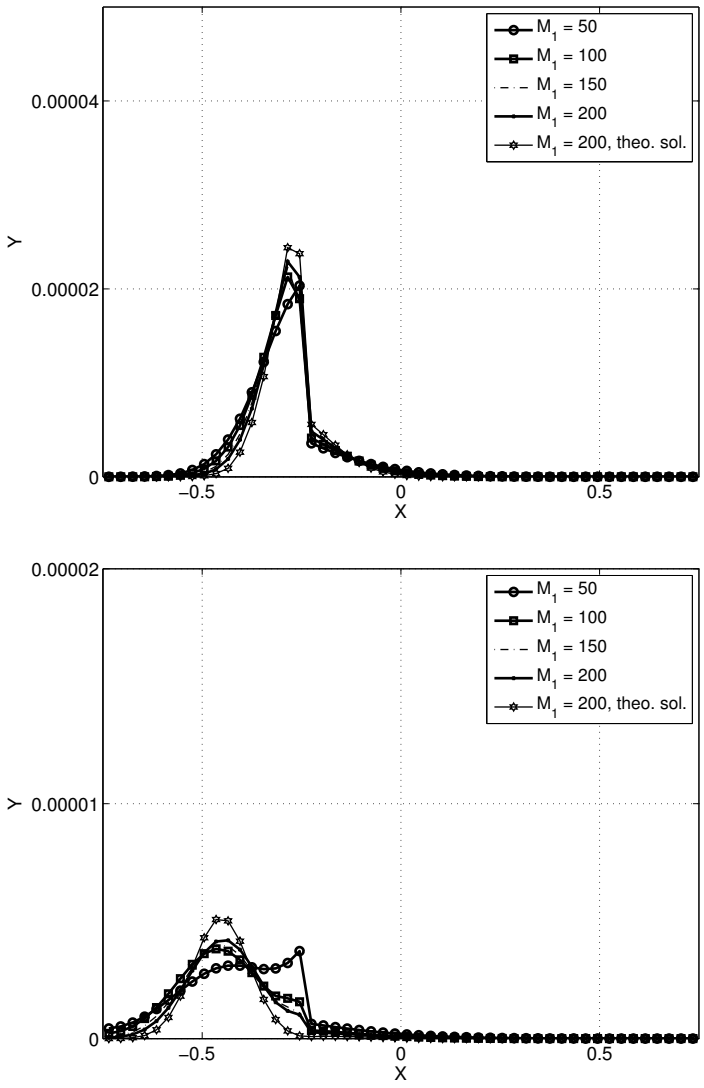

Figure 5.30: Contour of the energy densities for the second corrective scheme (*Example 3*), at the coordinate $x_2 = 0$, and at time steps, $t = 0.34$s and $t = 0.50$s.

5.2 Curved (slanted) interface

We present here the results obtained in case of a curved interface. More precisely, the theory presented in the Section 4.4, is illustrated on examples, that point out the interest of the method in terms of energy conservation. The schemes presented, correct the error due to a classical interpolation of the specific intensities on the mesh of wave vectors at $\mathcal{I}$, which is now chosen as a curved interface. In order to check the results obtained with a curved interface, and to verify the convergence of the solutions, we compare the latter with the results obtained, in case of a straight interface. We consider the reflection, and transmission of an initial condition, on a slanted line, which allows to compare the results obtained with a theoretical solution. The accuracy, and convergence of the solution can be verified, this way. We also compare the results to the ones obtained with the corresponding initial condition, that impinges on a straight line, parallel to the ordinate axis (case of a straight interface treated in the first part of the Chapter).

We observe, for each example presented here, the convergence of the energy density, with the discretization step following the space variables, by comparing the energy densities for different values of the discretization step. And also, by the computation of the L^2-error, of the energy density, to the theoretical one, defined on the rays. The dependance of the numerical scheme observed, toward the time and space variable, are in agreement with the first order approximation, used in the discretization of the derivatives of the Liouville equation. The convergence remains slow, in space and in time.

We also consider the total energy density obtained, (L^1-norm of the energy density). The latter is conserved for the $c \times \mathbf{k}$ corrective scheme, during the whole simulations, as in case of a straight interface. Note here, that we only present the results obtained for the second corrective scheme. The first interpolation method, is not presented here, since, it requires, more than 4-points interpolations (see the Section 4.4), and since the second corrective method fixes this drawback, in case of transmission from the slow to the fast medium. The results are similar to the ones obtained in case of a straight interface. As in the latter case, one may show, that the error obtained with a classical scheme, may be important. We thus, focus on the interest of a conservative scheme, that allows to cancel, or reduce the loss of energy, at the crossing of $\mathcal{I}$, and on the convergence of the energy density, to the theoretical one. We consider two examples, of initial conditions of the form (5.1), which illustrate the interest of the numerical schemes presented above. (We treat here exclusively, the case of transmission from the slow to the fast medium.) The parameters of each examples are given by:

Parameters	*Example 4*	*Example 5*
$\mathbf{v}-\mathbf{u}$	(0.5, -0.5)	(2.4., 0.4)
Initial position, $\mathbf{u}$	(-0.5, 0)	(-0.3, 0)
$\mathcal{I}$	$x_1 = x_2$	$x_1 = (1/6)x_2$
c^-	1.0	1.0
c^+	3.0	3.0
$N_1 = N_2$	50	50
$M_1 = M_2$	100	100

Table 5.2: The different parameters for each of the examples presented further.

5.2.1 *Example 4*: conservative numerical scheme, in case of normal incidence

We consider an initial condition of the form (5.1), where the amplitude is Gaussian, with respect to the space variable, and with a Dirac distribution with respect to the wave vectors variable, as in case of a straight interface. We recall, that we use initial conditions, with energy distributed on a small number of wave vectors, which allow to illustrate the efficiency of the method, and that correspond to a peak of energy following the wave vectors variable. We focus on the conservation of the energy through a slanted line, and on the convergence of the energy density to a theoretical solution.

In the *Example 4*, the interface $\mathcal{I}$ is the slanted line, defined by the equation:

$$x_1 - x_2 = 0\,.$$

The computational domain $\mathcal{O}_h$ is the square $[-1,\,1]\times[-1,\,1]$, split into two triangles, by $\mathcal{I}$. The physical parameters as the celerity, and the density are chosen in each sub-domain of the computational domain $\mathcal{O}_h$ equal respectively to $c^- = 1.0$ and $c^+ = 3.0$, and $\rho^- = \rho^+ = 1.0$. The Dirac distribution of (5.1) is discretized on a small number of wave vectors, (see 5.2), while the parameters of the Gaussian amplitude of the initial condition, are given by:

$$\mathbf{u} = (-0.5,\,0.0),\;\; \mathbf{v} = (-1.0,\,0.5)\,,$$

while the characteristic lengths r_1, r_2 and r_1', r_2' are both chosen equal, $r_1 = r_2 = 0.01$, and $r_1' = r_2' = 1/\sqrt{2}$. The initial condition, defined by the above parameters, is a peak, that propagates through the interface from the slow to the fast medium. The peak propagates toward $\mathcal{I}$ in the direction defined by $\mathbf{u} - \mathbf{v} = (0.5,\,-0.5)$, such that it impinges on $\mathcal{I}$ in the normal direction, and should reflect and transmit through $\mathcal{I}$ with the respective coefficients $\mathcal{R}^- = 0.25$ and $\mathcal{T}^- = 0.75$.

The total energy variation is plotted on the Figure 5.31, for the discretization numbers $M_1^- = M_1^+ = M_2^- = M_2^+ = 50$, and $N_1 = N_2 = 25$, for the corrective method, where one may observe, that the latter is conserved at the crossing of $\mathcal{I}$, such that the numerical scheme defined in the Section 4.4.2, gives satisfying results on this example, in terms of energy conservation. A comparison to the classical scheme (with the same discretization steps), on this example, shows that the loss of energy is very important.

We then observe, the energy densities plotted in the Figure 5.32 for instance, that shows different discretization steps, and shows the convergence of the numerical solutions to the theoretical one. This convergence can also be observed directly in Figure 5.33, by the comparison of the L^2-error of the densities obtained for the different discretization numbers mentionned above.

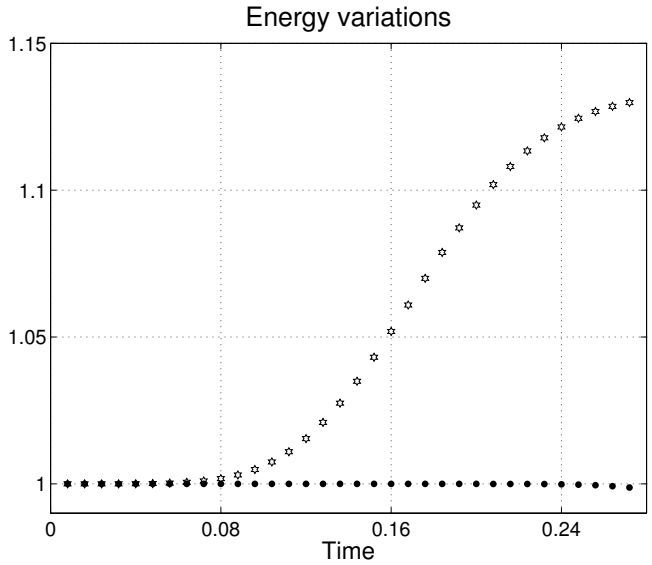

Figure 5.31: Total energy variation of the corrected scheme for the *Example 4*, of a slanted line with equation $x_1 = x_2$, between the times steps 0s and 0.24s.

One observes, before the peak of the energy pulse reaches $\mathcal{I}$, that the behavior is linear in time. Once the peak, reaches $\mathcal{I}$ one observes, a change in the slope of each curve, and after that, a decrease of the error, while the peak crosses $\mathcal{I}$ from the slow to the fast medium. The convergence of the solution to the theoretical one is also linear in the space variable. This is confirmed, in the Figure 5.34, where the L^2 errors of the numerical solution is plotted at different time steps, as a function of the discretization step,

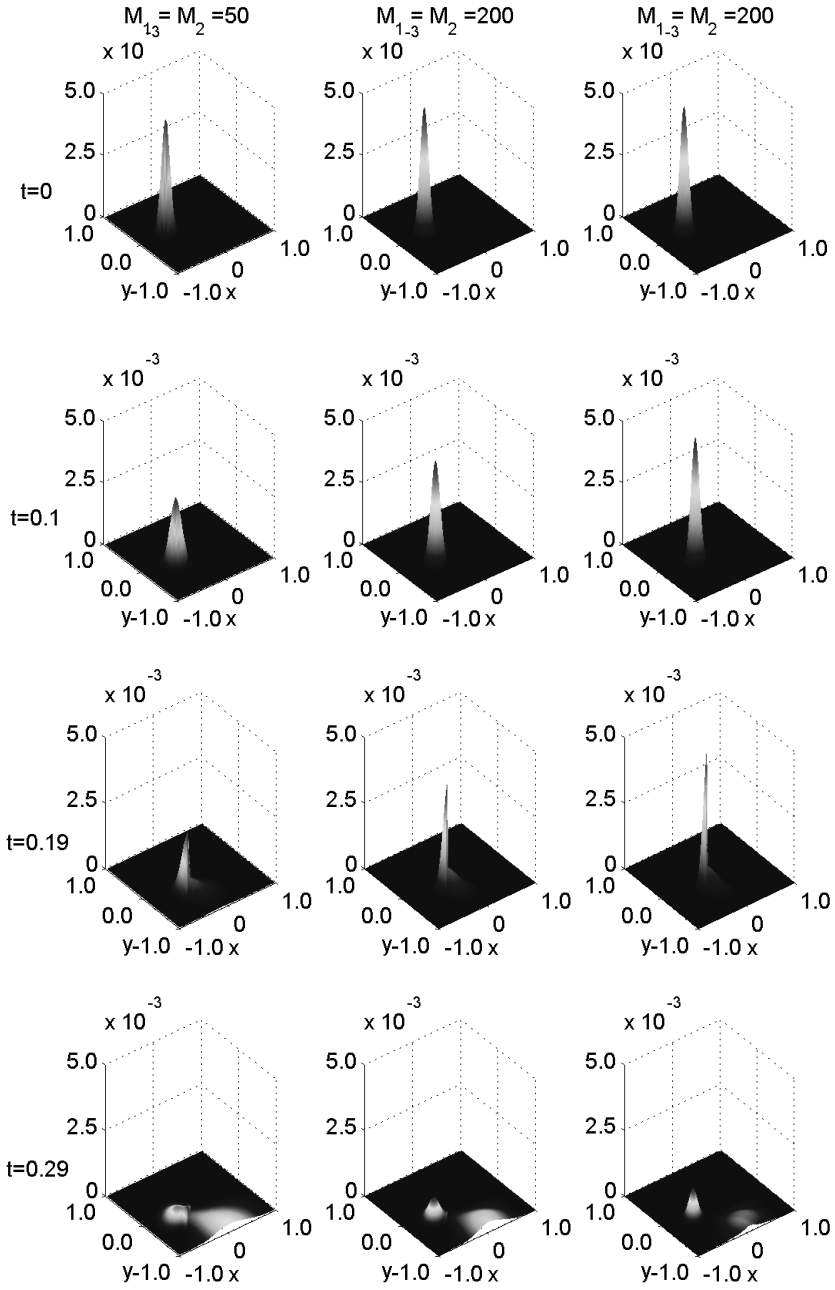

Figure 5.32: Energy density for the *Example 4*, plotted at times steps $t = 0.0$s, $t = 0.096$s, $t = 0.192$s and $t = 0.288$s, for discretization numbers, $M_1^- = M_1^+ = 25$ at the top, and $M_1^- = M_1^+ = 50$ at the bottom.

along the space variable. One observes, that this dependance is almost linear in space. The convergence to the theoretical solution remains slow, which is in agreement with the FD theory (see [69]). The linear behavior traduces a first order approximation of the numerical scheme used for the resolution of the transport equation. The same kind of considerations apply in case of non-normal incidence on a slanted line, as explained in the next subsection.

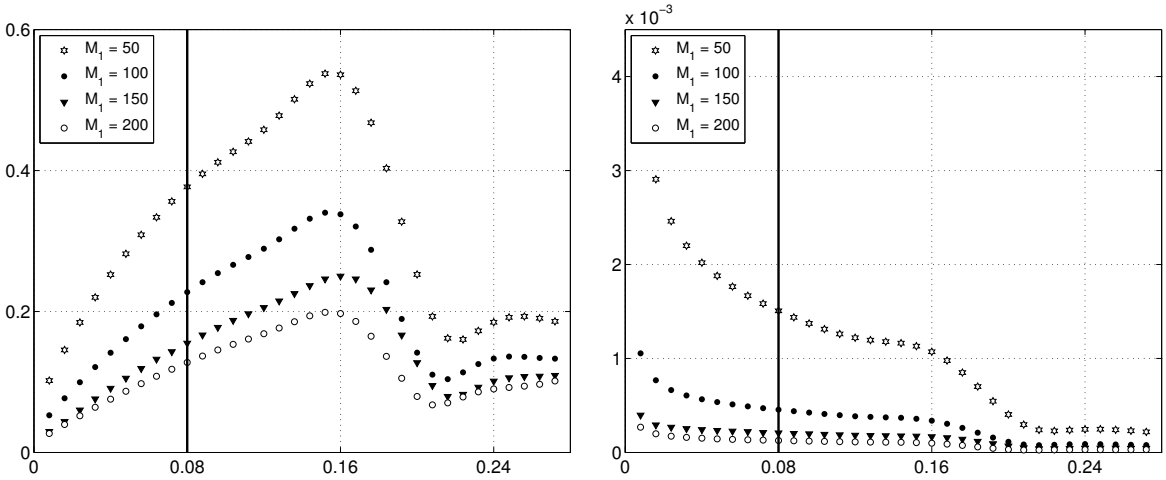

Figure 5.33: L^2-error between the $c \times \mathbf{k}$ corrected and the theoretical solution, for the *Example 4*. The discretization numbers takes the values $M_1^- = M_1^+ = 25$ (white dots), $M_1^- = M_1^+ = 50$ (black dots), $M_1^- = M_1^+ = 75$ (black triangles), and $M_1^- = M_1^+ = 100$ (white stars). L^2-error of the corrected solution, for the discretization numbers along the x_1 coordinates $M_1 = M_2 = 50$ to $M_1 = M_2 = 200$ from the top to the bottom, *Example 2* (normal incidence, with $\mathbf{u} = (-0.3, 0)$, $\mathbf{v} = (-1.9, 0)$, and $N_1 = N_2 = 50$). One observes the L^2-error of the corrected solution (left), and the L^2-error $\times \frac{1}{M_1 t}$ (right). The thick vertical line indicates the time at which the peak of the pulse reaches the interface.

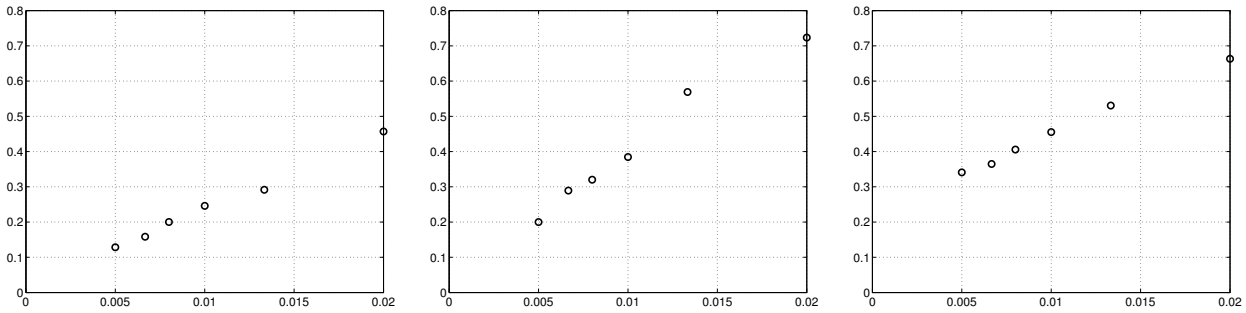

Figure 5.34: L^2-error for the *Example 4* (initial condition with normal incidence on the line $x_1 = x_2$), plotted at time $t = 0.08$s, $t = 0.19$s and $t = 0.29$s, as a function of the discretization step following the space variable, $\Delta x = \frac{1}{M_1}$.

5.2.2 *Example 5*: conservative numerical scheme, in case of a slanted incidence

The *Example 5*, corresponds to a slanted line, with an equation given by:

$$x_2 - 1/\tan(\theta) x_1 = 0\,,$$

where $\tan(\theta) = \frac{1}{6}$ is the angle of incidence, of the initial condition, defined hereafter, on the slanted interface. More precisely, the initial condition impinges on $\mathcal{I}$ with a direction parallel to the x_1 axis, and is partly reflected and partly transmitted. It corresponds exactly, to the *Example 3*, with an orthogonal frame $\mathcal{R}'$, of which x-axis, is parallel to the direction $\mathbf{u} - \mathbf{v}$, and is centered on the intersection O' of the y-axis of the canonical frame, and the ray $(\mathbf{u}, \mathbf{u} - \mathbf{v})$, where $\mathbf{u}$ and $\mathbf{v}$ are given hereafter. The Dirac distribution of the initial conditions, of the form (5.1), is discretized on a few number of wave vectors, as

in the previous cases (see 5.2). And the parameters of the Gaussian, initial condition, are given by:

$$\mathbf{u} = (-0.3,\, 0.0)\,,\ \ \mathbf{v} = (-2.7,\, -0.4)\,,$$

for the main vectors, and $r_1 = r_2 = 0.01$, $r_1' = r_2' = 1/\sqrt{2}$ for the characteristic lengths. We observe the propagation of the initial peak, along the x_1 abscissa, until it reflects and is transmitted through the slanted interface $\mathcal{I}$. One may observe, that the total energy variation, plotted on the Figure 5.35, can be considered as null, while the peak crosses the interface. This energy is thus conserved, and as in the previous example, the numerical scheme gives satisfying results from this point of view.

Figure 5.36 shows the snapshots of the energy density obtained with the $c \times \mathbf{k}$ corrected scheme (CKS) at several time steps and for several level of refinement in the slowness space ($M_1 = M_2 = 50$ and $M_1 = M_2 = 200$), showing a good convergence towards the analytical solution. These results are very similar to those plotted in Figure 5.25, once rotated with an angle $\arctan 1/6$.

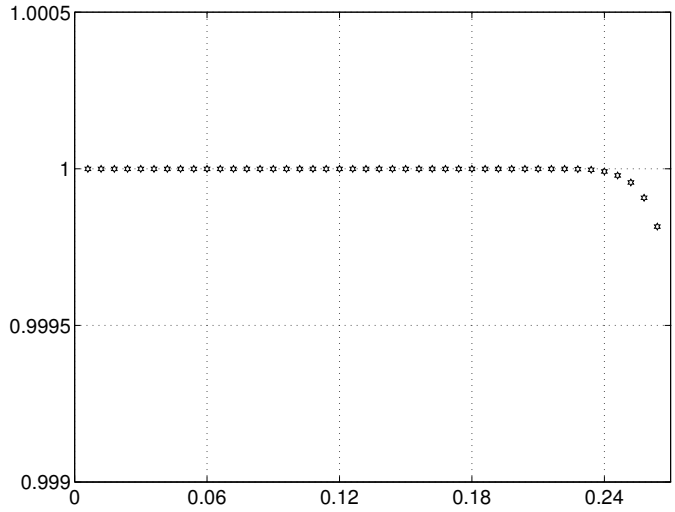

Figure 5.35: Total energy variation, through a slanted line, for the *Example 5*, with the parameters, $M_1^- = M_1^+ = 100$.

In order to draw a better comparison between the corrected scheme, and the theoretical solution, one may consider the L^2 error between both types of solutions, plotted on the Figure 5.37.

Once again, the L^2-error, is linear in time and space variable. As for the previous example, the slope of the error changes, as the peak crosses the interface $\mathcal{I}$. The error decreases, at the crossing of the interface, and one observes, that the error is linear in time. Figure 5.38, presents this error, for different discretization numbers, along the space variables. They show the convergence of the solution obtained with the corrected method, to the theoretical solution.

5.3 Conclusions

We observe on the different examples, that the schemes proposed allow to correct the loss of energy. The different schemes proposed give interesting results. One observes the convergence of the solutions obtained, with the discretization number following the space variable. This convergence remains slow (it is of frist order, in time and space vaiable). In case of a straight interface, we compare the numerical scheme to a theoretical solution.

The solution obtained are thus validated in case of normal, and slanted incidence. We also observe, that the numerical schemes allow to conserve the toteal energy variation in comaprison, to the classical numerical schemes used. The same results are obtained in case of a curved interface, where the schemes are validated for a slanted interface. We observe the convergence of the solution with the same order.

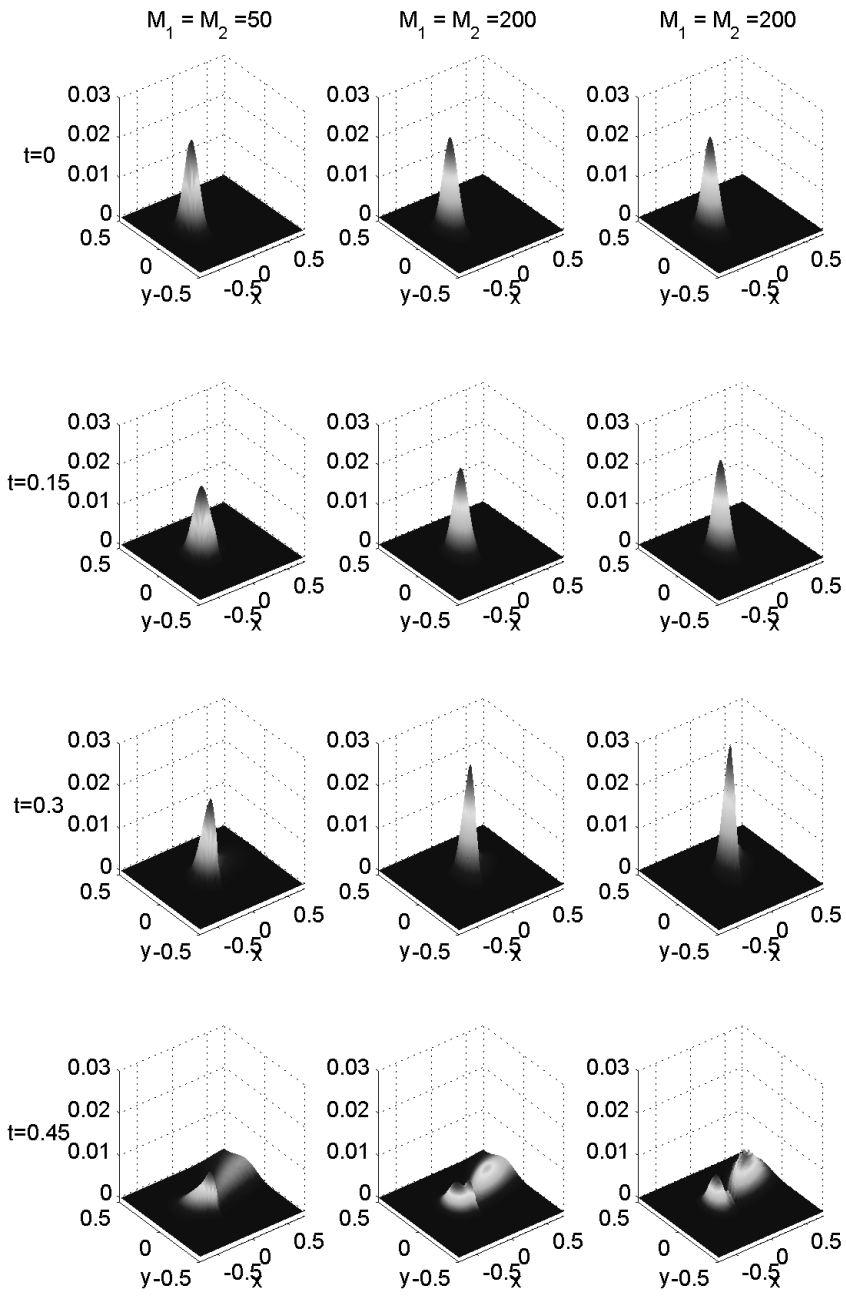

Figure 5.36: Energy density for a peak that propagates through a slanted line, *Example 5*, with the parameters $M_1^- = M_1^+ = 25$ and $M_1^- = M_1^+ = 100$. The time steps are $t = 0$s, $t = 0.15$s, $t = 0.30$s and $t = 0.45$s.

They are obtained, the smae way for normal, and slanted incidence. The latter are obtained in case of transmission from the slow to the fast medium. In the other cases, the same type of methods should help to reduce partly this loss. This should be investigated in details in some other work, and is not considered here.

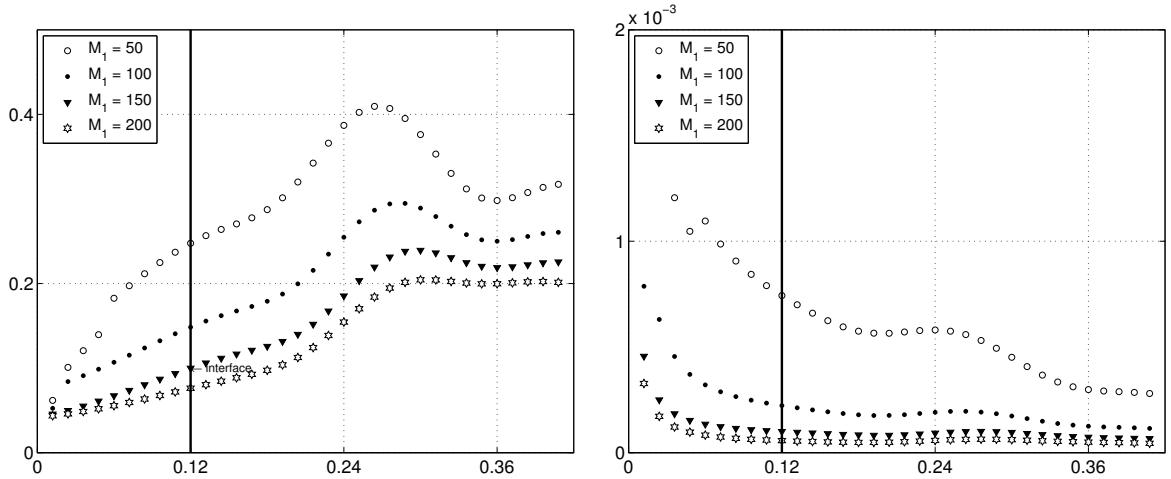

Figure 5.37: L^2-error obatained by the $c \times \mathbf{k}$ corrected schemes to the theoretical solution, *Example 5*, for the discretization numbers $M_1^- = M_1^+ = 25$ (white dots), $M_1^- = M_1^+ = 50$ (black dots), $M_1^- = M_1^+ = 75$ (black triangles) and $M_1^- = M_1^+ = 100$ (white stars). L^2-error of the corrected solution, for the discretization numbers along the x_1 coordinates $M_1 = M_2 = 50$ to $M_1 = M_2 = 200$ from the top to the bottom, *Example 2* (normal incidence, with $\mathbf{u} = (-0.3, 0)$, $\mathbf{v} = (-1.9, 0)$, and $N_1 = N_2 = 50$). One observes the L^2-error of the corrected solution (left), and the L^2-error $\times \frac{1}{M_1 t}$ (right).

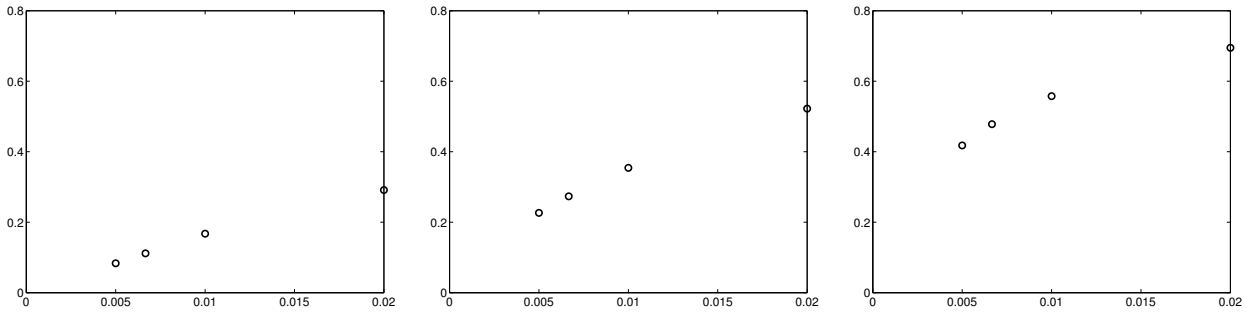

Figure 5.38: L^2-error for the *Example 5* (initial condition with normal incidence on the line $x_1 = x_2$), plotted at time $t = 0.15$s and $t = 0.30$s, and $t = 0.45$s, as a function of the discretization steps following the space variable, $\Delta x = \frac{1}{M_1}$.

6

General Conclusions

The work presented in this thesis deals with the modeling of high-frequency wave propagation in heterogeneous acoustic or elastic media. It is more particularly focused to the consideration of the boundary phenomena, such as the reflection and transmission of waves at the interfaces of the homogeneous subdomains of a piecewise homogeneous medium. They have been described in the chapter 2, together with teh various approaches developed so far in order to address high-frequency waves. However the diffraction phenomena when the waves get trapped by the interfaces and propagate along them have been disregarded, because we lack a theoretical model for them at present. Our approach is based on the resolution of transport equations in phase space of the Liouville type, that describe wave propagation in acoustic or elastic media in terms of the energy density associated to the high-frequency solutions of the underlying wave equations. This model has been summarized more particularly in the section 2.4. The Liouville equations are then solved numerically by finite difference (FD) methods. The adopted schemes have been outlined in the chapter 3. One of the main purpose of the thesis is the implementation of numerical schemes able to conserve the total energy, which may be numerically dissipated by reflection and transmission of the waves at the interfaces of the medium. The classical scheme developed in [27–31] and references therein does not preserve the total energy, as discussed in the section 4.3.1 for straight interfaces, or in the section 4.4.1 for curved interfaces. The limits of these scheme are detailed in the section 3.4 and must be corrected by modifying the numerical fluxes considered in the standard FD method of [27–31]. The corrected schemes proposed in this thesis (see the sections 4.3.2, 4.3.3 and 4.4.2) are summarized in the next section. Their limits and potential extensions are discussed in the subsequent one.

6.1 Main results

Approaching acoustic or elastic wave propagation by a kinetic model determines a system of transport equations of the Liouville type for the so-called specific intensities, which are angularly resolved (in terms of the wave vectors) energy densities. They are associated to the high-frequency limit solutions of the underlying wave equations. At the interfaces of the propagation medium, the Snell-Descartes laws that rule the behavior of the waves are characterized by reflection and transmission coefficients for the corresponding power flows. This approach is summarized in 2.4. Now solving for the Liouville equations together with the reflection and transmission phenomena at interfaces in a piecewise homogeneous medium allows to compute the energy and energy flux densities pointwise in that medium, and track the energy paths. The main purpose of this work is to develop numerical schemes that allow to conserve numerically the total energy, starting with the case of acoustic (scalar) waves. For straight interfaces we have derived FD schemes that fulfill this property for transmission from a fast to a slow medium and from a slow to a fast medium, when the sound speeds on both sides are different (see the chapter 4). The numerical methods we have considered are of two types, depending on the particular choice of the numerical fluxes applied to a standard FD discretization of the transport partial differential equation. At first, upwind fluxes with an adapted interpolations of the transmitted specific intensities that corrects the observed

loss of energy, have been developed in the section 4.3.2 for a straight interface (the FCS scheme).Such interpolations are required on account of the irregular distribution of the wave vectors obtained by backward transmission through straight or curved interfaces. A second class of upwind fluxes is developed considering a global correction of the distribution of the wave vectors both for the case of a straight interface in the section 4.3.3, and the case of a curved interface in the section 4.4.2 (the CKS scheme). It is achieved through the use of a mesh adaptation that uses two grids in order to compensate the difference of scales of the wave vector distribution on each side of the interfaces due to the differences in sound speeds. With both schemes (FCS and CKS) one obtains the conservation of the total energy, *i.e.* ℓ^1–stability and ℓ^∞–boundedness. It is also possible to show their convergence as the discretization steps go to zero.

These results are established by a formal analysis and verified on several numerical examples described in the chapter 5, in particular for a configuration with a straight interface where a theoretical solution is known. The ℓ^1–stability of the solution is observed on this example. We have also verified that the proposed schemes are of first order, which means that their convergence is linear with respect to the time and space variables–so it is relatively slow (we also refer to [28] and [32] on this issue). In the case of a curved interface though, the situation is slightly different. We have derived a numerical scheme with a global correction of the wave vector distribution (see the section 4.4.2 of the chapter 4) and a dedicated interpolation of the transmitted specific intensities. It is a quasi-conservative numerical scheme for transmission from the slow to the fast medium (see the last paragraph of the section 4.4.2), when we make some assumption on the discrete wave vector distribution obtained by backward transmission of the actual discrete wave vectors. As for the case of a straight interface, we have obtained numerical schemes which preserve the discretized total energy within the computational domain and exhibit the desired convergence properties. We have also verified with numerical examples that they are of first order in the time and space variables, so that their convergence is again linear with respect to the time and space variables (see the section 5.2 of the chapter 5). Here we have used the example of a straight slanted line with respect to the spatial mesh in order to illustrate and verify the results obtained for a curved interface, since a theoretical solution is also known in that situation. The properties of the proposed schemes for curved interfaces are the ℓ^1 convergence and ℓ^∞ boundedness of the numerical solutions, and the conservation of the total energy within the computational domain (under certain assumptions) in the case of transmission from the slow to the fast medium.

However, contrary to what has been done for a straight interface, the cases of total reflection and transmission from the fast to the slow medium with a curved interface have not been investigated in this thesis. In fact, it may be observed in some situations that it is not possible to cancel the increments of the discretized total energy, due to the geometrical adaptation of such an interface on the grid. Indeed the actual unit normal vector of a curved interface and its discretized version may be different to such a degree that it becomes irrelevant to express the continuity of the normal energy flux in a discrete setting. In this configuration, which is not discussed further in this work, it is no longer possible to obtain conservative numerical schemes, and the latter must be adapted in order to reduce the loss of energy at the interfaces. We refer to the end of the chapter 4 on this issue.

6.2 Limits and prospects

The kinetic model used for the analysis of the high-frequency solutions of the wave equation in acoustics can be applied to the high-frequency solutions of the Navier equation in elastodynamics, or to the Maxwell equations in electromagnetism. It yields a system of coupled Liouville equations for these physics, since elastic or electromagnetic waves are polarized. However the coupled transport equations can be solved numerically by the same type of methods, though some adaptations are necessary. Considering elastic waves for instance, the analysis of transmission from a slow to a fast medium, and from a fast to a slow medium can be carried on along the same lines as in acoustics [29]. However additional difficulties arise due to the possible conversion of longitudinal and transverse polarizations P and S, respectively, at the crossing of the interfaces. In the case of a straight interface, the different upwind fluxes for the FD schemes developed in this thesis can be adapted without any important difficulties. In the case of a curved interface, the scheme used for transmission from a slow to a fast medium can be adapted to

elastodynamics. The situation of transmission from a fast to a slow medium raises several difficulties discussed at the end of the chapter 4, which precludes a straightforward adaptation of the numerical schemes proposed in this thesis to elastodynamics. Another approach should be investigated in that case.

Another limit of the proposed FD schemes stems from the important number of degrees of freedom used to discretize the phase-space computational domain, such that the volume of stored data grows significantly with the discretization refinement and the physical dimension. We observe however that the proposed upwind fluxes remain conservative even for a small number of degrees of freedom (coarse meshes with small discretization numbers), which underlines their main advantage. Additionally it could be argued that the methods used in this thesis are limited to the two-dimensional problems considered for the numerical examples (chapter 5), and should be adapted to three-dimensional problems. However in the case of straight interfaces, the different numerical schemes developed in this work may be easily adapted to three-dimensional geometries, since the only difference with the two-dimensional ones is given by the tangential component of the wave vectors. The latter becomes a two-dimensional vector, which is in any case conserved by the reflection and transmission processes. The interpolation of the normal component remains the same though. In the case of curved interfaces, the consideration of transmission from a slow to a fast three-dimensional medium can be adapted from the developments expounded in the chapter 4. The interfaces are discretized using the same procedure, and the different sub-cases exhibited for two-dimensional problems can be identified by the same principles. All this requires only slight adjustments of the numerical codes developed so far. The consideration of transmission from the fast to the slow medium and of total reflection raises the same difficulties as in two-dimensional geometries and calls for additional developments. The latter may be addressed by defining partially non-conservative numerical schemes, with the objective of reducing the total energy that is lost at the interfaces. Both the two-dimensional and three-dimensional geometries require further investigations on these aspects.

At last, it is emphasized again that the diffraction phenomena [11, 35, 41] arising from the occurrence of glancing energy rays or corner refractions have not been taken into account in this research. An interesting prospect would be to try to adapt the different methods proposed here to such a situation. We refer to [31, 33] for some early developments on this issue.

A

Reflexion/transmission coefficients for elastic waves at a straight interface

We consider the case of an impinging P-wave (see Figure 2.2) that generates a reflected and a transmitted P-wave, and a reflected and a transmitted SV-wave, corresponding to the case presented in Section 2.1.3. We adopt here the notations of that section and write the continuity of displacements and stress vectors at the interface $\mathcal{I}$ between the two homogeneous media $\mathcal{O}^-$ and $\mathcal{O}^+$. Their Lamé parameters are denoted by μ^-, λ^- in $\mathcal{O}^-$, and by μ^+, λ^+ in $\mathcal{O}^+$. The material densities are ρ^- and ρ^+ respectively, and the corresponding P and S wave celerities are denoted by $c_{\rm P}^-$, $c_{\rm S}^-$, $c_{\rm P}^+$ and $c_{\rm S}^+$.

Let us first recall the continuity equation (2.29) at $\mathcal{I}$ for the displacement fields:

$$\hat{\mathbf{k}}\,\mathrm{e}^{-\,\mathrm{i}\,\mathbf{k}'\cdot\mathbf{x}'} + A_{\rm PR}\mathbf{d}_{\rm PR}\,\mathrm{e}^{-\,\mathrm{i}\,\mathbf{k}'_{\rm PR}\cdot\mathbf{x}'} + A_{\rm SR}\mathbf{d}_{\rm SR}\,\mathrm{e}^{-\,\mathrm{i}\,\mathbf{k}'_{\rm SR}\cdot\mathbf{x}'} = A_{\rm PT}\mathbf{d}_{\rm PT}\,\mathrm{e}^{-\,\mathrm{i}\,\mathbf{k}'_{\rm PT}\cdot\mathbf{x}'} + A_{\rm ST}\mathbf{d}_{\rm ST}\,\mathrm{e}^{-\,\mathrm{i}\,\mathbf{k}'_{\rm ST}\cdot\mathbf{x}'}\,, \qquad \text{(A.1)}$$

for all $\mathbf{x}'$ on $\mathcal{I}$. The above relation implies the equality of all phase terms, which provides with the Snell-Descartes law stating that the tangential components are equal for all $m \in \{\mathrm{PR}, \mathrm{SR}, \mathrm{PT}, \mathrm{ST}\}$: $\mathbf{k}' = \mathbf{k}'_m$. It is then deduced that:

$$\begin{aligned}
\mathbf{d}_m &= \frac{1}{|\mathbf{k}_m|}\Big(\mathbf{k}' + (\mathbf{k}_m\cdot\mathbf{n})\mathbf{n}\Big)\,, && m = \mathrm{PR}\,, \mathrm{PT}\,,\\
\mathbf{d}_m &= \frac{1}{|\mathbf{k}_m|}\Big(-(\mathbf{k}_m\cdot\mathbf{n})\hat{\mathbf{k}}' + |\mathbf{k}'|\mathbf{n}\Big)\,, && m = \mathrm{SR}\,, \mathrm{ST}\,,
\end{aligned}$$

with $\omega = c_{\rm P}^-|\mathbf{k}_{\rm PR}| = c_{\rm S}^-|\mathbf{k}_{\rm SR}| = c_{\rm P}^+|\mathbf{k}_{\rm PT}| = c_{\rm S}^+|\mathbf{k}_{\rm ST}|$ and $\hat{\mathbf{k}}' = \mathbf{k}'/|\mathbf{k}'|$. By projecting Eq. (A.1) on $\mathbf{k}'$ and $\mathbf{n}$ (see the figure 2.2), we obtain successively two equations for the reflected and transmitted amplitudes:

$$c_{\rm P}^-|\mathbf{k}'|(1 + A_{\rm PR}) - \sqrt{\omega^2 - (c_{\rm S}^-|\mathbf{k}'|)^2}\,A_{\rm SR} = c_{\rm P}^+|\mathbf{k}'|A_{\rm PT} + \sqrt{\omega^2 - (c_{\rm S}^+|\mathbf{k}'|)^2}\,A_{\rm ST} \qquad \text{(A.2)}$$

and

$$\sqrt{\omega^2 - (c_{\rm P}^-|\mathbf{k}'|)^2}\,(A_{\rm PR} - 1) + c_{\rm S}^-|\mathbf{k}'|A_{\rm SR} = -\sqrt{\omega^2 - (c_{\rm P}^+|\mathbf{k}'|)^2}\,A_{\rm PT} + c_{\rm S}^+|\mathbf{k}'|A_{\rm ST}\,. \qquad \text{(A.3)}$$

Second, the continuity of the stress vectors (2.30) reads:

$$\begin{aligned}
\Big[|\mathbf{k}|(\lambda^-\mathbf{I} + 2\mu^-\hat{\mathbf{k}}\otimes\hat{\mathbf{k}})\,\mathrm{e}^{-\,\mathrm{i}\,\mathbf{k}'\cdot\mathbf{x}'} + A_{\rm PR}|\mathbf{k}_{\rm PR}|(\lambda^-\mathbf{I} + 2\mu^-\hat{\mathbf{k}}_{\rm PR}\otimes\hat{\mathbf{k}}_{\rm PR})\,\mathrm{e}^{-\,\mathrm{i}\,\mathbf{k}'_{\rm PR}\cdot\mathbf{x}'}\\
+ A_{\rm SR}|\mathbf{k}_{\rm SR}|(2\mu^-\mathbf{d}_{\rm SR}\otimes_s\hat{\mathbf{k}}_{\rm SR})\,\mathrm{e}^{-\,\mathrm{i}\,\mathbf{k}'_{\rm SR}\cdot\mathbf{x}'}\Big]\mathbf{n} =\\
\Big[A_{\rm PT}|\mathbf{k}_{\rm PT}|(\lambda^+\mathbf{I} + 2\mu^+\hat{\mathbf{k}}_{\rm PT}\otimes\hat{\mathbf{k}}_{\rm PT})\,\mathrm{e}^{-\,\mathrm{i}\,\mathbf{k}'_{\rm PT}\cdot\mathbf{x}'} + A_{\rm ST}|\mathbf{k}_{\rm ST}|(2\mu^+\mathbf{d}_{\rm ST}\otimes_s\hat{\mathbf{k}}_{\rm ST})\,\mathrm{e}^{-\,\mathrm{i}\,\mathbf{k}'_{\rm ST}\cdot\mathbf{x}'}\Big]\mathbf{n}\,. \qquad \text{(A.4)}
\end{aligned}$$

Introducing $\kappa_- = \frac{c_{\rm P}^-}{c_{\rm S}^-}$ and $\kappa_+ = \frac{c_{\rm P}^+}{c_{\rm S}^+}$, and projecting the relation (A.4) on $\mathbf{n}$ and $\mathbf{k}'$, respectively, leads to:

$$\frac{\mu^-}{c_{\rm P}^-}\kappa_-^2\left(\omega^2 - 2(c_{\rm S}^-|\mathbf{k}'|)^2\right)(1 + A_{\rm PR}) + 2\mu^-|\mathbf{k}'|\sqrt{\omega^2 - (c_{\rm S}^-|\mathbf{k}'|)^2}\,A_{\rm SR} = \frac{\mu^+}{c_{\rm P}^+}\kappa_+^2\left(\omega^2 - 2(c_{\rm S}^+|\mathbf{k}'|)^2\right)A_{\rm PT} - 2\mu^+|\mathbf{k}'|\sqrt{\omega^2 - (c_{\rm S}^+|\mathbf{k}'|)^2}\,A_{\rm ST}\,, \quad \text{(A.5)}$$

and

$$\mu^-|\mathbf{k}'|\sqrt{\omega^2 - (c_{\rm P}^-|\mathbf{k}'|)^2}\,(A_{\rm PR} - 1) - \frac{\mu^-}{2c_{\rm S}^-}\left(\omega^2 - 2(c_{\rm S}^-|\mathbf{k}'|)^2\right)A_{\rm SR} = -\mu^+|\mathbf{k}'|\sqrt{\omega^2 - (c_{\rm P}^+|\mathbf{k}'|)^2}\,A_{\rm PT} - \frac{\mu^+}{2c_{\rm S}^+}\left(\omega^2 - 2(c_{\rm S}^+|\mathbf{k}'|)^2\right)A_{\rm ST}\,. \quad \text{(A.6)}$$

In order to solve the system of equations (A.2), (A.3), (A.5) and (A.6), we follow the steps of [20] and introduce the unknowns $\rm D_S$, $\rm S_S$, $\rm D_P$, $\rm S_P$:

$$\mathrm{D_P} = A_{\rm Pi} - A_{\rm PR}\,, \quad \mathrm{S_P} = A_{\rm Pi} + A_{\rm PR}\,, \quad \mathrm{D_S} = -A_{\rm SR}\,, \quad \mathrm{S_S} = A_{\rm SR}\,,$$

with $A_{\rm Pi} = 1$ in the present case. This enables to rewrite this system of equations in the form:

$$c_{\rm P}^-|\mathbf{k}'|\mathrm{S_P} + \sqrt{\omega^2 - (c_{\rm S}^-|\mathbf{k}'|)^2}\,\mathrm{D_S} = c_{\rm P}^+|\mathbf{k}'|A_{\rm PT} + \sqrt{\omega^2 - (c_{\rm S}^+|\mathbf{k}'|)^2}\,A_{\rm ST}\,,$$

$$-\sqrt{\omega^2 - (c_{\rm P}^-|\mathbf{k}'|)^2}\,\mathrm{D_P} + c_{\rm S}^-|\mathbf{k}'|\mathrm{S_S} = -\sqrt{\omega^2 - (c_{\rm P}^+|\mathbf{k}'|)^2}\,A_{\rm PT} + c_{\rm S}^+|\mathbf{k}'|A_{\rm ST}\,,$$

$$\frac{\mu^-}{c_{\rm P}^-}\kappa_-^2\left(\omega^2 - 2(c_{\rm S}^-|\mathbf{k}'|)^2\right)\mathrm{S_P} - 2\mu^-|\mathbf{k}'|\sqrt{\omega^2 - (c_{\rm S}^-|\mathbf{k}'|)^2}\,\mathrm{D_S} = \frac{\mu^+}{c_{\rm P}^+}\kappa_+^2\left(\omega^2 - 2(c_{\rm S}^+|\mathbf{k}'|)^2\right)A_{\rm PT} - 2\mu^+|\mathbf{k}'|\sqrt{\omega^2 - (c_{\rm S}^+|\mathbf{k}'|)^2}\,A_{\rm ST}\,,$$

$$\mu^-|\mathbf{k}'|\sqrt{\omega^2 - (c_{\rm P}^-|\mathbf{k}'|)^2}\,\mathrm{D_P} + \frac{\mu-}{c_{\rm S}^-}\left(\omega^2 - 2(c_{\rm S}^-|\mathbf{k}'|)^2\right)\mathrm{S_S} = \mu^+|\mathbf{k}'|\sqrt{\omega^2 - (c_{\rm P}^+|\mathbf{k}'|)^2}\,A_{\rm PT} + \frac{\mu^+}{c_{\rm S}^+}\left(\omega^2 - 2(c_{\rm S}^+|\mathbf{k}'|)^2\right)A_{\rm ST}\,.$$

The previous system is divided into two subsystems: $(\mathrm{S_P}, \mathrm{D_S})$ on the one hand, and $(\mathrm{S_S}, \mathrm{D_P})$ on the other hand. These two subsystems are solved easily, which leads to:

$$\mathrm{S_P} = \alpha_1 A_{\rm PT} + \beta_1 A_{\rm ST}\,, \quad \mathrm{D_S} = \alpha_2 A_{\rm PT} + \beta_2 A_{\rm ST}\,,$$

where:

$$\begin{aligned}
\alpha_1 &= \frac{2\mu^- c_{\rm P}^+|\mathbf{k}'|^2 + \frac{\mu^+}{c_{\rm P}^+}\kappa_+^2\left(\omega^2 - 2(c_{\rm S}^+|\mathbf{k}'|)^2\right)}{2\mu^- c_{\rm P}^-|\mathbf{k}'|^2 + \frac{\mu^-}{c_{\rm P}^-}\kappa_-^2\left(\omega^2 - 2(c_{\rm S}^-|\mathbf{k}'|)^2\right)}\,,\\
\beta_1 &= \frac{2\left(\frac{\mu^+}{\mu^-} - 1\right)c_{\rm P}^-|\mathbf{k}'|\sqrt{\omega^2 - (c_{\rm S}^+|\mathbf{k}'|)^2}}{2(c_{\rm P}^-|\mathbf{k}'|)^2 + \kappa_-^2\left(\omega^2 - 2(c_{\rm S}^-|\mathbf{k}'|)^2\right)}\,,\\
\alpha_2 &= \frac{c_{\rm P}^+|\mathbf{k}'|\left(\frac{\mu^+}{\mu^-}\frac{c_{\rm S}^{-2}}{c_{\rm S}^{+2}}\left(\omega^2 - 2(c_{\rm S}^+|\mathbf{k}'|)^2\right) - \left(\omega^2 - 2(c_{\rm S}^-|\mathbf{k}'|)^2\right)\right)}{\sqrt{\omega^2 - (c_{\rm S}^-|\mathbf{k}'|)^2}}\,,\\
\beta_2 &= \left(\left(2\frac{\mu^+}{\mu^-} + 1\right)(c_{\rm S}^-|\mathbf{k}'|)^2 - \omega^2\right)\sqrt{\frac{\omega^2 - (c_{\rm S}^+|\mathbf{k}'|)^2}{\omega^2 - (c_{\rm S}^-|\mathbf{k}'|)^2}}\,,
\end{aligned} \quad \text{(A.7)}$$

and:

$$\mathrm{S_S} = \alpha_3 A_{\mathrm{PT}} + \beta_3 A_{\mathrm{ST}}\,, \quad \mathrm{D_P} = \alpha_4 A_{\mathrm{PT}} + \beta_4 A_{\mathrm{ST}}\,,$$

where:

$$\begin{aligned}
\alpha_3 &= \frac{\left(\frac{\mu^+}{\mu^-} - 1\right) c_{\mathrm{S}}^- |\mathbf{k}'| \sqrt{\omega^2 - (c_{\mathrm{P}}^+ |\mathbf{k}'|)^2}}{\omega^2 - (c_{\mathrm{S}}^- |\mathbf{k}'|)^2}\,,\\
\beta_3 &= \frac{\frac{\mu^+}{\mu^-}\frac{c_{\mathrm{S}}^-}{c_{\mathrm{S}}^+}\left(\omega^2 - 2(c_{\mathrm{S}}^+ |\mathbf{k}'|)^2\right) + c_{\mathrm{S}}^- c_{\mathrm{S}}^+ |\mathbf{k}'|^2}{\omega^2 - (c_{\mathrm{S}}^- |\mathbf{k}'|)^2}\,,\\
\alpha_4 &= \frac{\omega^2 + \frac{\mu^+}{\mu^-}(c_{\mathrm{S}}^- |\mathbf{k}'|)^2}{\omega^2 - (c_{\mathrm{S}}^- |\mathbf{k}'|)^2} \sqrt{\frac{\omega^2 - (c_{\mathrm{P}}^+ |\mathbf{k}'|)^2}{\omega^2 - (c_{\mathrm{P}}^- |\mathbf{k}'|)^2}}\,,\\
\beta_4 &= \frac{-\frac{\mu^+}{\mu^-}\frac{c_{\mathrm{S}}^-}{c_{\mathrm{S}}^+} c_{\mathrm{S}}^- |\mathbf{k}'| \left(\omega^2 - 2(c_{\mathrm{S}}^+ |\mathbf{k}'|)^2\right) + c_{\mathrm{S}}^+ |\mathbf{k}'| \left(\omega^2 - 2(c_{\mathrm{S}}^- |\mathbf{k}'|)^2\right)}{\left(\omega^2 - (c_{\mathrm{S}}^- |\mathbf{k}'|)^2\right) \sqrt{\omega^2 - (c_{\mathrm{P}}^+ |\mathbf{k}'|)^2}}\,.
\end{aligned} \tag{A.8}$$

Owing to the normalisation $A_{\mathrm{Pi}} = 1$ one then has:

$$\begin{aligned}
1 &= -\mathrm{R}_{\mathrm{PP}}^-(\mathbf{k}) + \alpha_1 \mathrm{T}_{\mathrm{PP}}^-(\mathbf{k}) + \beta_1 \mathrm{T}_{\mathrm{PS}}^-(\mathbf{k})\,,\\
0 &= \mathrm{R}_{\mathrm{PS}}^-(\mathbf{k}) + \alpha_2 \mathrm{T}_{\mathrm{PP}}^-(\mathbf{k}) + \beta_2 \mathrm{T}_{\mathrm{PS}}^-(\mathbf{k})\,,\\
0 &= -\mathrm{R}_{\mathrm{PS}}^-(\mathbf{k}) + \alpha_3 \mathrm{T}_{\mathrm{PP}}^-(\mathbf{k}) + \beta_3 \mathrm{T}_{\mathrm{PS}}^-(\mathbf{k})\,,\\
1 &= \mathrm{R}_{\mathrm{PP}}^-(\mathbf{k}) + \alpha_4 \mathrm{T}_{\mathrm{PP}}^-(\mathbf{k}) + \beta_4 \mathrm{T}_{\mathrm{PS}}^-(\mathbf{k})\,,
\end{aligned}$$

where we use the notations (2.31) introduced in the Section 2.1.3. Finally the expressions for the amplitude reflection qnd trqnsmission coefficients are given by:

$$\begin{aligned}
\mathrm{R}_{\mathrm{PP}}^-(\mathbf{k}) &= \frac{(\beta_2 + \beta_3)(\alpha_1 - \alpha_4) + (\alpha_2 + \alpha_3)(\beta_4 - \beta_1)}{(\alpha_1 + \alpha_4)(\beta_2 + \beta_3) - (\alpha_2 + \alpha_3)(\beta_1 + \beta_4)}\,,\\
\mathrm{R}_{\mathrm{PS}}^-(\mathbf{k}) &= \frac{2(\alpha_3\beta_2 - \alpha_2\beta_3)}{(\alpha_1 + \alpha_4)(\beta_2 + \beta_3) - (\alpha_2 + \alpha_3)(\beta_1 + \beta_4)}\,,\\
\mathrm{T}_{\mathrm{PP}}^-(\mathbf{k}) &= \frac{2(\beta_2 + \beta_3)}{(\alpha_1 + \alpha_4)(\beta_2 + \beta_3) - (\alpha_2 + \alpha_3)(\beta_1 + \beta_4)}\,,\\
\mathrm{T}_{\mathrm{PS}}^-(\mathbf{k}) &= \frac{-2(\alpha_2 + \alpha_3)}{(\alpha_1 + \alpha_4)(\beta_2 + \beta_3) - (\alpha_2 + \alpha_3)(\beta_1 + \beta_4)}\,.
\end{aligned}$$

The same kind of computations can be made for an SV-wave that crosses the interface $\mathcal{I}$ from $\mathcal{O}^-$ to $\mathcal{O}^+$ and symetrically for P and SV waves crossing $\mathcal{I}$ from $\mathcal{O}^+$ to $\mathcal{O}^-$. One may notice here that it is assumed that the determinant of the above system is non zero. In that case where it is zero, we obtain an equation that defines a so-called Stoneley wave. This case is not treated here.

An expression for the reflection and transmission power flows is obtained by computing the ratio of the normal components of the reflected and transmitted flux vectors, to the normal component of the incident flux vector. The elastic intensity, or flux vector being $\boldsymbol{\pi}_m = -\boldsymbol{\sigma}_m \overline{\partial_t \mathbf{u}}_m$, expressions of the energy flux reflection coefficients are then deduced as:

$$\mathcal{R}_{\mathrm{PP}}^-(\mathbf{k}) = (\mathrm{R}_{\mathrm{PP}}^-(\mathbf{k}))^2\,, \quad \mathcal{R}_{\mathrm{PS}}^-(\mathbf{k}) = \frac{c_{\mathrm{S}}^- \hat{\mathbf{k}}_{\mathrm{SR}} \cdot \mathbf{n}}{c_{\mathrm{P}}^- \hat{\mathbf{k}}_{\mathrm{Pi}} \cdot \mathbf{n}} (\mathrm{R}_{\mathrm{PS}}^-(\mathbf{k}))^2\,,$$

while expressions of the energy flux transmission coefficients are given by:

$$\mathcal{T}_{\mathrm{PP}}^-(\mathbf{k}) = \frac{\rho^+ c_{\mathrm{P}}^+ \hat{\mathbf{k}}_{\mathrm{PT}} \cdot \mathbf{n}}{\rho^- c_{\mathrm{P}}^- \hat{\mathbf{k}}_{\mathrm{Pi}} \cdot \mathbf{n}} (\mathrm{T}_{\mathrm{PP}}^-(\mathbf{k}))^2\,, \quad \mathcal{T}_{\mathrm{PS}}^-(\mathbf{k}) = \frac{\rho^+ c_{\mathrm{S}}^+ \hat{\mathbf{k}}_{\mathrm{ST}} \cdot \mathbf{n}}{\rho^- c_{\mathrm{P}}^- \hat{\mathbf{k}}_{\mathrm{Pi}} \cdot \mathbf{n}} (\mathrm{T}_{\mathrm{PS}}^-(\mathbf{k}))^2\,.$$

B

Determination of the caustic curve

We aim at determining an expression (equation or parametrization) for the caustic curve, and to this purpose we use the notations of Section 2.2.3.0. As explained in this Section, the caustic is defined as the envelop of the rays which are staight lines here. The rays are parametrized by their distance to the caustic, which is denoted $\delta(\phi)$, where $\phi \in [0,\, 2\pi]$ is the angle between the ray and the x abscissa (see Figure B.2). For a point given by $(R,\, \theta)$ in $\mathbb{R}^2$, we can determine the rays passing through this point, using the curve $C_p = \left\{(\delta(\phi),\, \phi + \frac{\pi}{2}),\, \phi \in [0,\, 2\pi]\right\}$ as described on Figure B.1. We may then define ϕ as a function of R and θ. The rays are characterized by the set of points for which $\phi(R,\, \theta) = \phi_0$ is a constant. One may note that for one point $(R,\, \theta)$ there are several possible angles $\phi(R,\, \theta)$. We suppose that the shape of the caustic is such that a unique ray $(\delta(\phi),\, \phi)$ can be defined contrary to the example given on the right-side of Figure B.1.

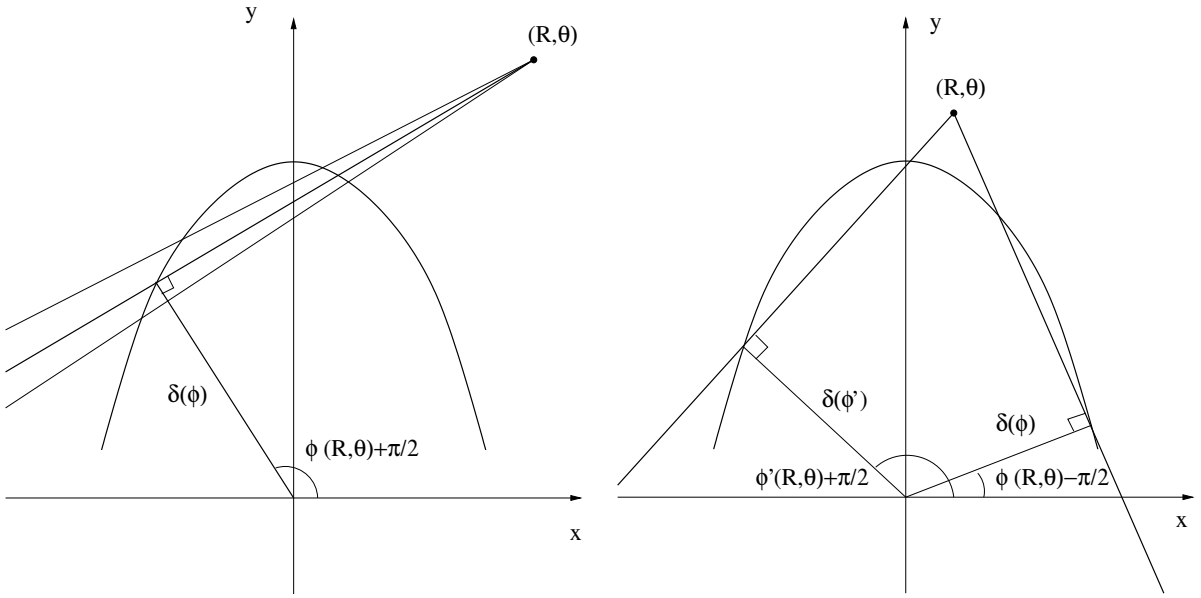

Figure B.1: Determining the angle $\phi(R,\, \theta)$

We explain now how to determine an equation of the caustic curve. The phase S solution of the Eikonal Equation (see (2.48)) on the rays is expressed as a function of the polar coordinates $(R,\, \theta)$. Using, Equation (2.52) and the relation between polar and caustic coordinates (see Figure B.2). Leads to:

$$S = S_0 + R\cos(\phi - \theta)\,,$$

where S_0 is the phase at the point $(\delta(\phi),\, \phi)$ and can be determined by making use of the Sommerfeld

condition (2.51). In effect, the form (2.46) of the solution implies, that for a given point along the ray of parameter ϕ, $S_0 = \mathrm{a}(\phi)$. (since θ tends to ϕ along the ray as R tends to $+\infty$). An equation for the rays

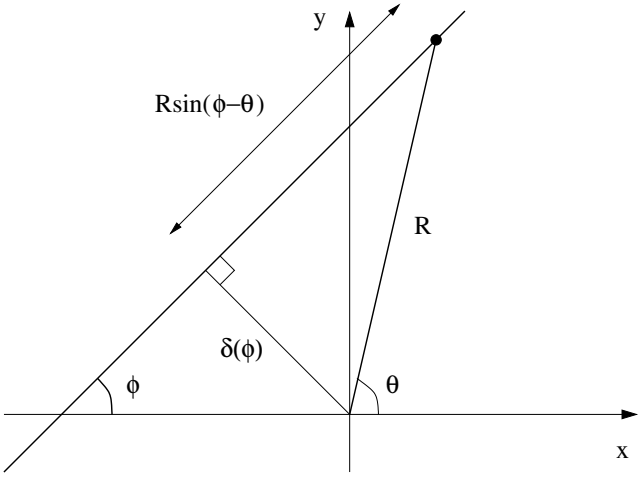

Figure B.2: Relations between polar and caustic coordinates

is obtained in polar coordinates by writing that along the rays ϕ is a constant, and ∇S is a unit vector in the direction of the ray. Thus, if ϕ is considered as a function of (R, θ), one obtains by computing ∇S, that $\nabla_{\mathbf{x}}\phi \cdot \nabla_{\mathbf{x}} S = 0$ that:

$$\frac{\mathrm{d}S}{\mathrm{d}\phi} = \mathrm{a}'(\phi) - R\sin(\phi - \theta) = 0\,. \tag{B.1}$$

Note that this implies that:

$$\delta(\phi) = \mathrm{a}'(\phi), \tag{B.2}$$

which links the shape of the curve S and the function $\mathrm{a}(\phi)$. (B.1) is then an equation for the rays. Let:

$$f(\phi,\, \mathbf{r}) = \mathrm{a}'(\phi) - R\sin(\phi - \theta)\,,$$

where $\mathbf{r} = R\mathbf{u}_r$ is the position vector, we seek a parametrization of the caustic in the form $\mathbf{r}(\phi)$, $\phi \in [0,\, 2\pi]$. The points $\mathbf{r}(\phi)$ on the caustic satisfy:

$$f(\phi,\, \mathbf{r}(\phi)) = 0\,,\;\; \nabla_{\mathbf{r}} f(\phi,\, \mathbf{r}(\phi)) \cdot \frac{\mathrm{d}\mathbf{r}}{\mathrm{d}\phi} = 0\,,\;\; \phi \in [0,\, 2\pi]\,.$$

Thus deriving the function $\phi \to f(\phi, \mathbf{r}(\phi))$ leads to:

$$\mathrm{a}''(\phi) - R\cos(\phi - \theta) = 0\,.$$

We deduce a parametric representation of the caustic from the above equation and from Equation (B.1):

$$\begin{aligned} R(\phi) &= \sqrt{\mathrm{a}''(\phi)^2 + \mathrm{a}'(\phi)^2}\,, \\ \theta(\phi) &= \phi - \arctan\frac{\mathrm{a}'(\phi)}{\mathrm{a}''(\phi)} \mod[\pi]\,. \end{aligned} \tag{B.3}$$

C

First expansion at a caustic: details of the computation

We detail in the present appendix the computations performed in order to obtain the first expansion of the solution p of the Helmholtz equation at a caustic.

C.1 Derivation of the transport equation in the caustic coordinates

Let $f(s,t)$ be a function in the caustic coordinates, α_1 a unit vector tangent to the caustic at the point (s,t), α_2 a unit vector normal to the caustic and a the radius of curvature. The gradient of f and its partial derivatives toward s and t can be decomposed as $\nabla f = (\nabla f \cdot \alpha_1)\alpha_1 + (\nabla f \cdot \alpha_2)\alpha_2$, while following relations hold between the components of ∇f and its partial derivative:

$$\frac{\partial f}{\partial t}(s,t) = \nabla f \cdot \alpha_1 \,,$$
$$\frac{\partial f}{\partial s}(s,t) = \nabla f \cdot \alpha_1 + \frac{t}{r}\nabla f \cdot \alpha_2 \,.$$

This leads to an expression of ∇f using the relations between the caustic coordinates and the Cartesian coordinates:

$$\nabla f = \frac{\partial f}{\partial t}\alpha_1 + \frac{\mathrm{a}}{t}(\frac{\partial f}{\partial s} - \frac{\partial f}{\partial t})\alpha_2 \,.$$

The Laplacian Δf of f can be directly deduced from the previous expression by applying the definition of Δf and by using the fact that $|\alpha_i|^2 = 1$, $i \in \{1,2\}$ and $\alpha_1 \cdot \alpha_2 = 0$:

$$\Delta f = \frac{1}{t}\partial_t[t\partial_t(f)] + \frac{\mathrm{a}}{t}(\partial_s - \partial_t)[\frac{\mathrm{a}}{t}(\frac{\partial f}{\partial s} - \frac{\partial f}{\partial t})] \,. \tag{C.1}$$

This last expression enables to obtain the Equation (2.54) in a neighborhood of the caustic.

C.2 Expression of p for an expansion outside of the boundary layer

We suppose that p is expanded in powers of the wave number k following (2.55). We recall that this expansion writes for the incoming ray, and the outgoing ray as follows:

$$p = \mathrm{h}(k)\sum_{n=0}^{\infty} \mathrm{v}_n(s,t)k^{-n} \,, \tag{C.2}$$

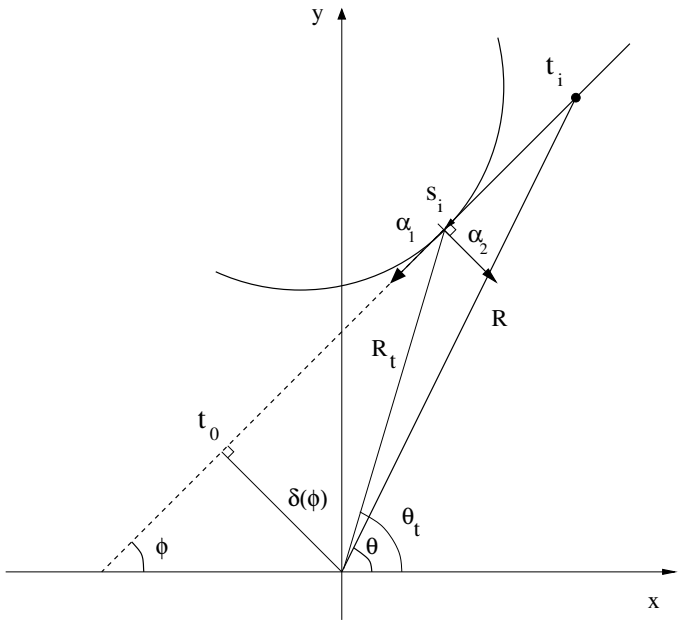

Figure C.1: Relations between polar coordinates and caustic coordinates

where $p = p_i$, p_o, and $\mathrm{v} = \mathrm{v}^i$, v^o. Using this expression in Equation (2.54), we obtain:

$$\mathrm{i}(2\frac{\partial}{\partial t} + \frac{1}{t})\mathrm{v}_n = -\Delta \mathrm{v}_{n-1}\ ,\ \mathrm{v}_{-1} = 0\,, \tag{C.3}$$

where the Laplacian is given by above expression (C.1). This system of differential equations can be solved by seeking a solution to the homogeneous problem, and a particular solution to (C.3) with its RHS. We obtain the general form for the solution:

$$\mathrm{v}_n(s,\, t) = \frac{\mathrm{G}_n(s)}{\sqrt{t}} + \frac{\mathrm{i}}{2}\int_{t_0}^{t} \Delta \mathrm{v}_{n-1}(s,\, t')\sqrt{\frac{t'}{t}}\mathrm{d}t'\,, \tag{C.4}$$

where t_0 denotes a real number or $-\infty$. The first term in the above expansion for the incoming ray can be determined as follows. Let us follow an incoming ray arriving, with an incidence ϕ and tangent to the caustic at the point $(R_t,\, \theta_t)$ (given by its polar coordinates). The relation between the polar coordinates and the caustic coordinates of a point are given by the following relation (see Figure (C.1)):

$$\begin{aligned} R\cos(\phi-\theta) &= -t_i + R_t\cos(\phi-\theta_t) = -t_i + K_t(\phi)\,,\\ R\sin(\phi-\theta) &= \delta(\phi)\,,\\ R &= \sqrt{\delta(\phi)^2 + (-t_i + R_t\cos(\phi-\theta_t))^2}\,. \end{aligned} \tag{C.5}$$

Replacing the approximation of p (see Eq. (2.55)) in the boundary conditions (2.51), and noticing that:

$$\partial_R p = \nabla p\cdot \mathbf{u}_R = \frac{\partial p}{\partial t_i}\alpha_1\cdot\mathbf{u}_R + \frac{\mathrm{a}}{t_i}(\frac{\partial p}{\partial s_i} - \frac{\partial p}{\partial t_i})\alpha_2\cdot\mathbf{u}_R\,,$$

where we use the notations introduced in the previous paragraph, leads to:

$$\begin{aligned}
&\frac{1}{2\,\mathrm{i}\,k}\sqrt{R}(\mathrm{i}\,kp_i - \partial_R p_i)e^{-\,\mathrm{i}\,kS}\mathrm{h}_i(k)^{-1}\\
&= \sqrt{R}\sum_{n=0}^{\infty}\{\frac{1}{k^n}\mathrm{v}_n^i\frac{1-\alpha_1\cdot\mathbf{u}_R}{2} - \frac{1}{2\,\mathrm{i}\,k^{n+1}}(\frac{\partial \mathrm{v}_n^i}{\partial t_i}\alpha_1\cdot\mathbf{u}_R + \frac{\mathrm{a}}{t_i}(\frac{\partial \mathrm{v}_n^i}{\partial s_i} - \frac{\partial \mathrm{v}_n^i}{\partial t_i})\alpha_2\cdot\mathbf{u}_R)\}\\
&= \sqrt{R}\mathrm{v}_0^i\frac{1-\alpha_1\cdot\mathbf{u}_R}{2} + \sqrt{R}\sum_{n=1}^{\infty}\frac{1}{k^n}\{\mathrm{v}_n^i\frac{1-\alpha_1\cdot\mathbf{u}_R}{2} - \frac{1}{2\,\mathrm{i}}(\frac{\partial \mathrm{v}_{n-1}^i}{\partial t_i}\alpha_1\cdot\mathbf{u}_R + \frac{\mathrm{a}}{t_i}(\frac{\partial \mathrm{v}_{n-1}^i}{\partial s_i} - \frac{\partial \mathrm{v}_{n-1}^i}{\partial t_i})\alpha_2\cdot\mathbf{u}_R)\}\\
&\to \mathrm{I}(\phi(s_i))e^{\mathrm{i}\,k\mathrm{a}(\phi)}\,,
\end{aligned} \tag{C.6}$$

where it can be proved recursively from (C.4), that the serie of functions above is uniformly convergent, and that each term in the sum is of the form $O(\frac{1}{\sqrt{-t_i}})$ as t_i tends to $-\infty$. As v_0^i is solution of the associated homogeneous Equation (C.3), it has the form $\mathrm{v}_0^i(s_i,\,t_i) = \frac{\mathrm{G}_i(s)}{\sqrt{-t_i}}$ (see Equation (C.4)). The previous equality, the relations (C.5) and the fact that $\alpha_1\cdot\mathbf{u}_R = \cos(\theta-\psi)\to -1$ when $R\to\infty$ lead to:

$$\mathrm{h}_i(k)\mathrm{G}_i(s)\sqrt{R}\to \mathrm{I}(\phi(s_i))\,,\;\; \mathrm{G}_i(s) = \mathrm{I}(\phi(s_i))\,,\;\; \mathrm{h}_i(k) = 1\,.$$

We finally obtain:

$$p_0^i(s_i,t_i) = \frac{\mathrm{I}(\theta(s_i))}{\sqrt{-t_i}}\,,\;\; p_n^i(s_i,t_i) = \frac{\mathrm{i}}{2}\int_{-\infty}^{t_i}\sqrt{\frac{t_i}{t'}}\Delta p_{n-1}(s_i,\,t')\mathrm{d}t'\,,$$

The complete expansion for h_o is determined in the Section C.5 of this appendix. In particular we observe, that in a neighborhood of the caustic, the amplitude $\mathrm{v}_0^i(s_\mathrm{i},\,t_\mathrm{i})$ is unbounded as $t_i\to 0$. This suggests to seek another expansion for p in this area and to model the caustic with a boundary layer, as done in the next section.

C.3 Solving the transport equation inside the boundary layer

The transport equation (2.57) is obtained by a stretching method in the boundary layer: it is solved by replacing p by its expansion in powers of k, requiring that the highest power of k inside of the brackets in the transport Equation be equal to the highest power of k in front of $2\partial_\tau p + \frac{1}{\tau}p$. We find that $r = \frac{1}{3}$ and that the previous equation rewrites:

$$k^{\frac{4}{3}}\mathrm{N}_1 p + k\mathrm{N}_2 p + k^{\frac{2}{3}}\mathrm{N}_3 p = 0\,, \tag{C.7}$$

where the operators N_1, N_2 and N_3 are deduced from (2.57) taken with $r=\frac{1}{3}$. In order to solve the equation (C.7), a second expansion of the solution in powers of $k^{-\frac{1}{3}}$ is introduced, in the form:

$$\mathrm{H}(k) = \sum_{n=0}^{\infty}\mathrm{V}_n(s,\tau)k^{-\frac{n}{3}}\,. \tag{C.8}$$

Plugging this expression (C.8) in (C.7), so as to cancel each coefficient in powers of k, leads to:

$$\mathrm{N}_1\mathrm{V}_n = -\mathrm{N}_2\mathrm{V}_{n-1} - \mathrm{N}_3\mathrm{V}_{n-2}\,,\quad \mathrm{V}_{-1}\equiv\mathrm{V}_{-2}\equiv 0\,. \tag{C.9}$$

A basis of the solutions space of the corresponding homogeneous equation (C.9), $\mathrm{N}_1\mathrm{V}_n = 0$, is given by the two linearly independent functions:

$$\begin{aligned}
\mathcal{L}(s,\tau) &= \mathrm{e}^{-\frac{\mathrm{i}\,\tau^3}{3\mathrm{a}^2}}\,\mathrm{Ai}\left[-\left(\frac{\mathrm{a}}{2}\right)^{\frac{2}{3}}\left(\frac{\tau}{\mathrm{a}}\right)^2\mathrm{e}\,\mathrm{i}\,\frac{2\pi}{3}\right]\,,\\
\mathcal{M}(s,\tau) &= \mathrm{e}^{-\frac{\mathrm{i}\,\tau^3}{3\mathrm{a}^2}}\,\mathrm{Ai}\left[-\left(\frac{\mathrm{a}}{2}\right)^{\frac{2}{3}}\left(\frac{\tau}{\mathrm{a}}\right)^2\mathrm{e}^{-\,\mathrm{i}\,\frac{2\pi}{3}}\right]\,.
\end{aligned} \tag{C.10}$$

In the above Ai denotes the Airy function defined by:

$$\mathrm{Ai}(x) = \frac{1}{2\pi}\int_{-\infty}^{\infty} \cos\left(xs + \frac{s^3}{3}\right) \mathrm{d}s\,, \tag{C.11}$$

which is solution of the ordinary differential equation:

$$\mathrm{Ai}''(x) = x\mathrm{Ai}(x)\,.$$

A solution of the homogeneous differential equation corresponding to (C.9) is:

$$\mathrm{V}_0(s,\tau) = \mathrm{c}_0(s)\mathcal{L}(s,\tau) + \mathrm{d}_0(s)\mathcal{M}(s,\tau)\,, \tag{C.12}$$

while a solution of (C.9) reads:

$$\mathrm{V}_n(s,\tau) = \mathrm{V}_{n,0}(s,\tau) + \int_{\pm 1}^{\tau} \frac{\mathcal{L}(s,\tau)\mathcal{M}(s,\tau') - \mathcal{M}(s,\tau)\mathcal{L}(s,\tau')}{\mathcal{W}(\mathcal{L},\mathcal{M})(s,\tau')}(\mathrm{N}_2\mathrm{V}_{n-1} - \mathrm{N}_3\mathrm{V}_{n-2})(s,\tau')\mathrm{d}\tau'\,, \tag{C.13}$$

where $\mathrm{V}_{n,0}(s,\tau)$ has the form given by Eq. (C.12), and $\mathcal{W}(\mathcal{L},\mathcal{M}) = \mathcal{L}\mathcal{M}' - \mathcal{M}\mathcal{L}'$ is the Wronskian of $(\mathcal{L}\,,\mathcal{M})$. One may verify that an expression of $\mathcal{W}(\mathcal{L},\mathcal{M})$ on the rays is given by:

$$\mathcal{W}(\mathcal{L},\mathcal{M}) = \left(\frac{\mathrm{a}^4}{2}\right)^{\frac{1}{3}} \mathrm{i}\,\pi\tau \exp\left(\frac{2\,\mathrm{i}\,\tau^3}{3\mathrm{a}^2}\right)\,.$$

C.4 Connexion between the expansions obtained inside and outside the boundary layer

We suppose that the two previous expressions (C.2) and (C.8) are valid for the following values of t_i:

$$t_\mathrm{i} = -k^{-\frac{1}{6}}\epsilon \;(\Leftrightarrow\; \tau_i = -k^{\frac{1}{6}}\epsilon)\,,\; 0 < \epsilon < \infty\,.$$

The condition of compatibility of both expansions derived above leads to:

$$\mathrm{h}_i(k)\mathrm{v}_0^i(s_\mathrm{i}, -k^{-\frac{1}{6}}\epsilon) = \mathrm{H}_i(k)\mathrm{V}_0^i(s_\mathrm{i}, -k^{\frac{1}{6}}\epsilon)\,,\; 0 < \epsilon < \infty\,, \tag{C.14}$$

at the 0 order term, where V_0^i has the form given by the expression (C.12), and we have seen that $\mathrm{h}_i(k)$ is equal to 1. Using the previous relations and (D.2) of the appendix D, yields:

$$\frac{\mathrm{I}(\theta(s_\mathrm{i}))}{\sqrt{\epsilon}}k^{\frac{1}{12}} = \mathrm{H}_i(k)\mathrm{c}_0(s_i)[\frac{1}{\sqrt{\pi}}e^{\mathrm{i}\frac{\pi}{12}}\rho^{\frac{1}{3}}\frac{k^{-\frac{1}{12}}}{\sqrt{\epsilon}}]e^{\frac{2\,\mathrm{i}\,\epsilon^3\sqrt{k}}{3\rho^2}} + \mathrm{H}_i(k)\mathrm{d}_0(s_i)[\frac{1}{\sqrt{\pi}}e^{-\mathrm{i}\frac{\pi}{12}}\rho^{\frac{1}{3}}\frac{k^{-\frac{1}{12}}}{\sqrt{\epsilon}}]\,.$$

This last equality is satisfied only if the term in front of $e^{\frac{2\,\mathrm{i}\,\epsilon^3\sqrt{k}}{3\rho^2}}$ vanishes, since the equality holds for all $\epsilon \in [0,\infty[$. We obtain:

$$\mathrm{c}_0 = 0\,,\;\; \mathrm{H}_i(k) = k^{\frac{1}{6}}\,,\;\; \mathrm{d}_0(s_i) = \mathrm{I}[\theta(s_i)]\sqrt{\pi}2^{\frac{5}{6}}e^{\mathrm{i}\frac{\pi}{12}}\rho^{-\frac{1}{3}}\,.$$

This leads to the expression of V_0^i inside of the boundary layer:

$$\mathrm{V}_0^i(s_\mathrm{i},\tau_i) = \mathrm{I}[\theta(s_\mathrm{i})]2^{\frac{5}{6}}\sqrt{\pi}e^{\mathrm{i}\frac{\pi}{12}}\rho^{-\frac{1}{3}}\mathrm{Ai}[-\frac{\rho}{2}^{\frac{2}{3}}\tau_i^2\rho^{-2}e^{-\frac{2\,\mathrm{i}\,\pi}{3}}]\,.$$

The same considerations can be done for the outgoing ray, and yield the following relations:

$$p_0^o(s_\mathrm{o},t_\mathrm{o}) = \frac{\mathrm{G}_o(s_0)}{\sqrt{t_0}}\,,\;\; \mathrm{H}_o(k) = k^{\frac{1}{6}}\mathrm{h}_o(k)\,,$$
$$\mathrm{V}_0^0(s_\mathrm{o},\tau_o) = \mathrm{G}_o(s_0)2^{\frac{5}{6}}\sqrt{\pi}\mathrm{a}^{-\frac{1}{3}}e^{-\mathrm{i}\frac{\pi}{12}}\exp\left(-\frac{\mathrm{i}\,\tau_o^3}{3\mathrm{a}^2}\right)\mathrm{Ai}[-\frac{\mathrm{a}}{2}^{\frac{2}{3}}\tau_o^2\mathrm{a}^{-2}e^{\frac{2\,\mathrm{i}\,\pi}{3}}]\,.$$

The functions h_o and G_o are determined by a condition inside of the caustic. The expansion obtained in the boundary layer is equated to an expansion inside of the caustic as explained in the following paragraph.

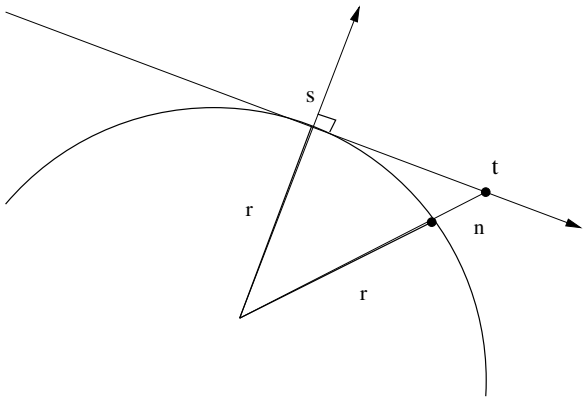

Figure C.2: Expansion in the caustics normal direction

C.5 Expansion inside of the caustic

In order to find $\mathrm{h}_o(k)$ and $\mathrm{G}_o(s)$, an expansion of the amplitude inside of the caustic is also performed. To this purpose, the distance between the caustic and a point $\mathbf{x}$ along the normal is denoted n (n > 0 if it is located outside of the caustic, or n < 0 if it is inside of it). The phase value at the point, where the normal reaches the caustic is denoted $\underline{s}$, and we define:

$$\bar{\mathrm{n}} = k^{\frac{2}{3}}\mathrm{n}\,.$$

Writing τ_i, τ_o, s_i and s_o in terms of $\underline{s}$, $\bar{\mathrm{n}}$ and k leads to the following expansion for p:

$$p \sim e^{\mathrm{i}\,k\underline{s}}k^{\frac{1}{6}}\pi^{\frac{1}{2}}2^{-\frac{5}{6}}\mathrm{a}^{-\frac{1}{3}} \times \left\{ e^{\frac{\mathrm{i}\,\pi}{12}}\mathrm{I}[\theta(\underline{s})]\mathrm{Ai}[-(\frac{2}{\mathrm{a}})^{\frac{1}{3}}\bar{\mathrm{n}}e^{-\mathrm{i}\,\frac{2\pi}{3}}] + e^{-\frac{\mathrm{i}\,\pi}{12}}\mathrm{h}_o(k)\mathrm{G}_o(\underline{s})\mathrm{Ai}[-(\frac{2}{\mathrm{a}})^{\frac{1}{3}}\bar{\mathrm{n}}e^{\mathrm{i}\,\frac{2\pi}{3}}] \right\} + \ldots\,, \quad \text{(C.15)}$$

since we have the following relations in the neighborhood of the caustic at the first order in $\bar{\mathrm{n}}$ as illustrated on Figure C.2:

$$s_\mathrm{o} + t_\mathrm{o} = \bar{\mathrm{n}}\,, \text{ and } \mathrm{n} = \frac{t^2}{2\mathrm{a}}\,.$$

If we use the expansion of the Airy functions (see Eq. (D.2)) in the previous Eq. (C.15), we obtain an expression of p in terms of the functions Ai and Bi and deduce an asymptotic behavior of Bi (see the Appendix D for the definition of Ai and Bi):

$$\mathrm{Bi}[(\frac{2}{\mathrm{a}})^{\frac{1}{3}}k^{\frac{2}{3}}|\mathrm{n}|] =_{\mathbf{k}\to\infty} \mathrm{O}[\exp\left\{\frac{2}{3}(\frac{2}{\mathrm{a}})^{\frac{1}{2}}k|\mathrm{n}|^{\frac{3}{2}}\right\}]\,,$$

its coefficient must be equal to zero, so that the expressions of $\mathrm{h}_o(k)$ and $\mathrm{G}_o(\underline{s})$ are given by:

$$\mathrm{h}_o(k) = 1\,,\ \ \mathrm{G}_o(\underline{s}) = e^{-\frac{\mathrm{i}\,\pi}{2}}\mathrm{I}[\theta(\underline{s})]\,.$$

This determines entirely the expansion at the first order for p inside and outside of the boundary layer.

D

Connecting expansions inside and outside the boundary layer about the caustics

The Airy function defined by:

$$\mathrm{Ai}(x) = \frac{1}{\pi}\int_0^\infty \cos\left(\frac{1}{3}t^3 + xt\right)\mathrm{d}t\,, \quad x \in \mathbb{C}\,,$$

is solution of the following differential equation:

$$y''(x) - xy(x) = 0\,. \tag{D.1}$$

The Airy function of the second kind Bi also satisfies the previous Eq. (D.1) on $\mathbb{R}$, for the following initial conditions:

$$\mathrm{Bi}(0) = \frac{1}{3^{\frac{1}{6}}\Gamma(\frac{2}{3})}\,, \quad \mathrm{Bi}'(0) = \frac{3^{\frac{1}{6}}}{\Gamma(\frac{1}{3})}\,.$$

Let $\xi = \frac{2}{3}x^{\frac{3}{2}}$, these functions admit the first order expansions for $x > 0$:

$$\begin{aligned}
\mathrm{Ai}(-x) &\underset{x\to\infty}{\simeq} \frac{1}{\sqrt{\pi}x^{\frac{1}{4}}}\cos\left(\xi - \frac{\pi}{4}\right)\,,\\
\mathrm{Bi}(-x) &\underset{x\to\infty}{\simeq} -\frac{1}{\sqrt{\pi}x^{\frac{1}{4}}}\sin\left(\xi - \frac{\pi}{4}\right)\,.
\end{aligned}$$

They yield the following expansions:

$$\begin{aligned}
\mathrm{Ai}^+(-x) &= \frac{\mathrm{e}^{\frac{\mathrm{i}\pi}{3}}}{2}[\mathrm{Ai}(-x) - \mathrm{i}\,\mathrm{Bi}(-x)] \underset{x\to\infty}{\simeq} \frac{1}{2\sqrt{\pi}}\,\mathrm{e}^{\frac{\mathrm{i}\pi}{12}}\,\frac{1}{x^{\frac{1}{4}}}\,\mathrm{e}^{\mathrm{i}\frac{2}{3}x^{\frac{3}{2}}}\,,\\
\mathrm{Ai}^-(-x) &= \frac{\mathrm{e}^{-\frac{\mathrm{i}\pi}{3}}}{2}[\mathrm{Ai}(-x) + \mathrm{i}\,\mathrm{Bi}(-x)] \underset{x\to\infty}{\simeq} \frac{1}{2\sqrt{\pi}}\,\mathrm{e}^{-\frac{\mathrm{i}\pi}{12}}\,\frac{1}{x^{\frac{1}{4}}}\,\mathrm{e}^{-\mathrm{i}\frac{2}{3}x^{\frac{3}{2}}}\,.
\end{aligned}$$

With the help of the above formula we can give explicit expressions of $\mathcal{L}(s, -k^{\frac{1}{6}})$ and $\mathcal{M}(s, -k^{\frac{1}{6}})$ and plug them in Eq. (C.14). We obtain successively:

$$\begin{aligned}
\mathrm{Ai}^+\left[-k^{\frac{1}{6}}\left(\frac{\epsilon^3}{2\rho^2}\right)^{\frac{2}{3}}\right] &\underset{\epsilon\to\infty}{\simeq} \frac{2^{-\frac{5}{6}}}{\sqrt{\pi}}\rho^{\frac{1}{3}}\,\mathrm{e}^{\frac{\mathrm{i}\pi}{12}}\,\frac{k^{-\frac{1}{12}}}{\sqrt{\epsilon}}\,\mathrm{e}^{\frac{\mathrm{i}\epsilon^3\sqrt{k}}{3\rho^2}}\,,\\
\mathrm{Ai}^-\left[-k^{\frac{1}{6}}\left(\frac{\epsilon^3}{2\rho^2}\right)^{\frac{2}{3}}\right] &\underset{\epsilon\to\infty}{\simeq} \frac{2^{-\frac{5}{6}}}{\sqrt{\pi}}\rho^{\frac{1}{3}}\,\mathrm{e}^{-\frac{\mathrm{i}\pi}{12}}\,\frac{k^{-\frac{1}{12}}}{\sqrt{\epsilon}}\,\mathrm{e}^{-\frac{\mathrm{i}\epsilon^3\sqrt{k}}{3\rho^2}}\,.
\end{aligned} \tag{D.2}$$

These relations are used to determine an expression of the solution in the boundary layer defined about the caustics.

E

Eigenvectors and eigenvalues of the elastic dispersion matrix

E.1 Dispersion matrix for elastic waves

We consider the system of Eq. (2.67) for wave propagation in an isotropic elastic medium. The 10×10 symmetric matrices $\mathbf{A}$, $\mathbf{D}_1$, $\mathbf{D}_2$ and $\mathbf{D}_3$ of Eq. (2.65) are described by the following formula:

$$\mathbf{A} = \mathrm{diag}\left(\rho \mathbf{I}_3, \frac{1}{2\mu}\mathbf{I}_3, \frac{1}{\mu}\mathbf{I}_3, \frac{1}{\lambda}\right) ,$$

and:

$$\begin{aligned}
\mathbf{D}_1 &= -\left(\mathbf{e}_1 \otimes \mathbf{e}_4 + \mathbf{e}_1 \otimes \mathbf{e}_{10} + \mathbf{e}_2 \otimes \mathbf{e}_9 + \mathbf{e}_3 \otimes \mathbf{e}_8\right) , \\
\mathbf{D}_2 &= -\left(\mathbf{e}_1 \otimes \mathbf{e}_9 + \mathbf{e}_2 \otimes \mathbf{e}_5 + \mathbf{e}_2 \otimes \mathbf{e}_{10} + \mathbf{e}_2 \otimes \mathbf{e}_{10}\right) , \\
\mathbf{D}_3 &= -\left(\mathbf{e}_1 \otimes \mathbf{e}_8 + \mathbf{e}_2 \otimes \mathbf{e}_7 + \mathbf{e}_3 \otimes \mathbf{e}_6 + \mathbf{e}_3 \otimes \mathbf{e}_{10}\right) .
\end{aligned}$$

The dispersion matrix $\mathbf{L} = \mathbf{A}^{-1} k_j \mathbf{D}_j$ reads:

$$\mathbf{L} = \begin{pmatrix} \mathbf{0} & \frac{1}{\rho}\mathbf{K}(\mathbf{k}) & \frac{1}{\rho}\mathbf{M}(\mathbf{k}) & \frac{1}{\rho}\mathbf{k} \\ 2\mu\mathbf{K}(\mathbf{k}) & \mathbf{0} & \mathbf{0} & \mathbf{0} \\ \mu\mathbf{M}(\mathbf{k}) & \mathbf{0} & \mathbf{0} & \mathbf{0} \\ \lambda\mathbf{k}^t & \mathbf{0} & \mathbf{0} & \mathbf{0} \end{pmatrix} ,$$

where the 3×3 matrices $\mathbf{K}(\mathbf{k})$ and $\mathbf{M}(\mathbf{k})$ are given by:

$$\mathbf{M}(\mathbf{k}) = \begin{pmatrix} 0 & k_3 & k_2 \\ k_3 & 0 & k_1 \\ k_2 & k_1 & 0 \end{pmatrix} , \qquad \mathbf{K}(\mathbf{k}) = \begin{pmatrix} k_1 & 0 & 0 \\ 0 & k_2 & 0 \\ 0 & 0 & k_3 \end{pmatrix} .$$

The dispersion matrix $\mathbf{L}$ has the following eigenvalues:

$$\begin{aligned}
&\omega_0 = 0 , && \text{with multiplicity } 4 , \\
&\omega_{\mathrm{P}}^{\pm} = \pm c_{\mathrm{P}} |\mathbf{k}| , && \text{with multiplicity } 1 , \\
&\omega_{\mathrm{S}}^{\pm} = \pm c_{\mathrm{S}} |\mathbf{k}| , && \text{with multiplicity } 2 ,
\end{aligned}$$

where we recall the celerities of the P and S waves:

$$c_{\mathrm{P}} = \sqrt{\frac{\lambda + 2\mu}{\rho}} , \quad c_{\mathrm{S}} = \sqrt{\frac{\mu}{\rho}} .$$

E.2 Eigenvectors and eigenvalues

Let α be an eigenvalue, and $\mathbf{b}$ be and eigenvector of $\mathbf{L}$. If $\alpha = 0$ the form of matrix $\mathbf{L}$ shows that its kernel is isomorphic to the kernel of the following matrix:

$$\begin{bmatrix}\mathbf{K}(\mathbf{k}) & \mathbf{M}(\mathbf{k}) & \mathbf{k}\end{bmatrix},$$

which obviously has dimension equal to 4, since its lines are independent. One may verify that a basis of the kernel ($\alpha = 0$) is given by the following eigenvectors $\mathbf{b}_0^j(\mathbf{x},\mathbf{k})$, $1 \leq j \leq 4$:

$$\begin{aligned}
\mathbf{b}_0^j(\mathbf{x},\mathbf{k}) &= \left(\mathbf{0}, \sqrt{2\mu}\mathbf{K}(\mathbf{z}^j)\mathbf{z}^j, \sqrt{\mu}2\mathbf{M}(\mathbf{z}^j)\mathbf{z}^j, 0\right)^{\mathsf{T}}, \quad j = 1,2,\\
\mathbf{b}_0^3(\mathbf{x},\mathbf{k}) &= \left(\mathbf{0}, \sqrt{2\mu}\mathbf{K}(\mathbf{z}^1)\mathbf{z}^2, \sqrt{\mu}2\mathbf{M}(\mathbf{z}^1)\mathbf{z}^2, 0\right)^{\mathsf{T}},\\
\mathbf{b}_0^4(\mathbf{x},\mathbf{k}) &= \left(\mathbf{0}, \frac{2\sqrt{\lambda\mu}\mathbf{K}(\hat{\mathbf{k}})\hat{\mathbf{k}}}{\sqrt{2(\lambda+2\mu)}}, \sqrt{\frac{\lambda\mu}{2(\lambda+2\mu)}}\mathbf{M}(\hat{\mathbf{k}})\hat{\mathbf{k}}, -\frac{2\sqrt{\lambda\mu}}{\sqrt{2\,(\lambda+\mu)}}\right)^{\mathsf{T}},
\end{aligned}$$

where the vectors $\hat{\mathbf{k}} = \mathbf{k}/|\mathbf{k}|$, $\mathbf{z}_1$ and $\mathbf{z}_2$ form an orthonormal triplet defined as follows. Let $(1,\theta,\phi)$ be the spherical coordinates of $\hat{\mathbf{k}}$ in the canonical basis of $\mathbb{R}^3$, we have:

$$\hat{\mathbf{k}} = \begin{pmatrix}\sin\theta\cos\phi\\ \sin\theta\sin\phi\\ \cos\theta\end{pmatrix}, \quad \mathbf{z}_1 = \begin{pmatrix}\cos\theta\cos\phi\\ \cos\theta\sin\phi\\ -\sin\theta\end{pmatrix}, \quad \mathbf{z}_2 = \begin{pmatrix}-\sin\phi\\ \cos\phi\\ 0\end{pmatrix}.$$

Otherwise, if $\alpha \neq 0$, the equality $\mathbf{L}\mathbf{w} = \alpha\mathbf{w}$ leads to the system of equations below:

$$\alpha\begin{pmatrix}w_1\\ w_2\\ w_3\end{pmatrix} = \frac{1}{\rho}\mathbf{K}(\mathbf{k})\begin{pmatrix}w_4\\ w_5\\ w_6\end{pmatrix} + \frac{1}{\rho}\mathbf{M}(\mathbf{k})\begin{pmatrix}w_7\\ w_8\\ w_9\end{pmatrix} + \frac{\lambda}{\rho}w_{10}\mathbf{k}, \tag{E.1}$$

$$\alpha\begin{pmatrix}w_4\\ w_5\\ w_6\end{pmatrix} = 2\mu\mathbf{K}(\mathbf{k})\begin{pmatrix}w_1\\ w_2\\ w_3\end{pmatrix}, \quad \alpha\begin{pmatrix}w_7\\ w_8\\ w_9\end{pmatrix} = \mu\mathbf{M}(\mathbf{k})\begin{pmatrix}w_1\\ w_2\\ w_3\end{pmatrix}, \quad \alpha w_{10} = \lambda\mathbf{k}\cdot\begin{pmatrix}w_1\\ w_2\\ w_3\end{pmatrix}, \tag{E.2}$$

and:

$$\alpha^2\begin{pmatrix}w_1\\ w_2\\ w_3\end{pmatrix} = \left[\frac{\mu}{\rho}|\mathbf{k}|^2 + \frac{\lambda+\mu}{\rho}\mathbf{k}\otimes\mathbf{k}\right]\begin{pmatrix}w_1\\ w_2\\ w_3\end{pmatrix}.$$

Taking (w_1, w_2, w_3) in the above system orthogonal to $\mathbf{k}$, which means:

$$\begin{pmatrix}w_1\\ w_2\\ w_3\end{pmatrix} \in \mathrm{Span}\left\{\mathbf{w}_1 = \begin{pmatrix}k_2\\ -k_1\\ 0\end{pmatrix}, \mathbf{w}_2 = \begin{pmatrix}0\\ k_3\\ -k_2\end{pmatrix}\right\} = \mathrm{Span}\left\{\begin{pmatrix}k_2\\ -k_1\\ 0\end{pmatrix}, \begin{pmatrix}k_3\\ 0\\ -k_1\end{pmatrix}\right\} = \mathrm{E},$$

we obtain that:

$$\alpha^2 = \frac{\mu}{\rho}|\mathbf{k}|^2,$$

and the corresponding eigenvalues of $\mathbf{L}$ are thus $\omega_{\mathrm{S}}^{\pm} = \pm c_{\mathrm{S}}|\mathbf{k}|$, each having multiplicity 2. To each couple of vector $\mathbf{w} \in \mathrm{E}$ and eigenvalue $\alpha = \omega^{\pm}$ corresponds an eigenvector $\mathbf{v} = (\mathbf{w}, \mathbf{v}'_\alpha)$ for the eigenvalue α, given by (E.1) and (E.2). We give the expressions of the eigenvectors for the S modes here:

$$\begin{aligned}
\mathbf{b}_{\mathrm{S1}}^{\pm} &= \frac{1}{|\mathbf{k}|}\left(\mathbf{w}_1, \pm 2\sqrt{\frac{\mu}{\rho}}\mathbf{K}(\mathbf{k})\mathbf{w}_1, \pm\sqrt{\frac{\rho}{\mu}}\mathbf{M}(\mathbf{k})\mathbf{w}_1, 0\right)^{\mathsf{T}},\\
\mathbf{b}_{\mathrm{S2}}^{\pm} &= \frac{1}{|\mathbf{k}|}\left(\mathbf{w}_2, \pm 2\sqrt{\frac{\mu}{\rho}}\mathbf{K}(\mathbf{k})\mathbf{w}_2, \pm\sqrt{\frac{\rho}{\mu}}\mathbf{M}(\mathbf{k})\mathbf{w}_2, 0\right)^{\mathsf{T}}.
\end{aligned}$$

Now if (w_1, w_2, w_3) is equal to $\mathbf{k}$ one obtains:

$$\alpha^2 = \frac{2\mu + \lambda}{\rho} |\mathbf{k}|^2 ,$$

and the corresponding eigenvalues of $\mathbf{L}$ are thus $\omega_{\mathrm{P}}^{\pm} = \pm c_{\mathrm{P}} |\mathbf{k}|$, each having multiplicity 1. The corresponding eigenvectors are given by:

$$\mathbf{b}_{\mathrm{P}}^{\pm} = \frac{1}{|\mathbf{k}|} \left(\mathbf{k}, \pm \frac{2\mu\sqrt{\rho}}{\sqrt{\lambda + 2\mu}} \mathbf{K}(\mathbf{k})\mathbf{k}, \pm \frac{\mu\sqrt{\rho}}{\sqrt{\lambda + 2\mu}} \mathbf{M}(\mathbf{k})\mathbf{k}, \pm \frac{\lambda\sqrt{\rho}}{\sqrt{\lambda + 2\mu}} |\mathbf{k}| \right)^{\mathsf{T}} .$$

F

CKS scheme with a piecewise linear approximation of the specific intensity

We consider here the case when energy is computed using piecewise linear functions to approximate the specific intensity following the k_1 variable instead of step functions as described in the section 4.2. The definition of the discretized energy on the grid is given by Eq. (4.2), and an equivalent definition is given for the restriction of this quantity to the cell $\mathcal{C}_\alpha$:

$$\mathcal{E}_\alpha^n = \frac{1}{2}\sum_\beta \left(\mathrm{a}_{\alpha\beta}^n + \mathrm{a}_{\alpha,\beta+\boldsymbol{\delta}^1}^n\right)\Delta\mathbf{k}\Delta\mathbf{x}\,,$$

where for all multi-indices α, $(\beta)_1$ and $n \in \mathbb{N}^*$, we extend the definition of $\{\mathrm{a}_{\alpha\beta}^n\}_{\alpha,\beta}$ to the index $\beta_1 = N_1 + 1$ by setting $\mathrm{a}^n_{\alpha,(\beta)_1+(N_1+1)\boldsymbol{\delta}^1}$ to zero. We also make the assumption that for all indices $\alpha_j \in \{1,\dots N_j\}$, $j \geq 2$, $\beta_j \in \{1,\dots N_j\}$, $j \geq 2$, and $\alpha_1 \in \{1,\dots \alpha_1^1\}$ we have:

$$\mathrm{a}^0_{\alpha,\,(\beta)_1+\boldsymbol{\delta}^1} = \mathrm{a}^0_{\alpha,\,(\beta)_1+(N_1+1)\boldsymbol{\delta}^1} = 0,$$

and consider that during the whole simulation, the propagation of the initial condition does not reach the boundaries of $\mathcal{O}_h$. Then we proceed as in the section 4.3.3 and define the change of grid and the transmitted specific intensity with the definition of energy given above. Let us reconsider the problem of computation of energy on the fine mesh with linear functions. The definition of energy on the coarse mesh of points for instance, still requires the set of values $\{\mathrm{a}_{\alpha\beta}^n\}_{\beta\in\mathcal{K}^+}$ and of wave vector steps Δk_1^- and Δk_j. The set of "incident" discretized wave vectors $\{\mathbf{k}_\beta^+\}_\beta$, and their image obtained by backward transmission using the function f, define two types of wave vector distributions for which the energy is computed. The discrete change of variable between these two distributions (we refer to its definition on the third paragraph of the section 4.3.3) induced by the very function f, is denoted by c_β and is defined as in the computation of the energy by piecewise constant functions by Eq. (4.24) and Eq. (4.25). The definition of $\{\mathrm{b}^n_{\alpha^-\beta}\}$ relies on the same equality that expresses the conservation of energy flux density at $\mathcal{I}$. It reads:

$$\begin{aligned}\frac{1}{2}\sum_{(\alpha)_1}\sum_{\beta\in\mathcal{K}^+}(c^+\hat{\mathbf{k}}_\beta^+\cdot\mathbf{n})\Delta k_1^+\left(\mathrm{b}^n_{\alpha^-\beta}+\mathrm{b}^n_{\alpha^-,\beta+\boldsymbol{\delta}^1}\right)&\\ = \frac{1}{2}\sum_{(\alpha)_1}\sum_{\beta\in\mathcal{K}^+}(c^-\hat{\mathbf{k}}_\beta^{\mathrm{T}}\cdot\mathbf{n})c_\beta\Delta k_1^+\mathcal{T}^-(\mathbf{k}_\beta^{\mathrm{T}})\left(\tilde{\mathrm{a}}^n(\mathbf{X}_{\alpha^-},\mathbf{k}_\beta^{\mathrm{T}})+\tilde{\mathrm{a}}^n(\mathbf{X}_{\alpha^-},\mathbf{k}^{\mathrm{T}}_{\beta+\boldsymbol{\delta}^1})\right)&,\end{aligned}$$

which leads now to the following definition of the transmitted specific intensity $\mathrm{b}^n_{\alpha^-\beta}$:

$$\mathrm{b}^n_{\alpha^-\beta} = \mu_\beta^-\tilde{\mathrm{a}}^n(\mathbf{X}_{\alpha^-},\mathbf{k}_\beta^{\mathrm{T}})\,, \tag{F.1}$$

where μ_β^- is taken equal to:

$$\mu_\beta^- = \begin{cases} \dfrac{1}{\nu}\dfrac{(\hat{\mathbf{k}}_\beta^{\mathrm{T}}\cdot\mathbf{n})c_\beta\mathcal{T}^-(\mathbf{k}_\beta^{\mathrm{T}}) + (\hat{\mathbf{k}}_{\beta-\boldsymbol{\delta}^1}^{\mathrm{T}}\cdot\mathbf{n})c_{\beta-\boldsymbol{\delta}^1}\mathcal{T}^-(\mathbf{k}_{\beta-\boldsymbol{\delta}^1}^{\mathrm{T}})}{\hat{\mathbf{k}}_\beta^+\cdot\mathbf{n} + \hat{\mathbf{k}}_{\beta-\boldsymbol{\delta}^1}^+\cdot\mathbf{n}} & \text{if} \quad 2\leq\beta_1\leq N_1\,, \\ \dfrac{1}{\nu}\dfrac{(\hat{\mathbf{k}}_\beta^{\mathrm{R}}\cdot\mathbf{n})c_\beta\mathcal{T}^-(\mathbf{k}_\beta^{\mathrm{T}})}{\hat{\mathbf{k}}_\beta^+\cdot\mathbf{n}} & \text{if} \quad \beta_1 = 1\,, \end{cases}$$

where the multi-indices α^- and α^+ are defined by Eq. (4.6). Note that by replacing the above expression of the "transmitted" specific intensities in Eq. (4.8), we can rewrite the sum S_2^n in the form:

$$\begin{aligned} S_2^n &= \frac{\Delta t}{\Delta x_1}\sum_{(\alpha)_1}\sum_{\beta\in\mathcal{K}^+}\left(c^-\Delta k_1^-\hat{k}_{\beta_1}^-(1-\mathcal{R}^-(\mathbf{k}_\beta^-))\mathrm{a}_{\alpha^-\beta}^n - c^+\Delta k_1^+\hat{k}_{\beta_1}^+\tilde{\mathrm{a}}^n(\mathbf{X}_{\alpha^-},\mathbf{k}_\beta^{\mathrm{T}})\right), \\ &= \frac{\Delta t}{\Delta x_1}\sum_{(\alpha)_1}\sum_{\beta'\in\mathcal{K}_c^+}\left(c^-\Delta k_1^-\gamma'_{\beta'} - c^+\Delta k_1^+\left(\sum_{k_{\beta'_1}^-\leq k_\beta^{\mathrm{T}}<k_{\beta'_1+1}^-}\gamma_\beta^0 + \sum_{k_{\beta'_1-1}^-\leq k_\beta^{\mathrm{T}}<k_{\beta'_1}^-}\gamma_\beta^1\right)\right)\mathrm{a}_{\alpha^-\beta'}^n\,, \end{aligned}$$

where γ'_β and γ_β^i, $i=0,1$, are defined here by:

$$\gamma'_{\beta'} = \hat{k}_{\beta'_1}^-\mathcal{T}^-(\mathbf{k}_{\beta'}^-)\,,\ \ \gamma_\beta^0 = \hat{k}_{\beta_1}^+\frac{k_{\beta'_1}^- + \Delta k_1^- - k_\beta^{\mathrm{T}}}{\Delta k_1^-}\mu_\beta^-\,,\ \ \gamma_\beta^1 = \hat{k}_{\beta_1}^+\frac{k_\beta^{\mathrm{T}} - k_{\beta'_1}^-}{\Delta k_1^-}\mu_\beta^-\,,$$

and where the parameter μ_β^- is defined above together with Eq. (F.1).

The same considerations done in the case of transmission from the fast to the slow medium, lead to the following expression of the "transmitted" specific intensity:

$$\mathrm{b}_{\alpha^+\beta}^n = \mu_\beta^+\tilde{\mathrm{a}}^n(\mathbf{X}_{\alpha^+},\mathbf{k}_\beta^{\mathrm{T}})\,, \tag{F.2}$$

where μ_β^+ is given by:

$$\mu_\beta^+ = \begin{cases} \nu\dfrac{(\hat{\mathbf{k}}_\beta^{\mathrm{T}}\cdot\mathbf{n})c_\beta\mathcal{T}^+(\mathbf{k}_\beta^{\mathrm{T}}) + (\hat{\mathbf{k}}_{\beta-\boldsymbol{\delta}^1}^{\mathrm{T}}\cdot\mathbf{n})c_{\beta-\boldsymbol{\delta}^1}\mathcal{T}^+(\mathbf{k}_{\beta-\boldsymbol{\delta}^1}^{\mathrm{T}})}{\hat{\mathbf{k}}_\beta^-\cdot\mathbf{n} + \hat{\mathbf{k}}_{\beta-\boldsymbol{\delta}^1}^-\cdot\mathbf{n}} & \text{if} \quad 2\leq\beta_1\leq N_1\,, \\ \nu\dfrac{(\hat{\mathbf{k}}_\beta^{\mathrm{T}}\cdot\mathbf{n})c_\beta\mathcal{T}^+(\mathbf{k}_\beta^{\mathrm{T}})}{\hat{\mathbf{k}}_\beta^-\cdot\mathbf{n}} & \text{if} \quad \beta_1 = 1\,. \end{cases}$$

The above definitions of the numerical scheme are supplemented by the interpolation of the transmitted specific intensities, given by Eq. (4.18). They completely define the numerical scheme together with Eq. (F.1) and Eq. (F.2). We may observe here that the choice of the grid points and of the way the energy is computed enables to modify the variation of the latter between two time steps t_n and t_{n+1}. Thus it may be interesting to compare the loss of energy obtained during a simulation for the scheme presented in this appendix, with the loss of energy obtained for the classical scheme, in order to underline the interest of the method and its efficiency.

G

Interpolation coefficients for reflection and transmission with a curved interface

We show here how to derive interpolation coefficients for transmission from a slow to a fast medium, in case of a curved interface. We first give an expression of the sum S_2^n, in terms of the reflected and transmitted specific intensity, at cells that share one common edge and two common edges with $\mathcal{I}$. We then discuss, if the different incident, reflected, and transmitted sums, may be cancelled. We finally derive interpolation coefficients, that conserve energy through the curved interface $\mathcal{I}$.

The sum S_2^n defined by Eq. (4.40) can be simplified for both types of cells $\mathcal{C}_\alpha$ that share one or two different edges with $\mathcal{I}$. For a given index α' such that $\mathcal{C}_{\alpha'}$ shares two edges with $\mathcal{I}$:

$$\alpha' = (\alpha)_i + \alpha_i^1 \boldsymbol{\delta}^i = (\alpha)_j + \alpha_j^1 \boldsymbol{\delta}^j \,,$$

we choose for example the same values of the reflected and transmitted specific intensities at the respective edges of the cell (that is, $\mathrm{b}^n_{\alpha'\beta} = \mu_\beta^- \tilde{\mathrm{a}}^n(\mathbf{X}_{\alpha'}, \mathbf{k}^{\mathrm{T}}_\beta)$ is the same along the i-th coordinate and along the j-th coordinate, and $\tilde{\mathrm{a}}^n_i(\mathbf{X}_{\alpha'}, \mathbf{k}^{\mathrm{R}}_\beta) = \tilde{\mathrm{a}}^n_j(\mathbf{X}_{\alpha'}, \mathbf{k}^{\mathrm{R}}_\beta)$). The sum S_2^n then reads:

$$
\begin{aligned}
S_2^n = &- \sum_{i=1,\,2} \frac{\Delta t}{\Delta x_i} \Bigg[\sum_{\substack{\alpha' = (\alpha)_i + \alpha_i^1 \boldsymbol{\delta}^i, \\ \neq (\alpha)_j + \alpha_j^{1,\,2} \boldsymbol{\delta}^j,\ j \neq i}} \sum_{\beta \in \mathcal{K}_c^-(\mathbf{n})} (c^- \hat{\mathbf{K}}_\beta^- \cdot \mathbf{N}) \Delta \mathbf{k}^- \mathrm{a}_{\alpha'\beta}^n - \sum_{\beta \in \mathcal{K}^-(\mathbf{n})} (c^+ \hat{\mathbf{K}}_\beta^+ \cdot \mathbf{N}) \Delta \mathbf{k}^+ \mu_\beta^- \tilde{\mathrm{a}}^n \left(\mathbf{X}_{\alpha'}, \mathbf{k}_\beta^{\mathrm{T}} \right) \\
&\qquad + \sum_{\beta \in \mathcal{K}_c^+(\mathbf{n})} (c^- \hat{\mathbf{K}}_\beta^- \cdot \mathbf{N}) \mathcal{R}^-(\mathbf{K}_\beta^-) \Delta \mathbf{k}^- \tilde{\mathrm{a}}^n \left(\mathbf{X}_{\alpha'}, \mathbf{k}_\beta^{\mathrm{R}} \right) \Bigg] \\
&- \frac{\Delta t}{\Delta x_2} \Bigg[\sum_{\substack{\alpha'' = (\alpha)_2 + \alpha_2^2 \boldsymbol{\delta}^2, \\ \neq (\alpha)_1 + \alpha_1^1 \boldsymbol{\delta}^1,}} \sum_{\beta \in \mathcal{K}_c^-(\mathbf{n})} (c^- \hat{\mathbf{K}}_\beta^- \cdot \mathbf{N}) \Delta \mathbf{k}^- \mathrm{a}_{\alpha''\beta}^n - \sum_{\beta \in \mathcal{K}^-(\mathbf{n})} (c^+ \hat{\mathbf{K}}_\beta^+ \cdot \mathbf{N}) \Delta \mathbf{k}^+ \mu_\beta^- \tilde{\mathrm{a}}^n \left(\mathbf{X}_{\alpha''}, \mathbf{k}_\beta^{\mathrm{T}} \right) \\
&\qquad + \sum_{\beta \in \mathcal{K}_c^+(\mathbf{n})} (c^- \hat{\mathbf{K}}_\beta^- \cdot \mathbf{N}) \Delta \mathbf{k}^- \mathcal{R}^-(\mathbf{K}_\beta^-) \tilde{\mathrm{a}}^n \left(\mathbf{X}_{\alpha''}, \mathbf{k}_\beta^{\mathrm{R}} \right) \Bigg] \\
&- \frac{\Delta t}{\Delta x_1} \Bigg[\sum_{\substack{\alpha' = (\alpha)_1 + \alpha_1^1 \boldsymbol{\delta}^1, \\ = (\alpha)_2 + \alpha_2^{1,\,2} \boldsymbol{\delta}^2}} \sum_{\beta \in \mathcal{K}_c^-(\mathbf{n})} (c^- \hat{\mathbf{K}}_\beta^- \cdot \mathbf{N}) \Delta \mathbf{k}^- \mathrm{a}_{\alpha'\beta}^n - \sum_{\beta \in \mathcal{K}^-(\mathbf{n})} (c^+ \hat{\mathbf{K}}_\beta^+ \cdot \mathbf{N}) \Delta \mathbf{k}^+ \mu_\beta^- \tilde{\mathrm{a}}^n \left(\mathbf{X}_{\alpha'}, \mathbf{k}_\beta^{\mathrm{T}} \right) \\
&\qquad + \sum_{\beta \in \mathcal{K}_c^+(\mathbf{n})} (c^- \hat{\mathbf{K}}_\beta^- \cdot \mathbf{N}) \Delta \mathbf{k}^- \mathcal{R}^-(\mathbf{K}_\beta^-) \tilde{\mathrm{a}}^n \left(\mathbf{X}_{\alpha'}, \mathbf{k}_\beta^{\mathrm{R}} \right) \Bigg] + \dots
\end{aligned}
\tag{G.1}
$$

where the discretized normal vector $\mathbf{N}$ is defined for the spatial cells $\mathcal{C}_{\alpha'}$ and $\mathcal{C}_{\alpha''}$ that share one common edge with $\mathcal{I}$ by:

$$
\mathbf{N} = \begin{cases} -\boldsymbol{\delta}^1 & \text{if} \quad \alpha' = (\alpha)_1 + \alpha_1^1 \boldsymbol{\delta}^1 \,, \\ -\boldsymbol{\delta}^2 & \text{if} \quad \alpha' = (\alpha)_2 + \alpha_2^1 \boldsymbol{\delta}^2 \,, \\ \boldsymbol{\delta}^2 & \text{if} \quad \alpha'' = (\alpha)_2 + \alpha_2^2 \boldsymbol{\delta}^2 \,. \end{cases}
$$

For the spatial cells $\mathcal{C}_{\alpha'}$ that share two common edges with $\mathcal{I}$, it is defined as:

$$
\mathbf{N} = \begin{cases} -\boldsymbol{\delta}^1 - \dfrac{\Delta x_1}{\Delta x_2} \boldsymbol{\delta}^2 & \text{if} \quad \alpha' = (\alpha)_1 + \alpha_1^1 \boldsymbol{\delta}^1 = (\alpha)_2 + \alpha_2^1 \boldsymbol{\delta}^2 \,, \\ -\boldsymbol{\delta}^1 + \dfrac{\Delta x_1}{\Delta x_2} \boldsymbol{\delta}^2 & \text{if} \quad \alpha' = (\alpha)_1 + \alpha_1^2 \boldsymbol{\delta}^1 = (\alpha)_2 + \alpha_2^2 \boldsymbol{\delta}^2 \,, \end{cases}
$$

such that each term in S_2^n may be rewritten in the same form. The terms in the sum above labelled by the index α', correspond to indices in J_j^1 (see the notations introduced in the sections 3.1.2 and 3.2.3), while the terms labelled by the index α'' correspond to indices in J_2^2. The above computation shows that the sum S_2^n may be written in the form (4.41). It is thus useful now to seek interpolations of $\tilde{\mathrm{a}}^n(\mathbf{X}_{\alpha'/\alpha''}, \mathbf{k}_\beta^{\mathrm{R}})$ and $\tilde{\mathrm{a}}^n(\mathbf{X}_{\alpha'/\alpha''}, \mathbf{k}_\beta^{\mathrm{T}})$, such that the above sums cancel.

Let us show that it is possible to cancel the sums by considering their different terms. Let $\mathbf{N}$ be a given vector and $\mathbf{K}_{\beta'}^-$ denote an incident wave vector ($\mathbf{K}_{\beta'}^- \cdot \mathbf{n} < 0$), we suppose that $\mathbf{K}_{\beta'}^-$ is a subcritical vector. We consider the sets of wave vectors, $\mathrm{IC}_{\beta'}^{\mathrm{R}}$ and $\mathrm{IC}_{\beta'}^{\mathrm{T}}$ defined from the set $\mathrm{IC}_{\beta'}$ by reflection and transmission:

$$
\mathrm{IC}_{\beta'}^{\mathrm{R}} = \left\{ \mathbf{k} \,|\, \mathbf{k}^{\mathrm{R}} \in \mathrm{IC}_{\beta'} \right\} \,, \quad \mathrm{IC}_{\beta'}^{\mathrm{T}} = \left\{ \mathbf{k} \,|\, \mathbf{k}^{\mathrm{T}} \in \mathrm{IC}_{\beta'} \right\} \,.
$$

where $\mathbf{k}^{\mathrm{R}}$ is defined by the equations (3.27) and (3.19), and $\mathbf{k}^{\mathrm{T}}$ is defined as follows:

$$
\mathbf{k}^{\mathrm{T}} = -f(k_{\mathbf{n}}, \mathbf{k}')\mathbf{n} + \mathbf{k}' \,.
$$

We compare the sign of $\hat{\mathbf{K}}_{\beta'}^- \cdot \mathbf{N}$ with the sign of $\hat{\mathbf{K}}_\beta^- \cdot \mathbf{N}$, for $\mathbf{K}_\beta^-$ in $\mathrm{IC}_{\beta'}^{\mathrm{R}} \cap \mathcal{M}_{\mathbf{k}}^-$, and $\mathbf{K}_\beta^+$ in $\mathrm{IC}_{\beta'}^{\mathrm{T}} \cap \mathcal{M}_{\mathbf{k}}^+$. There are different possible cases.

We suppose, that $\mathbf{n} \cdot \mathbf{N} > 0$, and for example, that $\mathbf{t} \cdot \mathbf{N} < 0$. Let us suppose, for instance, that $\hat{\mathbf{K}}_{\beta'}^- \cdot \mathbf{N} < 0$. If for all $\mathbf{K}_\beta^-$ in $\mathrm{IC}_{\beta'}^{\mathrm{R}}$, $\mathbf{K}_\beta^- \cdot \mathbf{N} > 0$, we observe, that the term corresponding to reflection in

S_2^n, may cancel the incident term. In that case, it must be possible to derive interpolation coefficients, chosen, such that S_2^n vanishes. The latter are derived further.

Suppose, now, that for all $\mathbf{k}$ in $\mathrm{IC}^{\mathrm{R}}_{\beta'}$, $\mathbf{k}\cdot\mathbf{N}<0$. We suppose, that for all $\mathbf{k}$ in $\mathrm{IC}^{\mathrm{R}}_{\beta'}$, $\mathbf{k}\cdot\mathbf{n}>0$. It can be deduced from this, since $\mathbf{n}\cdot\mathbf{N}>0$, that for all $\mathbf{k}$ in $\mathrm{IC}_{\beta'}$, $\mathbf{k}\cdot\mathbf{N}<0$. Let us show, that for all $\mathbf{K}^+_\beta$ in $\mathrm{IC}^{\mathrm{T}}_{\beta'}\bigcap\mathcal{M}^+_{\mathbf{k}}$, $\mathbf{K}^+_\beta\cdot\mathbf{N}<0$. If $\mathbf{K}^+_\beta\in\mathrm{IC}^{\mathrm{T}}_{\beta'}\bigcap\mathcal{M}^+_{\mathbf{k}}$, the vector $\mathbf{k}^{\mathrm{T}}_{\beta,\,\mathrm{R}}$ obtained by reflection from the transmitted vector $\mathbf{k}^{\mathrm{T}}_\beta$ belongs to the set $\mathrm{IC}^{\mathrm{R}}_{\beta'}$, since the reflection on the interface $\mathcal{I}$ is involutive. We deduce, that $\mathbf{k}^{\mathrm{T}}_{\beta,\,\mathrm{R}}\cdot\mathbf{N}<0$, such that $\mathbf{K}^+_\beta$, which writes as a linear combination of $\mathbf{k}^{\mathrm{T}}_\beta$ and $\mathbf{k}^{\mathrm{T}}_{\beta,\,\mathrm{R}}$ with positive coefficients, also satisfies $\mathbf{K}^+_\beta\cdot\mathbf{N}<0$.

We now suppose, that $\mathrm{IC}^{\mathrm{R}}_{\beta'}$ has an intersection with both subsets $\{\mathbf{k},\,\mathbf{k}\cdot\mathbf{N}>0\}$ and $\{\mathbf{k},\,\mathbf{k}\cdot\mathbf{N}<0\}$, and we suppose, that $\mathrm{IC}^{\mathrm{R}}_{\beta'}\bigcap\{\mathrm{IC}_{\beta'}\}$ is empty. If $\mathrm{IC}^{\mathrm{R}}_{\beta'}$ is included in one of the two subsets $\{\mathbf{k},\,\mathbf{k}\cdot\mathbf{t}>0\}$ or $\{\mathbf{k},\,\mathbf{k}\cdot\mathbf{t}<0\}$, it is possible to deduce from the latter hypothesis, that for all $\mathbf{k}\in\mathrm{IC}_{\beta'}$, $\mathbf{k}\cdot\mathbf{N}$ has the same sign, which is necessarely negative. Then, from the fact, that $\mathbf{t}\cdot\mathbf{N}<0$, we obtain, that for all $\mathbf{K}^+_\beta$ in $\mathrm{IC}^{\mathrm{T}}_{\beta'}\bigcap\mathcal{M}^+_{\mathbf{k}}$, (which write as a linear combination of $\mathbf{k}^{\mathrm{T}}_\beta$ and $\mathbf{t}$ with positive coefficients), $\mathbf{K}^+_\beta\cdot\mathbf{N}<0$. In case, when $\mathrm{IC}^{\mathrm{R}}_{\beta'}$ has an intersection with both subsets $\{\mathbf{k},\,\mathbf{k}\cdot\mathbf{t}>0\}$ and $\{\mathbf{k},\,\mathbf{k}\cdot\mathbf{t}<0\}$, it is more difficult to conclude, and we will exclude this case. Finally, we consider the case when $\mathrm{IC}^{\mathrm{R}}_{\beta'}\bigcap\{\mathrm{IC}_{\beta'}\}$ is not empty. It is possible to show, under critical incidence, and under a certain assumption on the discretization step, and the incident wave vectors length, that this case does not occur. Let, k_0 denote the lower boundary for the incidence wave vectors lengths, and θ_c denote the critical angle, and $\theta=\pi/2-\theta_c$, we make the assumption that: $\max(\Delta k^j_-)/k_0\leq 1/\sqrt{2}\tan(\theta)$. One may verify, that under this assumption, the intersection of the two sets considered above is empty.

In case, when $\hat{\mathbf{K}}^-_{\beta'}\cdot\mathbf{N}>0$, one observes, that either for all $\mathbf{k}$ in $\mathrm{IC}_{\beta'}$, $\mathbf{k}\cdot\mathbf{N}>0$, such that, in the same manner, it can be proved, that for all $\mathbf{k}\in\mathrm{IC}^{\mathrm{T}}_{\beta'}$, $\mathbf{k}\cdot\mathbf{N}>0$. We make the assumption, that the case, when $\mathrm{IC}_{\beta'}$ contains, both type of vectors $\mathbf{k}$, such that $\mathbf{k}\cdot\mathbf{N}>0$ and $\mathbf{k}\cdot\mathbf{N}<0$, does not occur.

We now summarize the different cases discussed above. Let us show that it is possible to derive interpolation coefficients so that the different sums in S_2^n cancel. We observe that in all the different cases considered above, except in particular cases, we have either for all $\mathbf{k}$ in $\mathrm{IC}^{\mathrm{T}}_{\beta'}$, $\mathbf{k}\cdot\mathbf{N}$ has the same sign as $\hat{\mathbf{K}}^-_{\beta'}\cdot\mathbf{N}$, or for all $\mathbf{k}$ in $\mathrm{IC}^{\mathrm{R}}_{\beta'}$, $\mathbf{k}\cdot\mathbf{N}$ and $\hat{\mathbf{K}}^-_{\beta'}\cdot\mathbf{N}$ have opposite signs. We thus define the interpolation coefficients as follows. Let A_u and B_u be defined by:

$$A_u=\begin{cases}1 & \text{if } \mathrm{Card}(\mathcal{C}_{\beta'-\boldsymbol{\delta}^u}\bigcap\left\{\mathbf{k}^{\mathrm{R}}_\beta,\,\mathbf{K}^-_\beta\in\mathrm{IC}^{\mathrm{R}}_{\beta'}\right\}>0\\ 0 & \text{if } \mathrm{Card}(\mathcal{C}_{\beta'-\boldsymbol{\delta}^u}\bigcap\left\{\mathbf{k}^{\mathrm{R}}_\beta,\,\mathbf{K}^-_\beta\in\mathrm{IC}^{\mathrm{R}}_{\beta'}\right\}=0\end{cases}$$

with $A=\sum_u A_u$ and:

$$B_u=\begin{cases}1 & \text{if } \mathrm{Card}(\mathcal{C}_{\beta'-\boldsymbol{\delta}^u}\bigcap\left\{\mathbf{k}^{\mathrm{T}}_\beta,\,\mathbf{K}^+_\beta\in\mathrm{IC}^{\mathrm{T}}_{\beta'}\right\}>0\\ 0 & \text{if } \mathrm{Card}(\mathcal{C}_{\beta'-\boldsymbol{\delta}^u}\bigcap\left\{\mathbf{k}^{\mathrm{T}}_\beta,\,\mathbf{K}^+_\beta\in\mathrm{IC}^{\mathrm{T}}_{\beta'}\right\}=0\end{cases}$$

with $B=\sum_u B_u$. We make the assumption that with a four-point interpolation, $A+B>0$ for all index β'. Let $C_{a,u}$ and $C_{b,u}$ be defined by:

$$C_{a,u}=\frac{\hat{\mathbf{K}}^-_{\beta'}\cdot\mathbf{N}}{\sum_{\mathbf{k}^{\mathrm{R}}_\beta\in\mathcal{C}_{\beta'-\boldsymbol{\delta}^u}}(\hat{\mathbf{K}}^-_\beta\cdot\mathbf{N})\mathcal{R}^-(\mathbf{K}^-_\beta)}\,,\quad C_{b,u}=\frac{\hat{\mathbf{K}}^-_{\beta'}\cdot\mathbf{N}}{\sum_{\mathbf{k}^{\mathrm{T}}_\beta\in\mathcal{C}_{\beta'-\boldsymbol{\delta}^u}}(\hat{\mathbf{K}}^+_\beta\cdot\mathbf{N})\mathcal{T}^-(\mathbf{k}^{\mathrm{T}}_\beta)}\,,$$

if $A_u>0$ and $B_u>0$, and by 0 in the other cases. Let a_u and b_u be defined by:

$$a_u=\begin{cases}\mathcal{R}^-(\mathbf{K}^-_{\beta'}) & \text{if}\quad C_{a,u}<0\,,\quad C_{b,u}>0\,,\\ (1+\mathcal{T}^-(\mathbf{K}^-_{\beta'})) & \text{if}\quad C_{a,u}<0\,,\quad C_{b,u}<0\,,\\ -\mathcal{R}^-(\mathbf{K}^-_{\beta'}) & \text{if}\quad C_{a,u}>0\,,\end{cases}$$

and:

$$b_u=\begin{cases}\mathcal{T}^-(\mathbf{K}^-_{\beta'}) & \text{if}\quad C_{a,u}<0\,,\quad C_{b,u}>0\,,\\ (1+\mathcal{R}^-(\mathbf{K}^-_{\beta'})) & \text{if}\quad C_{a,u}>0\,,\quad C_{b,u}>0\,,\\ -\mathcal{T}^-(\mathbf{K}^-_{\beta'}) & \text{if}\quad C_{b,u}<0\,.\end{cases}$$

Then the interpolation coefficients $C^-_{\beta'+\boldsymbol{\delta}^u}$ and $\Gamma^-_{\beta'+\boldsymbol{\delta}^u}$ are defined by:

$$C^-_{\beta'+\boldsymbol{\delta}^u} = -\frac{1}{A} a_u C_{a,u} \quad \Gamma^-_{\beta'+\boldsymbol{\delta}^u} = \nu \frac{1}{B} b_u C_{b,u} \,.$$

One may verify that the above coefficients cancel the terms in the sum S_2^n that correspond to reflection and transmission.

H

Theoretical solution of the Liouville equation in case of a straight interface

We consider here a WKB initial condition of the form of Eq. (2.32) (or Eq. (2.45)), and recall that the corresponding specific intensity reads in the general case 2.83 (or in our case (2.87)). In an homogeneous subdomain of $\mathcal{O}_h$ of $\mathbb{R}^d$, the Liouville equation can be solved as a transport equation on the rays, or with the help of the computation of the solution $\mathrm{a}^+(t,\mathbf{x},\mathbf{k})$ in terms of the amplitude and phase of the WKB initial condition. The solution can thus be determined in the homogeneous subdomain of $\mathcal{O}_h$ where the initial condition is defined. One obtains, for given vectors $\mathbf{X}_\alpha$ with $\alpha_1 < 0$, $\mathbf{K}_\beta$ with $\beta_1 > 0$ and a time t before the interface is reached, that:

$$\mathrm{a}^+(t,\mathbf{X}_\alpha,\mathbf{K}_\beta) = \mathrm{a}^+(0,\mathbf{X}_\alpha - c^- t\hat{\mathbf{K}}_\beta,\mathbf{K}_\beta)\,,$$

and $\hat{\mathbf{K}}_\beta = \frac{\mathbf{K}_\beta}{|\mathbf{K}_\beta|}$. As the initial conditions used in our examples are defined on a few number of discretized wave vectors of the mesh, we consider propagation exclusively along them, and denote:

$$E_0 = \left\{ \mathbf{K}_0 + \sum_{j=1}^{d} u_j \boldsymbol{\delta}^j,\ u_j = 0 \text{ or } \Delta k_j \right\}\,,$$

the set of these discretized wave vectors, where $\mathbf{K}_0$ is a given vector of $\mathcal{M}_\mathbf{k}$. We may then define the reflected specific intensity for $\mathbf{X}_\alpha$ with $\alpha_1 < 0$, $\mathbf{K}_\beta$ with $\beta_1 < 0$, and a time $t > t_1$ by:

$$\mathrm{a}^+_\mathrm{R}(t,\mathbf{X}_\alpha,\mathbf{K}_\beta) = \mathcal{R}^-(\mathbf{k}^\mathrm{R}_\beta)\mathrm{a}^+(0,\mathbf{x}_\mathcal{I} - c^- t_1 \hat{\mathbf{k}}^\mathrm{R}_\beta, \mathbf{k}^\mathrm{R}_\beta)\,,$$

where $\mathbf{k}^\mathrm{R}_\beta = (-K_{\beta_1}, \mathbf{K}'_\beta)$, $\mathbf{x}_\mathcal{I} = \mathbf{X}_\alpha - c^-(t-t_1)\hat{\mathbf{K}}_\beta$ is the point where the ray in $\mathbf{X}_\alpha$ and direction $\mathbf{K}_\beta$ at time t has reached $\mathcal{I}$ at time t_1 (we recall that in our examples the origin of the computational domain belongs to $\mathcal{I}$), and t_1 is given by:

$$t_1 = t - \frac{X_{\alpha_1}}{c^- \hat{K}_{\beta_1}}\,.$$

Likewise, the transmitted specific intensity is defined for $\mathbf{X}_\alpha$ with $\alpha_1 > 0$, $\mathbf{K}_\beta$ with $\beta_1 > 0$, and a time $t > t_1$, with the help of the numerical scheme used for the computation. If the discretized transmitted specific intensity $\tilde{\mathrm{a}}^n(\mathbf{X}_\alpha, \mathbf{k}^\mathrm{T}_\beta)$ is defined by an interpolation of the form $\tilde{\mathrm{a}}^n(\mathbf{X}_\alpha, \mathbf{k}^\mathrm{T}_\beta) = \sum_{\beta_i=\beta_m}^{\beta_M} \gamma_i \mathrm{a}^n_{\alpha\beta_i}$ (see Eq. (4.14) or Eq. (4.15)), and the set of vectors $E = E_0 \cap \{\mathbf{K}_{\beta_i}\}_{\beta_m \le \beta_i \le \beta_M}$ is not empty, then the transmitted specific intensity reads:

$$\mathrm{a}^+_\mathrm{T}(t,\mathbf{X}_\alpha,\mathbf{K}_\beta) = \sum_{\mathbf{k}_i \in E} \gamma_i \mathcal{T}^-(\mathbf{k}_i)\mathrm{a}^+(0,\mathbf{x}_\mathcal{I} - c^- t_1 \hat{\mathbf{k}}_i, \mathbf{k}_i)\,,$$

where $\mathbf{x}_\mathcal{I} = \mathbf{X}_\alpha - c^+(t-t_1)\hat{\mathbf{K}}_\beta$ and $\hat{\mathbf{k}}_i = \frac{\mathbf{k}_i}{|\mathbf{k}_i|}$.

Bibliography

[1] J. D. Achenbach. Wave Propagation in Elastic Solids, North-Holland Publishing Company, Amsterdam, 1973.

[2] S. Alinhac. Hyperbolic Partial Differential Equations, Springer, Dordrecht, 2009 [DOI:10.1007/978-0-387-87823-2].

[3] J.-L. Akian. Étude des mesures de Wigner pour la propagation d'énergie à haute fréquence dans les matériaux visco-élastiques, Technical Report RT 2/07950 DDSS, ONERA, décembre 2003, 57 pages.

[4] J.-L. Akian, R. Alexandre, S. Bougacha. A Gaussian beam approach for computing Wigner measures in convex domains. Kinetic and Related Models **4**, 589-631 (2011) [DOI :10.3934/krm.2011.4.589].

[5] J.-L. Akian. Space-time semiclassical measures for three-dimensional elastodynamics: Boundary conditions for the hyperbolic set. Asymptotic Analysis **78**, 37-83 (2012) [DOI :10.3233/ASY-2011-1084].

[6] V. M. Babich, V. S. Buldyrev, I. A. Molotkov. Space-Time Ray Method, Leningrad University Press, Leningrad, 1985.

[7] G. Bal, G. C. Papanicolaou, L. V. Ryzhik. Probabilistic theory of transport processes with polarization, SIAM Journal on Applied Mathematics **60**, 1639-1666 (2000) [DOI:10.1137/S003613999935696X].

[8] G. Bal. Kinetics of scalar wave fields in random media, Wave Motion **43**, 132-157 (2005) [DOI:10.1016/j.wavemoti.2005.08.002].

[9] G. Bal, T. Komorowski, L. Rhyzik. Kinetic limits for waves in a random medium, Kinetic and Related Models **3**, 529-644 (2010) [DOI:10.3934/krm.2010.3.529].

[10] O. M. Bouthier, R. J. Bernhard. Models of space-averaged energetics of plates, AIAA Journal **30**, 616-623 (1992) [DOI:10.2514/3.10964].

[11] R. N. Buchal, J. B. Keller. Boundary layer problems in diffraction theory, Communications on Pure and Applied Mathematics **13**, 85-114 (1960) [DOI:10.1002/cpa.3160130109].

[12] Y. Capdeville, E. Chaljub, J.-P. Vilotte, J.-P. Montagner. Coupling the spectral element method with a modal solution for elastic wave propagation in global Earth models, Geophysical Journal International **152**, 34-67 (2003) [DOI:10.1046/j.1365-246X.2003.01808.x].

[13] V. Červený. Seismic Ray Theory, Cambridge University Press, Cambridge, 2001.

[14] Y. M. Chen. Diffraction by a smooth transparent object, Journal of Mathematical Physics **5**, 820-832 (1964) [DOI:10.1063/1.1704183].

[15] Y. M. Chen. Diffraction by a smooth transparent object II, Diffraction by a cylindrical cavity, Journal of Mathematical Physics **6**, 1332-1333 (1965) [DOI:10.1063/1.1704779].

[16] G. Cohen, P. Joly, J. E. Roberts, N. Tordjman. Higher order triangular finite elements with mass lumping for the wave equation, SIAM Journal on Numerical Analysis **38**, 2047-2078 (2001) [DOI:10.1137/S0036142997329554].

[17] G. Cohen. Higher-Order Numerical Methods for Transient Wave Equations, Springer-Verlag, Berlin, 2002 [DOI:10.1007/978-3-662-04823-8].

[18] B. Engquist, O. Runborg. Computational high-frequency wave propagation, Acta Numerica **12**, 181-266 (2003) [DOI:10.1017/S0962492902000119].

[19] A. Erdélyi. Asymptotic Expansions, Dover Publications, New York NY, 1956.

[20] W. M. Ewing, W. S. Jardetzky, F. Press, Waves in Layered Media, Mc-Graw Hill, New York NY, 1957.

[21] S. Fauqueux. Éléments Finis Mixtes Spectraux et Couches Absorbantes Parfaitement Adaptées pour la Propagation d'Ondes Élastiques en Régime Transitoire, PhD thesis, Université Paris IX-Dauphine, 2003 [http ://tel.archives-ouvertes.fr/tel-00007445].

[22] P. Gérard, P. A. Markowich, N. J. Mauser, F. Poupaud. Homogenization limits and Wigner transforms, Communications on Pure and Applied Mathematics **50**, 323-379 (1997) [DOI:10.1002/(SICI)1097-0312(199704)50:4<323::AID-CPA4>3.0.CO;2-C].

[23] E. Godlewski, P. A. Raviart. Numerical Approximation of Hyperbolic Systems of Conservation Laws, Applied Mathematical Sciences **118**, Springer, New York NY, 1996.

[24] B. Gustafsson. The convergence rate for difference approximations to mixed initial-boundary value problems, Mathematics of Computation **29**, 396-406 (1975) [DOI:10.1090/S0025-5718-1975-0386296-7].

[25] B. Gustafsson. The convergence rate for difference approximations to general mixed initial-boundary value problems, SIAM Journal of Numerical Analysis **18**, 179-190 (1981) [DOI:10.1137/0718014].

[26] P. C. Herdic, B. H. Houston, M. H. Marcus, E. G. Williams, A. M. Baz The vibro-acoustic response and analysis of a full-scale aircraft fuselage section for interior noise reduction, Journal of the Acoustical Society of America **117**, 3667-3678 (2005) [DOI:10.1121/1.1887125].

[27] S. Jin, X. Wei. A Hamiltonian-preserving scheme for the Liouville equation of geometrical optics with partial transmissions and reflections, SIAM Journal on Numerical Analysis **44**, 1801-1828 (2006) [DOI:10.1137/050631343].

[28] S. Jin, X. Wen. Hamiltonian-preserving schemes for the Liouville equation of geometrical optics with discontinuous local wave speeds, Journal of Computational Physics **214**, 672-697 (2006) [DOI:10.1016/j.jcp.2005.10.012].

[29] S. Jin, X. Liao. A Hamiltonian-preserving scheme for high-frequency elastic waves in heterogeneous media, Journal of Hyperbolic Differential Equations **3**, 741-777 (2006) [DOI:10.1142/S0219891606000999].

[30] S. Jin, X. Wen. Computation of transmissions and reflections in geometrical optics via the reduced Liouville equation, Wave Motion **43**, 667-688 (2006) [DOI:10.1016/j.wavemoti.2006.06.001].

[31] S. Jin, D. Yin. Computational high frequency waves through curved interfaces via the Liouville equation and geometric theory of diffraction, Journal of Computational Physics **227**, 6106-6139 (2008) [DOI:10.1016/j.jcp.2008.02.029].

[32] S. Jin, X. Wen. The ℓ^1–stability of a Hamiltonian-preserving scheme for the Liouville equation with discontinuous potentials, Journal of Computational Mathematics **27**, 45-67 (2009) [DOI:].

[33] S. Jin, D. Yin. Computational high frequency wave diffraction by a corner via the Liouville equation and geometric theory of diffraction, Kinetic and Related Models **4**, 295-316 (2011) [DOI:10.3934/krm.2011.4.295].

[34] D. Komatitsch, J.-P. Vilotte. The Spectral Element method: an efficient tool to simulate the seismic response of 2D and 3D geological structures, Bulletin of the Seismological Society of America **88**, 368-392 (1998) [DOI:].

[35] J. B. Keller. Geometrical theory of diffraction, Journal of the Optical Society of America **52**, 116-130 (1962) [DOI:10.1364/JOSA.52.000116].

[36] L. E. Kinsler, A. R. Frey, A. B. Coppens, J. V. Sanders. Fundamentals of Acoustics, 4th Edition, Wiley, New York NY, 2000.

[37] R. S. Langley. On the vibrational conductivity approach to high frequency dynamics for two-dimensional structural components, Journal of Sound and Vibration **182**, 637-657 (1995) [DOI:10.1006/jsvi.1995.0223].

[38] B. Lapeyre, É. Pardoux, R. Sentis. Introduction to Monte-Carlo Methods for Transport and Diffusion Equations, Oxford University Press, Oxford, 2003.

[39] Y. Lase, M. N. Ichchou, L. Jézéquel. Energy flow analysis of bars and beams: theoretical formulation, Journal of Sound and Vibration **192**, 281-305 (1996) [DOI:10.1006/jsvi.1996.0188].

[40] R. J. LeVeque. Numerical Methods for Conservation Laws, Birkhäuser Verlag, Basel, 1990.

[41] R. M. Lewis, N. Bleistein, D. Ludwig. Uniform asymptotic theory of creeping waves, Communications on Pure and Applied Mathematics **20**, 295-328 (1967) [DOI:10.1002/cpa.3160200205].

[42] B. Lombard. Modélisation Numérique de la Propagation des Ondes Acoustiques et Élastiques en Présence d'Interfaces, PhD thesis, Université Aix-Marseille II, 2002 [http ://tel.archives-ouvertes.fr/tel-00009907].

[43] B. Lombard, J. Piraux. Numerical treatment of two-dimensional interfaces for acoustic and elastic waves, Journal of Computational Physics **195**, 90-116 (2004) [DOI :10.1016/j.jcp.2003.09.024].

[44] B. Lucquin. Équations aux Dérivées Partielles et leurs Approximations. Ellipses, Paris, 2004.

[45] P.-L. Lions, T. Paul. Sur les mesures de Wigner, Revista Matemática Iberoamericana **9**, 553-618 (1993).

[46] Y. Liu, M. K. Sen. A new time-space domain high-order finite difference method for the acoustic wave equation, Journal of Computational Physics **228**, 8779-8806 (2009) [DOI:10.1016/j.jcp.2009.08.027].

[47] D. Ludwig. Uniform asymptotic expansions at a caustic, Communications on Pure and Applied Mathematics **19**, 215-250 (1966) [DOI:10.1002/cpa.3160190207].

[48] R. H. Lyon, G. Maidanik. Power flow between linearly coupled oscillators, Journal of the Acoustical Society of America **34**, 623-639 (1962) [DOI:10.1121/1.1918177].

[49] R. H. Lyon. Statistical Energy Analysis of Dynamical Systems: Theory and Application. MIT Press, Cambridge MA, 1975.

[50] R. H. Lyon, R. G. DeJong. Theory and Application of Statistical Energy Analysis, 2nd Edition. Butterworth-Heinemann, Boston MA, 1995.

[51] Y. Maday, A. T. Patera. Spectral element methods for the incompressible Navier-Stokes equations, in State of the Art Surveys in Computational Mechanics (A. Noor ed.), 71-143, 1989.

[52] L. Miller. Refraction of high-frequency waves density by sharp interfaces and semi-classical measures at boundary, Journal de Mathématiques Pures et Appliquées **79**, 227-269 (2000) [DOI:10.1016/S0021-7824(00)00158-6].

[53] V. Mukhina. Diffraction by a smooth interface between two inhomogeneous media, Journal of Mathematical Sciences **3**, 109-124 (1975) [DOI:10.1007/BF01084810].

[54] D. J. Nefske, S. H. Sung. Power flow finite element analysis of dynamic systems: basic theory and application to beams, ASME Journal of Vibration, Acoustics, Stress and Reliability in Design, **111**, 94-100 (1989) [DOI:10.1115/1.3269830].

[55] P. Olsson. High-Order Difference Methods and Data Parallel Implementation, PhD thesis, Department of Scientific Computing, Uppsala University, Sweden, 1992 [http://urn.kb.se/resolve?urn=urn:nbn:se:uu:diva-106918].

[56] P. Olsson. Summation by parts, projections, and stability. I, Mathematics of Computation **64**, 1035-1065 (1995) [DOI:10.1090/S0025-5718-1995-1297474-X].

[57] P. Olsson. Summation by parts, projections, and stability. II, Mathematics of Computation **64**, 1473-1493 (1995) [DOI:10.1090/S0025-5718-1995-1308459-9].

[58] B. Perthame, C. W. Shu. On positivity preserving finite volume schemes for Euler equations, Nümerische Mathematik **73**, 119-130 (1996) [DOI:10.1007/s002110050187].

[59] M. M. Popov. Ray Theory and Gaussian Beam Method for Geophysicists, Editora de Universidade Federal da Bahia, Salvador BA, 2002 [http://www.cpgg.ufba.br/publicacoes/popov.pdf].

[60] E. Priolo, J. M. Carcione, G. Seriani. Numerical simulation of interface waves by high-order spectral modeling techniques, Journal of the Acoustical Society of America **95**, 681-693 (1994) [DOI:10.1121/1.408428].

[61] L. V. Ryzhik, G. C. Papanicolaou, J. B. Keller. Transport equations for elastic and other waves in random media, Wave Motion **24**, 327-370 (1996) [DOI:10.1016/S0165-2125(96)00021-2].

[62] É. Savin. Midfrequency Vibrations of a Complex Structure: Experiments and Comparison with Numerical Simulations, AIAA Journal **40**, 1876-1884 (2002) [DOI :10.2514/2.1867].

[63] É. Savin. Discontinuous finite element solution of radiative transfer equations, Technical Report RT 2/12683 DTIM, ONERA, December 2007, pp. 136–157.

[64] É. Savin. A transport model for high-frequency vibrational power flows in coupled heterogeneous structures, Interaction and Multiscale Mechanics **1**, 53-81 (2007).

[65] C. Sparber, P. A. Markowitch, N. J. Mauser. Wigner functions versus WKB-methods in multivalued geometrical optics, Asymptotic Analysis **33**, 153-187 (2003) [DOI:].

[66] J. Staudacher, É. Savin. Conservative finite-difference scheme for high-frequency acoustic waves propagating at an interface between two media, Communications in Computational Physics **11**, 351-366 (2012) [DOI:10.4208/cicp.111209.240710s].

[67] C. R. Steele. Application of the WKB method in solid mechanics, in Mechanics Today (S. Nemat-Nasser ed.) Vol. **3**, Franklin Book Co., Elkins Park PA, pp. 243-295 (1976).

[68] B. Strand. Simulations of acoustic wave phenomena using high-order finite difference approximations, SIAM Journal of Scientific Computing **20**, 1585-1604 (1999) [DOI:10.1137/S1064827596312523].

[69] T. Tang, Z. H. Teng. The sharpness of Kuznetsov's $O(\sqrt{\Delta x})$ L^1–error estimate for monotone difference schemes, Mathematics of Computation **64**, 581-589 (1995) [DOI:10.1090/S0025-5718-1995-1270625-9].

[70] Q.-A. Ta, D. Clouteau, R. Cottereau. Modeling of random anisotropic elastic media and impact on wave propagation, European Journal of Computational Mechanics **19**, 241-253 (2010) [DOI:10.3166/ejcm.19.241-253]

[71] L. Tartar. H-measures, a new approach for studying homogenisation, oscillations and concentration effects in partial differential equations, Proceedings of the Royal Society of Edinburgh **115A**, 193-230 (1990) [DOI:10.1017/S0308210500020606].

[72] J. Virieux. SH-wave propagation in heterogeneous media: Velocity-stress finite-difference method, Geophyscis **49**, 1933-1942 (1984) [DOI:10.1190/1.1441605].

[73] K. S. Yee. Numerical solution of initial boundary value problems involving Maxwell's equations in isotropic media, IEEE Transactions on Antennas and Propagation **14**, 302-307 (1966) [DOI:10.1109/TAP.1966.1138693].

[74] X. Zhang, C.-W. Shu. Maximum-principle-satisfying and positivity-preserving high-order schemes for conservation laws: survey and new developments, Proceedings of the Royal Society A **467**, 2752-2776 (2011) [DOI:10.1098/rspa.2011.0153].